

UC Riverside

UC Riverside Electronic Theses and Dissertations

Title

Subversion of Innate Immunity by Ebola Virus

Permalink

<https://escholarship.org/uc/item/5kh3f5q4>

Author

Menicucci, Andrea Rivera

Publication Date

2018

Peer reviewed|Thesis/dissertation

UNIVERSITY OF CALIFORNIA
RIVERSIDE

Subversion of Innate Immunity by Ebola Virus

A Dissertation submitted in partial satisfaction
of the requirements for the degree of

Doctor of Philosophy

in

Biomedical Sciences

by

Andrea Rivera Menicucci

June 2018

Dissertation Committee:

Dr. Ilhem Messaoudi, Co-Chairperson

Dr. Emma Wilson, Co-Chairperson

Dr. Thomas Girke

Copyright by
Andrea Rivera Menicucci
2018

The Dissertation of Andrea Rivera Menicucci is approved:

Committee Co-Chairperson

Committee Co-Chairperson

University of California, Riverside

ACKNOWLEDGEMENTS

To Ilhem Messaoudi: Thank you for letting me join the lab and contribute to amazing research. You have given me every opportunity to learn, whether it was to troubleshoot a new technique, take courses to be able to analyze my data, or review/write a manuscript or grant. This, in addition to our discussions about finding a story hidden in our massive datasets, has helped me on my way to become an independent scientist.

To the Messaoudi Lab: Thank you all for your help and support. Thank you for letting me bounce ideas off you whether or not they were good.

To Dr. Wilson and Dr. Girke: Thank you for being on my committee and taking the time to give me advice and support. Dr. Wilson, thank you for also being a great graduate student advisor I could confide in. Dr. Girke, thank you for teaching me about data analysis in genome biology and always advising me on different ways to interpret my data.

The text of this dissertation, in part or in full is a reprint of the material as it appears in the *Journal of Leukocyte Biology* 2016 (Chapter 1), *Nature Scientific Reports* 2017 (Chapter 2), and *Frontiers in Immunology* 2017 (Chapter 3). The corresponding author Ilhem Messaoudi listed in those publications directed and supervised the research that forms the basis for this dissertation. Data that are described in Chapters 4 and 5 will be submitted for publication.

Animal infections with ZEBOV-Makona or the VP35 mutant were performed in collaboration with Dr. Thomas Geisbert (Department of Microbiology and Immunology, University of Texas Medical Branch) and Dr. Chris Basler (Center for Microbial Pathogenesis, Georgia State University). Gene expression data following rVSV-ZEBOV vaccination and ZEBOV infection were generated in collaboration with Drs. Heinz Feldmann and Andrea Marzi (Laboratory of Virology, Division of Intramural Research, NIAID, NIH).

This work was funded by the National Institute of Allergy and Infectious Diseases, National Institute of Health, and NIH grant 5U19A109945.

ABSTRACT OF THE DISSERTATION

Subversion of Innate Immunity by Ebola Virus

by

Andrea Rivera Menicucci

Doctor of Philosophy, Graduate Program in Biomedical Sciences

University of California, Riverside, June 2018

Dr. Ilhem Messaoudi, Co-Chairperson

Dr. Emma Wilson, Co-Chairperson

Ebolavirus (EBOV) is amongst the deadliest human viruses that cause hemorrhagic fever. The Zaire species (ZEBOV) is responsible for most outbreaks and highest mortality rates, with the newly identified variant, Makona (ZEBOV-Makona) responsible for the recent epidemic in West Africa. The high virulence of ZEBOV is attributed to its ability to subvert innate immune responses, notably type I interferon (IFN) production, and causes excessive inflammation. However, studies investigating how ZEBOV modulates innate immunity has mostly been extrapolated from *in vitro* experiments. Therefore, ZEBOV-host interactions *in vivo* are not fully understood. In this dissertation, I address this gap in knowledge by investigating longitudinal host responses in peripheral blood collected from cynomolgus macaques infected with ZEBOV using both immunological assays and transcriptomic analysis. We first comprehensively analyzed ZEBOV-Makona pathogenesis and discovered correlations between: increased IFN α and interferon stimulated genes (ISGs); higher inflammatory transcripts and non-classical monocytes;

decreased expression of lymphocyte related genes and lymphopenia. This data also showed ZEBOV-Makona infection results in less severe and delayed appearance of clinical symptoms compared to previously identified variants. Second, transcriptomic analysis of purified immune cell subsets isolated from ZEBOV-Makona infected animals revealed that monocytes, but not T or B cells, support ZEBOV infection. Importantly, monocytes are one of the key players in mediating ZEBOV pathogenesis by initiating events that contribute to the characteristic symptoms of Ebola virus disease (EVD). Next, gene expression changes in animals infected with a recombinant ZEBOV containing mutations in VP35, which abrogate its ability to inhibit type I IFN, were indicative of a regulated innate immune response and successful development of adaptive immunity, which effectively immunized these animals against subsequent ZEBOV-Makona challenge. This data highlights the importance of type I IFN signaling and VP35 as a key virulence factor. Lastly, a promising vaccine candidate, rVSV-ZEBOV, has been shown to provide rapid protection to macaques against ZEBOV challenge. Transcriptomic analysis of animals vaccinated 7 or 3 days before challenge indicate that early expression of antiviral ISGs engendered by the vaccine can rapidly protect animals while paving the way for development of an adaptive immune response.

TABLE OF CONTENTS

Acknowledgements	iv
Abstract	vi
List of Figures	xi
List of Tables	xiv
CHAPTER 1: Introduction and Review of Literature	1
1.1 Ebola outbreaks	1
1.2 Clinical manifestations of Ebola infection	3
1.3 Ebola structure and life cycle	3
1.4 Animal models	8
1.5 Overview of immunity to viral infections	9
1.6 Subversion of innate immune response by Ebola	12
1.7 Dysregulated adaptive immune response after Ebola infection	16
1.8 Vascular permeability and coagulation defects	19
1.9 Long-term health outcomes in Ebola survivors	21
1.10 Clinical correlates and host factors that predict disease outcome	24
1.11 Vaccines against Ebola	27
1.12 Therapeutics against Ebola	31
1.13 Thesis overview and aims	37
CHAPTER 2: Infection with the Makona variant results in a delayed and distinct host immune response compared to previous Ebola virus variants	39
Abstract	40

Introduction	41
Materials and Methods	44
Results	53
Discussion	85
CHAPTER 3: Transcriptome Analysis of circulating immune cell subsets	91
highlight the role of monocytes in Zaire Ebola virus Makona pathogenesis	
Abstract	92
Introduction	93
Materials and Methods	96
Results	105
Discussion	121
CHAPTER 4: Modulation of host immunity by Ebola VP35	132
Abstract	133
Introduction	134
Materials and Methods	137
Results	142
Discussion	157
CHAPTER 5: rVSV-ZEBOV vaccination induces an antiviral innate	161
response that confers rapid protection	
Abstract	162
Introduction	163
Materials and Methods	166

Results	169
Discussion	194
CHAPTER 6: Discussion and Future Directions	200
References	208

LIST OF FIGURES

Figure 1.1. Ebola virus life cycle	7
Figure 1.2. Ebola virus pathogenesis	14
Figure 1.3. ZEBOV evades type I IFN responses	15
Figure 1.4. Long-term post-EBOV consequences	22
Figure 2.1. Flow cytometry gating strategy	49
Figure 2.2. Disease signs correlate with viral replication	55
Figure 2.3. Plasma levels of cytokines, chemokines and growth factors	58
Figure 2.4. ZEBOV-Makona infection results in early activation of innate immune cells and lymphopenia	61
Figure 2.5. NK cell subset frequencies and T cell proliferation	63
Figure 2.6. ZEBOV-Makona infection induces sustained large transcriptional changes in innate immune genes	67
Figure 2.7. ZEBOV reads mapping to open reading frames and intergenic regions	69
Figure 2.8. Gene expression changes 5 DPI reflect increased number of granulocytes	70
Figure 2.9. End-stage disease is characterized by upregulation of genes important for cell death and inflammation	71
Figure 2.10. ZEBOV-Makona pathogenesis is characterized by downregulation of genes critical for T-cell activation and translation	76
Figure 2.11. Comparison of DEGs detected in PBMC and WB	77
Figure 2.12. DEGs detected only in PBMC fraction play a role in regulating blood clotting, response to oxidative stress and vasculature development	79
Figure 2.13. Immgen analysis of PBMC 6 DPI	81
Figure 2.14. Comparison of host transcriptional profile following ZEBOV-Makona or ZEBOV-Kikwit infection at 4 DPI	82

Figure 2.15. Comparison of host transcriptional profile following ZEBOV-Makona or ZEBOV-Kikwit infection at 6 DPI	83
Figure 3.1. Cell subset separation strategy	99
Figure 3.2. Monocytes support ZEBOV-Makona replication and are major contributors of inflammation	106
Figure 3.3. Comparison of viral transcript profiles detected in each cell subset	107
Figure 3.4. ZEBOV-Makona infection induces expression of genes involved in defense response and type I IFN signaling in monocytes	108
Figure 3.5. Monocytes contribute significantly to ZEBOV-associated inflammation	111
Figure 3.6. Network displaying correlation between gene expression changes in monocytes and plasma levels of immune mediators 6 DPI	114
Figure 3.7. ZEBOV-Makona infection induces limited differential gene expression in T cells	115
Figure 3.8. ZEBOV-Makona infection induces limited differential gene expression in B cells	118
Figure 3.9. Monocytes contribute a significant proportion of transcriptional changes detected in PBMC	119
Figure 3.10. Comparison of transcriptional profiles between PBMC and monocytes 6 DPI	120
Figure 3.11. Expression of T cell activation inhibitors in purified T cells 6 DPI	125
Figure 3.12. Comparison of transcriptional changes in monocytes/macrophages following ZEBOV-Makona infection or LPS stimulation	128
Figure 4.1. VP35m infection results in mild clinical signs	143
Figure 4.2. VP35m infection induces robust gene expression changes within PBMC	147
Figure 4.3. Cluster 1 genes are involved in cell cycle and cellular metabolism	148

Figure 4.4. Cluster 2 genes are involved in cell cycle and cellular metabolism	149
Figure 4.5. VP35m infection induces a regulated innate immune response	150
Figure 4.6. VP35 infection engenders development of adaptive immunity	152
Figure 4.7. Animals challenged with VP35m are protected against subsequent WT ZEBOV challenge	155
Figure 4.8. Detection of transcriptional changes following WT ZEBOV infection	156
Figure 5.1. rVSV-ZEBOV vaccination elicits transcriptional changes suggestive of antiviral innate immunity and B cell activation	172
Figure 5.2. Immgen and DCQ analysis of transcriptional changes 7 days post rVSV-ZEBOV vaccination	176
Figure 5.3. Negative control animals exhibit gene expression changes consistent with EVD	178
Figure 5.4. Negative control animals display gene expression changes consistent with dysregulated inflammatory response and lymphopenia	179
Figure 5.5. Animals that were vaccinated 2 or more weeks prior to challenge show limited gene expression changes	181
Figure 5.6. ZEBOV-Makona challenge 1 week after vaccination induces a recall response	185
Figure 5.7. Animals vaccinated 1 week before challenge exhibit large transcriptional changes associated with adaptive immunity	186
Figure 5.8. Animals vaccinated 3 days before challenge display distinct Immune responses that correlate with disease outcome	191
Figure 5.9. Surviving animals in the day-3 group exhibit transcriptional changes consistent with resolution of immune response	193

LIST OF TABLES

Table 2.1. Antibodies used for flow cytometric analysis of immune cell subsets	48
Table 2.2. Clinical scores used to determine disease progression	57
Table 3.1. Average cell subset purity (%) per day	100

CHAPTER 1: Introduction and Review of Literature

1.1 Ebola outbreaks

The filoviruses, Ebola virus (EBOV) and Marburg virus (MARV), are amongst the deadliest re-emerging viruses. Infection in humans results in hemorrhagic fever with case fatality rates (CFR) of 90% in some outbreaks. The first identified instance of filovirus hemorrhagic fever occurred in 1967 in Marburg, Germany when animal staff and lab workers became infected while processing tissues from *Cercopithecus aethiops* monkeys that were imported from Uganda to produce kidney cell cultures needed for the production of a live poliomyelitis vaccine [1, 2]. Electron microscopy identified the causative agent as Marburg virus [3]. In the following years, small sporadic outbreaks of MARV occurred in Africa with the largest occurring in 2004 in Angola, with 252 cases and CFR of 90% [4, 5].

Hemorrhagic fever caused by a second filovirus, Ebola, was first reported in 1976 when simultaneous outbreaks occurred in northern Zaire, now the Democratic Republic of the Congo (DRC), and Sudan with 318 cases (CFR of 88%) and 284 cases (CFR of 53%) respectively [6]. These two epidemics were caused by two species of Ebola virus, Zaire Ebola virus (ZEBOV) and Sudan Ebola virus (SEBOV). Subsequent outbreaks of EBOV revealed the presence of 3 additional species with varying pathogenicity in humans. In 1989, the Reston Ebola virus (REBOV) was discovered in the United States during an outbreak of viral hemorrhagic fever among cynomolgus macaques imported from the

Philippines and was found to be non-pathogenic in humans [7]. In 1994, the Ivory Coast Ebola virus (CIEBOV) was isolated from an infected ethologist while conducting a necropsy on a chimpanzee in the Tai Forest reserve in Cote d'Ivoire; it was nonfatal and remains the only documented case [8]. Finally, Bundibugyo Ebola virus (BEBOV) was discovered in 2007 in Uganda where it caused an outbreak with 149 cases with a 25% lethality rate. The natural reservoir may be bats based on the presence of filovirus RNA in tissues and sera from bats in Africa and Asia [9]. Moreover, filoviruses do not seem to be pathogenic in bats, despite displaying high virulence in humans and non-human primates [10]. Lastly, the most recently identified filovirus, Lloviu virus, was identified in bats in Spain, and its pathogenic potential remains unknown [11].

ZEBOV is responsible for the most Ebola outbreaks with multiple strains identified. From 1976 until the end of 2013, there have been 1,383 ZEBOV cases, 779 SEBOV cases, and 185 BEBOV cases. These outbreaks were quickly contained due to small populations in remote regions of central Africa [12]. However, in December 2013, ZEBOV emerged in Guinea, then quickly spread to Sierra Leone and Liberia, leading to the first EBOV epidemic in history. Over 28,600 confirmed, probable and suspected cases of ZEBOV disease and 11,310 deaths were reported across 10 countries (Guinea, Liberia, Sierra Leone, United States, Mali, Nigeria, Senegal, Spain, United Kingdom, and Italy). The new ZEBOV strain responsible for this epidemic was named Makona after the river that borders these three countries. Concurrently, in August 2014, the WHO was notified of an unrelated ZEBOV outbreak in DRC, that resulted in 66 cases and 74% lethality rate. Although

sporadic cases of Ebola virus continued to occur in Sierra Leone (14th of January 2016) and Guinea in (17th of March 2016), WHO declared the end of the Public Health Emergency of International Concern regarding the Ebola virus disease (EVD) outbreak in West Africa on the 29th of March 2016. Since then, 8 suspected cases of EVD were reported on May 11, 2017 with 4 deaths [13]. A study that compared the virulence of Makona with that of Mayinga (responsible for the 1976 outbreak), in cynomolgus macaques, showed that although infection with both strains was uniformly lethal, disease progression was delayed in Makona-infected animals [14]. The mechanisms underlying differences in disease severity and fatality rates between species and strains are not fully understood.

1.2 Clinical manifestations of Ebola infection

Filovirus infections are acquired by direct contact with infected bodily fluids and enter the human body via breaks in the skin or through mucosal surfaces [15]. The incubation period ranges from 2 to 21 days with an average of 5-7 days [15]. Early symptoms are nonspecific including fever, chills, malaise and myalgia. Subsequent symptoms that signal multi-system involvement are gastrointestinal (anorexia, nausea, vomiting, abdominal pain, diarrhea), respiratory (chest pain, shortness of breath, cough, nasal discharge), and vascular (postural hypotension, edema). During the terminal stage of the disease, there is an increase in vascular permeability, massive tissue injury, dysregulation of the coagulation cascade and hemorrhage. Hemorrhagic manifestations include petechiae, ecchymoses and mucosal hemorrhages. Multiorgan failure and shock are usually the main causes of death, which occur 7-14 days after the onset of initial symptoms [8, 16-19]. Laboratory diagnosis of

filovirus infections can be achieved by measuring EBOV-specific IgG and IgM antibodies (ELISA), viral nucleic acid (RT-PCR), or viral antigen (ELISA) [20].

1.3 Ebola structure and life cycle

Ebola virus is a filamentous enveloped virus containing a 19 kb negative strand RNA genome that encodes 7 genes and 9 proteins [21]. At the genome ends, short extragenic regions, called leader and trailer sequences, contain encapsidation signals as well as replication and transcription promoters. The leader region contains signals for initiation of RNA synthesis by the viral RNA-dependent RNA polymerase in addition to signals that direct packaging of full-length negative strand copies of the viral genome in nucleocapsids. The trailer region, located at the 3' end of the antigenome RNA, contains the promoter for genome replication [22-24].

The 9 proteins encoded by EBOV genome include glycoprotein (GP), RNA dependent RNA polymerase (L), nucleoprotein (NP), and four viral proteins (VP) 24, 30, 35 and 40. GP is the only surface protein on the viral envelope and is important in mediating receptor binding and fusion [25-27]. EBOV also encodes soluble forms of GP, sGP and ssGP through RNA editing [28-30]. VP40 is a matrix protein located beneath the viral membrane where it maintains structural integrity of viral particles [26, 31]. Expression of VP40 alone in mammalian cells can also induce its own release and formation of virus like particles (VLP) in the absence of other viral proteins and, thus, is important in filovirus budding [32]. VP24 is a secondary matrix protein that contributes to nucleocapsid formation. NP,

VP35, VP30 and L are associated with the viral RNA genome, forming the nucleocapsid [23, 33]. NP is the structural component of the nucleocapsid complex but can also catalyze replication and transcription of the RNA genome. The active polymerase complex is composed of VP35 (a polymerase cofactor) and L (polymerase) [23, 24]. VP30 is a transcriptional activator and a major component of the RNA-dependent RNA polymerase. VP24 and VP35 also contribute to innate immune evasion by antagonizing type I interferon responses. GP has also been shown to antagonize tetherin, an interferon stimulated gene (ISG) that prevents virus budding [34].

Host receptors utilized by the virus to gain entry include: asialoglycoprotein receptor on hepatocytes, folate receptor alpha on epithelial cells; C-type lectins such as DC-SIGN and DC-SIGNR on DCs, macrophages, and endothelial cells; and human macrophage lectin specific for galactose/N-acetylgalactosamine (hMGL) on macrophages [35, 36]. Once EBOV attaches to the cell membrane by its surface GP, virions are taken up by macropinocytosis or clathrin-mediated endocytosis [37, 38]. The acidification of the endosome is followed by fusion of virus and host membranes, and the release of EBOV into the cytoplasm [39-42] (**Figure 1.1**). Specifically, cleavage of GP by cellular proteases cathepsin B and cathepsin L allow GP to interact with host protein Niemann-Pick C1, resulting in a conformational change in GP that triggers membrane fusion and release of the viral ribonucleocapsid into the cytoplasm [43-46]. Within the cytoplasm, the negative-strand RNA genome undergoes transcription, which requires NP, VP35, L and VP30. EBOV mRNA synthesis is detectable by 6-7 hours post-infection [47]. The EBOV RNA

dependent RNA polymerase (L) binds a site within the leader region of each negative-sense genome and slides along the RNA template transcribing individual genes sequentially in a 3' to 5' direction [48]. Each gene is delineated by highly conserved transcription start and stop signals with polyadenylation sites marking the termini of the mRNAs [26]. Additionally, EBOV mRNAs are shown to be capped at the 5' end [49]. NP is the most transcribed gene, while L is the least transcribed in Vero E6 cells [50]. EBOV transcription is dependent on the presence of transcription factor VP30 [24]. The initial transcription and translation of virus genes leads to a buildup of viral proteins, especially NP, which triggers viral replication [23, 24]. During replication, which requires NP, VP35 and L, the promoter at the 3' end of genomic RNA drives synthesis of full-length positive-sense antigenomic RNA, which in turn serve as a template for production of progeny negative-sense genomes [48]. When sufficient levels of negative-sense genomes and viral proteins are reached, they are assembled at the plasma membrane where VP40 induces budding of filoviruses [50] (**Figure 1.1**).

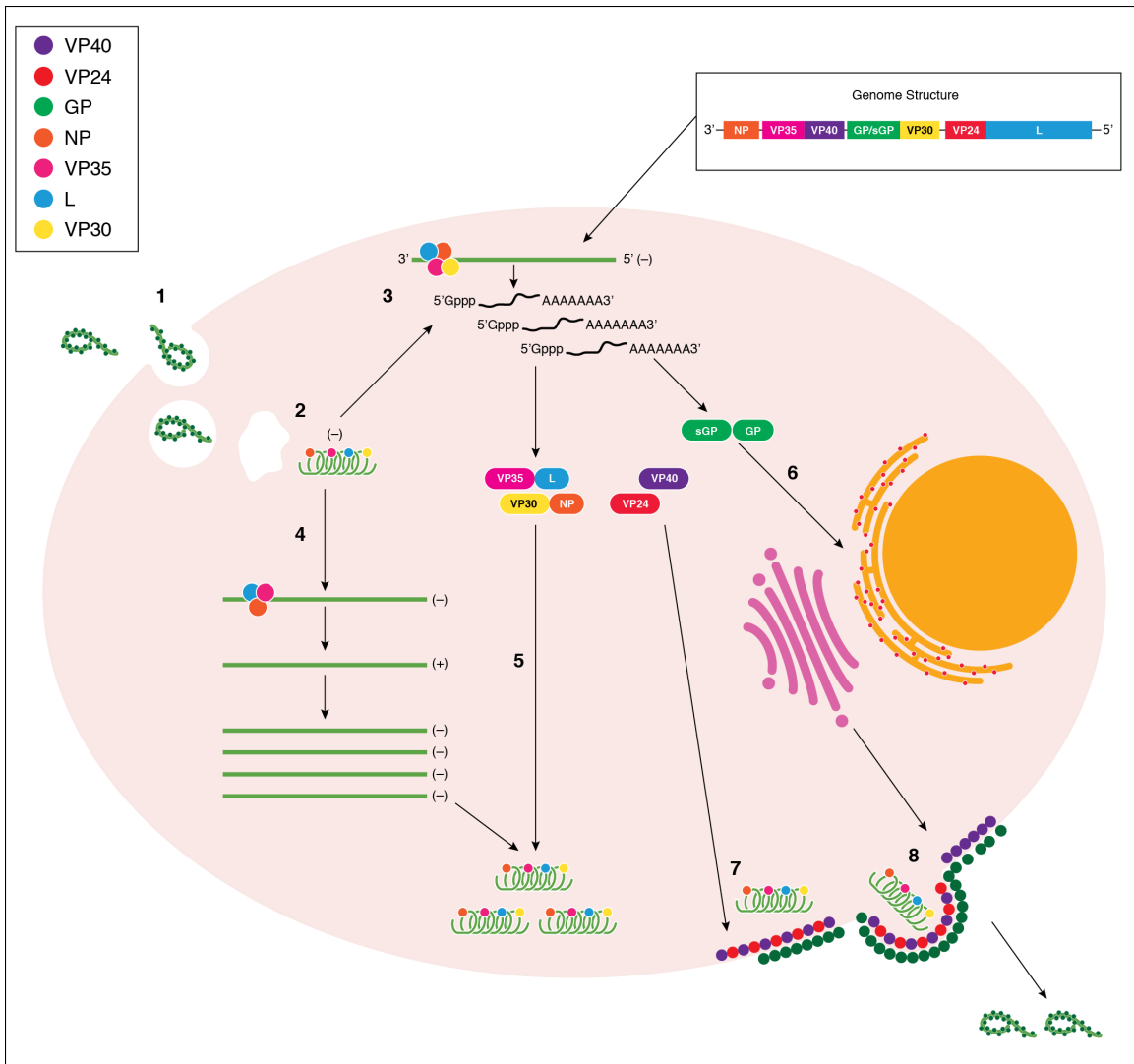


Figure 1.1. Ebola virus life cycle. (1) EBOV gains cell entry by macropinocytosis or receptor-mediated endocytosis. (2) Acidification of the endocytic vesicle followed by fusion of virus and host membranes releases the EBOV nucleocapsid into the cytoplasm. (3) The RNA dependent RNA polymerase transcribes individual mRNA from the negative-sense genome in a 3' to 5' direction. Each mRNA are capped at the 5' end and contain a poly-A tail. (4) During replication, the promoter at the 3' end of genomic RNA drives synthesis of full-length positive-sense antigenomic RNA, which in turn serve as a template for production of progeny negative-sense genomes. (5) Nucleocapsid proteins (VP35, L, VP30 and NP) associate with negative-sense genome progeny while (6) GP and sGP are further modified in the ER and Golgi Body. (7) When sufficient levels of negative-sense genomes and viral proteins are reached, they are assembled at the plasma membrane with membrane associated proteins (matrix proteins VP24 and VP40, and GP). (8) Complete virions bud from the cell surface.

1.4 Animal models

Rodent models, including guinea pigs and inbred mice, are not ideal for studying ebola hemorrhagic fever (EHF) since both models require the use of a mouse-adapted ZEBOV (MA-ZEBOV), which was obtained by serial passage of wild type ZEBOV in newborn mice [8, 51]. Although lethal infection of mice with MA-ZEBOV can be achieved by intraperitoneal injection, no significant coagulation disorders or other characteristics of hemorrhagic fever are observed [52]. Clinical manifestations in MA-ZEBOV infected mice include increased levels of inflammatory cytokines, infection of mononuclear phagocytes, lymphopenia, and disseminated viremia with death occurring 5-7 days post-infection [52]. Compared to WT-ZEBOV, MA-ZEBOV possesses 13 amino acid mutations in: VP35 (1), VP24 (1), VP40 (1), GP (3), NP (2), L (3), and noncoding regions (2) [53]. It was shown that two amino acid mutations in NP, which is essential for initiating viral replication, and VP24, which is critical for virus evasion of IFN-induced antiviral responses, are the determinants of virulence of MA-ZEBOV in mice [53]. Recently, a new mouse model was developed using the Collaborative Cross resource, a large panel of genetically diverse recombinant inbred strains (CC-RI) derived from a cross of eight different mice strains, referred to as founders [54]. Different CC-RI strains can be crossed with one another to generate an intercrossed (CC-RIX) F1 progeny. Rasmussen et al., assessed the pathogenic phenotype following intraperitoneal infection with MA-ZEBOV in 47 CC-RIX lines and observed a spectrum of disease outcomes, including coagulation defects in 16 CC-RIX lines [55]. However, this model still requires the use of MA-ZEBOV. To date, hu-BLT mice, which are engrafted with human immune cells, is the only rodent model susceptible

to WT ZEBOV. While hu-BLT mice exhibit some features of human EVD, including dysregulation of cytokine and chemokine secretion, this model does not exhibit hemorrhaging and coagulopathies [56].

In contrast, several nonhuman primate species are susceptible to the same ZEBOV strains that cause disease in humans including African green monkeys (*Chlorocebus aethiops*), hamadryad baboons (*Papio hamadryas*), cynomolgus macaques (*Macaca fascicularis*), and rhesus macaques (*Macaca mulatta*) [57]. However, cynomolgus macaques and rhesus macaques are the gold standard animal models used in filovirus study because of the strong resemblance of disease symptoms and kinetics as well as host responses to those observed in human infections [58, 59]. The macaque model uses a challenge dose and route (1000 PFU; intramuscular injection) that reflects a likely laboratory exposure and is uniformly lethal with animals succumbing to infection 6-7 days after challenge [20]. It should be noted that MA-ZEBOV is not virulent in macaques. Only two out of three rhesus macaques challenged with a large dose of MA-ZEBOV (5000 PFU) showed mild illness [52].

1.5 Overview of immunity to viral infections

The immune system protects the host against foreign pathogens while limiting damage through the coordination of both innate and adaptive immune system. Innate immunity is the first line of defense that recognizes conserved pathogen-associated molecular patterns (PAMPs) using germline-encoded receptors, referred to as pathogen recognition receptors (PRRs). In contrast, the adaptive immune system can detect specific pathogens through a

highly diverse set of receptors (T cell receptor and B cell receptor) that is generated through recombination and somatic mutation. Additionally, adaptive immunity is characterized by the ability to develop long lasting immunological memory, which results in an enhanced effector response upon re-exposure to the same antigen.

The innate immune system is composed primarily of neutrophils, monocytes/macrophages, dendritic cells (DCs), and natural killer (NK) cells. Neutrophils are the most abundant white blood cell and are able to destroy pathogens via phagocytosis of infected cells, degradative enzymes and respiratory burst [60]. Monocytes and DCs are scavenging cells that serve as antigen-presenting cells (APC) responsible for processing and presenting foreign antigen peptides to T cells, thereby bridging innate and adaptive immunity [61]. Furthermore, DCs can be further subdivided into myeloid DCs (mDCs), which can present antigen to naïve T cells , and plasmacytoid DCs (pDCs), which are potent producers of type I IFN in response to viral infections [62, 63]. NK cells are able to destroy virally infected cells through the release of cytolytic molecules and antibody dependent cell-mediated cytotoxicity [64].

The most well known PRRs in recognizing viral invasion are 1) toll-like receptors (TLRs), particularly TLRs 3, 7, 8 and 9; 2) Retinoic acid-inducible gene I-like receptors (RLRs); 3) the nucleotide oligomerization domain-like receptors (NLRs); 4) and cytosolic DNA sensors [65]. After recognition of foreign antigens, PRRs initiate intracellular signaling that results in the production of molecules that inhibit viral replication and spread. A critical

component for innate immunity against viral infection is the interferon (IFN) response. Viral dsRNA in the cytosol is detected by viral sensors retinoic acid-inducible gene-I (RIG-I) and melanoma differentiation associated gene-5 (MDA-5). Upon activation, RLRs signal through the adaptor molecule interferon promoter stimulator-1 (IPS-1), which induces the kinases Tank binding kinase-1 (TBK-1) and I-Kappa-B kinase epsilon (IKK ϵ) to phosphorylate interferon regulatory factors (IRF) 3 and 7 [66]. Phosphorylated IRF3/7 dimerize and move to the nucleus, where they activate the transcription of IFN α/β . Binding of IFN α/β to receptors IFNAR1/2 activates the Janus kinase (JAK) and signal transducer and activator of transcription (STAT) pathway [66]. Phosphorylation of JAK1 by tyrosine kinase 2 (TYK2) leads to phosphorylation of STAT1 and STAT2. Phosphorylated STAT1/STAT2 dimerize and translocate to the nucleus where they activate transcription of interferon-stimulated genes (ISGs), which are important in inhibiting viral replication [66, 67] (**Figure 1.2**).

Adaptive immune responses are mediated by T and B cells. T cells are responsible for cell-mediated responses against viruses and are generated in the thymus where they differentiate into naïve CD4 or CD8 T cells [68]. T cells use T cell receptors (TCRs) to recognize antigens presented on either MHC-I or MHC-II molecules, the latter of which are only found on APCs [68]. CD8 T cells are cytotoxic T cells that recognize peptide bound to MHC-I and upon recognition, induce apoptosis of infected cells by producing granzymes and perforin [69]. CD4 T cells, which are also known as helper T cells and recognize peptides bound to MHC-II, can be further categorized as T helper 1 (Th1), Th2,

Th17, regulatory T cells (Tregs) and follicular helper (Tfh) CD 4 T cells [70-72]. Th1 CD4 T cells are important for viral infections since they produce pro-inflammatory cytokines such as IL-2, IFN γ , and TNF α and can help priming of CD8 T cells [70, 71]. Tfh CD4 T cells play an important role in promoting germinal cell B cell responses [72]. Upon activation of the B cell receptor (BCR), B cells proliferate and differentiate into long-lived memory B cells or Ig-secreting plasma cells [73, 74]. Antibodies are important in neutralizing virus and together with NK cells, can kill infected cells via antibody-dependent cell-mediated cytotoxicity [75].

1.6 Subversion of innate immune response by Ebola

While ZEBOV displays broad tropism, studies in macaques have shown that antigen-presenting cells (APCs), notably monocytes/macrophages and dendritic cells (DCs), are the first and preferred targets of ZEBOV [58, 76] (**Figure 1.2**). Due to the migratory potential of APCs, infection of these cells allows transport of the virus to lymph nodes, spleen and liver where the virus can infect resident tissue macrophages and DCs [58, 59]. Filovirus infection of monocytes and macrophages *in vitro* triggers the robust expression of inflammatory mediators including IL-1 β , IL-6, IL-8, MIP-1 α , MIP-1 β and MCP-1, and TNF α [77-79]. Increased levels of these inflammatory mediators, in addition to reactive oxygen and nitrogen species, have been detected in the plasma of humans and animal models following ZEBOV exposure [77, 80-84]. Chemokines released from virus-infected cells may recruit additional monocytes and macrophages to sites of infection, increasing the availability of target cells. Increased inflammatory mediators may also contribute to the

impairment of the vascular system and disseminated intravascular coagulation [76, 79, 85, 86]. In contrast, *in vitro* infection of DCs results in their failure to: 1) upregulate co-stimulatory molecules CD40, CD80 and CD86 as well as MHC class II; and 2) produce chemokine/cytokines [87, 88]. Therefore, ZEBOV infection may impair the ability of DCs to mature into mobile, antigen presenting cells, that can stimulate T and B cell responses needed to clear infection [89] (**Figure 1. 2**). Indeed, T and B cell responses are absent in fatal ZEBOV cases as discussed in 1.7.

ZEBOV can prevent production of and cellular responses to type I IFN. *In vitro* studies have shown that ZEBOV VP35 can block RIG-I-like receptor signaling by binding to dsRNA or binding PKR activating protein (PACT), thereby preventing production of antiviral cytokines IFN α/β [90, 91] (**Figure 1.3**). VP35 can also prevent the phosphorylation of IRF3 by IKK ϵ [92, 93]. Furthermore, VP35 can interact with host SUMOylation machinery, including SUMO E2 enzyme Ubc9 and E3 ligase PIAS1, to promote the degradation of IRF7/IRF3 [94]. Interestingly, infection of guinea pigs with recombinant ZEBOV possessing two point mutations in VP35, that impair its dsRNA binding activity, resulted in loss of virulence and protected animals against subsequent WT ZEBOV challenge [95]. ZEBOV VP24 binds to the nuclear importer protein karyopherin α -1 (KPN α 1) and prevents it from binding to phosphorylated STAT1, thereby limiting the accumulation of nuclear STAT1 and preventing IFN-induced gene expression [96-99] (**Figure 1.3**).

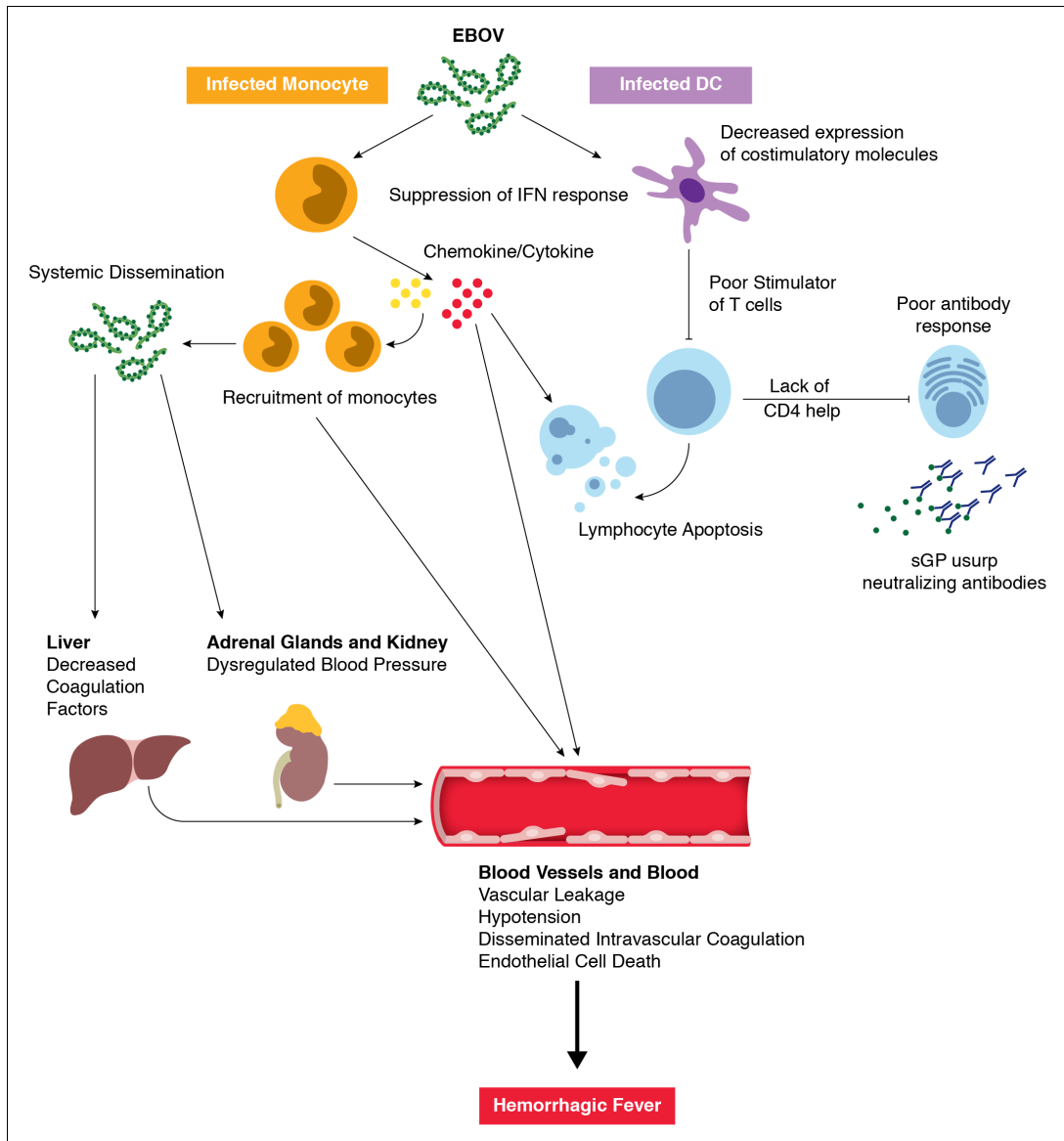


Figure 1.2. Ebola virus pathogenesis. ZEBOV initially and preferentially infects monocytes, macrophages, and dendritic cells. Infection of dendritic cells impairs their maturation and suppresses type I IFN responses thereby preventing T cell activation. Infection of monocytes and macrophages leads to the robust expression of inflammatory mediators. Secreted chemokines can recruit more monocytes, which act as new targets for viral infection. Inflammatory mediators, reactive oxygen species and nitric oxide, can induce apoptosis leading to lymphocyte death. The lack of lymphocytes such as CD4 T cells inhibit the ability of the virus to induce an antibody response. Production of ZEBOV soluble glycoprotein (sGP) usurps any GP-specific antibodies that are made. Eventually, the inflammatory cytokines are responsible for vascular leakage. ZEBOV systemically disseminates to liver, kidneys, and adrenal glands, which contribute to symptoms associated with hemorrhagic fever.

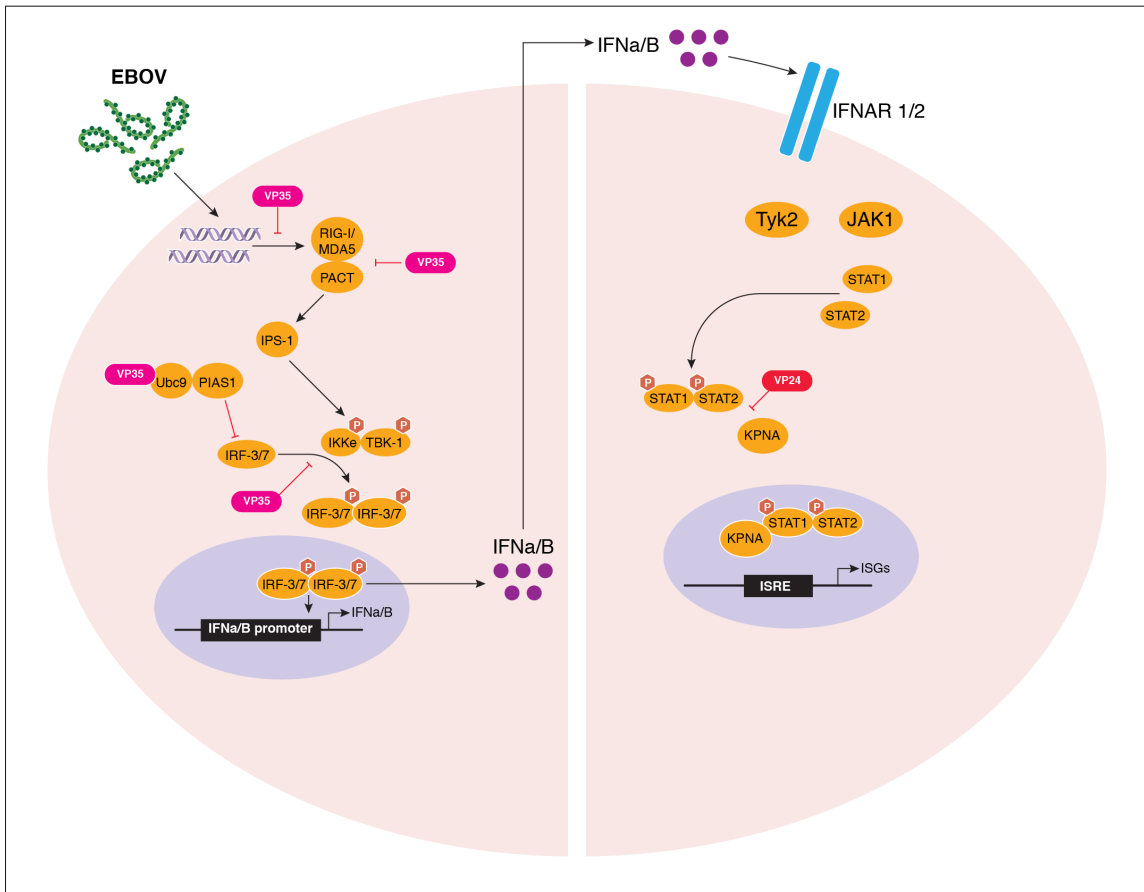


Figure 1.3. ZEBOV evades type I IFN responses. ZEBOV can prevent production of and cellular responses to type I IFN. *In vitro* studies have shown that ZEBOV VP35 can block RIG-I-like receptor signaling by binding to dsRNA or binding PKR activating protein (PACT), preventing production of IFN α/β . VP35 can interact with host SUMOylation machinery, including SUMO E2 enzyme Ubc9 and E3 ligase PIAS1, to promote the degradation of IRF7/IRF3. VP35 can also prevent the phosphorylation of IRF3 by IKK ϵ . ZEBOV VP24 can prevent cellular responses to IFN α/β by binding to the nuclear importer protein karyopherin α -1 (KPN α 1), preventing it from binding to phosphorylated STAT1, thus limiting the accumulation of nuclear STAT1 and preventing IFN-induced gene expression.

Neutrophilia has been observed in ZEBOV infected macaques after detection of viremia, suggesting widespread recruitment to sites of infection. Although not productively infected by ZEBOV, neutrophils can be activated by viral particles and contribute to the overall inflammation by secretion of pro-inflammatory cytokines [58, 100]. Frequency of peripheral natural killer cells (NK) were reported to decline during ZEBOV infection in cynomolgus macaques and humans [58, 101]. Their importance in controlling ZEBOV infection has yet to be elucidated.

1.7 Dysregulated adaptive immune response after Ebola infection

Severe lymphopenia and destruction of lymphoid tissue is one of the hallmarks of Ebola infection [102] (**Figure 1.2**). Loss of peripheral blood CD4 and CD8 T cells has been documented in mice [103], cynomolgus macaques [59, 101] and human peripheral blood mononuclear cell (PBMC) cultures [104] following ZEBOV infection. Loss of B cells is more controversial with some studies demonstrating apoptosis of B lymphocytes using double staining for CD20 and TUNEL in mice and macaques [76], while other studies show no changes in B lymphocyte counts in cynomolgus macaques [101]. *In vivo* and *in vitro* studies using TUNEL staining and transmission electron microscopy confirm apoptosis as the main mechanism of lymphocyte loss during ZEBOV infection [76]. In humans, percentages of peripheral blood CD4 and CD8 T cells expressing the apoptotic marker CD95 were higher in fatally infected patients compared to healthy individuals [84]. Increased expression of CD95 was also observed in cynomolgus macaques [101].

Increased levels of soluble Fas (sFas) and 41/7 nuclear matrix protein, which is cleaved and solubilized during apoptosis, have been detected in plasma of patients during the last 5 days of life following infection with ZEBOV [105]. Similarly, an upregulation of Fas and FasL mRNA levels was detected using RT-PCR in PBMC of infected patients [105]. Moreover, mice deficient in the expression of Fas-associated death domain or overexpressing the anti-apoptotic molecule Bcl-2 were resistant to MA-ZEBOV induced lymphocyte apoptosis, suggesting lymphocyte death can occur via both extrinsic (death receptor) and intrinsic (mitochondrial) pathways [106]. Furthermore, while patients who survived ZEBOV infection showed an up-regulation of Bcl-2 mRNA in PBMC, those who succumbed showed a significant decrease of Bcl-2 mRNA expression during the terminal stage of infection [105]. The decreased expression of Bcl-2 was coincident with the loss of CD3, CD8, and TCR-V β mRNA in PBMC [105].

However, infection of human PBMC *in vitro* with ZEBOV did not result in increased expression of Fas but rather an increase in mRNA levels of TNF related apoptosis inducing ligand (TRAIL) in CD4 and CD8 T cells at 7 days post infection (DPI) [104]. These data suggest that additional inflammatory mediators released *in vivo* during infection result in the increased Fas expression and that apoptosis of lymphocytes during ZEBOV infection is not due to viral replication (**Figure 1.2**). Indeed, analysis of ZEBOV-infected nonhuman primate tissues clearly shows the presence of ZEBOV antigens within mononuclear phagocytic cells but not in lymphocytes even after *in vitro* infection [76, 85]. Some inflammatory mediators produced after ZEBOV infection, such as TNF α , nitric oxide and

reactive oxygen species, can induce apoptosis [107-109]. Moreover, 90% of ZEBOV infected adherent human macrophages were positive for TRAIL by immunohistochemistry, flow cytometry, and RNA analysis [77] and can therefore induce apoptosis in lymphocytes via the extrinsic pathway.

The lymphopenia observed during ZEBOV infection in part explains the lack of ZEBOV-specific T and B cell responses. The lack of T cell response is evident by the absence of T cell derived cytokines (IL-2, IL-3, IL-4, IL-5, IL-9, IL-13) in the plasma of fatally infected patients [84, 88, 110, 111]. In addition, lack of activated T lymphocytes was reported in the peripheral blood of ZEBOV-infected macaques [87, 101] and mice [112]. Since CD4 T cells are required for B cell isotype class switching, the loss of CD4 T cells may explain the lack of Ebola specific IgM and IgG antibodies observed in fatally infected patients [105]. Moreover, the ZEBOV envelope is covered in a dense concentration of N- and O-linked glycans [113, 114], that interfere with binding of neutralizing antibodies [115-117]. Finally, secreted glycoproteins (sGP), which account for about 70% of glycoprotein mRNA transcripts [118], act as decoys that usurp the much-needed neutralizing antibodies [119] (**Figure 1.2**). Subversion of the adaptive immune response, coupled with inactivation of the innate immune branch, allows ZEBOV to disseminate systemically.

The magnitude of the recent ZEBOV epidemic and the large number of survivors has provided a unique opportunity to study host immune responses in EVD patients who survived infection. Four patients treated at Emory Hospital with various combinations of

the antibody cocktail ZMapp, an siRNA against ZEBOV, a DNA polymerase inhibitor, and convalescent serum as early as 1 day and as late as 10 days post symptom onset exhibited increased frequencies of activated CD8 T cells, CD4 T cells and plasmablasts 2-3 weeks after the onset of symptoms. Lymphocyte activation coincided with a decline in viral loads during the 2nd week, that reached nadir by week 3 post symptom onset [120]. ZEBOV-specific IgG responses peaked 2-3 weeks after symptom onset and the strongest T cell responses were directed against ZEBOV NP. Surprisingly, the number of activated T cells remained elevated up to 30 days following discharge, suggesting potential persistence of ZEBOV antigen [120]. A second study of T cell immune responses in EVD patients managed at Ebola Treatment Centers in Guinea (47 in Gueckedou and 157 Coyah) showed that while there was robust CD4 and CD8 T cell activation (measured by co-expression of CD38 and HLA-DR) in all EVD cases, an increase in the co-expression of the negative T cell regulators CTLA-4 and PD-1 significantly correlated with fatalities [121]. These studies indicate that dysregulation of the T cell response, in addition to lymphopenia, contributes to EVD pathology.

1.8 Vascular permeability and coagulation defects

In addition to inducing apoptosis within lymphocytes, the large release of TNF α from infected monocytes/macrophages can increase endothelial permeability, resulting in vascular leakage [77]. *In vitro* studies show that increased endothelial permeability is temporally associated with the release of TNF α from MARV infected human monocytes/macrophages [1]. Similarly, the release of nitric oxide, which is an important

effector molecule in the homeostasis of the cardiovascular system, can result in loss of vascular smooth-muscle tone and hypotension [82, 122]. In addition, ZEBOV infection of macrophages leads to the upregulation of surface tissue factor (TF) as well as the release of membrane microparticles containing TF, resulting in the over-activation of the extrinsic pathway of coagulation and the development of disseminated intravascular coagulation [86]. Expression of TF is further upregulated by pro-inflammatory cytokines, notably IL-6, that are abundant during acute ZEBOV infection, exacerbating the intravascular coagulation phenotype [123].

In addition, ZEBOV-induced paralysis of the host response facilitates viral dissemination to hepatocytes, adrenal cortical cells and endothelial cells of connective tissue in cynomolgus macaques [58] (**Figure 1.2**). Hepatocellular necrosis results in decreased synthesis of coagulation proteins while infection and necrosis of adrenocortical cells may negatively affect blood pressure homeostasis, leading to hemorrhage [58]. Coagulation abnormalities are initiated early during ZEBOV infection in cynomolgus macaques. Specifically, a dramatic decrease in plasma levels of anticoagulant protein C occurs as early as 2 DPI. This is followed by an increase of both tissue plasminogen activator (tPA), which is involved in dissolving blood clots, and fibrin-degradation products (D-dimers) at day 5 post-infection [86]. Thrombocytopenia and prolonged pro-thrombin time are indicators of dysregulated blood coagulation and fibrinolysis during ZEBOV infection and may manifest as petechiae, ecchymoses, mucosal hemorrhages, and congestion [52, 86]. Towards the terminal stage of infection and after the onset of hemorrhagic abnormalities,

ZEBOV replicates in endothelial cells [59]. However, while infection of endothelial cells is thought to play a role in pathogenesis, the molecular mechanisms of endothelial damage are not yet fully understood.

1.9 Long-term health outcomes in Ebola survivors

The recent ZEBOV outbreak in West Africa has resulted in an unprecedented number of survivors and highlighted the complexity of EVD sequelae in clinically recovered patients (**Figure 1.4**). A study in which clinical and laboratory records of surviving patients treated in Port Loko, Sierra Leone were assessed showed a higher incidence of arthralgia, ocular symptoms (including uveitis), and auditory problems. Moreover, a higher ZEBOV viral load at clinical presentation was associated with higher incidence of uveitis and other ocular symptoms [124]. A second study of surviving patients showed increased incidence of anorexia, arthralgia, myalgia, and chest/back pain [125] (**Figure 1.4**). These observations are similar to those reported in survivors of BEBOV infection. One retrospective study collected health status, functional limitations, demographics, blood chemistry, hematology and filovirus antibody titers from 49 survivors and 157 seronegative contacts 29 months following the 2007 Bundibugyo outbreak in Uganda. Results showed that while no differences in blood analysis were observed, survivors were at a significantly greater risk for ocular problems (retro-orbital pain and blurred vision), loss of hearing, difficulty swallowing, difficulty sleeping, arthralgia, abdominal and back pain, fatigue, impotence, severe headaches, memory problems and confusion [126].

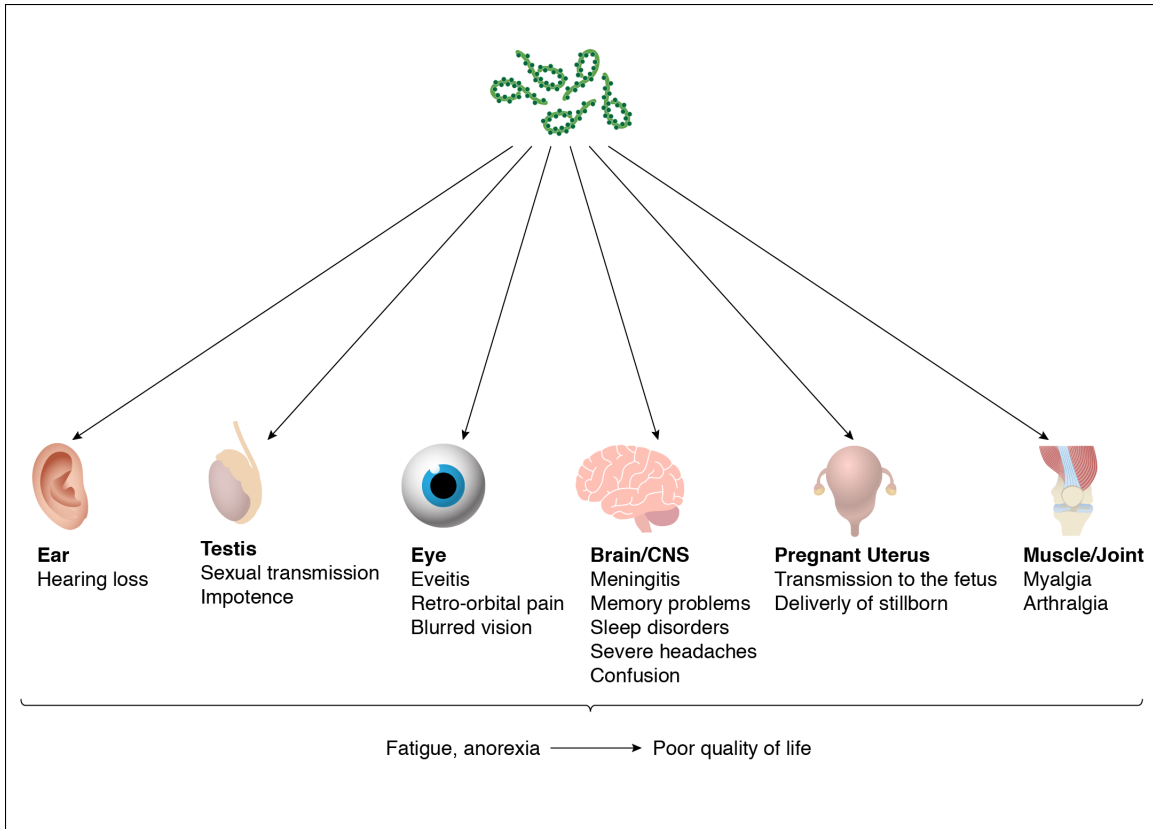


Figure 1.4. Long-term post-EBOV consequences. EBOV entry and persistence into organs that are immune privileged, including ear, testis, eye, central nervous system, pregnant uterus, and muscle tissue have been observed in clinically recovered patients, resulting in Ebola disease sequelae.

Further investigation of recovering survivors revealed that ZEBOV persists in the semen, ocular fluid, cerebrospinal fluid (CSF), placenta, and amniotic fluid. A study of 93 male survivors in Sierra Leone showed that 100% of men (n=9) who provided a semen specimen 2-3 months after the onset of EVD had positive qRT-PCR results despite absence of viremia. Of 40 samples obtained 4-6 months after onset, 26 tested positive (65%), while 11 out of 43 (26%) specimens collected at 7-9 months after onset were positive [127]. Recently, genetic sequencing of ZEBOV strain confirmed a female patient who succumbed to ZEBOV infection, acquired the virus via sexual transmission from a survivor whose semen tested positive for ZEBOV by qRT-PCR 199 days after his recovery [128]. These data suggest that infectious virus, not only viral RNA, can persist in the semen for months after viremia ceases. In one case, although tear-film specimen and peripheral blood tested negative for ZEBOV RNA by qRT-PCR, virus was detected in aqueous humor 9 weeks after cessation of viremia [129]. ZEBOV was also detected in the cerebral spinal fluid of a nurse who developed meningitis 9 months after recovery from EVD [130]. Finally, ZEBOV persisted in amniotic fluid and placenta after clearance from the blood in two pregnant women, resulting in delivery of stillborn fetuses in both cases [131].

Collectively, these observations indicate that ZEBOV can persist in organs that were traditionally considered immune privileged sites (**Figure 1.4**). The ability of immune cells to access these sites (anterior chamber of the eye, central nervous system, testes and pregnant uterus) is limited in order to reduce the risk of irreparable damage to these critical organ system [132]. The persistence of ZEBOV in these sites well after recovery raises

many questions regarding the mechanisms and the kinetics by which this virus gains access to and is able to persist in these sites.

1.10 Clinical correlates and host factors that predict disease outcome

It is currently not well understood why some patients develop fulminant EVD and succumb to infection while others survive. The recent outbreak provided an opportunity to address this critical question using large patient cohorts. One of the strongest predictors of outcome is the initial viral load at the time of admission. Patients that succumbed to disease presented on average with 2 log₁₀ higher genome equivalents (GEQ)/mL than those who survived [133]. Association between initial viral load and disease outcome was also reported by the Jui Government Hospital in Sierra Leone who showed that patients who were admitted with a viral load higher than 10⁶ copies/mL had significantly shorter survival time than patients with viral loads lower than 10⁶ copies/mL. Moreover, advanced age was significantly negatively associated with survival [110, 134]. These observations were confirmed in a second study where EVD patients under the age of 21 had a lower case fatality rate than those over the age of 45 years [135]. From a clinical perspective, AST (but not ALT) and D-Dimer levels are important prognostic factors in EVD [136].

Niemann-Pick C1 (NPC1) and heat shock 70kDA protein 5 (HSPA5) have also been identified as host factors that can modulate severity of ZEBOV infection. NPC1 is an endo/lysosomal cholesterol transporter protein that can affect endosome/lysosome fusion. Administration of U18666A, a small molecule that targets NPC1, to Vero and HAP1 cells

inhibited infection by rVSV-ZEBOV-GP (replication-competent vesicular stomatitis virus bearing Ebola virus glycoprotein). Knock out of NPC1 in HAP1 cells also had significantly lower amount of cellular infection by rVSV-ZEBOV-GP, suggesting that membrane fusion and entry mediated by ZEBOV glycoproteins requires NPC1 [44]. HSPA5 is an endoplasmic reticulum chaperone that may play an important role in the maturation of viral proteins. Administration of the HSPA5 inhibitor epigallocatechin gallate (EGCG) to HeLa cells prior to infection, results in a significant decrease in viral infection. Similarly, transfection of 293T cells with siRNA targeting HSPA5 before ZEBOV infection resulted in a significant drop in viral transcription and VP24/VP40 protein levels. Lastly, *in vivo* targeting of HSPA5 using phosphorodiamidate morpholino oligomers (PMOs) in mice (C57BL/6) before MA-ZEBOV challenge resulted in increased survival rates [137].

Liquid chromatography-linked tandem mass spectrometry of purified ZEBOV and MARV virions produced in Vero E6 cells identified 66 virion-associated host proteins; 53 of which were identified only in ZEBOV. Virion-associated host proteins were involved in cell adhesion, cytoskeleton formation, cell signaling, intracellular trafficking, membrane organization and protein folding [138]. Spurgers et al., examined the biological relevance of these host proteins by performing an siRNA library-mediated knockdown of gene expression in 293T cells followed by ZEBOV or MARV infection 24 hours later. They identified 11 genes that influence viral replication as measured by qRT-PCR [138]. Knockdown of HSPA5, RPL18, UBC, RPL3, RPL5, RPS6, DNAJB2, and Hist1H2BO reduced ZEBOV infection whereas knockdown of HSPB1, DCD and ARF1 increased

infectivity rates. In line with the proteomics data, knockdown of only HSPA5, RPL18 and UBC reduced MARV infectivity [138].

Following the SEBOV Uganda outbreak in 2000-2001, HLA-B typing was performed using leukocytes isolated from 77 patients (35 survivors and 42 fatalities) in order to determine if the major histocompatibility complex (MHC) class I genes of infected patients could influence the course of disease using predictive discriminant analysis (PDA) and epitope prediction software [139]. Alleles B*07, B*14, B*35 and B*40 were associated with patient survival. In contrast, alleles B*67, B*13, and B*42 were associated with fatal outcomes. Epitopes predicted to bind strongly to HLA B07 were identified within the L polymerase, NP, and VP35 proteins [139]. Another study evaluated the association of killer immunoglobulin-like receptors (KIR) with the outcome of human ZEBOV infection. KIRs are expressed on the surface of NK cells and bind to HLA class I alleles to either activate or inhibit NK cell function. Chi-square test and a Fisher's exact test was used to compare KIR among four populations: 1) 54 controls from rural regions of Gabon who were seronegative for ZEBOV-specific IgG; 2) 68 healthy subjects that were sero-positive for ZEBOV-specific IgG and defined as contacts; 3) 21 survivors of ZEBOV infection (outbreaks in Gabon from 1996-2001); 4) 15 fatalities of ZEBOV infection (from epidemics in Gabon from 2001-2002). Results showed that only 9.5% of survivors, compared to 35.2% of controls, had the activating KIR2DS3 gene, suggesting that the KIR2 family may be associated with ZEBOV fatal outcome. More importantly, activating

KIR2S1 and KIR2DS3 were significantly more frequent in fatalities (46.8% and 53.3%, respectively) than in survivors (4.6% and 9.5%, respectively) [140].

1.11 Vaccines against Ebola

Several vaccine platforms against ZEBOV have been developed including viral protein antigen-based vaccines (virus like particles), replication deficient vaccines (DNA vaccines and recombinant adenovirus vectors (rAd)), and replication competent recombinant viral vector based platforms (recombinant human parainfluenza virus (rHPIV3), recombinant rabies virus (RABV), recombinant cytomegalovirus (CMV), and recombinant vesicular stomatitis virus (rVSV)) [141]. Among these various vaccine strategies, two vaccine candidates have advanced the furthest in clinical trials: rAd and rVSV vectors expressing ZEBOV-GP.

Recombinant adenovirus serotype 5 expressing the ZEBOV glycoprotein gene (rAd5-EBOVGP) is a replication deficient vector. Immunization of cynomolgus macaques with a single dose of 10^{10} rAd5-EBOVGP particles resulted in the production of ZEBOV-GP specific antibodies and GP-specific CD8 T cells, and provided 100% protection against ZEBOV challenge 21 days after vaccination [142]. Passive transfer of ZEBOV specific IgG purified from nonhuman primates vaccinated with DNA and rAd5 vectors expressing ZEBOV-GP prior to ZEBOV challenge only protected 25% of naïve animals. In contrast, CD8 T cell depletion of NHPs immunized with rAd5-EBOVGP 4 days before challenge resulted in 80% mortality, suggesting a major role for CD8 T cells in mediating protection

in this vaccine platform [143]. However, a large percentage of humans have preexisting immunity against Ad5, which interferes with the efficacy of the rAd5-EBOVGP vaccine. Indeed, individuals with anti-Ad5 antibodies generated lower GP-specific humoral responses after rAd5-EBOVGP vaccination compared to Ad5 seronegative subjects [144, 145].

To address this challenge, alternate rAd based vaccine platforms were explored. Recombinant Ad26 and Ad35, which have lower seroprevalence in humans, can engender GP-specific T and B cell responses after 2 vaccinations, and provide 100% protection in nonhuman primates against ZEBOV infection [146]. Immunization of cynomolgus macaques with a single inoculation of recombinant chimpanzee adenovirus 3 (ChAd3) expressing ZEBOV-GP (rChAd3-EBOVGP) resulted in complete protection when ZEBOV challenge occurred 5 weeks after vaccination but only 50% protection when the animals were challenged 10 months after immunization [147]. The addition of a booster vaccination using recombinant modified vaccinia Ankara expressing ZEBOV-GP 8 weeks after the rChAd3-EBOVGP vaccination resulted in complete protection at 10 months [147]. In September 2014, two Phase I clinical trials conducted by the National Institute of Allergy and Infectious Diseases (NIAID) and Wellcome Trust evaluated the ChAd3-EBOVGP safety and immunogenicity in 80 participants in a dose-escalation design. Reactivity and immunogenicity to rChAd3 was dose dependent [148], but antibody and T cell responses were lower compared to those associated with protection in macaques [149]. This vaccine platform, now has entered a Phase II/III trial sponsored by the NIAID called

Partnership for Research on Ebola Vaccines in Liberia (PREVAIL) that will enroll 27,000 healthy adults. Currently, Phase II studies demonstrated this vaccine is safe and well tolerated in 500 participants, producing sustained immune responses up to one year post vaccination [150].

Replicating vaccine platforms have several advantages over non-replicating ones including longer durability, but they also have several challenges such as risk of reversion to wild type and potential adverse events in patients with deficient or compromised immunity. VSV is a member of the Rhabdoviridae family with a nonsegmented, negative-stranded RNA genome. A single vaccination with only 10^7 PFU rVSV-ZEBOV for nonhuman primates and 2 PFU for mice provides complete protection against ZEBOV challenge 28 days later [151, 152]. A single dose of rVSV-ZEBOV confers complete protection against ZEBOV infection for up to 6 months in macaques and 18 months in mice and guinea pigs [153, 154]. Moreover, this vaccine platform confers complete protection in macaques against MARV challenge as late as 14 months after vaccination, further demonstrating the durability of this vaccine platform against filoviruses [155]. In contrast to rAd based vaccines, antibody responses are the main mode of protection conferred by rVSV-ZEBOV [156]. In a nonhuman primate study in which groups of cynomolgus macaques were either depleted of CD4 or CD8 T cells during vaccination or depleted of CD4 T cells during challenge, only the animals depleted of CD4 T cells during vaccination, and which lacked GP-specific antibodies, succumbed to ZEBOV challenge 28 days after immunization [156].

Because rVSV-ZEBOV is a live-attenuated virus, several studies have investigated its safety. No adverse events have been observed in over 80 nonhuman primates immunized with rVSV-MARV or rVSV-ZEBOV [151, 157]. Moreover, no evidence of disease was observed in immunocompromised animal models (NOD-SCID mice and simian human immunodeficiency infected (SHIV) rhesus macaques), further confirming the safety of this vaccine [152, 157]. Vaccination of cynomolgus macaques with a mixture containing rVSV-MARV, rVSV-ZEBOV, and rVSV-SEBOV resulted in protection following infection with MARV, ZEBOV, SEBOV and CIEBOV, indicating that a multivalent rVSV vaccine is efficacious [158]. Finally, rVSV-ZEBOV is effective post-exposure and confers 50% and 100% protection in rhesus macaques given rVSV-ZEBOV or rVSV-SEBOV, respectively, when administered 20-30 minutes after challenge [159, 160]. More recently, complete and partial protection was achieved when cynomolgus macaques were immunized with rVSV-ZEBOV 7 and 3 days before challenge with the 2014 variant Makona, respectively. Because these animals lacked detectable ZEBOV-GP specific antibodies at the time of challenge, these data suggest that early innate immune responses to this vaccine can provide rapid protection [161].

Multiple Phase I clinical trials across Europe and Africa evaluated the safety and immunogenicity of this vaccine platform. Data from these studies show this vaccine to be safe and immunogenic [162, 163]. More importantly, results from a cluster-randomized ring Phase III trial, in which 7,651 people were vaccinated with 2×10^7 PFU of rVSV-

ZEBOV, show this vaccine to be 100% efficacious [164]. Furthermore, ZEBOV-GP specific antibodies were demonstrated to be sustained up to 2 years following vaccination with $1-5 \times 10^6$ PFU of rVSV-ZEBOV [165]. Importantly, as described for macaques, this vaccine has the potential to be a successful post exposure treatment option in humans. In March 2009, a single dose of rVSV-ZEBOV was administered to a virologist 48 hours after a ZEBOV needle stick injury. The subject developed acute fever and rVSV viremia, but did not develop EVD [166]. Similarly, during the 2014 outbreak, a physician who sustained a needle-stick injury while working in an Ebola treatment unit in Sierra Leone was given rVSV-ZEBOV as an emergency post-exposure vaccination 43 hours later. The patient developed a self-limited febrile syndrome in addition to ZEBOV-GP specific adaptive immune responses following vaccination and recovered [167]. Although these two promising vaccine candidates have been accelerated for clinical trials, correlates and durability of protection in humans remain to be determined.

1.12 Therapeutics against Ebola

Strategies for developing experimental postexposure treatments against ZEBOV focus on: 1) preventing the development of filovirus-associated coagulopathies (recombinant nematode anticoagulant protein (rNAPc2) and recombinant human activated protein C (rhAPC)); 2) inhibiting viral replication or translation such as nucleotide analogs (Favipiravir, BCX4430, Brincidofovir) and antisense therapeutics (PMOs and siRNA); or 3) limiting viremia and virus spread (monoclonal antibody cocktails). Several of these post-exposure therapeutic candidates are currently in clinical trials.

Favipiravir (T-705), developed by Toyoma Chemical, Japan, is an oral nucleotide analog that has been licensed for the treatment of influenza. It inhibits viral RNA-dependent RNA polymerase by directly competing with GTP after it is converted to its active metabolite form (ribofuranosyl triphosphate). Favipiravir has been shown to suppress ZEBOV replication in Vero E6 cells when added 1 hour after infection [168]. Favipiravir is also effective when given 1 hour following ZEBOV aerosol challenge in immunodeficient IFN α/β receptor knockout (IFNAR $^{-/-}$) mice for 14 days [169]. To date, Favipiravir has been used to treat 1 French nurse infected with Ebola in the 2014-2015 outbreak who recovered [170]. A non-randomized Phase II clinical trial tested the efficacy of Favipiravir in 126 patients with EVD in Guinea. Of these 126, 111 were analyzed and divided into 3 groups: 1) 55 who had a baseline Ct ≥ 20 (5×10^7 genome copies/mL); 2) 44 with Ct < 20 ; and 3) 12 young children between 1-6 years of age (median Ct value of 19.9). All groups received favipiravir within a median of 4 days from the first symptoms. Sixty participants died with 20% mortality in the group with Ct ≥ 20 , 90% mortality in the group with Ct < 20 , and 75% mortality in the group of young children. This data shows that initial viral load and age are predictors of EVD outcome. The 51 surviving patients had a mean initial viral load of 6.65 log₁₀ copies/mL with a mean decrease of 0.33 log₁₀ copies/mL each day after favipiravir initiation. Moreover, the trial showed the antiviral was well tolerated and of the 99 adults and adolescents, viral loads and mortality were not significantly different in patients who received Favipiravir less than 72 hours from symptom onset than patients who received treatment more than 3 days from symptom onset [171].

BCX4430 is an adenosine analog that is incorporated into the nascent viral RNA chain and terminates transcription. Similar to Favipiravir, it is not incorporated into mammalian RNA or DNA. Treatment of cynomolgus macaques with BCX4430 as late as 48 hours after MARV challenge confers 100% protection [172]. BioCryst Pharmaceuticals and NIAID have initiated a Phase I clinical trial of BCX4430 in the UK. Brincidofovir (CMX001), developed by Chimerix, is a lipid conjugate of cidofovir (known to inhibit replication of DNA viruses including cytomegalovirus and adenovirus) that inhibits ZEBOV replication *in vitro* although the mechanism is unknown [173]. Due to the small number of new EVD cases, a clinical trial study of Brincidofovir has been terminated [174]. Warren et al. has reported a novel nucleoside triphosphate, GS-5734, which exhibits antiviral activity against ZEBOV and provided 100% protection in 12 infected rhesus macaques when administered a daily 10mg/kg starting 2 or 3 days post-exposure for 12 days. Importantly, when administered intravenously GS-5734 is able to reach immune privileged sites including testes, eyes, and brain [175].

Phosphorodiamidate morpholino oligomers (PMO) are synthetic antisense molecules that target mRNA in a sequence-specific manner and suppress translation through steric hindrance rather than targeting mRNA for degradation. AVI-6002 consists of PMO AVI-7537 and AVI-7539, which target VP24 and VP35, respectively. AVI-6002 protects 62.5% of rhesus macaques when given 30-60 minutes following ZEBOV infection and daily for 14 days [176]. Interestingly, treatment with AVI-7537 alone protected 6/8 cynomolgus

macaques when administered 1.5 hours after ZEBOV challenge and daily for 14 days, while treatment with AVI-7539 alone did not [172, 177]. Data from Phase I clinical trial revealed that AVI-6002 is safe with doses ranging from 0.05 to 4.5mg/kg [177].

Stable nucleic acid-lipid particles (SNALP) were developed to deliver siRNAs *in vivo* and this combination has been shown to efficiently target the ZEBOV polymerase L gene resulting in complete protection of guinea pigs when given daily starting 1 hour after challenge [178]. TKM-Ebola, developed by Tekmira Pharmaceuticals, which consists of SNALP carrying siRNAs that target ZEBOV L polymerase, VP24 and VP35 protected 2/3 macaques when given 30 minutes after challenge and daily thereafter [179]. Although TKM-Ebola entered Phase I trials early in 2014, studies were halted when elevated cytokine levels were observed in healthy participants. The FDA however, has extended access to TKM-Ebola in a state of emergency [180].

Based on experimental and clinical data supporting the importance of antibody-mediated protection against ZEBOV infections, monoclonal treatment strategies were developed. Initial studies that used monoclonal antibodies (mAb) showed very limited success if any. The human monoclonal antibody, KZ52, which targets an epitope in ZEBOV-GP failed to protect rhesus macaques against ZEBOV challenge when administered 1 day before and 4 days after challenge [181]. However, when a combination of two human-mouse chimeric neutralizing mAbs were given to 3 nonhuman primates 1 day before and 1 and 3 days after ZEBOV challenge, 1/3 was protected and another animal had delayed time-to-death [182].

Furthermore, passive transfer of polyclonal IgG isolated from vaccinated nonhuman primates that survived ZEBOV or MARV challenge as late as 48h after infection protected naïve macaques against both MARV and ZEBOV challenge [183]. These studies strongly indicate that protection against ZEBOV requires targeting of multiple epitopes on GP and that neutralization potential may not be a good predictor of protection.

To test this hypothesis, several ZEBOV-GP specific mAbs produced following rVSV-ZEBOV-GP vaccination were evaluated in immunocompetent mice and guinea pigs individually or as pools. As previously described, individually administered mAbs were ineffective whereas pools of 3 mAbs provided complete protection when administered as late as 2 days post infection [184]. These studies eventually led to the development of two cocktails of mAbs termed MB-003 (clones c13C6, h13F6 and c6D8) and ZMab (clones m1H3, m2G4 and m4G7). These cocktails conferred protection to NHPs when given as late as 3 days post ZEBOV challenge [185]. ZMapp™, developed jointly by the Public Health Agency of Canada and Mappbio Pharmaceuticals (USA) contains the monoclonal antibodies from MB-003 and ZMab with the highest efficacy (c13C6, c2G4 and c4G7). Three doses of ZMapp™ spread evenly over 9 days, protected NHPs even when administered 5 days post-exposure and after the appearance of clinical symptoms [186]. During the 2014-2015 outbreak, ZMapp™ was used to treat 7 ZEBOV patients, 5 of whom survived [187]. In February 2015, NIAID initiated Phase I clinical trials of ZMapp™ in which patients positive for ZEBOV RNA will be randomly assigned to a control group who will receive the current standard of care, and a second group who will receive

ZMapp™. A total of 72 patients were enrolled and evaluated; death occurred in 13/35 patients who received the current standard of care and in 8/36 patients who received ZMapp [188]. With no current cases, a complete evaluation of the efficacy of this treatment has yet to be completed. The slow production of antibodies in tobacco plants has delayed the clinical evaluation of this treatment. New methods to increase yields of the monoclonal antibody cocktail are being developed. MIL-77 (developed by mabworks, China) is a cocktail of the same antibodies used for ZMapp generated in Chinese hamster ovary (CHO) cells. Although currently there are no efficacy data in monkeys, the WHO reports MIL-77 is comparable to ZMapp™ in conferring protection in NHPs following ZEBOV infection [189, 190]. To date, only one monoclonal antibody, mAb114, has been shown to fully protect 3 rhesus macaques when given as late as 5 days after ZEBOV challenge [191]. Structural studies show that mAb114 interacts with the glycan cap of GP, inhibiting the binding of the cleaved GP to its receptor [192].

1.13 Thesis overview and aims

Most studies investigating the mechanisms of innate immune evasion by filoviruses have been carried out through *in vitro* studies which are limited by the use of immortalized cell lines and high multiplicity of infection (MOI), which may not accurately recapitulate natural pathogenesis. Additionally, a majority of human biological samples are collected from patients after the onset of symptoms, resulting in a paucity of data on initial host immune responses. Consequently, there remains a critical gap in knowledge in understanding how ZEBOV subverts host innate immunity *in vivo*. In this dissertation, I address this knowledge gap by investigating longitudinal host responses in peripheral

blood collected from cynomolgus macaques infected with ZEBOV using both immunological assays and transcriptomic analysis. I first use this model to characterize the host response to the most recently identified ZEBOV variant, Makona. In the second aim of my dissertation, I elucidate the role of individual immune cell subsets in mediating ZEBOV pathogenesis. Since ZEBOV VP35 has been shown to inhibit type I IFN production *in vitro*, I determined the importance of VP35 as a key virulence factor *in vivo*. Finally, the rVSV-ZEBOV vaccine has been shown to provide protection in cynomolgus macaques as late as 3 days before challenge. However, the mechanisms underlying rapid protection conferred by this vaccine are not fully understood. Therefore, in my last aim, I investigate the innate immune signatures engendered by rVSV-ZEBOV vaccination important in protecting against ZEBOV infection. Data from these studies provide novel insight into ZEBOV pathogenesis and indicate that virus interaction with the innate immune system early in the course of infection plays a key role in determining disease outcome.

CHAPTER 2: Infection with the Makona variant results in a delayed and distinct host immune response compared to previous Ebola virus variants

Krista Versteeg^{1,2#}, Andrea R. Menicucci^{3#}, Courtney Woolsey^{1,2}, Chad E. Mire^{1,2}, Joan B. Geisbert^{1,2}, Robert W. Cross^{1,2}, Krystle N. Agans^{1,2}, Daniel Jeske³, Ilhem Messaoudi^{4*} and Thomas W. Geisbert^{1,2*}

¹**Galveston National Laboratory, Galveston, TX, USA.**

²**Department of Microbiology and Immunology, University of Texas Medical Branch, Galveston, TX, USA.**

³**Division of Biomedical Sciences, University of California-Riverside, Riverside, CA, USA.**

⁴**Department of Molecular Biology and Biochemistry, University of California-Irvine, Irvine, CA, USA**

***To whom Correspondence should be addressed**

#These authors contributed equally to this work.

A version of this chapter is published in Nature Scientific Reports [193]

Abstract

Zaire Ebolavirus (ZEBOV) continues to pose a significant threat to human health as highlighted by the recent epidemic that originated in West Africa and the ongoing outbreak in the Democratic Republic of the Congo. Although the ZEBOV variant responsible for this epidemic (Makona) shares significant genetic similarity with previously identified variants (Kikwit and Mayinga), recent reports suggest slower disease progression in nonhuman primates. However, the pathogenesis caused by the new variant is not fully understood. We present the first comprehensive approach in understanding ZEBOV-Makona pathogenesis in cynomolgus macaques by measuring changes in immune cell frequencies, plasma levels of immune mediators, and differentially expressed genes (DEGs) within whole blood (WB) and peripheral blood mononuclear cells (PBMC). Our combined approach revealed a link between: 1) increased interferon-stimulated gene expression, IFN α levels, and activated plasmacytoid dendritic cells; 2) higher pro-inflammatory gene expression, cytokine and chemokine levels, and non-classical monocytes; 3) gene signature of leukocyte activation and increased granulocytes; and 4) decreased expression of lymphocyte related genes and lymphopenia. In addition, our data strongly indicate delayed disease progression as well as limited overlap (~30%) in host transcriptome changes following ZEBOV-Makona infection compared to ZEBOV-Kikwit. These observations provide novel insight into the molecular mechanisms of ZEBOV-Makona pathogenesis.

Introduction

Zaire Ebolavirus (ZEBOV) is a member of the *Filovirus* family with a single strand, negative sense RNA genome encoding 9 viral proteins [26]. ZEBOV infection in humans is characterized by hemorrhage, lymphopenia, high levels of circulating pro-inflammatory mediators, liver failure, and disseminated intravascular coagulation, which culminate in death due to hypovolemic shock and multi-organ failure [84, 194-196]. The traditionally remote locations and small magnitudes of ZEBOV outbreaks have precluded in-depth studies of ZEBOV pathogenesis in humans. Therefore, different animal models have been used to elucidate disease progression and host responses to ZEBOV. Despite the experimental advantages that rodents offer, the need for adapted ZEBOV strains is a major limitation. Recently, a ferret model for ZEBOV infection has been described in which wild-type virus induces uniform lethality featuring many hallmark features of ZEBOV pathogenesis [197]; however, the current dearth of reagents available to study immune parameters limits the utility of this model to study immune responses. In contrast, infection of nonhuman primates (NHP, rhesus and cynomolgus macaques) with wild-type ZEBOV variants results in lethal disease [58, 198] with a similar presentation as humans [18]. Studies in NHP have demonstrated that ZEBOV initially infects monocytes and dendritic cells in draining lymph nodes before disseminating to the liver, adrenal gland, kidney, and lymphoid tissue [59]. In addition, consumption of clotting factors and high levels of fibrin degradation products contribute to the development of the characteristic petechial rash and hemorrhage from mucosal membranes. End-stage disease in macaques is typified by liver necrosis, loss of splenic structure, and lymphopenia [101, 199].

In December of 2013, a ZEBOV outbreak was reported in Guinea that quickly spread to Sierra Leone and Liberia resulting in the first and largest ZEBOV epidemic. Ultimately, 10 countries were affected with over 28,600 cases and 11,300 fatalities [200]. The ZEBOV variant responsible for the West Africa epidemic was named Makona, after the river that borders Guinea, Liberia and Sierra Leone. Although the end of the epidemic was declared in January 2016, sporadic cases continued to occur in Guinea and Sierra Leone, possibly due to the persistence of the virus in immune privileged sites, such as the testes, eyes, and central nervous system.

Sequence analysis indicates that ZEBOV-Makona has a 97% nucleotide identity to Mayinga and Kikwit ZEBOV variants [201]. In addition to the symptoms characteristic of Ebola hemorrhagic fever (EHF), ZEBOV-Makona infection has been associated with more pronounced gastrointestinal symptoms (severe vomiting and diarrhea). Moreover, recent NHP studies show a delay in disease progression after infection with ZEBOV-Makona compared to ZEBOV-Mayinga [14]. However, little is known about the progression of disease caused by this newly identified variant. To address this gap in knowledge, we conducted a longitudinal study to characterize the host immune response to ZEBOV-Makona infection in NHP using a multipronged approach that combined immunological assays and next generation sequencing in both whole blood (WB) and peripheral blood mononuclear cells (PBMC). Our data show delayed appearance of clinical symptoms as well as overlapping but distinct host transcriptome changes during ZEBOV-Makona

infection compared to ZEBOV-Kikwit in ZEBOV-Makona-infected animals thereby providing novel insight into ZEBOV-Makona pathogenesis.

Materials and Methods

Virus and Challenge

A laboratory seed stock of the Makona variant was grown from the serum of a 2014 fatal human case in Guékédou, Guinea and passaged twice in authenticated Vero E6 cells (ATCC, CRL-1586) to produce ZEBOV isolate H.sapiens-tc/GIN/2014/ Makona-Gueckedou-C07, accession number KJ660347.2. This clone is one of the earliest isolates from the recent ZEBOV epidemic and was used in recent nonhuman primate studies[14]. The University of Texas Medical Branch at Galveston Institutional Animal Care and Use Committee (IACUC) and the Institutional Biosafety Committee approved this study and all protocols are in accordance with state and federal statutes and regulations relating to experiments involving animals. Ten healthy, filovirus-negative male cynomolgus macaques 3-5 years of age and between 4-8 kg were challenged with 1000 PFU of ZEBOV-Makona intramuscularly with the dose divided equally into the left and right quadriceps. Animals were housed in the Biosafety Level 4 (BSL-4) laboratory in the Galveston National Laboratory (GNL) and monitored post challenge for clinical signs of disease.

Sample Collection and PBMC isolation

Blood was collected by venipuncture into EDTA and serum tubes according to the study design. WB was added to AVL buffer (Qiagen, Valencia, CA) to isolate RNA. To separate plasma and serum, tubes were spun at 2500 rpm for 10 minutes at 4°C. EDTA plasma and serum were stored at -80°C for future analysis and virus quantification. To isolate PBMC, WB was centrifuged over Histopaque (Sigma-Aldrich, St. Louis, MO) using AccuSpin

Tubes (Sigma-Aldrich, St. Louis, MO) at 1400 rpm for 45 minutes, room temperature with no brake. The PBMC buffy coat was extracted and washed in RPMI media. Isolated cells were counted on a TC20 Automated Cell Counter (Bio-Rad, Hercules, CA). 1.0×10^6 PBMC were put into Trizol (Invivogen) buffer for RNA isolation. An additional 5.0×10^6 PBMC were used for flow cytometry analysis.

Remaining PBMC cells were frozen and stored at -80°C (stable for 6 months) for future analysis.

Hematology and Clinical Chemistry

WB collected in EDTA was analyzed by a hematological analyzer (Beckman Coulter, Brea, CA) that measures: white blood cell and differentials, red blood cells, platelets, hematocrit values, hemoglobin, mean cell volumes, mean corpuscular volumes, and mean corpuscular hemoglobin concentrations. Serum was collected for clinical chemistry analysis using a Piccolo point-of-care analyzer and Biochemistry Panel Plus analyzer discs (Abaxis, Sunnyvale, CA) to measure concentrations of albumin, amylase, ALT, AST, ALP, GGT, glucose, cholesterol, total protein, total bilirubin (TBIL), blood urea nitrogen (BUN), CRE, and CRP.

Virus detection and quantification

Virus titer was measured by plaque assay on Vero E6 cells. Cells were plated in 6-well plates and grown to confluency. Virus was titrated from 10^{-1} to 10^{-6} in duplicate. Plaques were counted using neutral red stain; limit of detection was 25 PFU/ml. RNA was isolated from WB using AVL Buffer and Viral RNA mini-kit (Qiagen, Valencia, CA). As previously described, primers/probe targeting the VP30 gene of ZEBOV-Makona were used for RT-qPCR [202]. ZEBOV RNA was detected using the CFX96 detection system (BioRad Laboratories) using One-Step Probe qRT-PCR Kits (Qiagen) with the following cycle conditions: 50°C for 10 minutes, 95°C for 10 seconds, and 40 cycles of 95°C for 10 seconds followed by 59°C for 30 seconds. Threshold cycle values representing ZEBOV genome equivalents (GEq) were analyzed with CFX Manager Software, and data are shown as means \pm SD of technical replicates. To create the GEq standard, RNA from ZEBOV stocks was extracted and the number of ZEBOV genomes calculated using Avogadro's number and the molecular weight of the ZEBOV genome.

Cytokine, Chemokine and Growth Factor Analysis

Circulating cytokines were measured in the plasma using NHP Cytokine/Chemokine/Growth factor (eBioscience, San Diego CA) 37-plex panel that measures IFN γ , IFN α , TNF α , IL1RA, IL1b, IL2, IL4, IL5, IL6, IL7, IL8, IL10, IL12p70, IL13, IL15, IL17A, IL18, IP10, IL23, sCD40L, SCF, MCP1, MIP1 α , MIP1 β , MIG, Eotaxin, ITAC, BLC, SDF1 α , VEGFA, VEGFD, GCSF, GMCSF, BDNF, FGF2, NGF β , and PDGFBB.

Flow Cytometry Analysis

PBMC were stained in round bottom 96-well plates using 5 different panels to measure frequency and characterize phenotype of monocytes and dendritic cells (CD3, CD20, CD14, HLA-DR, CD16, CD11c, CD123), T-cells (CD4, CD8b, CD28, CD95, CCR7, Ki67), B-cells (CD20, IgD, CD27, Ki67), dendritic cell activation (CD3, CD20, CD14, HLA-DR, CD16, CD11c, CD123, CD80), and natural killer cells (CD3, CD20, CD8a, CD159a, Granzyme B, and CD16) [203]. Antibodies used are detailed in **Table 2.1**. For all panels, cells were stained and fixed according to manufacturer recommendations (Tonbo Biosciences, San Diego, CA). For panels requiring intracellular stains, cells were stained, fixed and permeabilized using CytoFix/CytoPerm (BD Biosciences, San Jose, CA), according to manufacturer recommendations. All samples were acquired using BD FACS Diva software on a BD FACS Canto-II Flow Cytometer (Becton Dickinson Biosciences, San Jose, CA). Live cells were identified by FSC and SSC and a minimum of 50,000 events were collected for each sample. Data were analyzed using FlowJo Analysis Software (FlowJo LLC, Ashland, OR) and Prism Software (Irvine, CA). Gating strategy is shown in **Figure 2.1**.

Antibody	Clone	Source
CCR7	G043H7	BioLegend, San Diego, CA
CD3	SP34-2	BD Biosciences, San Jose, CA
CD11c	3.9	BioLegend, San Diego, CA
CD123	6H6	BioLegend, San Diego, CA
CD14	M5E2	BioLegend, San Diego, CA
CD159a	Z199	Beckman Coulter, Brea, CA
CD16	3G8	BioLegend, San Diego, CA
CD20	2H7	BD Biosciences, San Jose, CA
CD27	O323	Tonbo Biosciences, San Diego, CA
CD28	CD28.2	Tonbo Biosciences, San Diego, CA
CD4	OKT4	Tonbo Biosciences, San Diego, CA
CD80	2D10	BioLegend, San Diego, CA
CD8a	RPA-T8	BioLegend, San Diego, CA
CD8b	2ST8.5H7	BD Biosciences, San Jose, CA
CD95	DX2	BD Biosciences, San Jose, CA
Granzyme B	GB11	BioLegend, San Diego, CA
HLA-DR	L243	BioLegend, San Diego, CA
IgG	HP6017	BioLegend, San Diego, CA
Ki67	B56	BD Biosciences, San Jose, CA

Table 2.1 Antibodies used for flow cytometric analysis of immune cell subsets

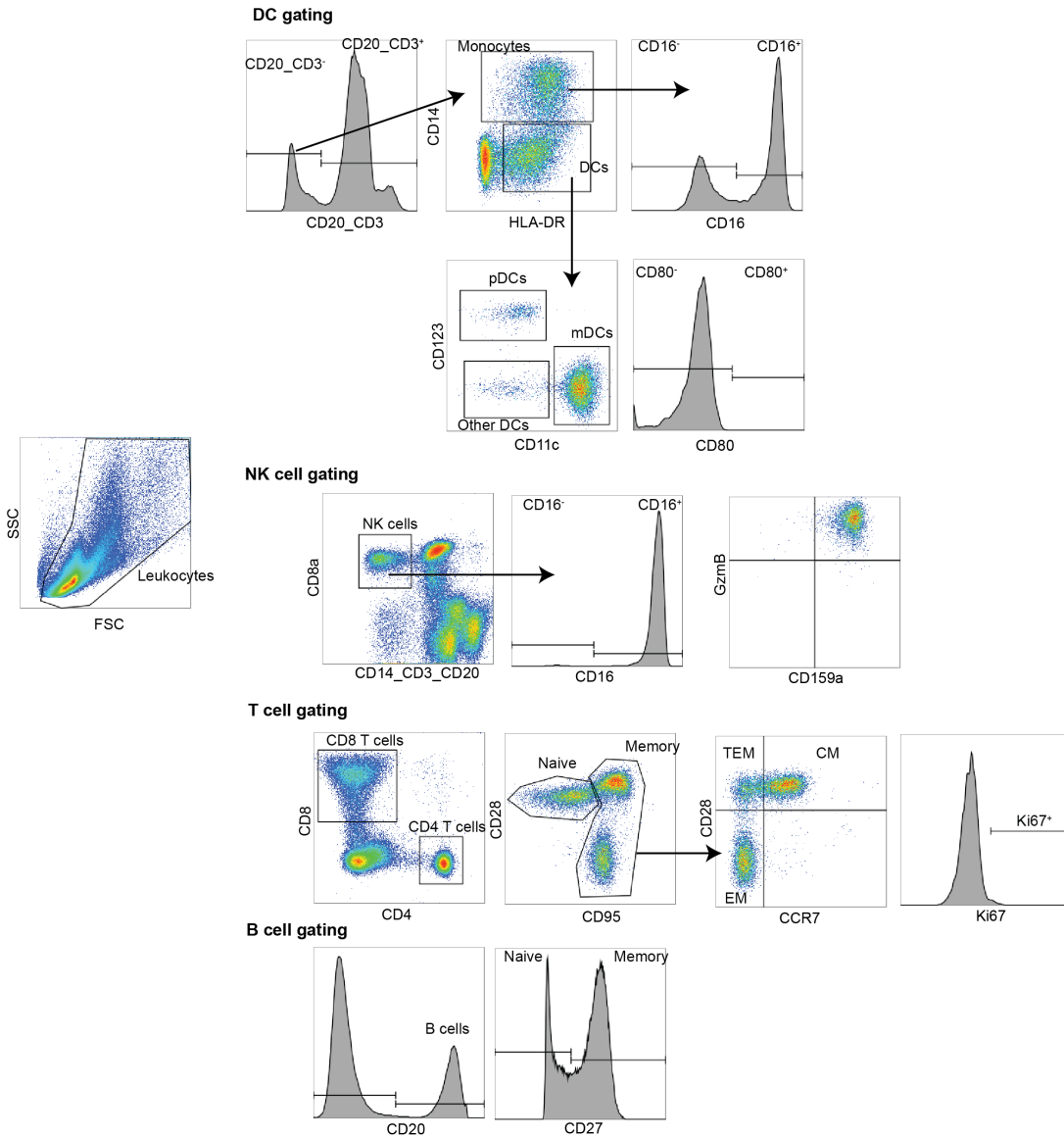


Figure 2.1. Flow cytometry gating strategy. First, lymphocytes expressing CD3 and CD20 were gated out. DC and monocytes were identified based on CD14 and HLA-DR expression. Monocytes were further subdivided based on CD16 expression. DCs were further subdivided into myeloid and plasmacytoid DC based on CD11c and CD123 expression. Activation of DCs was assessed based on CD80 expression levels. NK cells were identified based on absence of CD14, CD3 and CD20 and expression of CD8 α . NK cells were further subdivided based on CD16 expression. Activation and effector function of NK cells were monitored by expression of Granzyme B and CD159a. Memory T cells were first identified based on the expression of CD95, and then further subdivided into central (CM), transitional effector (TEM), and effector (EM) memory subsets based on the expression of CD28 and CCR7. T cell proliferation is assessed based on changes in Ki67 expression. Memory B cells were identified based on expression of CD27.

Library preparation for RNA-Seq

RNA from WB and PBMC was isolated using Zymo Research Direct-zol RNA mini-prep (Zymo Research) per manufacturer's instructions. Concentration and integrity of RNA was determined using an Agilent 2100 Bioanalyzer. Ribosomal RNA (rRNA) was depleted using the ClontechRibo-Gone rRNA Removal kit. Libraries were constructed using the Clontech SMARTer Stranded RNA-Seq kit. First, rRNA-depleted RNA was fragmented and converted cDNA. Adapters were ligated and the ~300 base pair (bp) fragments were then amplified by PCR and selected by size exclusion. Each library was prepared with a unique indexed primer for multiplexing. Quantitation and quality of libraries were confirmed on the Agilent 2100 Bioanalyzer. Multiplexed libraries were subjected to single-end 100 bp sequencing using the Illumina HiSeq2500 platform. RNA-sequencing data presented in this article were submitted to the National Center for Biotechnology Information Sequence Read Archive (Accession number PRJNA398558).

Bioinformatic analysis

Data analysis was performed with the RNA-Seq workflow module of the systemPipeR package available on Bioconductor [204] as previously described [205]. RNA-Seq reads were trimmed using Trim Galore with an average phred score cutoff of 30 and minimum length of 75 bp; 3 bp from the 5' end were trimmed as per Clontech's instruction. The *Macaca mulatta* genome sequence (Macaca_mulatta.MMUL_1.dna.toplevel.fa) and annotation file from Ensembl (Macaca_mulatta.MMUL_1.78.gtf) was used for alignment. In order to determine the kinetics of viral transcription, the ZEBOV-Makona genome

(H.sapiens-wt/GIN/2014/Makona- Gueckedou-C07) from Virus Pathogen Resource was adjoined to the *Macaca mulatta* reference. ZEBOV open reading frames (ORFs), intergenic regions (IGRs) and leader and trailing sequences were defined based on the ZEBOV-Makona genome annotation GTF file: NP (470-2689), VP35 (3129-4151), VP40 (4479-5459), GP (6039-8068), VP30 (8509-9375), VP24(10345-11100), L (11581-18219), Leader (1-469), IGR_NP_VP35 (2690-3128), IGR_VP35_VP40 (4152-4478), IGR_VP40_GP (5460-6038), IGR_GP_VP30 (8069-8508), IGR_VP30_VP24 (9376-10344), IGR_VP24_L (11101-11580), Trailing (18220-18959). RNA-Seq reads were aligned to a reference genome containing *Macaca mulatta* and ZEBOV-Makona genome sequences using Bowtie2/Tophat2. Statistical analysis of differentially expressed genes (DEGs) was performed using the *edgeR* package, which normalizes reads by the trimmed mean of M values (TMM) method. DEGs were defined as those with a fold change ≥ 2 compared to 0 DPI and a false discovery rate (FDR) corrected p-value ≤ 0.05 . Only protein coding genes with human homologs and an average of 5 reads per kilobase of transcript per million mapped reads (RPKM) were included for further analysis. Reads mapping to the ZEBOV-Makona genome were also normalized as RPKM. Statistical analysis of changes in normalized reads mapping to ZEBOV-Makona ORF, IGR, leader, trailing sequences, and entire genome was performed using *edgeR*. Heatmaps and venn diagrams were generated using R packages *gplot* and *VennDiagram*.

Functional enrichment

Functional enrichment of DEGs was done to identify clusters of genes mapping to specific biological pathways including Gene Ontology (GO) processes, Disease terms and Process networks using MetaCore™ (Thomson Reuters, New York, NY). Since this software requires human gene identifiers for analysis, rhesus DEGs were mapped to human homologs using BioMart.

Statistical analysis

Statistical analysis of viral genome copy number; hematology and clinical chemistry data; cytokine, chemokine, and growth factor data; and flow cytometry data was carried out using the SAS software, PROC MIXED. A repeated measures analysis was used to model each of the dependent variables. Intra-animal correlation was modeled using a compound symmetric variance-covariance structure. In some cases, a linear trend was used for the mean. In other cases, in which a linear trend was not a good fit, a nonparametric trend was used where each time point was modeled by its own mean. Missing data was handled by using maximum likelihood algorithms to fit the model. When a linear model was an adequate trend, the p-value for the estimated slope was reported. When each time point was modeled by its own mean, the mean response at each non-zero time point was contrasted with the mean response at the zero time point. Holm's multiple comparison method was used to adjust the p-values for each contrast [206].

Results

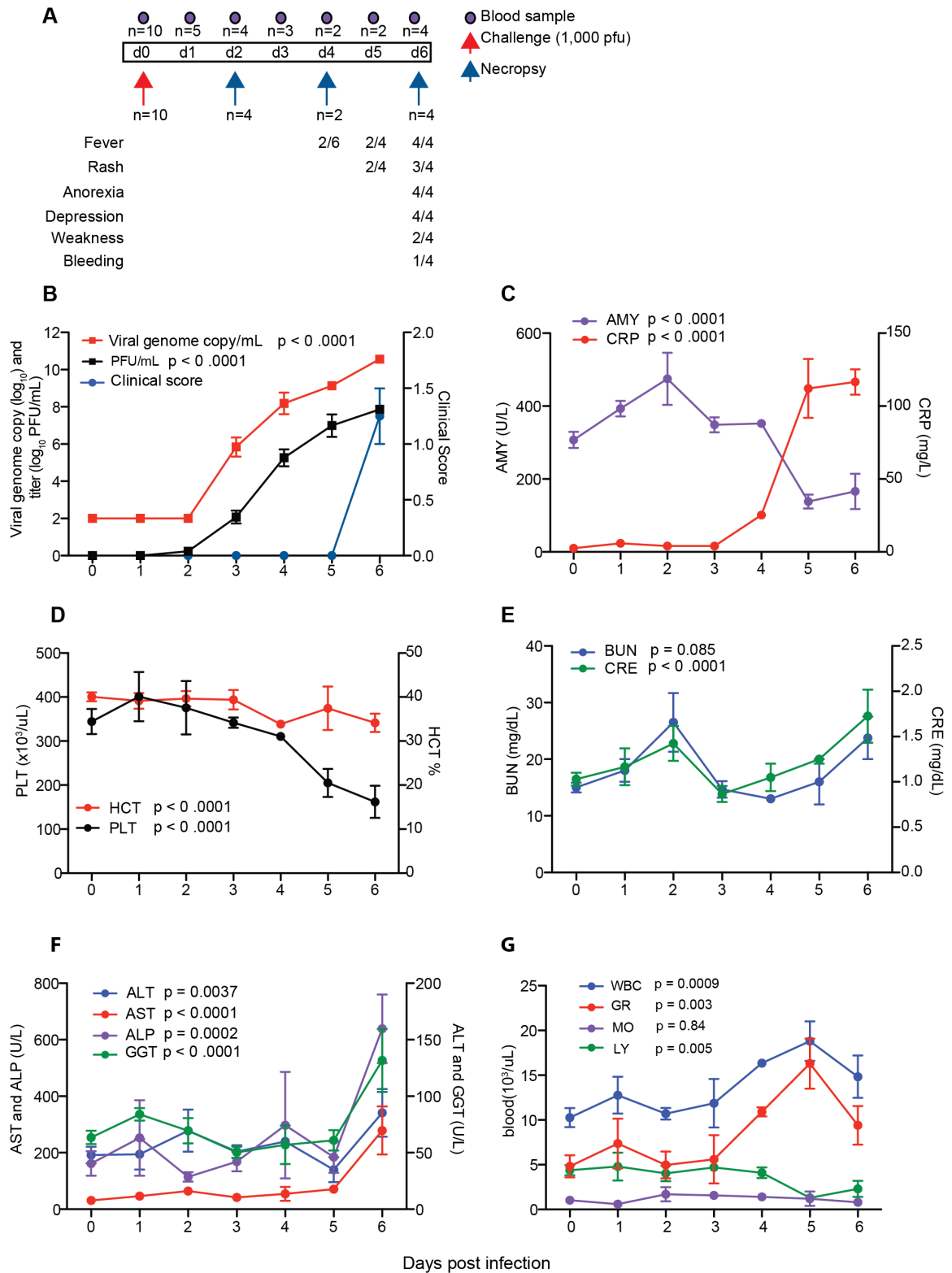
Disease signs correlate with viral replication

Ten male cynomolgus macaques were challenged with 1000 PFU of ZEBOV-Makona strain C07. We selected this isolate since it is one of the earliest and better characterized isolates from Guinea that was also used in a recent NHP study [14]. Fever (temperatures 2°F higher than baseline) was evident on or after 4 days post infection (DPI). Anorexia and mild to moderate depression were noted 6 DPI in 4/4 animals, whereas mild petechial rashes on arms, chest, and groin regions was evident in 3/4 animals. Two animals on day 6 exhibited a hunched posture and general weakness and one monkey had rectal bleeding (**Figure 2.2A**). However, these clinical signs became scorable only 6 DPI (**Table 2.2, Figure 2.2B**). Viral titers were measured in plasma by plaque assay and viral RNA was measured in whole blood using one-step RT-qPCR. Viremia was detected 4 DPI and significantly increased as infection progressed (**Figure 2.2B**).

Levels of circulating C-reactive protein (CRP), indicative of inflammation, correlated with viremia, and were increased slightly 4 DPI, followed by a large increase at 5 and 6 DPI (**Figure 2.2C**). Similarly, changes in blood amylase levels, characteristic of pancreatic injury, weren't detected until 5-6 DPI, when they significantly decreased (**Figure 2.2C**). Hematocrit and platelet numbers also decreased 5-6 DPI, which may be associated with coagulopathy and detrimental changes in microcirculation (**Figure 2.2D**). Levels of blood creatinine (CRE), indicative of kidney function, as well as liver enzymes (alanine transaminase (ALT), aspartate transaminase (AST), alkaline phosphatase (ALP), and

gamma-glutamyl transpeptidase (GGT)) significantly increased only 6 DPI when disease signs were more evident (**Figure 2.2E-F**). Total white blood cell numbers (WBC) increased 4-5 DPI driven by a significant increase in granulocytes (neutrophils) before declining 6 DPI due to loss of both granulocytes and lymphocytes, while monocyte numbers remained relatively consistent throughout the study (**Figure 2.2G**).

Changes in circulating immune mediators correlated with disease progression. In plasma, we detected significantly increased levels of inflammatory cytokines 6 DPI including IL-1 β , IL-18, IFN γ , and IL-6 as well as regulatory cytokines IL-1RA and IL-4 (**Figure 2.3A-B**). We also observed a sharp increase in IFN α , a potent antiviral cytokine, 6 DPI (**Figure 2.3B**). Lymphocyte populations were also likely impacted by significant decreases in levels of IL-7, which plays a role in B and T cell development and homeostasis, by 5-6 DPI (**Figure 2.3B**). Furthermore, ZEBOV-Makona infection resulted in upregulation of several chemokines 6 DPI (**Figure 2.3C**) including T-cell attractants, I-TAC (CXCL11) and MIG (CXCL9); leukocyte attractant, MIP1 α ; monocyte attractant, MCP-1; eosinophil attractant, eotaxin; and B-cell attractant, CXCL13. We also detected a significant decrease in growth factor PDGF-BB, which also coincides with characteristic thrombocytopenia seen in filovirus infection (**Figure 2.3C**).



(Previous Page) Figure 2.2. Disease signs correlate with viral replication. (A) Study time line and clinical observations. (B) Infectious virus was quantified by plaque assay on Vero cells and viral genome copies were measured using RT-qPCR with primers/probe targeting VP30. Average clinical scores as obtained by a scoring sheet (**Table 2.2**). (C) Amylase (AMY) and C-reactive protein (CRP) plasma levels. (D) Percentage hematocrit and platelets counts. (E) Blood urea nitrogen (BUN) and creatinine (CRE) levels. (F) Alanine aminotransferase (ALT), Aspartate aminotransferase (AST), alkaline phosphatase (ALP), gamma-glutamyltransferase (GGT) levels. (G) White blood cells (WBC), lymphocyte (LY), monocyte (MO), and granulocyte (GR) counts throughout infection. A linear model was used to perform statistical analysis; p-values listed for each parameter represent overall effect throughout infection.

Animal	DPI	Dyspnea (0-5)	Recumbency (0-9)	Unresponsiveness (0-5)	Bleeding Hemorrhage (0-5)	Total
091225	Day 2	0	0	0	0	0
100786	Day 2	0	0	0	0	0
133465	Day 2	0	0	0	0	0
133493	Day 2	0	0	0	0	0
080612 5	Day 4	0	0	0	0	0
100504 1	Day 4	0	0	0	0	0
903101	Day 6	0	0	1	0	1
090600 1	Day 6	0	0	1	0	1
133440	Day 6	0	0	1	0	1
133440	Day 6	0	0	1	1	2

Table 2.2. Clinical scores used to determine disease progression

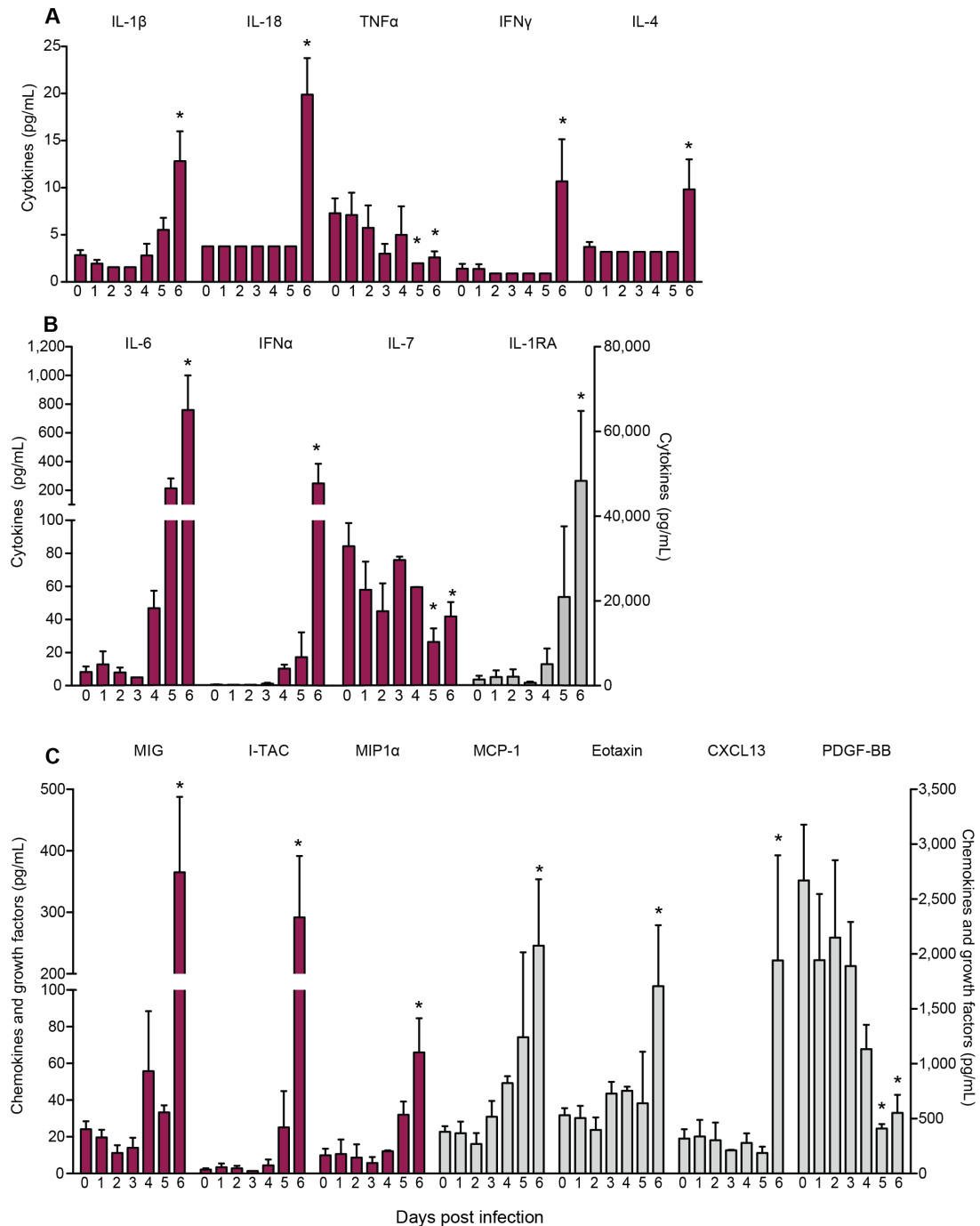


Figure 2.3. Plasma levels of cytokines, chemokines and growth factors. Cytokine (A-B), chemokine and growth factor (C) levels in plasma were determined using Luminex technology. Left axis (red bar) and right axis (gray bar). A nonparametric trend where each time point is modeled by its own mean was assumed for statistical analysis; * denote p-value ≤ 0.05 at the indicated time point compared to 0 DPI.

ZEBOV-Makona infection results in early activation of the innate immune cells

To characterize the immune response to ZEBOV-Makona, we used flow cytometry to measure changes in frequency and phenotype of circulating immune cells in PBMC (gating strategy described in **Figure 2.2**). Frequency of monocytes (defined as CD3⁻CD20⁻CD14⁺) remained relatively stable throughout infection with the exception of a small decrease 5 DPI (**Figure 2.4A**). Further analysis indicates a transient yet significant increased frequency of intermediate/non-classical monocytes (CD16⁺) ($p = 0.005$) 4 DPI (**Figure 2.4B**). This increased frequency of CD16⁺ monocytes returned to baseline values 6 DPI.

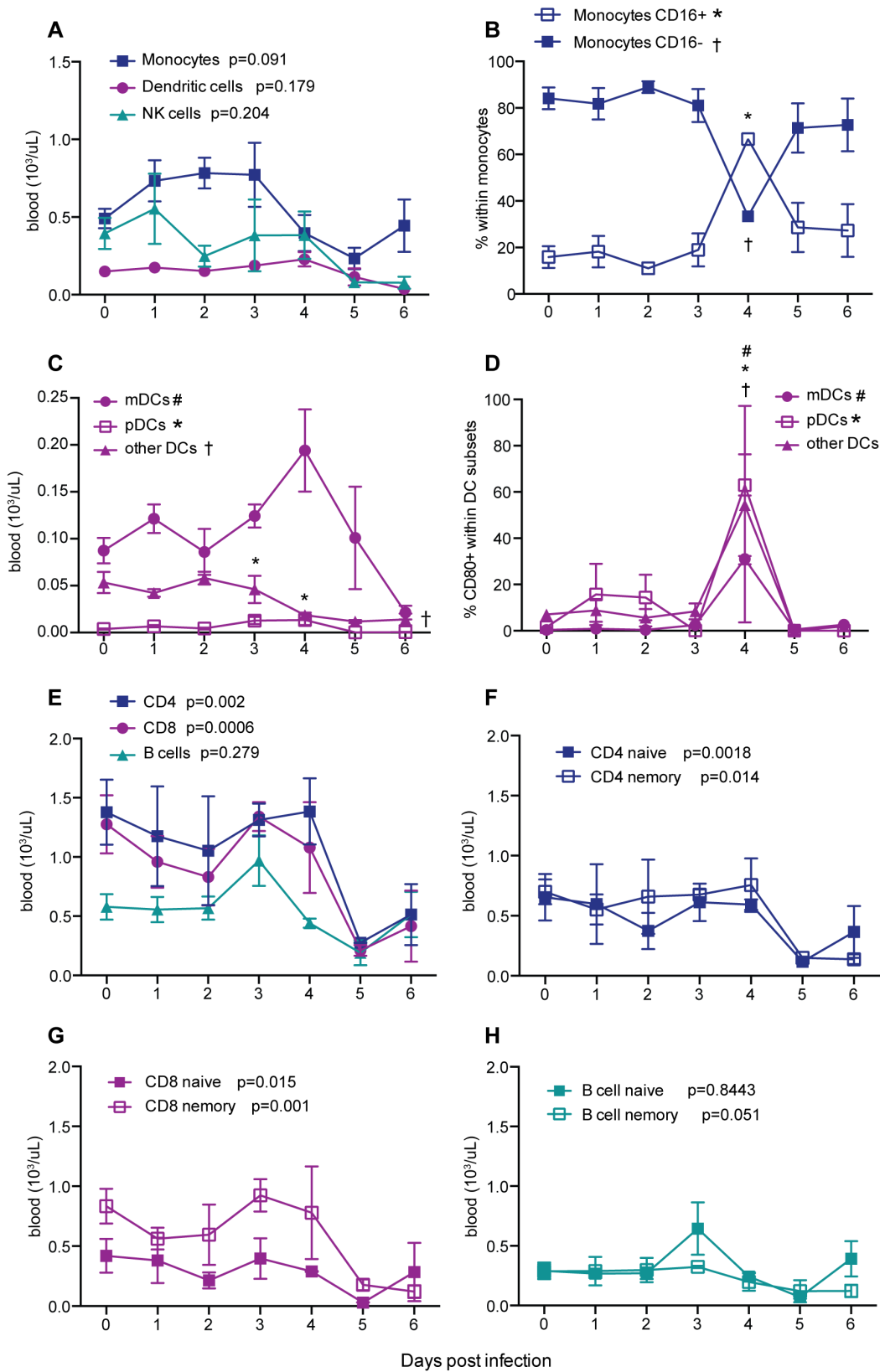
Total number of DCs (CD3⁻CD20⁻CD14⁻HLA-DR⁺) also remained stable with the exception of a small increase 4 DPI followed by a decline 5 DPI (**Figure 2.4A**). We then analyzed changes in the three distinct DC subsets: myeloid dendritic cells (mDC; CD11c⁺CD123⁻), plasmacytoid dendritic cells (pDC; CD11c⁻CD123⁺), and other dendritic cells (CD11c⁻CD123⁻) (**Figure 2.4C**). This analysis revealed that the increase in DC numbers 4 DPI was driven by a slight increase in the frequency of mDCs ($p = 0.116$) and a significant increase in pDCs 3 ($p = 0.0222$) and 4 DPI ($p = 0.0775$). The increase in mDC and pDC numbers 4 DPI was accompanied by increased expression of the activation marker CD80 by all three DC subsets (**Figure 2.4D**). The number of other DCs, in contrast, declined 6 DPI ($p = 0.033$) (**Figure 2.4C**).

We detected a small decrease in the total number of natural killer (NK) cells (CD3⁻CD20⁻CD14⁻CD8 α ⁺) at the later stages of the disease 5-6 DPI (**Figure 2.4A**). Although

frequencies of cytotoxic NK cells (CD16⁺) and cytokine-producing NK cells (CD16⁻) remained stable throughout infection (**Figure 2.5A**), the frequency of cytokine-producing NK cells expressing CD159 was transiently increased 1 DPI (p = 0.0072) (**Figure 2.5B**).

ZEBOV-Makona infection results in lymphopenia

PBMC were also analyzed by flow cytometry to determine changes in frequency of circulating lymphocytes (**Figure 2.4E-H**). CD4⁺ T cells (CD3⁺CD20⁻CD4⁺) and CD8⁺ T cells (CD3⁺CD20⁻CD8⁺) were classified into naïve (CD28⁺CD95⁻) and memory (CD28^{+/-}CD95⁺) subsets (**Figure 2.4F-G**). Similarly, B cells (CD3⁻CD20⁺) were also classified as naïve (CD27⁻) or memory (CD27⁺) (**Figure 2.4H**). Overall, T cell numbers, both memory and naïve, declined 5 and 6 DPI (**Figure 2.4E-G**). Although the number of total B cells remained stable, memory B cells significantly decreased 5-6 DPI (**Figure 2.4H**). In addition to analyzing frequency of T and B cell subsets, we assessed proliferation by measuring changes in the expression of Ki67, a nuclear protein associated with DNA replication. Memory CD4⁺ and CD8⁺ T cells were further divided into three groups: central memory (CM; CD28⁺CD95⁺CCR7⁺), effector memory (EM; CD28⁻CD95⁺CCR7⁻) and transitional effector memory (TEM; CD28⁺CD95⁺CCR7⁻). In contrast to lymphocyte numbers, the proliferation of memory CD4⁺ and CD8⁺ T cell subsets significantly increased 4-6 DPI while that of naïve T cells remained unchanged (**Figure 2.5C-D**).



(Previous Page) Figure 2.4. ZEBOV-Makona infection results in early activation of innate immune cells and lymphopenia. **(A)** Frequency of dendritic cells (DCs, CD14⁻HLA-DR⁺), monocytes (CD14⁺HLA-DR^{+/-}), and NK cells (CD3⁻CD20⁻CD14⁻CD8 α ⁺) were measured by flow cytometry (FCM). **(B)** Frequency of classical (CD16⁻) and intermediate/non-classical (CD16⁺) monocytes. **(C)** Frequencies of myeloid DCs (mDC, CD123⁻CD11c⁺) and plasmacytoid DCs (pDC, CD123⁺CD11c⁻) and other DCs (CD123⁻CD11c⁻). **(D)** Frequency of DC subsets expressing CD80. **(E)** Frequency of CD20 B-cells, CD4 and CD8 T cells. **(F-G)** Frequency of naïve (CD28⁺CD95⁻) and memory (CD28^{+/-}CD95⁺) T cells within CD4 **(F)** and CD8 **(G)** subsets. **(H)** Frequency of naïve (CD27⁻) and memory (CD27⁺) B cells. For frequency changes in total monocyte(s), DCs, NK cells, CD4 T cells, CD8 T cells and B cells, a linear model was used to perform statistical analysis; p-values listed for each parameter represent overall effect throughout infection. For changes in subset frequencies within monocytes, DC, and NK cells, a nonparametric trend where each time point is modeled by its own mean was assumed for statistical analysis; symbols (*, †, #) denote p-value ≤ 0.05 at the indicated time point compared to 0 DPI: * for CD16⁺ Monocytes and pDCs; † for CD16⁻ Monocytes and other DCs; # for mDCs.

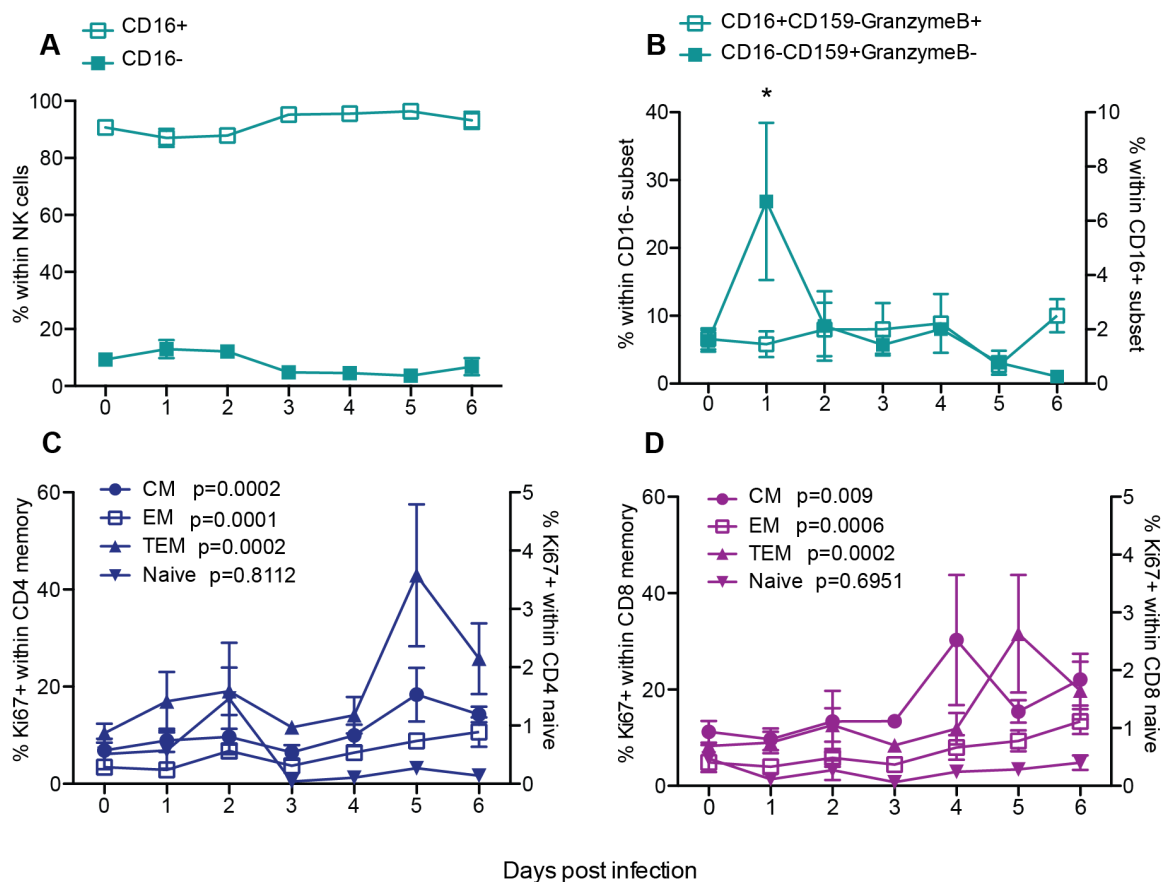


Figure 2.5. NK cell subset frequencies and T cell proliferation. (A) Frequency of CD16⁺ and CD16⁻ NK cells was measured by flow cytometry (FCM). (B) Frequency of CD159⁻GranzymeB⁺ cells within CD16⁺ NK cell subset and CD159a⁺GranzymeB⁻ cells within CD16⁻ NK cell subset. (C-D) The magnitude of CD4 T cell (C) and CD8 T cell (D) proliferation was determined by measuring changes in the frequency of Ki67⁺ cells within naïve, central (CM), effector (EM) and transitional effector (TEM) memory subsets. For frequency changes in T cell subsets, a linear model was used to perform statistical analysis; p-values listed for each parameter represent overall effect throughout infection. For changes in subset frequencies within NK cells, a nonparametric trend where each time point is modeled by its own mean was assumed for statistical analysis; * denote p-value ≤ 0.05 at the indicated time point compared to 0 DPI.

ZEBOV-Makona induces early and sustained upregulation of innate immune genes

We next determined longitudinal gene expression profiles in WB using RNA sequencing (RNA-Seq). The number of differentially expressed genes (DEGs), that are protein coding and have human homologs, correlated very tightly with viral replication with large changes observed 5 and 6 DPI (**Figure 2.6A**). We also determined the number of ZEBOV transcripts mapping to each ZEBOV open reading frame (ORF) and intergenic region (IGR) (**Figure 2.7A**). We detected a significant increase in transcripts from all ORFs and IGRs 5-6 DPI. Furthermore, NP had the highest number of transcripts while VP24 and L had the lowest, indicative of a productive ZEBOV transcriptional gradient. To understand the biological impact of the gene expression changes detected each DPI, we performed functional enrichment using MetaCore™ [207] to identify gene ontology (GO) processes, which are defined terms representing the biological processes of a gene set. DEGs upregulated 3 to 6 DPI enriched to GO processes associated with host defense (**Figure 2.6B**). As infection progressed, both the number of DEGs mapping to these GO processes and the false discovery rate (FDR)-corrected p-values became more significant (**Figure 2.6B**). Additionally, DEGs upregulated 5 and 6 DPI, when clinical signs are detected (**Figure 2.2A-B**), enriched to metabolism and leukocyte activation GO processes (**Figure 2.6B**). A significant number of downregulated DEGs was only detected 6 DPI and most of those genes enriched to GO processes associated with T cell activation and metabolic processes (**Figure 2.6C**).

The 30 DEGs that were detected 3 DPI remained upregulated throughout infection with fold changes that increased from ~ 20 at 3 DPI to ~ 150 at 6 DPI (**Figure 2.6D**). These 30 genes play a role in antiviral defense including: interferon stimulated genes such as *OAS1*, *MX1*, *IFI44*; and sensors of viral nucleic acids such as *DHX58* and *IFIH1* (**Figure 2.6E**). Similarly, the 68 upregulated genes that were newly detected 4 DPI remained upregulated 5-6 DPI (**Figure 2.6D**). Many of these genes were involved in inflammation including *SERPING1*, *CXCL10*, *S100A8*, and *TIFA* (**Figure 2.8A**). Other upregulated genes in this group activate innate immunity such as *TLR3* and *CD177*, while others encode negative regulators e.g. *IL1RN*, *SOCS3* and *TRAFD1*. Finally, some of these genes play a role in cell death such as *TNFSF10*, *CASP5*, and *CD274* (**Figure 2.8A**).

End-stage disease is characterized by upregulation of genes important for cell death and inflammation and downregulation of those important for T cell activation and translation

A substantial number of DEGs was detected 5 DPI (801). These DEGs enriched to GO processes associated with host defense as well as apoptosis and metabolism (**Figure 2.6B**). A network analysis of the DEGs that enriched to GO processes “Leukocyte activation” showed that several were regulated by a number of transcription factors critical to the inflammatory response, notably components of the NFκB complex *RELA/RELB* and *SP11* (**Figure 2.8B**). Interestingly, genes involved in B cell development such as *BCL6* and *BTK* as well as T cell activation including *LCP* and *FYB* were upregulated. Moreover, Toll-Like Receptors (*TLR*) 1-4 and 6 were upregulated (**Figure 2.8B**). Of the 119 DEGs detected

exclusively 5 DPI (**Figure 2.6D**), 34 enriched to “Immune system process” (FDR-adjusted p-value = 3.96^{-5}) and consisted of innate immune transcripts (i.e. *SI00A11*, *CASP10*, and *KLF6*) while 82 DEGs enriched to “Cellular metabolic process” (FDR-adjusted p-value = 2.382^{-4}) and consisted of genes that play a role in transcription (*EIF4E3*), signal transduction (*MAP4K4*), cellular respiration (*MT-CYB*) and apoptosis (*PIM2*).

Similarly, DEGs upregulated 6 DPI enriched to GO processes associated with host defense, cell death, and metabolic processes (**Figure 2.6B**). Of the 371 genes that mapped to “Immune system process”, 90 with known roles in inflammation directly interacted with one another (**Figure 2.9A**). Expression of these genes is regulated by: *NFKB1*, *STAT1/STAT2*, and *CEBPB*. DEGs regulated by these transcription factors included chemokines/cytokines such as *CCL2*, *CXCL10*, *TNF*, and *IL1B*; as well as their receptors, notably *C3AR1*, *CXCRI*, and *IL1RAP*. Several IFN stimulated genes (*ISG15* and *IFIT2*) and RNA helicases (*HERC5* and *DHX58*) were also part of this network. Other DEGs in this network play a role in generating or clearing reactive oxygen species e.g. *CYBB* and *SOD2* (**Figure 2.9A**). These upregulated genes are in line with the dysregulated immune activation often attributed to Ebola hemorrhagic fever (EHF). DEGs upregulated 6 DPI also play a role in 1) cell death including *FAS*, *TNFSF10*, *BCL2A1*, *TRPM2*; or 2) cell cycle progression such as *TCF7L1* and *OLFM4* (**Figure 2.9A-B**).

(Previous Page) Figure 2.6. ZEBOV-Makona infection induces sustained large transcriptional changes in innate immune genes. (A) Bar graph depicts number of protein-coding differentially expressed genes (DEGs; defined as those $\geq \log_2$ fold change compared to 0 DPI and FDR-corrected p-value ≤ 0.05) that have human homologues. Line graph indicates number of viral transcripts reported as normalized by reads per kilobase per million mapped (RPKM); the *EdgeR* package was used to determine statistically significant changes in viral reads; * denote p-value ≤ 0.05 at the indicated time point compared to 0 DPI. (B) Heatmap representing functional enrichment of DEGs 3-6 DPI; color intensity represents the statistical significance (shown as $-\log_{10}$ of the FDR-corrected p-value); range of colors is based on the lowest and highest $-\log_{10}(\text{FDR})$ values for the entire set of GO processes; the number of DEGs enriching to each GO process each day is listed within each box; blank boxes represent no statistical significance. (C) Bar graph depicting statistically significant GO processes to which downregulated genes 6 DPI enriched; the line graph represents $-\log_{10}(\text{FDR})$ of the enriched term. (D) 4-way venn diagram shows overlap of DEGs (protein-coding human homologs) detected 3, 4, 5 and 6 DPI. (E) Heatmap representing gene expression (shown as absolute normalized RPKM values) of the common 30 DEGs first detected 3DPI and upregulated throughout infection; range of colors is based on scaled and centered RPKM values of the entire set of genes (red represents increased expression while blue represents decreased expression); each column represents the median RPKM values for each DPI.

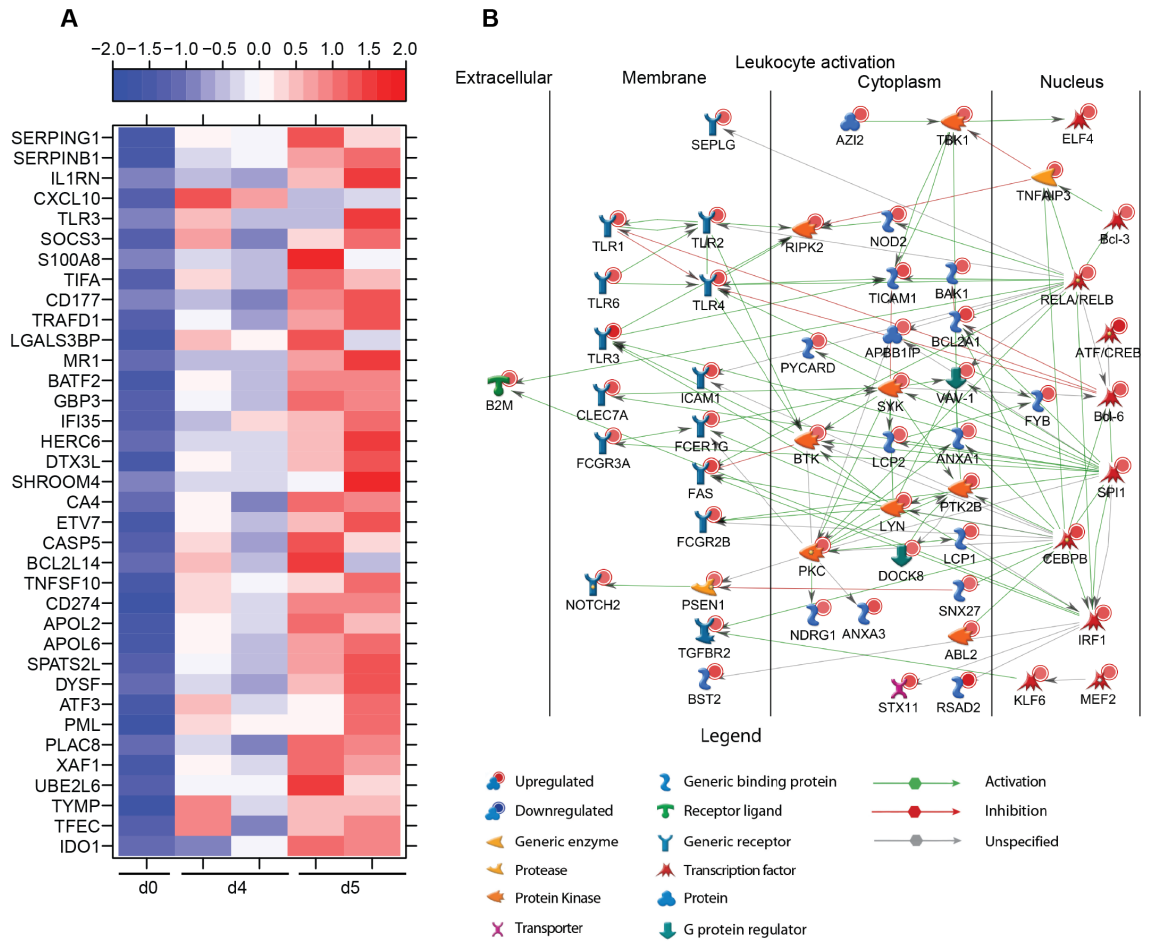


Figure 2.8. Gene expression changes 5 DPI reflect increased number of granulocytes. (A) Heatmap representing gene expression (shown as absolute normalized RPKM values) of DEGs upregulated 4 and 5 DPI with a FC ≥ 6.5 ; range of colors is based on scaled and centered RPKM values of the entire set of genes (red represents increased expression while blue represents decreased expression); day 0 is represented by the median RPKM value, while each column represents 1 animal for 4 and 5 DPI. **(B)** Network depicting direct interactions of DEGs upregulated 5 DPI that map to GO process "Leukocyte Activation".

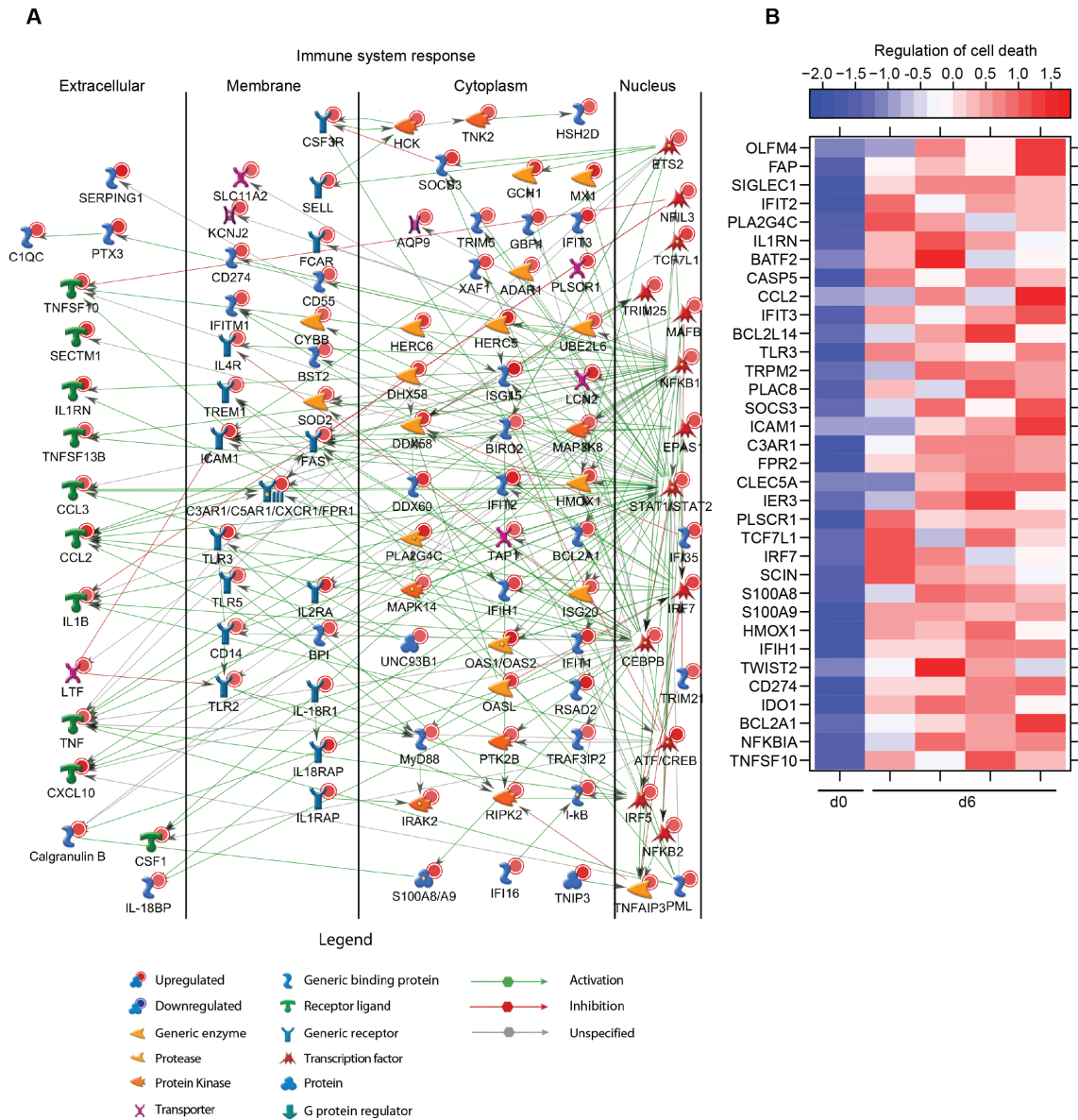


Figure 2.9. End-stage disease is characterized by upregulation of genes important for cell death and inflammation. (A) Network depicting direct interactions of DEGs upregulated 6 DPI that map to “Immune system response” with a FC ≥ 5.6 . **(B)** Heatmap representing gene expression (shown as absolute normalized RPKM values) of DEGs upregulated 6 DPI that map to “Regulation of cell death” with a FC ≥ 16 ; range of colors is based on scaled and centered RPKM values of the entire set of genes (red represents increased expression while blue represents decreased expression); day 0 is represented by the median RPKM value, while each column represents 1 animal for 6 DPI.

At day 6, changes in gene expression were also indicative of a suppressed adaptive immune response and cellular homeostasis (**Figure 2.6C**). Specifically, several downregulated genes mapping to “Immune system process” play a role in T-cell responses: *CD3*, *CD8*, *IL2RB*, *TRAC*, and *ZAP70* (**Figure 2.10A**). Additionally, genes encoding effector molecules *GZMB*, *PRF1*, and *CD244* were downregulated (**Figure 2.10A**). The second major group of downregulated genes enriched to GO process “translation” (**Figure 2.6C**) and contained translation initiation factors e.g. *EIF3E*; elongation factors such as *EEF2*; and ribosomal proteins e.g. *RPL22L1* (**Figure 2.10B**). Interestingly, several of the genes that enriched to the GO term “viral process” were also ribosomal proteins e.g. *RPS27* as well as genes that regulate nuclear import such as importins (*IPO5*) and nucleoporins (*NUP210*) (**Figure 2.10C**).

DEGs detected only in PBMC fraction play a role in regulating blood clotting, response to oxidative stress and vasculature development

In order to get a better understanding of the contributions of lymphocytes and antigen-presenting cells to gene expression changes, we next identified transcriptional changes within PBMC, which are devoid of granulocytes, erythrocytes, and platelets. The kinetics of host and viral gene expression changes in PBMC were similar as those described for WB, but the number of DEGs and viral reads was significantly smaller (**Figure 2.11A and Figure 2.7B**). As described for WB, 45 mostly interferon-stimulated genes were upregulated 3-6 DPI in PBMC with fold changes that increased from ~ 10 at 3 DPI to ~ 70 at 6 DPI as infection progressed (**Figure 2.11B-C**). Of these 45 DEGs, 27 were also

detected in WB 3 DPI (**Figure 2.11C**). The remaining 18 DEGs were detected in WB 4-5 DPI. Overall, a substantial number (50-75%) of DEGs detected in PBMC throughout infection were also detected in WB (**Figure 2.11D-G**).

Most of the 59 DEGs detected only in PBMC 4 DPI, were detected in WB 5-6 DPI such as *CIQC*, *BCL2A1*, *CYBB*, and *CASP4* (**Figure 2.11H**). DEGs detected only in PBMC 5 DPI enriched to GO process associated with blood regulation and response to oxidative stress (**Figure 2.12A**) including *ADAMDECI*, *NCF1*, *ATP2A2*, *THBS1*, and *F13A1* (**Figure 2.12B**).

Differences between the PBMC and WB gene expression profiles were most prominent 6 DPI (**Figure 2.11G**). DEGs upregulated only in PBMC enriched to immune related GO processes such as host defense and coagulation (**Figure 2.12C**). Upregulated genes that enriched to “Immune system process” include *MNDA*, and *NLRP12*. Genes that mapped to coagulation include *PTAFR*, and *THBD* (**Figure 2.12D**). Some of the downregulated genes detected only in PBMC 6 DPI play a role in host defense such as: *CD96*, *CD8B*, and *SLAMF6* (**Figure 2.12E-F**). Others were involved in vasculature development such as *CYSLTR2* and *ADRB2*, as well as coagulation e.g. *PRKCA* and *ENPP4* (**Figure 2.12F**). To better understand the source of the DEGs detected only in PBMC 6 DPI, we used the Immunological Genome Project Consortium database (ImmGen), a collaborative effort to delineate gene expression patterns across different leukocyte subsets [208] (**Figure 2.13**).

This analysis revealed that most of these DEGs are expressed by DCs and monocytes/macrophages.

ZEBOV-Makona induces overlapping but distinct gene expression changes compared to ZEBOV-Kikwit

To better understand the differences in pathogenesis caused by ZEBOV-Makona and the previously identified ZEBOV variant Kikwit, we compared our transcriptome results to those obtained from a recent study in which male cynomolgus macaques were challenged intramuscularly with 1000 PFU of Kikwit [205, 209]. Protocols for library preparation, sequencing, and bioinformatics analysis were the same, making these comparisons feasible. This comparison further supports delayed disease progression following challenge with Makona relative to Kikwit (**Figure 2.14**). Specifically, we observed significantly larger gene expression changes in both WB and PBMC 4 DPI following Kikwit infection compared to Makona (**Figure 2.14A-B**). Functional enrichment showed that DEGs detected 4 days following both Kikwit and Makona infection enriched to innate immunity while lymphocyte related transcripts were only downregulated following Kikwit infection, indicating lymphopenia occurs earlier compared to Makona infection[85, 105, 210] (**Figure 2.14C-D**).

At the terminal time point, widespread transcriptional responses were detected following infection with either ZEBOV variant and although there was significant overlap, we identified distinct gene expression profiles unique to Kikwit and Makona infection (**Figure**

2.15A-B). DEGs associated with inflammation and lymphopenia were detected with either variant. Since whole blood encompasses PBMC and functional enrichment was similar for both, we focused our analysis on differences between Kikwit and Makona infection in WB at the end stage of disease. Infection with either strain increased expression of ISGs (*GBPI*, *IFIT1*, *IRF7*) and reduced expression of lymphocyte related genes (*CD3D*, *CD8A*, *ZAP70*) (**Figure 2.15C**). However, DEGs unique to Makona infection suggest more widespread immune dysregulation (**Figure 2.15D-E**), while DEGs found exclusively during Kikwit infection were mostly involved with dysregulation of metabolism, cell cycle, and translation (**Figure 2.15F-G**).

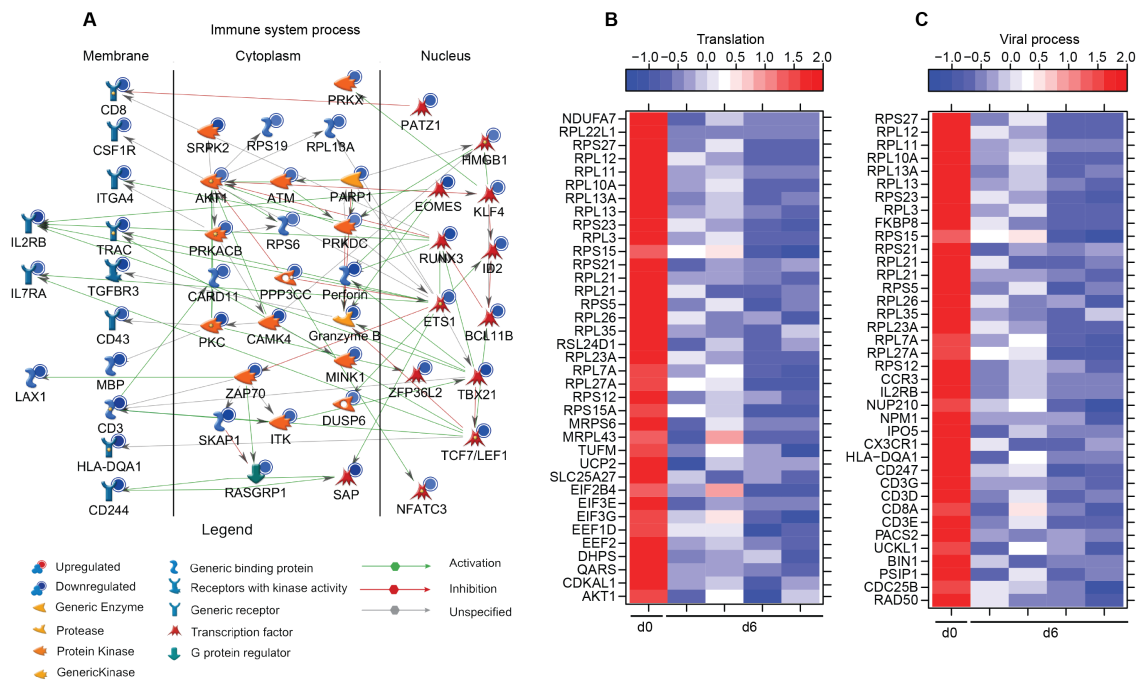
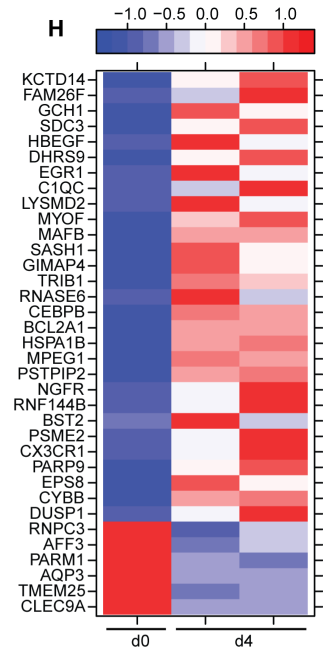
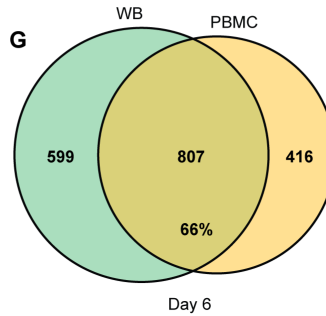
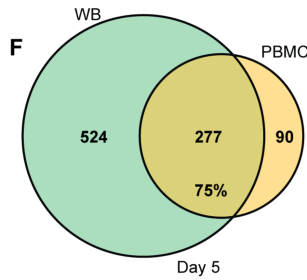
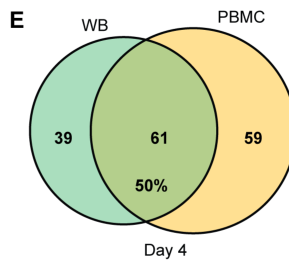
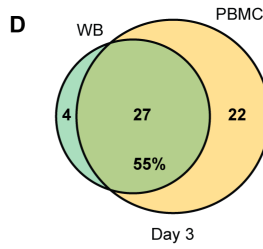
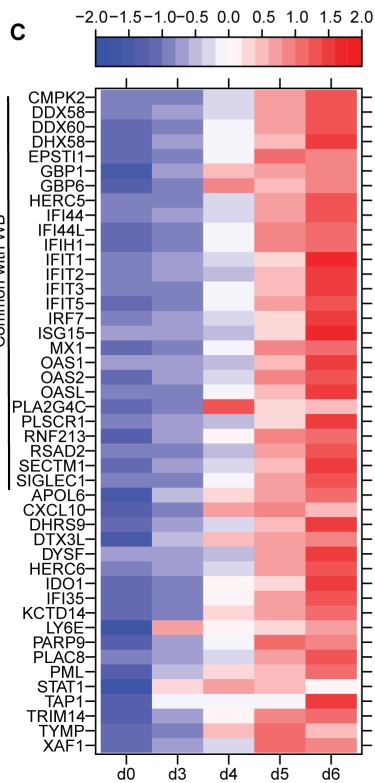
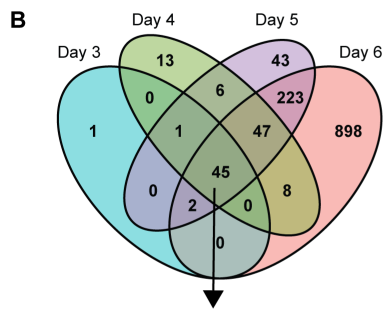
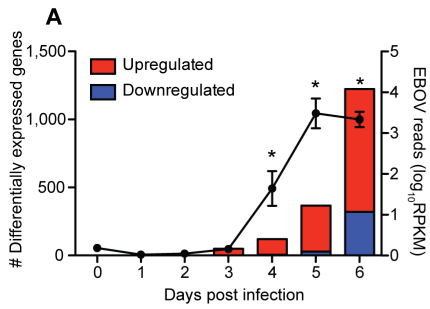
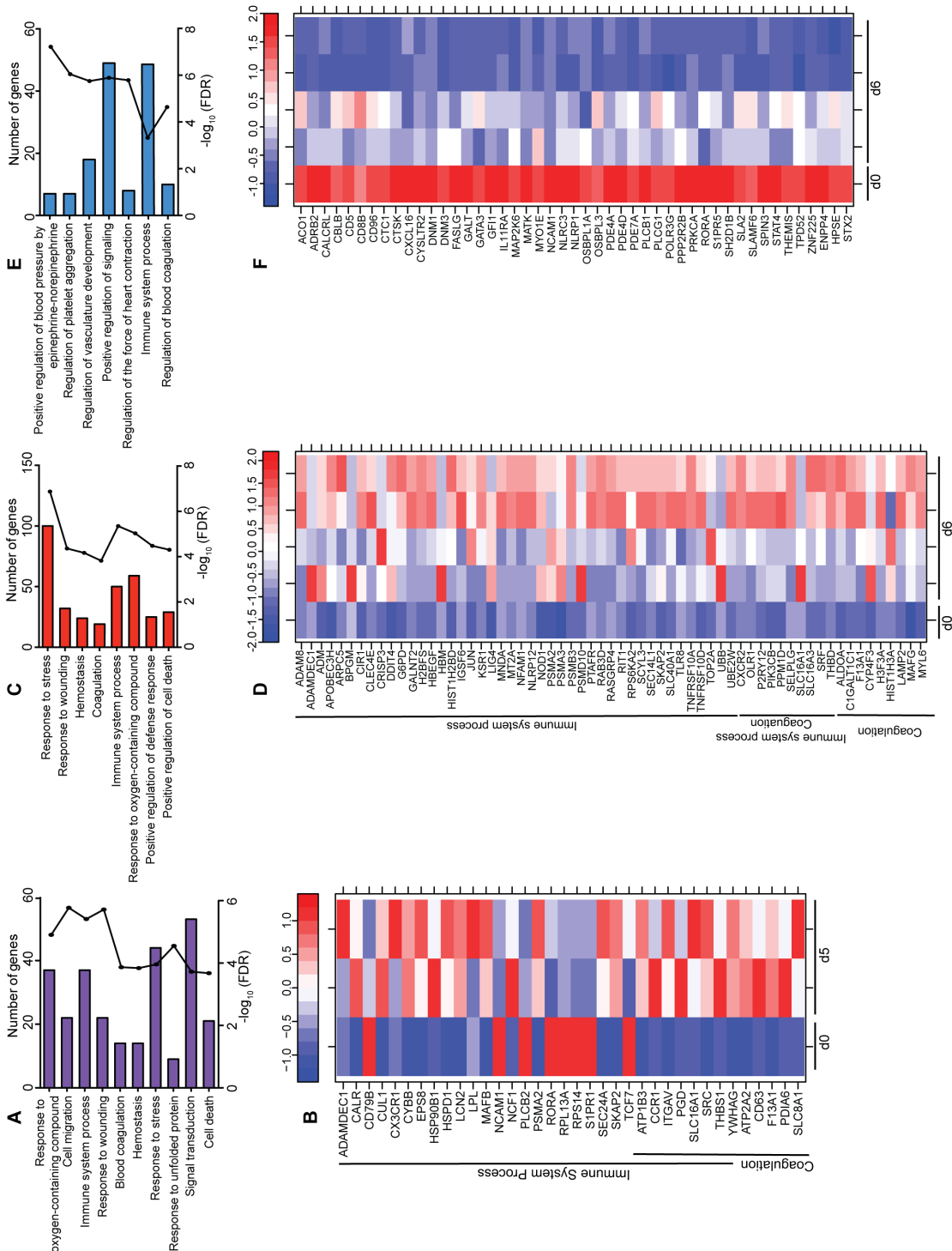


Figure 2.10. ZEBOV-Makona pathogenesis is characterized by downregulation of genes critical for T-cell activation and translation. (A) Network depicting direct interactions of DEGs downregulated 6 DPI that map to “Immune system response”. **(B-C)** Heatmap representing gene expression (shown as absolute normalized RPKM values) of DEGs downregulated 6 DPI that map to “Translation” with a FC ≥ 2.5 **(B)** and DEGs downregulated 6 DPI that map to “Viral process” with a FC ≥ 3.0 **(C)**; range of colors is based on scaled and centered RPKM values of the entire set of genes (red represents increased expression while blue represents decreased expression); day 0 is represented by the median RPKM value, while each column represents 1 animal for 6 DPI.



(Previous Page) Figure 2.11. Comparison of DEGs detected in PBMC and WB. (A) Bar graph depicts number of protein-coding differentially expressed genes (DEGs; defined as those $\geq \log_2$ fold change compared to 0 DPI and FDR-corrected p-value ≤ 0.05) that have human homologues. Line graph indicates number of viral transcripts reported as normalized by reads per kilobase per million mapped (RPKM); the *EdgeR* package was used to determine statistically significant changes in viral reads; * denote p-value ≤ 0.05 at the indicated time point compared to 0 DPI. **(B)** 4-way venn diagram shows overlap between DEGs detected 3, 4, 5 and 6 DPI. **(C)** Heatmap representing gene expression (shown as absolute normalized RPKM values) of all DEGs upregulated throughout infection; DEGs common with WB are noted; range of colors is based on scaled and centered RPKM values of the entire set of genes (red represents increased expression while blue represents decreased expression); each column represents the median RPKM values for each DPI. **(D-G)** Venn diagram shows overlap between DEGs in PBMC and WB 3 DPI **(D)**, 4 DPI **(E)**, 5 DPI **(F)**, and 6 DPI **(G)**. **(H)** Heatmap representing gene expression (shown as absolute normalized RPKM values) of DEGs found exclusively in PBMC 4 DPI with a FC ≥ 3.0 ; day 0 is represented by the median RPKM value, while each column represents 1 animal for 4 DPI.



(Previous Page) Figure 2.12. DEGs detected only in PBMC fraction play a role in regulating blood clotting, response to oxidative stress, and vasculature development. (A) Bar graph depicting statistically significant GO terms to which DEGs found exclusively in PBMC 5 DPI enriched; the line graph represents $-\log_{10}(\text{FDR})$ of the enriched term. (B) Heatmap representing gene expression (shown as absolute normalized RPKM values) of all DEGs found exclusively in PBMC 5 DPI that enriched to “Immune system process” and/or “Coagulation; day 0 is represented by the median RPKM value, while each column represents 1 animal for 5 DPI. (C) Bar graph depicting statistically significant GO

processes to which upregulated genes found exclusively in PBMC 6 DPI enriched; the line graph represents $-\log_{10}(\text{FDR})$ of the enriched term. **(D)** Heatmap representing gene expression (shown as absolute normalized RPKM values) of DEGs upregulated 6 DPI that map to “Coagulation” and/or “Immune system process”; range of colors is based on scaled and centered RPKM values of the entire set of genes (red represents increased expression while blue represents decreased expression); day 0 is represented by the median RPKM value, while each column represents 1 animal for 6 DPI. **(E)** Bar graph depicting statistically significant GO processes to which downregulated genes found exclusively in PBMC 6 DPI enriched; the line graph represents $-\log_{10}(\text{FDR})$ of the enriched term. **(F)** Heatmap representing gene expression (shown as absolute normalized RPKM values) of DEGs downregulated 6 DPI that map to “Immune system process”; range of colors is based on scaled and centered RPKM values of the entire set of genes (red represents increased expression while blue represents decreased expression); day 0 is represented by the median RPKM value, while each column represents 1 animal for 6 DPI.



Figure 2.13. Immgen analysis of PBMC 6 DPI. Heatmap profile showing expression profile of DEGs upregulated 6 DPI only in PBMC across various immune cell populations as predicted by ImmGen's MyGeneSet application. Red indicates high while blue indicates low likelihood of expression within indicated immune cell population.

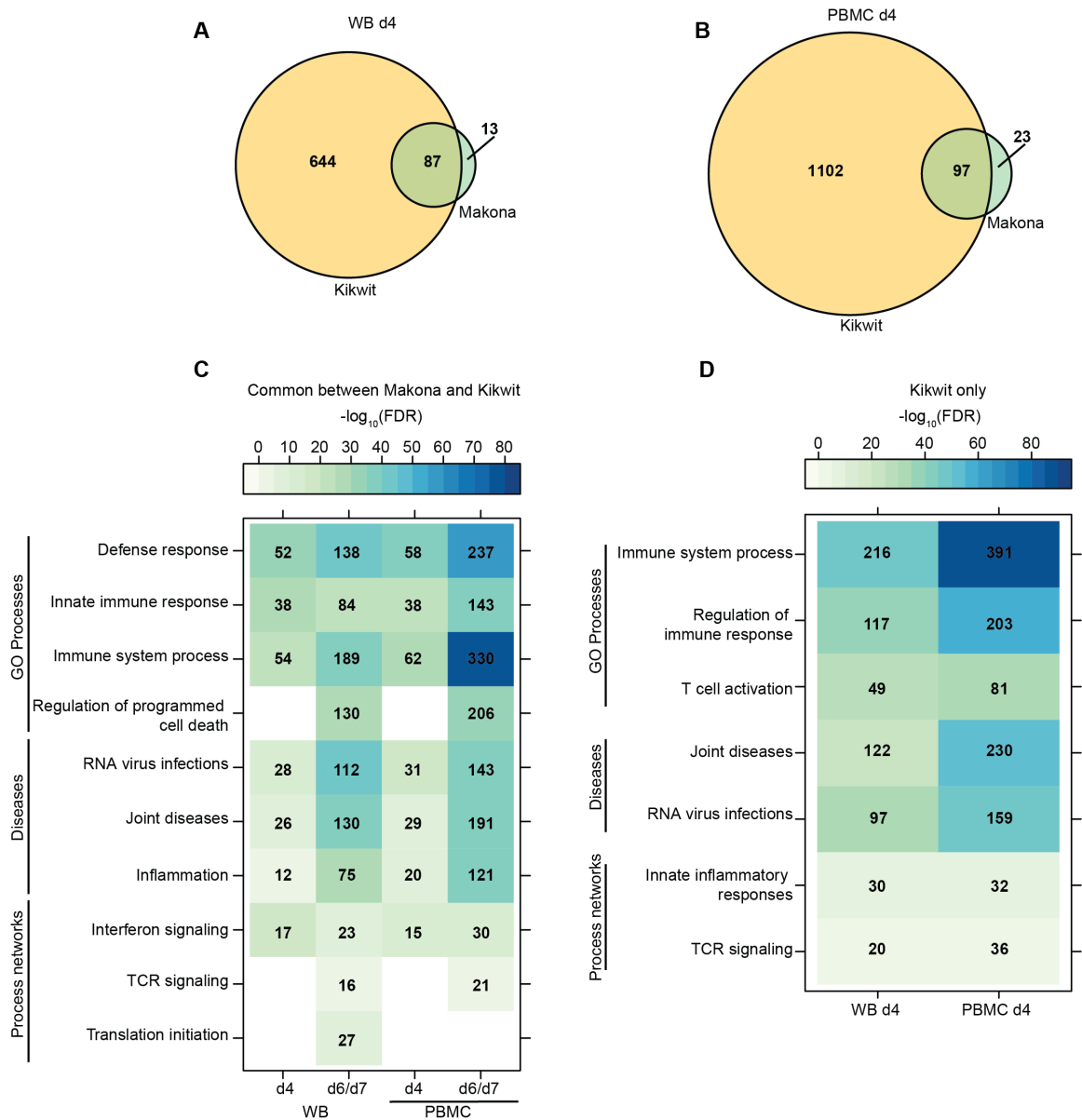
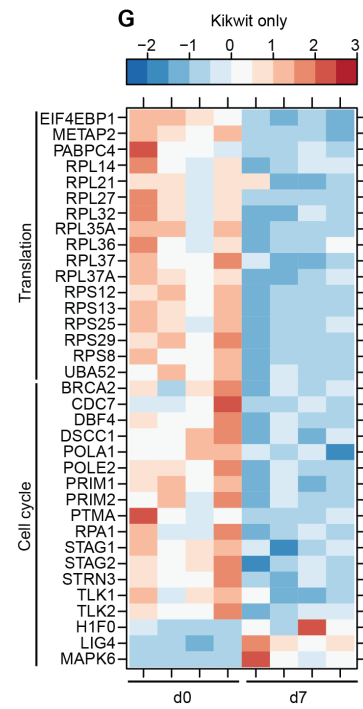
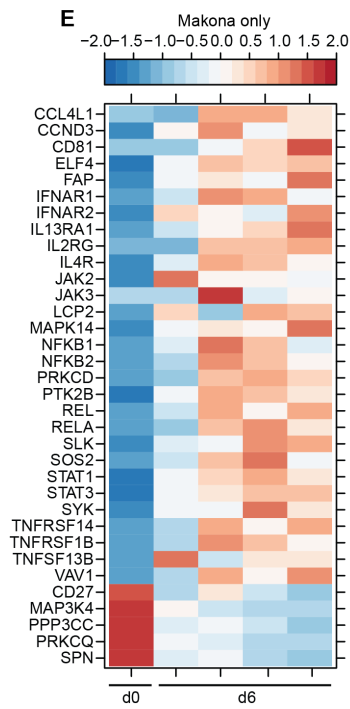
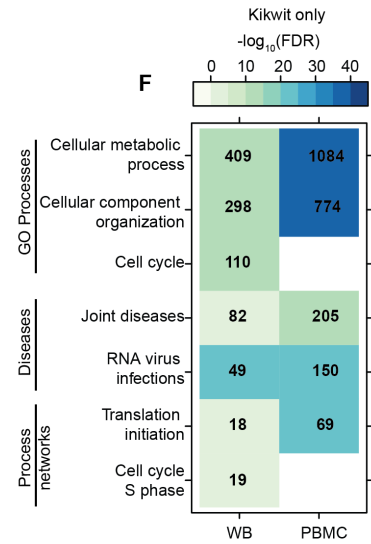
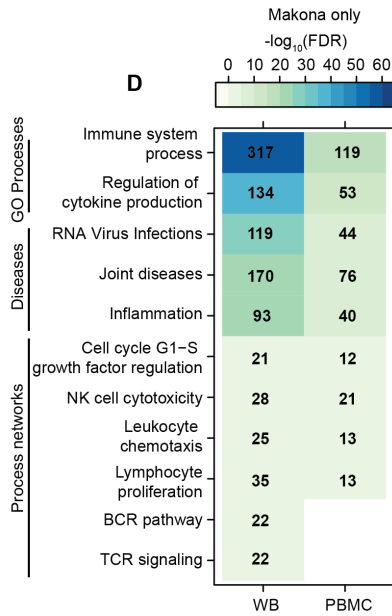
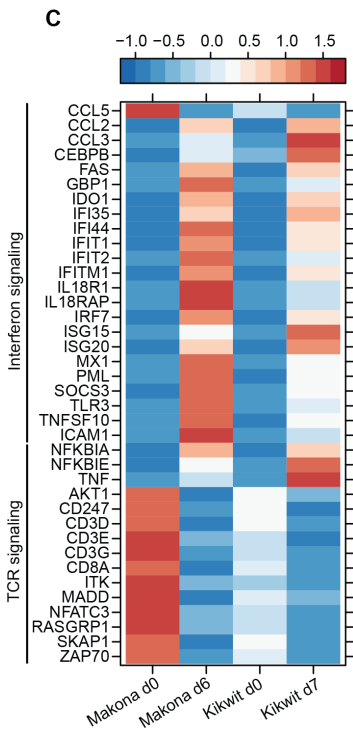
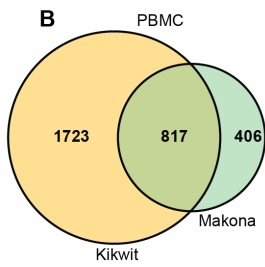
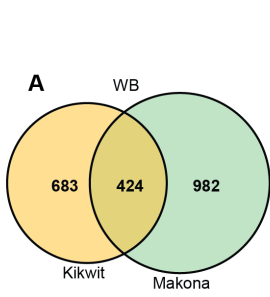


Figure 2.14. Comparison of host transcriptional profile following ZEBOV-Makona or ZEBOV-Kikwit infection at 4 DPI. (A-B) Venn diagram shows overlap between DEGs detected following Kikwit and Makona infection 4 DPI in WB (A) and PBMC (B). **(C-D)** Heatmap representing functional enrichment of DEGs common following Makona or Kikwit infection 4 DPI and at terminal time points (6 DPI for Makona and 7 DPI for Kikwit) (C) and DEGs exclusively detected following Kikwit infection 4 DPI (D); color intensity represents the statistical significance (shown as $-\log_{10}$ of the FDR-corrected p-Value); range of colors are based on the lowest and highest $-\log_{10}(\text{FDR})$ value for the entire set of terms; the number of DEGs enriching to each functional enrichment term each day is listed within each box; blank boxes represent no statistical significance.



(Previous Page) Figure 2.15. Comparison of host transcriptional profile following ZEBOV-Makona or ZEBOV-Kikwit infection at 6DPI. (A-B) Venn diagram shows overlap between DEGs detected following Makona and Kikwit infection 6 and 7 DPI, respectively, in WB **(A)** and PBMC **(B)**. **(C)** Heatmap representing gene expression (shown as absolute normalized RPKM values) of shared DEGs detected at end stage of disease following Kikwit or Makona infection that enriched to Process Network terms “Inflammation – Interferon signaling” and “Immune response – TCR signaling”; range of colors is based on scaled and centered RPKM values of the entire set of genes (red represents increased expression while blue represents decreased expression); each column represents the median RPKM values on each day for either Kikwit or Makona infection. **(D)** Heatmap representing functional enrichment of DEGs exclusively detected following Makona infection 6 DPI; color intensity represents the statistical significance (shown as $-\log_{10}$ of the FDR-corrected p-Value); range of colors is based on the lowest and highest $-\log_{10}(\text{FDR})$ values for the entire set of terms; the number of DEGs enriching to each functional enrichment term each day is listed within each box; blank boxes represent no statistical significance. **(E)** Heatmap representing gene expression (shown as absolute normalized RPKM values) of DEGs found only 6 DPI with Makona that enriched to “Proliferation – lymphocyte proliferation”; day 0 is represented by the median RPKM value, while each column represents 1 animal for 6 DPI. **(F)** Heatmap representing functional enrichment of DEGs exclusively detected following Kikwit infection 7 DPI. **(g)** Heatmap representing gene expression (shown as absolute normalized RPKM values) of DEGs found exclusively 7 DPI following Kikwit infection that enriched to “Translation” and “Cell cycle”; each column represents 1 animal 7 DPI.

Discussion

Although ZEBOV-Makona has high sequence homology to ZEBOV variants Mayinga and Kikwit, data from a recent study suggest Makona infection progresses less rapidly [14, 210]. However, the biological processes underlying altered disease course by ZEBOV-Makona is currently understudied. Therefore, we integrated flow cytometry and RNA-sequencing with clinical data to gain a more comprehensive understanding of ZEBOV-Makona pathogenesis. Here, we report that macaques infected with ZEBOV-Makona (isolate C07) presented with clinical signs typical of EHF including anorexia, hunching, fever, rash, and hemorrhaging. Clinical chemistry was also consistent with EHF and indicated damage to multiple organs, notably kidney, pancreas and liver. Moreover, lymphopenia and thrombocytopenia were observed at the later stages of disease together with sharp increases in plasma levels of pro-inflammatory cytokines (IL-1 β , IL-18, IL-6, and IFN α) and chemokines (I-TAC, MCP-1, and eotaxin), also characteristic of EHF.

Clinical scores, changes in liver and kidney enzymes, cytokine and chemokine levels, and pathology scores appeared later and were less severe than those previously reported in macaques infected with either the ZEBOV variants Mayinga or Kikwit [14, 58], despite comparable levels of viremia. It should be noted that early Makona isolates, including the C07 isolate used in this study, lack the A82V mutation in GP, which was observed in later Makona isolates and shown to confer increased infectivity of primate cells [211, 212]. Comparison of transcriptional changes also indicated that infection with ZEBOV-Makona established a distinct host transcriptional profile compared to the ZEBOV-Kikwit variant,

characterized by more robust changes in genes important for immunity and less pronounced changes in cellular metabolism and apoptotic pathways. It is possible that the delayed progression of disease led to enhanced immune activation following ZEBOV-Makona infection.

As previously reported for Mayinga and Kikwit [210, 213-215], ZEBOV-Makona infection induced early and sustained upregulation of genes important for antiviral immunity, notably ISGs. However, this increase was detected a day later than what was reported for ZEBOV-Kikwit infected macaques [210]. The initial upregulation of ISGs in our study correlated with the increased frequency of pDCs, which are potent producers of type I IFN. Additionally, the increased transcription of innate immune genes 4 DPI correlated with increased frequency of mDC and the upregulation of activation marker CD80 on all DC subsets. Since the frequency of DCs was significantly reduced 6 DPI, IFN α may be secreted from other infected cells or non-infected cells, such as endothelial cells, that are activated by viral debris. The magnitude of ISG expression was highest 6 DPI and correlated with levels of circulating IFN α .

These data contrast *in vitro* studies that show ZEBOV VP35 and VP24 prevent production and cellular responses to type I IFN, including failure to up-regulate CD80 and CD86 and mature into mobile antigen-presenting cells [87, 88, 216]. However, this discrepancy could be due to the infection rate likely being lower *in vivo*. Non-infected DCs may become activated by “shed” GP, which was recently shown to induce the secretion of pro-

inflammatory cytokines and expression of co-stimulatory molecules CD40, CD80, CD83, and CD86 on monocyte-derived DCs [217]. These data highlight the importance of delineating transcriptional profiles of individual immune cell subsets following *in vivo* infection in order to determine precisely how and in which cells ZEBOV evade host innate, and consequently, adaptive immune responses.

The sustained type I IFN response may lead to suppression of the adaptive immune response as recently reported in a mouse model of chronic lymphocytic choriomeningitis virus (LCMV) infection, where production of the immunosuppressive mediators IL-10 and PD-L1 was dependent on type I IFN signaling [218, 219]. Indeed, following upregulation of ISGs, we observed increased transcription of *CD274 (PD-L1)* 4-6 DPI, which preceded lymphopenia and reduced expression of genes typically expressed by lymphocytes. Therefore, it is possible that the high levels of circulating type I IFN contribute to the suppression of the adaptive immune responses following ZEBOV infection. The increased expression of PD-L1 is in line with recent clinical studies that reported increased numbers of CD4 and CD8 T cells expressing the inhibitory molecules CTLA-4 and PD-1 in ZEBOV-Makona fatalities [121].

Although the number of monocytes was unchanged, the percentage of non-classical monocytes (CD16⁺) significantly increased 4 DPI. Non-classical monocytes can produce large amounts of pro-inflammatory cytokines in an acute inflammatory state [220, 221] and may be largely responsible for the upregulation of pro-inflammatory mediators

(*SERPING1*, *CXCL10*, *S100A8*, *TIFA*) 4 DPI. “Shed” GP has also been shown to bind and activate monocytes, resulting in the production of inflammatory cytokines [217]. Our data contrasts a recent study reporting decreased levels of non-classical CD16⁺ monocytes in patients diagnosed with EHF in Guinea compared to febrile patients who tested negative for EHF [222]. However, the increase we observed was transient and preceded clinical signs. It is possible that the difficulties associated with a longitudinal study in a clinical setting precluded detection of early monocyte activation. Interestingly, we observed a transient increase in cytokine-producing NK cells 1 DPI. However, its clinical significance is unclear.

As infection progressed, we detected a robust upregulation of genes encoding cytokines and chemokines (*CCL2*, *CCL3*, *IL1B*, *CXCR1*, *IL1RN*) as well as granulocyte associated transcripts (*TLRs 1-4*, *SP11*, *S100A8*, *S100A9*, *CD177*), which correlated with the higher numbers of granulocytes 5 DPI. Granulocytosis was also reported following ZEBOV-Kikwit infection, albeit earlier at 4 DPI [58]. It is possible that the acute viral infection as well as the pro-inflammatory environment induced hematopoietic differentiation within the bone marrow, resulting in increased numbers of neutrophils [223, 224]. The largest gene expression changes (1400) were identified 6 DPI when a substantial decrease in many lymphocyte-related transcripts was detected (*CD3*, *CD8*, *IL2RB*, *LAX1*, and *ZAP70*, *GZMB*, *PRF1*). These changes correlated with a drop in CD4 T cells, CD8 T cells, B cells, and NK cells. Interestingly, proliferation of CD4 and CD8 T cells increased 4-6 DPI, possibly as an attempt to restore their numbers. We also detected a downregulation of genes

associated with translation and viral process 6 DPI such as translation initiation factors, elongation factors, and ribosomal proteins. These decreased transcripts suggest either cell death and/or an attempt by the host defense to prevent ZEBOV replication.

These observations are similar to the recent study by Liu and Speranza et al., [225] in which 2200 DEGs were identified in the WB from 88 patients who succumbed to ZEBOV-Makona infection (average of 5.9 days until symptom onset). These 2200 DEGs enriched to comparable biological processes reported in this study, notably those associated with innate immunity, type I interferon signaling, response to cytokine, cell death, T-cell activation, and coagulation. Moreover, in line with the early and sustained detection of ISGs in our study, Liu and Speranza et al. reported a higher number of ISGs in fatalities compared to surviving patients.

This study is the first to report a simultaneous analysis of gene expression changes within WB and PBMC from the same animals following ZEBOV infection. Interestingly, DEGs detected only in PBMC enriched to GO processes “Blood coagulation”, “Response to oxidative stress”, and “Vasculature development” 5-6 DPI. Further bioinformatics analysis confirmed that the majority of the DEGs unique in PBMC 5-6 DPI are primarily expressed by monocytes/macrophages and DCs. Upregulation of genes that enrich to response to oxidative stress may be attributed to reactive oxygen species produced by monocytes as suggested by increased transcripts of *NCF1*, an oxidase that can produce superoxide anion, and *CYBB*, a component of the microbicidal oxidase system of phagocytes [226].

Moreover, upregulation of DEGs that play a role in coagulation in PBMC including *PTAFR*, *THBD*, *P2RY12*, and *PRKCA* is in line with the potential role of ZEBOV-infected monocytes in initiating intra-vascular coagulation. Future studies will focus on transcriptional changes within ZEBOV-infected monocytes to assess to what degree inflammation, production of reactive oxygen species, and initiation of coagulation can be attributed to infected monocytes. Moreover, DEGs exclusively detected in WB suggest a significant role for granulocytes and platelets in ZEBOV-Makona pathogenesis.

CHAPTER 3: Transcriptome analysis of circulating immune cell subsets highlight the role of monocytes in Zaire Ebola virus Makona pathogenesis

Andrea R. Menicucci^{1#}, Krista Versteeg^{2,3#}, Courtney Woolsey^{2,3}, Chad E. Mire^{2,3}, Joan B. Geisbert^{2,3}, Robert W. Cross^{2,3}, Krystle N. Agans^{2,3}, Allen Jankeel⁴, Thomas W. Geisbert^{2,3*} and Ilhem Messaoudi^{4,*}

¹**University of California-Riverside, Division of Biomedical Sciences, Riverside, CA, USA.**

²**Galveston National Laboratory, Galveston, TX, 77555, USA.**

³**University of Texas Medical Branch, Department of Microbiology and Immunology, Galveston, TX, USA.**

⁴**University of California-Irvine, Department of Molecular Biology and Biochemistry, College of Biological Sciences, Irvine, USA**

***To whom Correspondence should be addressed**

These authors contributed equally to this work

A version of this chapter is published in *Frontiers in Immunology* [227]

Abstract

Existing models of Ebola virus disease (EVD) suggest antigen-presenting cells (APCs) are initial targets of *Zaire ebolavirus* (ZEBOV). *In vitro* studies have shown that ZEBOV infection of monocytes and macrophages results in the production of inflammatory mediators, which may cause lymphocyte apoptosis. However, these findings have not been corroborated by *in vivo* studies. In this study, we report the first longitudinal analysis of transcriptional changes in purified monocytes, T cells, and B cells isolated from the same cynomolgus macaques infected with ZEBOV-Makona (Chapter 2). Our data reveal monocytes as one of the major immune cell subsets that supports ZEBOV replication *in vivo*. In addition, we report a marked increase in the transcription of genes involved in inflammation, coagulation, and vascular disease within monocytes, suggesting that monocytes contribute to EVD manifestations. Further, genes important for antigen presentation and regulation of immunity were downregulated, potentially subverting development of adaptive immunity. In contrast, lymphocytes, which do not support ZEBOV replication, showed transcriptional changes limited to a small number of interferon stimulated genes (ISGs) and a failure to upregulate genes associated with an antiviral effector immune response. Collectively, these data suggest that ZEBOV-infected monocytes play a significant role in ZEBOV-Makona pathogenesis and strategies to suppress virus replication or modify innate responses to infection in these cells should be a priority for therapeutic intervention.

Introduction

Ebolaviruses (EBOV) are among the deadliest re-emerging viruses; causing hemorrhagic fever with case fatality rates (CFR) ranging from 40-90% depending on the species. Ebola virus disease (EVD) is characterized by an excessive inflammatory response, lymphocyte apoptosis, vascular impairment, hemorrhage, and coagulation defects leading to multi-organ failure and shock [18, 36]. *Zaire ebolavirus* (ZEBOV) is responsible for the highest CFRs and most outbreaks, including the largest epidemic that originated December 2013 in West Africa. The ZEBOV variant responsible for this epidemic, Makona, affected over 28,600 individuals and claimed over 11,300 lives [200].

Despite its impact on human health, the molecular basis for EVD is incompletely understood. Much of what is known about ZEBOV pathogenesis has been acquired through infectious studies in nonhuman primates (NHPs), particularly cynomolgus and rhesus macaques. Studies in macaques have shown that monocytes, macrophages, and dendritic cells (DCs), are the initial targets of ZEBOV [58]. Our understanding of how ZEBOV impacts function and behavior of DC and monocytes/macrophages has been primarily extrapolated from *in vitro* infections. Data from these studies show that *in vitro* infection of monocytes and macrophages with ZEBOV triggers a robust expression of inflammatory mediators including IL-1 β , IL-6, IL-8, MIP-1 α , MIP-1 β , MCP-1, and TNF α [77-79]; several of which have been detected in the plasma of humans and animal models following ZEBOV infection [77, 80-84]. Inflammatory mediators released by monocytes may also contribute to the impairment of the vascular system and disseminated intravascular

coagulation as well as lymphocyte death [76, 79, 85, 228]. However, whether monocytes are the major contributors to inflammation following ZEBOV infection *in vivo* remains to be elucidated. Moreover, the susceptibility of monocytes to ZEBOV remains contradictory. Some *in vitro* studies reported successful ZEBOV replication in both primary monocytes and macrophages [76, 78, 79]; others indicated ZEBOV entry is delayed in primary compared to differentiated monocytes and THP-1 cells are refractory to entry until PMA-induced differentiation [229].

Severe lymphopenia is a hallmark of ZEBOV infection [58, 84, 102, 105], observed as a loss of peripheral blood CD4 and CD8 T cells, as well as natural killer cells in cynomolgus macaques [58, 101] and humans [104]. The loss of B cells has been controversial with some NHP studies reporting apoptosis of B lymphocytes [76], while others observe no changes in B cell counts [101]. *In vivo* and *in vitro* studies using TUNEL staining and transmission electron microscopy confirm apoptosis as the main mechanism of lymphocyte loss during ZEBOV infection [76, 85]. Furthermore, while analysis of ZEBOV-infected NHP tissues shows the presence of ZEBOV antigens within phagocytic cells 3-4 days post challenge, no ZEBOV antigens have been observed in T and B cells throughout infection. This suggests lymphocyte apoptosis during ZEBOV infection is not due to direct viral replication but rather inflammatory mediators, such as TNF α , nitric oxide and reactive oxygen species. Presumably these cytokines and chemokines are produced in response to infection of phagocytes and other cells as well as immunosuppressive ZEBOV peptides

[42, 76, 230, 231]. However, the effects of ZEBOV infection and these mediators on T and B cell function remains incompletely defined.

Although many genomic studies have provided us with insight into the global transcriptional changes as disease progresses, studies that elucidate the role of individual immune cell subsets in viral pathogenesis are lacking. In this study, we used RNA sequencing (RNA-Seq) to uncover longitudinal gene expression profiles within monocytes, T cells, and B cells purified from ZEBOV-Makona infected cynomolgus macaque PBMC at different times post infection. Our data identify monocytes as one of the major targets of infection *in vivo*. Moreover, gene expression profiles at later stages of disease strongly support the role of monocytes as a significant source of inflammatory cytokines and chemokines during ZEBOV infection. In contrast, lymphocytes exhibited limited transcriptional activity and lacked significant signs of an effective adaptive immune response.

Materials and Methods

Study design

This study was designed to elucidate the role of specific immune cell subsets in mediating ZEBOV-Makona pathogenesis. For this purpose, monocytes, T cells, and B cells were isolated by magnetic bead separation from peripheral blood mononuclear cells (PBMC) collected on days 0 (n=10), 1 (n=5), 2 (n=4), 3 (n=3), 4 (n=2), 5 (n=2), and 6 (n=4) post ZEBOV-Makona infection from cynomolgus macaques (Chapter 2, [193]). Challenges with allowable volumes of blood collection and cell separation within a Biosafety Level 4 (BSL-4) lab precluded us from having n>2 for days 4 and 5 post infection. RNA-Seq was used to measure host gene expression changes within each cell subset.

Ethics statement

This study, including all protocols, were approved by the University of Texas Medical Branch at Galveston Institutional Animal Care and Use Committee (IACUC) in accordance with state and federal statutes and regulations relating to experiments involving animals and the Institutional Biosafety Committee.

Virus and challenge

A laboratory seed stock of the Makona variant isolate H.sapiens-tc/GIN/2014/ Makona-Gueckedou-C07 (accession number KJ660347.2) was grown from the serum of a 2014 fatal human case in Guékédou, Guinea and passaged twice in authenticated Vero E6 cells (ATCC, CRL-1586). This clone was selected because it is one of the earliest and well

characterized isolates from the ZEBOV epidemic in West Africa that was also used in a recent NHP study [14]. Ten healthy, filovirus-negative male cynomolgus macaques (*Macaca fascicularis*) 3-5 years of age and between 4-8 kg were challenged with 1000 PFU of ZEBOV-Makona intramuscularly with the dose divided equally into the left and right quadriceps. Animals were housed in the BSL-4 laboratory in the Galveston National Laboratory (GNL) and monitored post challenge for clinical signs of disease including temperature, weight loss, behavioral changes, changes in blood count, and blood chemistries.

Sample collection and PBMC isolation

Blood was collected by venipuncture into EDTA tubes. To isolate PBMC, whole blood was centrifuged over Histopaque (Sigma-Aldrich, St. Louis, MO) using AccuSpin Tubes (Sigma-Aldrich, St. Louis, MO) at ~400 x g for 45 minutes, room temperature with no brake. PBMC were counted on a TC20 Automated Cell Counter (Bio-Rad, Hercules, CA).

Magnetic bead cell separation

PBMC underwent sequential separations using magnetic microbeads (Miltenyi Biotec, San Diego, CA) as described in **Figure 3.1**. PBMC were initially stained with anti-CD2 microbeads to isolate T and NK cells. The CD2 negative cell population was then stained with anti-CD20 microbeads to isolate the B-cell population. The CD20 negative fraction was collected and stained with CD14 microbeads to isolate monocytes. Purity of the fractions was confirmed using flow cytometry (**Table 3.1**). All samples were acquired

using a BD FACS Canto-II (Becton Dickinson Biosciences, San Jose, CA) using BD FACS Diva software. Live cells were identified by FSC and SSC and a minimum of 50,000 events were collected for each sample. Data was analyzed using FlowJo Analysis Software (FlowJo LLC, Ashland, OR) and Prism Software (GraphPad Software, Irvine, CA). Only samples with purity above the cutoff of 60% were included in the analysis. The number of samples available at each time point were as follows: monocyte samples on days 0 (n=5), 1 (n=4), 2 (n=4), 3 (n=2), 4 (n=2), 6 (n=3) post infection; T cell samples on days 0 (n=7), 1 (n=4), 2 (n=4), 3 (n=2), 4 (n=2), 5 (n=2), 6 (n=3) post infection; and B cell samples on days 0 (n=2), 1 (n=4), 2 (n=4), 6 (n=4) post infection. Unfortunately, a sufficiently pure dendritic cell (DC) population could not be obtained, therefore in this study we focused on monocytes, T cells and B cells.

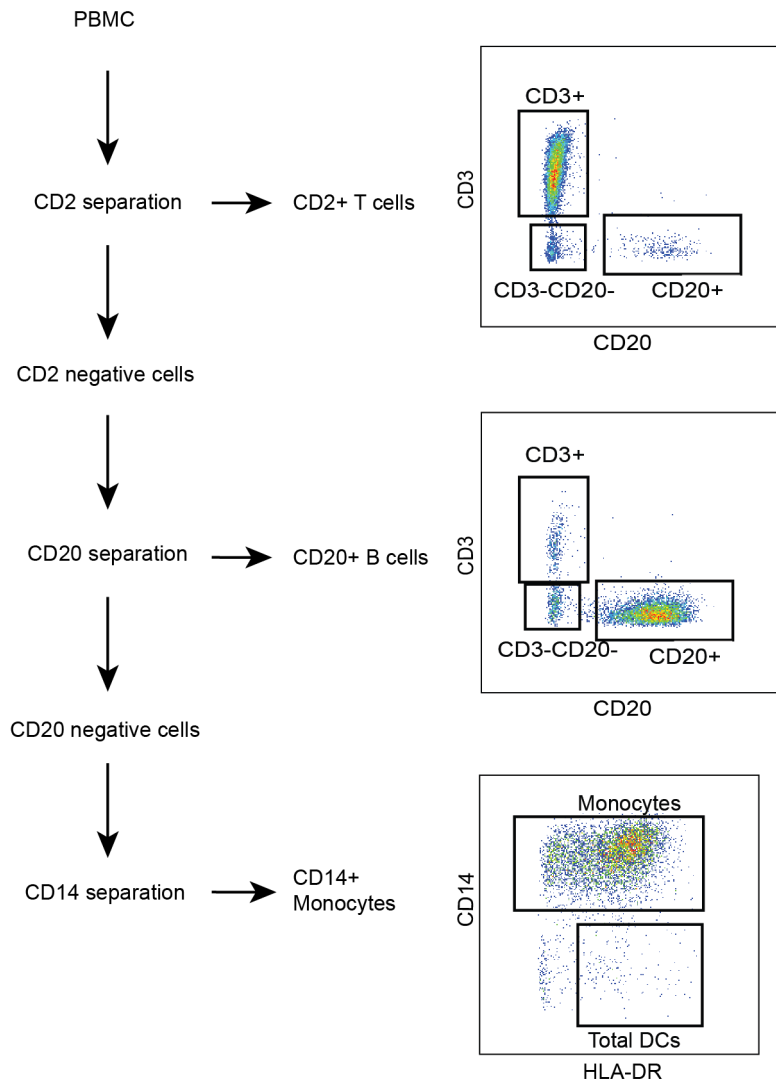


Figure 3.1. Cell subset separation strategy. PBMC were incubated with anti-CD2 microbeads in order to first isolate T and NK cells. The CD2 negative fraction was then incubated with anti-CD20 microbeads to isolate the B cell population. The CD20 negative fraction was collected and stained with CD14 microbeads to isolate monocytes. All cell fractions were confirmed for purity using flow cytometry staining for CD3, CD20, CD14, and HLA-DR.

Days post infection	d0	d1	d2	d3	d4	d5	d6
Monocytes	70.5	80.6	88.5	73.9	77.9	NA	73.5
T cells	11.76	8.43	1.67	18.15	6.93	NA	3.19
B cells	5.89	4.17	4.81	2.81	7.13	NA	9.36
Dendritic Cells	6.30	5.70	5.06	4.42	4.04	6.47	6.92
T cells	87.6	89.7	85.6	89.9	85.1	71.8	82.1
Monocytes	1.56	0.63	0.89	0.43	1.56	11.57	4.09
B cells	3.04	2.78	4.04	0.5	2.43	5.84	6.11
Dendritic Cells	2.00	1.66	1.73	2.52	2.68	4.74	1.07
B cells	65.2	65.7	72.8	NA	NA	NA	77.4
Monocytes	21.34	18.53	6.65	NA	NA	NA	7.37
T cells	3.08	2.72	3.69	NA	NA	NA	4.76
Dendritic Cells	4.45	5.75	4.12	NA	NA	NA	2.95

*NA: Samples not available

Table 3.1. Average cell subset purity (%) per day

Library preparation for RNA-Seq

RNA from each cell subset was isolated using Zymo Research Direct-zol RNA mini-prep (Zymo Research, Irvine, CA) per manufacturer's instructions. RNA concentration and integrity was determined using an Agilent 2100 Bioanalyzer (Agilent Technologies, Santa Clara, CA). Ribosomal RNA (rRNA) was depleted using the ClontechRibo-Gone rRNA Removal kit. Libraries were constructed using the Clontech SMARTer Stranded RNA-Seq kit (Takara Bio Inc., Kusatsu, Shiga, Japan). First, rRNA-depleted RNA was fragmented and converted to double stranded cDNA. Adapters were ligated and the ~300 base pair long fragments were then amplified by PCR and selected by size exclusion. Each library was prepared with a unique indexed primer for multiplexing. In order to ensure proper sizing, quantitation, and quality prior to sequencing, libraries were analyzed on the Agilent 2100 Bioanalyzer. Multiplexed libraries were subjected to single-end 100 base pair sequencing using the Illumina HiSeq2500 platform (Illumina, San Diego, CA).

Bioinformatic and statistical analysis

Data analysis was performed with the RNA-Seq workflow module of the systemPipeR package available on Bioconductor [204]. RNA-Seq reads were demultiplexed, quality filtered and trimmed using Trim Galore with an average phred score cutoff of 30 and minimum length of 75bp. Three base pairs from the 5' end were trimmed as per Clontech's instruction. Quality reports were generated with the FastQC function. Because the complete genome annotation for *Macaca fascicularis* is not available, the *Macaca mulatta* genome sequence (Macaca_mulatta.MMUL_1.dna.toplevel.fa) and annotation file from

Ensembl (Macaca_mulatta.MMUL_1.78.gtf) was used. In order to determine the level of viral transcription at different time points, the ZEBOV variant Makona genome (H.sapiens-wt/GIN/2014/Makona- Gueckedou-C07) from Virus Pathogen Resource was adjoined to the *Macaca mulatta* reference. ZEBOV open reading frames (ORFs), intergenic regions (IGRs) and leader and trailing sequences were defined based on the ZEBOV-Makona genome annotation GTF file: NP (470-2689), VP35 (3129-4151), VP40 (4479-5459), GP (6039-8068), VP30 (8509-9375), VP24(10345-11100), L (11581-18219), Leader (1-469), IGR_NP_VP35 (2690-3128), IGR_VP35_VP40 (4152-4478), IGR_VP40_GP (5460-6038), IGR_GP_VP30 (8069-8508), IGR_VP30_VP24 (9376-10344), IGR_VP24_L (11101-11580), and Trailing (18220-18959). RNA-Seq reads were mapped with the alignment suite Bowtie2/Tophat2 against a reference genome containing both *Macaca mulatta* and ZEBOV-Makona genome sequences. Raw expression values in the form of gene-level read counts were generated with the *summarizeOverlaps* function, counting only the reads overlapping exonic regions of genes, and discarding reads mapping to ambiguous regions of exons from overlapping genes. Normalization and statistical analysis of differentially expressed genes (DEGs) was performed using the *edgeR* package, which normalizes reads by the trimmed mean of M values (TMM) method. RNA-Seq data presented in this article were submitted to the National Center for Biotechnology Information Sequence Read Archive (BioProject accession PRJNA412109). DEGs were defined as those with a fold change ≥ 2 and a false discovery rate (FDR) corrected p-value ≤ 0.05 compared to 0 DPI. Only protein coding genes with human homologs and an average 5 reads per kilobase of transcript per million mapped reads (RPKM) were included for

further analysis. Reads mapping to the ZEBOV-Makona genome were normalized as RPKM. Heatmaps, venn diagrams, and a violin plot were generated using R packages gplot, DESeq2, VennDiagram, and ggplot2. Heatmaps for gene expression represent the absolute normalized expression (RPKM); range of colors is based on scaled and centered RPKM values of the entire set of genes (red represents increased expression while blue represents decreased expression). Heatmaps for functional enrichment of DEGs represent $-\log_{10}(\text{FDR-corrected p-value})$; range of colors is based on the lowest and highest $-\log_{10}(\text{FDR})$ values for the entire set of terms; the number of DEGs mapping to each functional enrichment term each day is listed within each box; blank boxes represent no statistical significance.

DEGs detected in monocytes 6 DPI were compared to the transcriptional profile of monocyte-derived macrophages (MDMs) and macrophages differentiated from human induced pluripotent stem cells following 6-hour lipopolysaccharide (LPS) stimulation [232] using R package VennDiagram.

Functional enrichment

Functional enrichment of DEGs was done to identify clusters of genes mapping to specific biological pathways, specifically Gene Ontology (GO) terms and Diseases (by Biomarkers) using MetaCore™ (Thomson Reuters, New York, NY). Significant functional enrichment terms were defined as those with a false discovery rate (FDR) corrected p-value

≤ 0.05 . Since this software requires human gene identifiers for analysis, rhesus DEGs were mapped to human homologs using BioMart.

Results

Monocytes support ZEBOV-Makona replication and are major contributors of inflammation

To investigate the impact of ZEBOV-Makona infection within monocytes, we determined longitudinal changes in gene expression profiles using RNA-Seq and compared them to our earlier analysis of total PBMC Chapter 2 [193]. The average purity of monocytes analyzed at the various time points was >70% (**Table 3.1**). Transcriptional changes correlated with ZEBOV reads (**Figure 3.2A**). We further investigated the total number of viral reads mapping to each ZEBOV ORF and IGR within purified monocytes (**Figure 3.2B**). At 6 DPI, viral transcripts were abundant with ORF L and the trailing end region having the lowest average RPKM values, while ORFs GP and NP had the highest. Based on Euclidean distances, the viral transcript profile in monocytes was most comparable to that observed in PBMC (**Figure 3.3**).

A small number of DEGs was detected 3 DPI within monocytes, which slightly increased 4 DPI, and then considerably increased 6 DPI (**Figure 3.2A**). DEGs detected 3 and 4 DPI enriched to GO terms associated with innate immunity such as type I IFN signaling pathways (**Figure 3.4A-B**). Only 2 DEGs were downregulated 3 DPI: *HBB* and transcription factor *JUN*, which plays an important role in inflammation [233] (**Figure 3.4C**). The 6 DEGs upregulated only 4 DPI included: *FAM3C*, which encodes Interleukin-Like EMT inducer; *HIP1R*, a component of clathrin-coated vesicles;

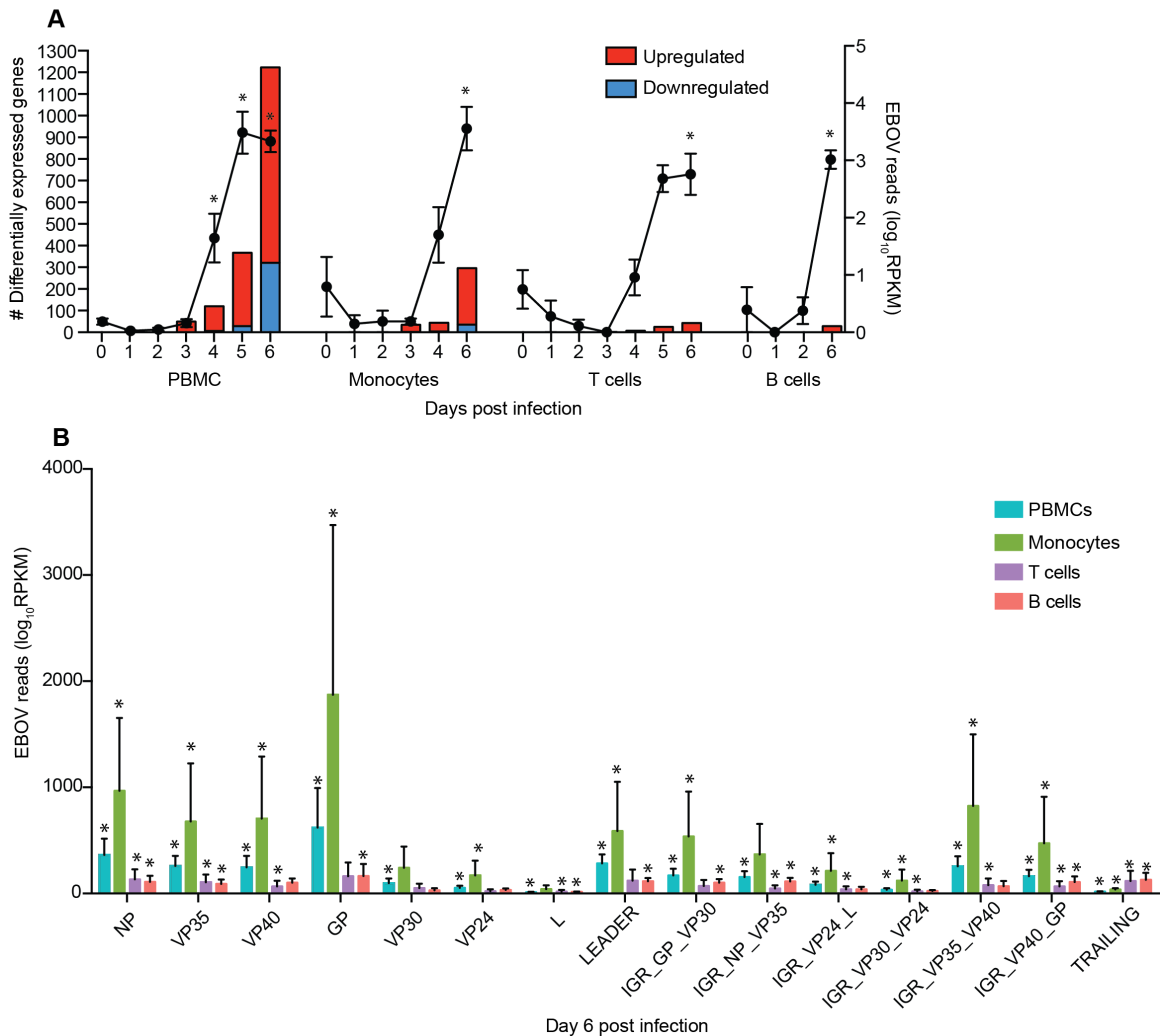


Figure 3.2. Monocytes support ZEBOV-Makona replication and are major contributors of inflammation. (A) Bar graph depicts number of protein coding differentially expressed genes (DEGs; defined as those ≥ 2 fold change and FDR corrected p-value ≤ 0.05 compared to 0 DPI) that have human homologues (red indicates upregulated while blue indicates downregulated DEGs) in PBMC, monocytes, T cells and B cells. Line graph represents number of normalized viral transcripts (RPKM); mean \pm SEM are shown; * p ≤ 0.05 compared to day 0. (B) RPKM normalized RNA-Seq reads mapping to each ZEBOV open reading frame (ORF), intergenic region (IGR), as well as leader and trailing sequences 6 DPI within PBMC, monocytes, T cells and B cells. FDR adjusted p-value was obtained following *EdgeR* analysis; mean \pm SEM are shown; * p ≤ 0.05 compared to day 0.

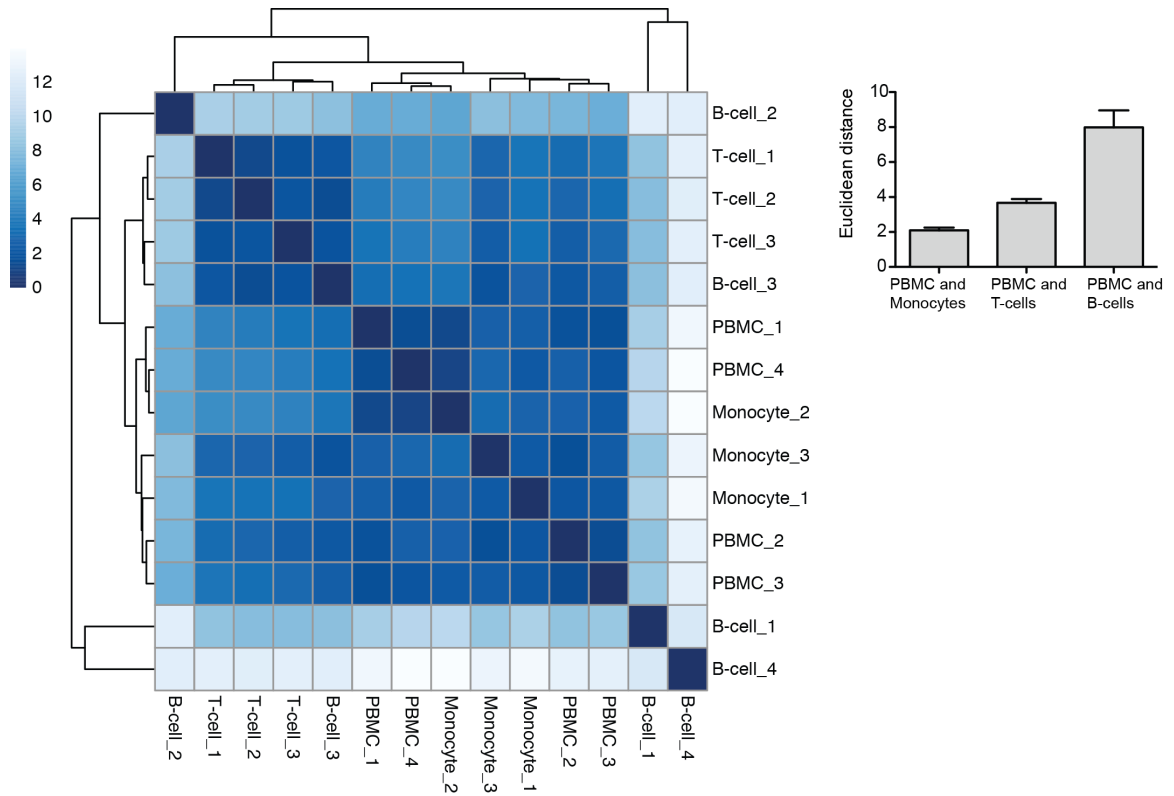


Figure 3.3. Comparison of viral transcript profiles detected in each cell subset. Heatmap showing the Euclidean distances of viral reads detected among each cell subset at 6 DPI calculated from log₂ transformation; bar graph depicts average Euclidean distance; mean ± SEM are shown.

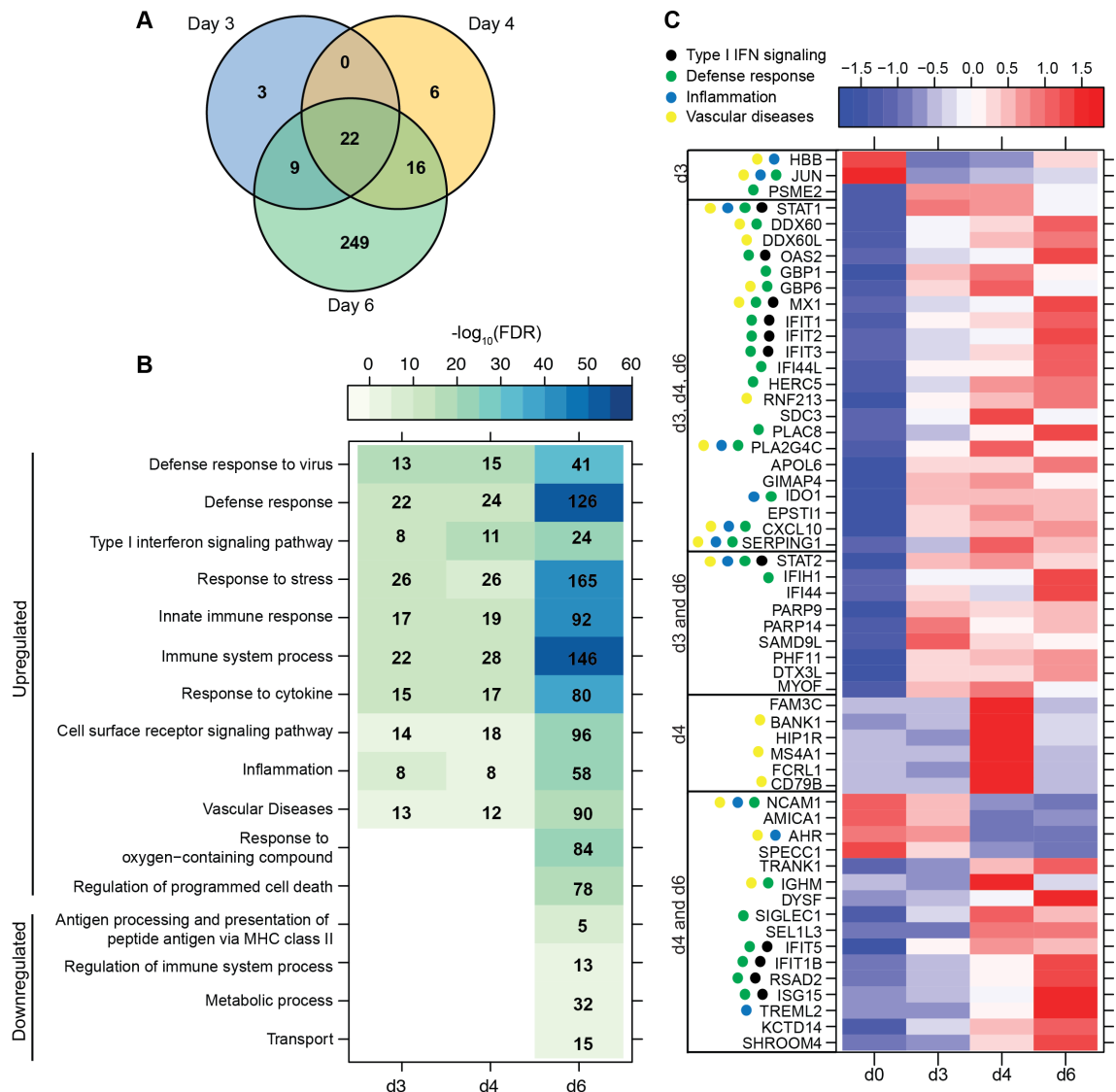


Figure 3.4. ZEBOV-Makona infection induces expression of genes involved in defense response and type I IFN signaling in monocytes. (A) 3 way Venn diagram displaying overlap between DEGs detected 3, 4 and 6 DPI in purified monocytes. (B) Heatmap representing functional enrichment of DEGs 3, 4 and 6 DPI; color intensity represents the statistical significance (shown as negative \log_{10} of the FDR-corrected p-value); range of colors is based on the lowest and highest $-\log_{10}(\text{FDR})$ values for the entire set of terms; the number of DEGs mapping to each functional enrichment term each day is listed within each box; blank boxes represent no statistical significance. (C) Heatmap representing gene expression (shown as absolute normalized RPKM values) of all DEGs detected 3 and 4 DPI; genes enriching to GO or disease term are indicated by colored dot; range of colors is based on scaled and centered RPKM values of the entire set of genes (red represents increased expression while blue represents decreased expression); each column represents the median RPKM values for each DPI.

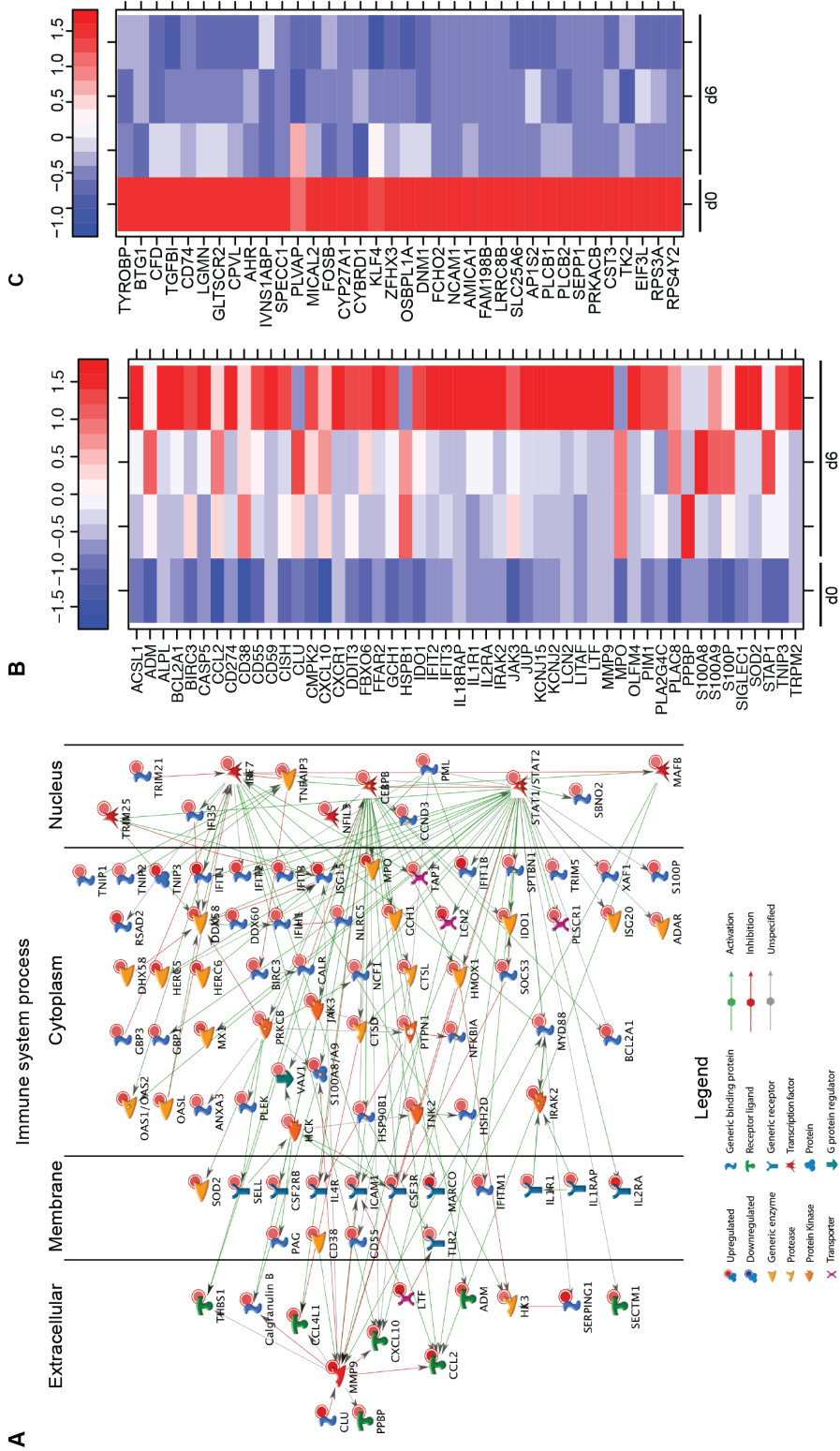
signaling adaptor *BANK1*; and receptor *FCRL1* (**Figure 3.4C**). Although these genes are mostly known to be expressed in B-cells, they are also expressed in activated monocytes and macrophages [234-238]. Their increased expression correlated with increased frequency of CD16⁺ nonclassical monocytes 4 DPI (**Figure 2.4B**).

Most of the 22 DEGs that were upregulated throughout infection in monocytes (**Figure 3.4A**) were interferon stimulated genes (ISGs) important in antiviral defense [66], notably *GBP1*, *OAS2*, *MX1* and *IFIT1-3* (**Figure 3.4C**). Also upregulated, were *STAT1* and 2, which serve as transcriptional activators of ISGs [66]. Other DEGs of note that were upregulated throughout infection include the monocyte chemoattractant *CXCL10* and the C1 inhibitor *SERPING1*. Additional ISGs such as *IFIT5*, *IFIT1B*, and as well as genes involved in receptor-mediated endocytosis such as *SIGLEC1* [239] were upregulated 4 and 6 DPI. In contrast, expression of adhesion molecules *NCAMI*, *AMICA* and *SPECCI* and transcription factor *AHR* were downregulated 4-6 DPI (**Figure 3.4C**).

A large number of DEGs were identified in monocytes 6 DPI. Upregulated DEGs enriched to GO terms related to defense response/inflammation, oxidative stress, and apoptosis (**Figure 3.4B**). Of the 146 DEGs that enriched to GO term “Immune system process”, 98 directly interacted with each other (**Figure 3.5A**). Expression of these genes was regulated by *STAT1*, *STAT2*, *IRF7*, and *CEBPB*. Downstream mediators of these transcription factors are involved in: leukocyte recruitment e.g. *CCL2* and *CCL4L1* [240, 241]; signaling e.g. *IRAK2* [242] and *CSF3R*; and pathogen recognition e.g. *TLR2* and *MYD88*. Other

upregulated genes in this network play a role in: coagulation such as *THBS1* [243]; apoptosis such as *BCL2A1* [244]; response to oxidative stress e.g. *SOD2* [245]; positive regulation of nitric oxide synthesis such as *GCHI* [246]; and vascular integrity e.g. *MMP9* [247]. Upregulated genes that also enriched to “Immune system process” but not included in the network include: *CD274* (PD-L1), which inhibits T-cell activation [248]; neutrophil chemoattractant *IL8* [249]; and monocyte chemoattractant *CCL8* [250]. Notable upregulated genes that play a role in apoptosis and oxidative stress include *DDIT3* [251], *HSPB1* [252] *CASP5* [253], and *BIRC3* [254] (**Figure 3.5B**).

The 36 genes downregulated 6 DPI enriched to metabolic and immune processes (**Figure 3.4B**). Some of the DEGs that enriched to “Antigen processing and presentation of peptide antigen via MHC class II” include *AP1S2*, *DNMI*, *OSBPL1A*, *CD74* (Major histocompatibility Complex, Class II), and *LGMN* (**Figure 3.5C**). We also observed downregulation of transcription factors *AHR*, *FOSB*, and *KLF4*. Finally, genes involved in translation i.e. *EIF3L*, *RPS3A* and *RPS4Y2* were also downregulated (**Figure 3.5C**).



(Previous Page) Figure 3.5. Monocytes contribute significantly to ZEBOV-associated inflammation. (A) Network showing direct interactions between DEGs upregulated 6 DPI in monocytes that enriched to “Immune system process”. **(B)** Heatmap representing gene expression (shown as absolute normalized RPKM values) of DEGs upregulated 6 DPI that enriched to “Regulation of programmed cell death” and “Response to oxygen containing compound” with a fold change ≥ 10.5 ; range of colors is based on scaled and centered RPKM values of the entire set of genes (red represents increased expression while blue represents decreased expression); day 0 is represented by the median RPKM value, while each column represents 1 animal for 6 DPI. **(C)** Heatmap representing gene expression (shown as absolute normalized RPKM values) of all downregulated genes 6 DPI; range of colors is based on scaled and centered RPKM values of the entire set of genes (red represents increased expression while blue represents decreased expression); day 0 is represented by the median RPKM value, while each column represents 1 animal for 6 DPI.

To investigate the association between transcriptional changes detected within monocytes and systemic inflammation, we performed a spearman correlation between plasma levels of cytokines and chemokines and RPKM values of DEGs detected in monocytes 6 DPI. We observed strong correlations ($R \geq 0.8$) between DEGs detected within monocytes 6 DPI and circulating inflammatory cytokines IL1 β (42 DEGs), IL6 (53 DEGs), IFN α (92 DEGs), IL7 (40 DEGs), IFN γ (40 DEGs), IL18 (74 DEGs) and IL4 (45 DEGs) as well as chemokines MIP1 α (110 DEGs), and MCP1 (45 DEGs) (**Figure 3.6**).

ZEBOV-Makona infection induces limited differential gene expression in lymphocytes

To understand the consequence of ZEBOV-Makona infection on the adaptive immune response, we next determined transcriptional changes within T and B cells following challenge. The average purity of T cells and B cells was >80% and >65%, respectively (**Table 3.1**). In contrast to monocytes, limited host and viral transcriptional changes were detected in T cells (**Figure 3.2A** and **Figure 3.7A**). In addition, DEGs detected in T cells were primarily involved in “Type I IFN signaling” (**Figure 3.7B**) and consisted of ISGs that play a role in antiviral immunity i.e. *DHX58*, *GBP1*, *IFIT1/2*, *OAS1-2*, and *MX1* (**Figure 3.7C**). Lastly, *PHF11* and *TREML2*, both of which are involved in T-cell activation [255, 256], were also upregulated 6 DPI. Similarly, we detected a limited

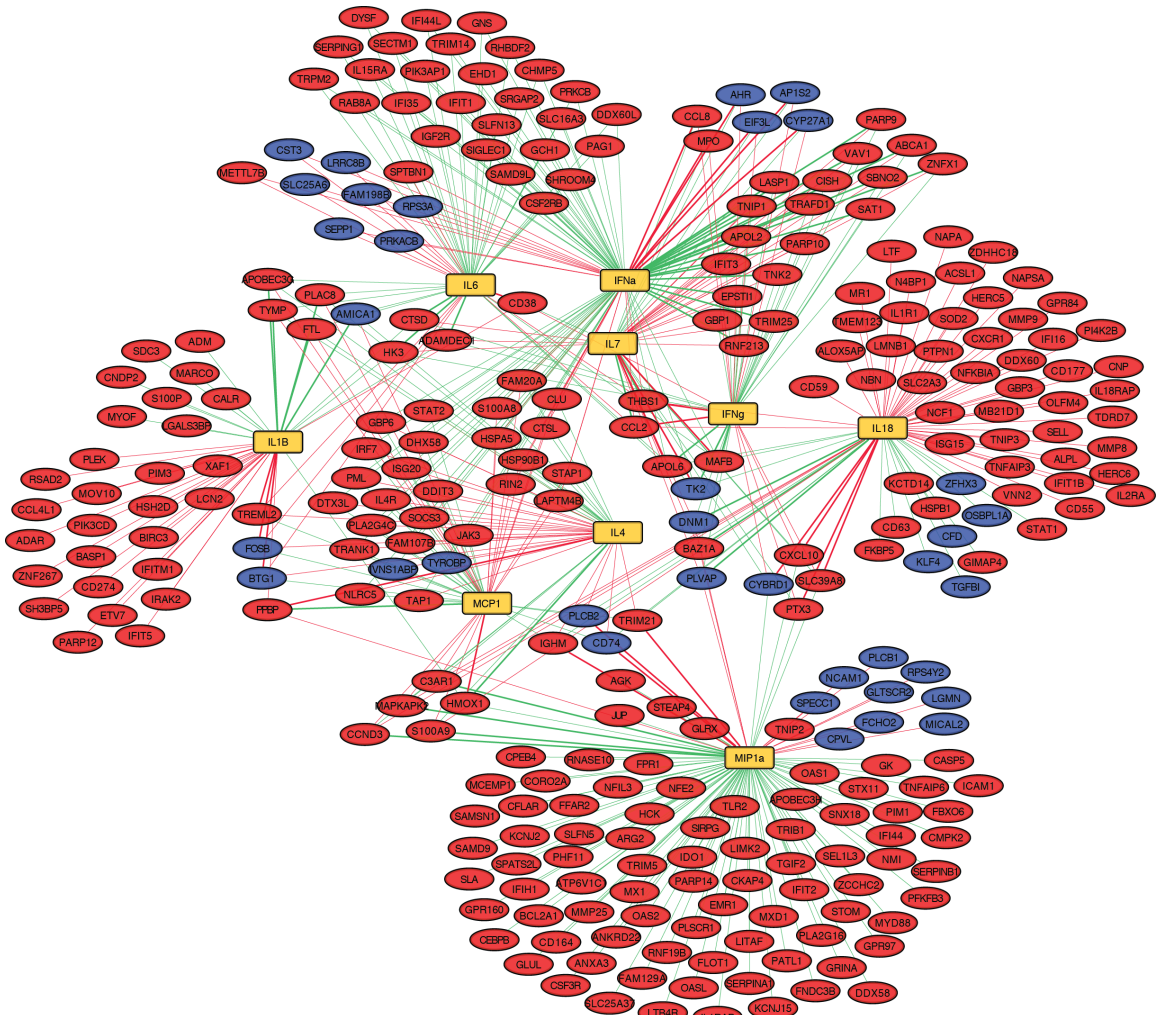


Figure 3.6. Network displaying correlation between gene expression changes in monocytes and plasma levels of immune mediators 6 DPI. Spearman correlation was used to investigate the association between immune mediators and DEGs. Yellow nodes represent immune mediators, blue nodes represent downregulated genes, red nodes represent upregulated genes, edges represent correlations (red indicates negative correlation, green indicates positive correlation). The width of each edge represents correlation strength. Correlations $R \geq 0.8$ are displayed.

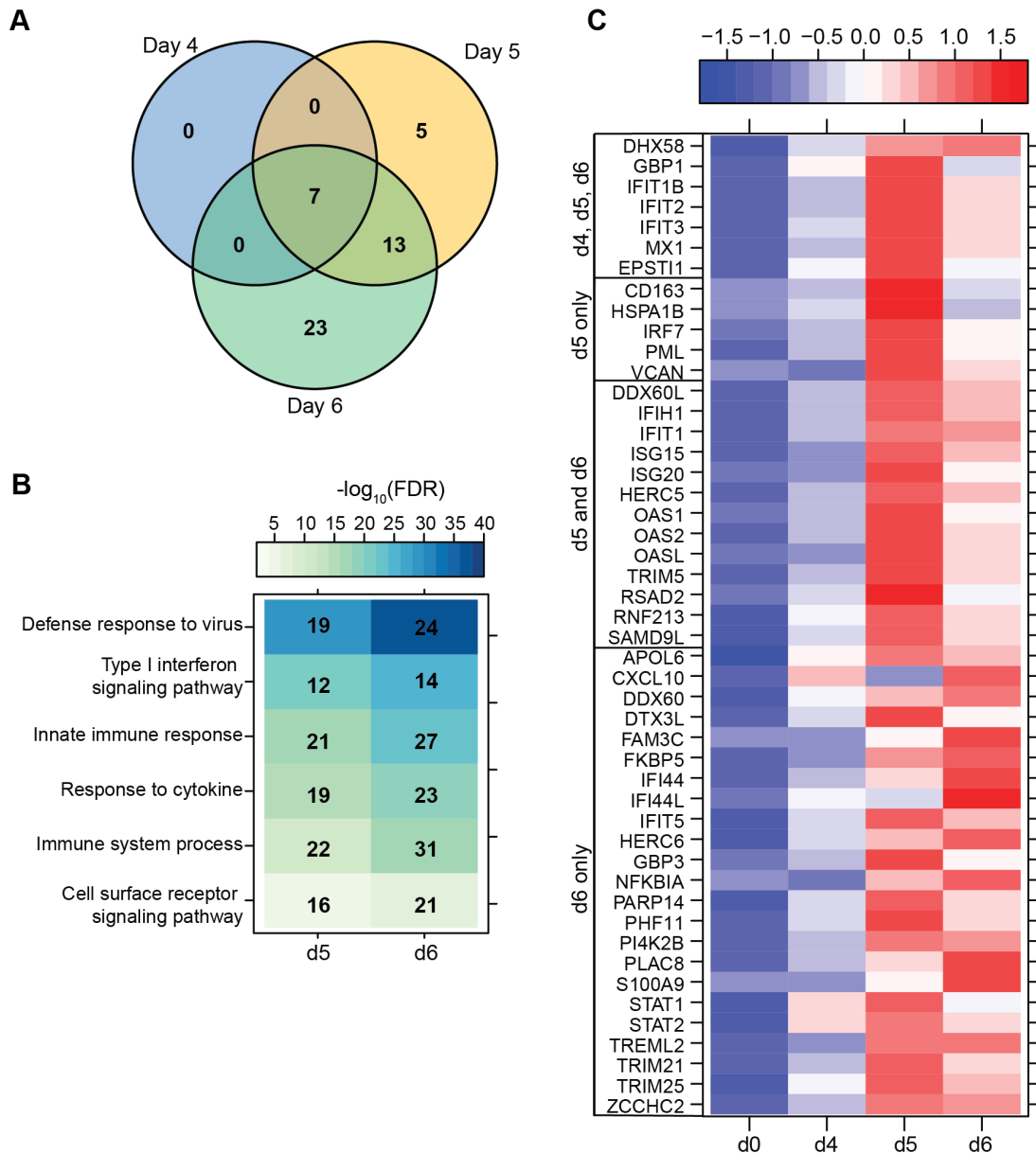


Figure 3.7. ZEBOV-Makona infection induces limited differential gene expression in T-cells. (A) 3 way Venn diagram displaying overlap between DEGs detected 4, 5 and 6 DPI. (B) Heatmap representing functional enrichment of DEGs 5 and 6 DPI; color intensity represents the statistical significance (shown as negative \log_{10} of the FDR-corrected p-value); range of colors is based on the lowest and highest $-\log_{10}(\text{FDR})$ values for the entire set of terms; the number of DEGs mapping to each GO term each day is listed within each box. (C) Heatmap representing gene expression (shown as absolute normalized RPKM values) of all DEGs detected 4, 5, and 6 DPI; range of colors is based on scaled and centered RPKM values of the entire set of genes (red represents increased expression while blue represents decreased expression); each column represents the median RPKM values for each DPI.

number of gene expression changes (31 DEGs) in B cells 6 DPI (**Figure 3.2A**), which also enriched to GO terms associated with innate immune defense to viral infection (**Figure 3.8A**) and consisted primarily of ISGs i.e. *DHX58*, *GBP1*, *IFIT1-3*, *5* (**Figure 3.8B**). Analysis of viral transcripts revealed that ZEBOV ORF and IGR transcripts in T and B cells were 2-12 fold lower compared to monocytes, with the exception of the trailing end region (**Figure 3.2B**). Euclidean distances also indicate that the viral transcript profile in T and B cells was more distant compared to that observed in PBMC (**Figure 3.3**).

Monocytes contribute a significant proportion of host transcriptional changes detected in PBMC

We next compared gene expression profiles of PBMC, monocytes, T cells, and B cells 6 DPI, the time point at which Makona-ZEBOV infection caused the most significant clinical signs and transcriptional changes (Chapter 2; [193]). Principle component analysis of normalized reads across all groups showed that monocytes were transcriptionally more similar to PBMC than T cells and B cells (**Figure 3.9A**). Comparison of all protein coding DEGs among the 4 groups revealed that 20% of DEGs detected in PBMC were also differentially expressed within monocytes. In contrast, the DEGs detected in T cells and B cells accounted for only 3.4% and 2.5% of the DEGs detected in PBMC (**Figure 3.9B**). As expected, the 24 DEGs common to all 4 groups play a role in type I IFN response (**Figure 3.9C**). The 971 genes that were only differentially expressed in PBMC had lower fold changes and their expression did not reach the statistical cutoff of FDR adjusted p-value ≤ 0.05 and average RPKM ≥ 5 in each individual cell subset (**Figure 3.9D**). The 250 DEGs

detected in both monocytes and PBMC enriched to GO terms linked to immunity and cell death (**Figure 3.10A**). Functional enrichment of the 971 genes exclusive to PBMC are involved in similar biological processes as the 250 DEGs found in monocytes related to host defense, innate immune response, and inflammation (**Figure 3.10B**). These data suggest that these DEGs are only significant when transcriptional changes across all subsets are included in the analysis. The 46 DEGs detected exclusively in monocytes 6 DPI mapped to GO terms such as “Innate immune response” and “Antigen processing and presentation of exogenous peptide antigen” and had higher magnitude of expression compared to PBMC, suggesting that their expression was diluted by the inclusion of the additional subsets in PBMC analysis (**Figure 3.10C-D**).

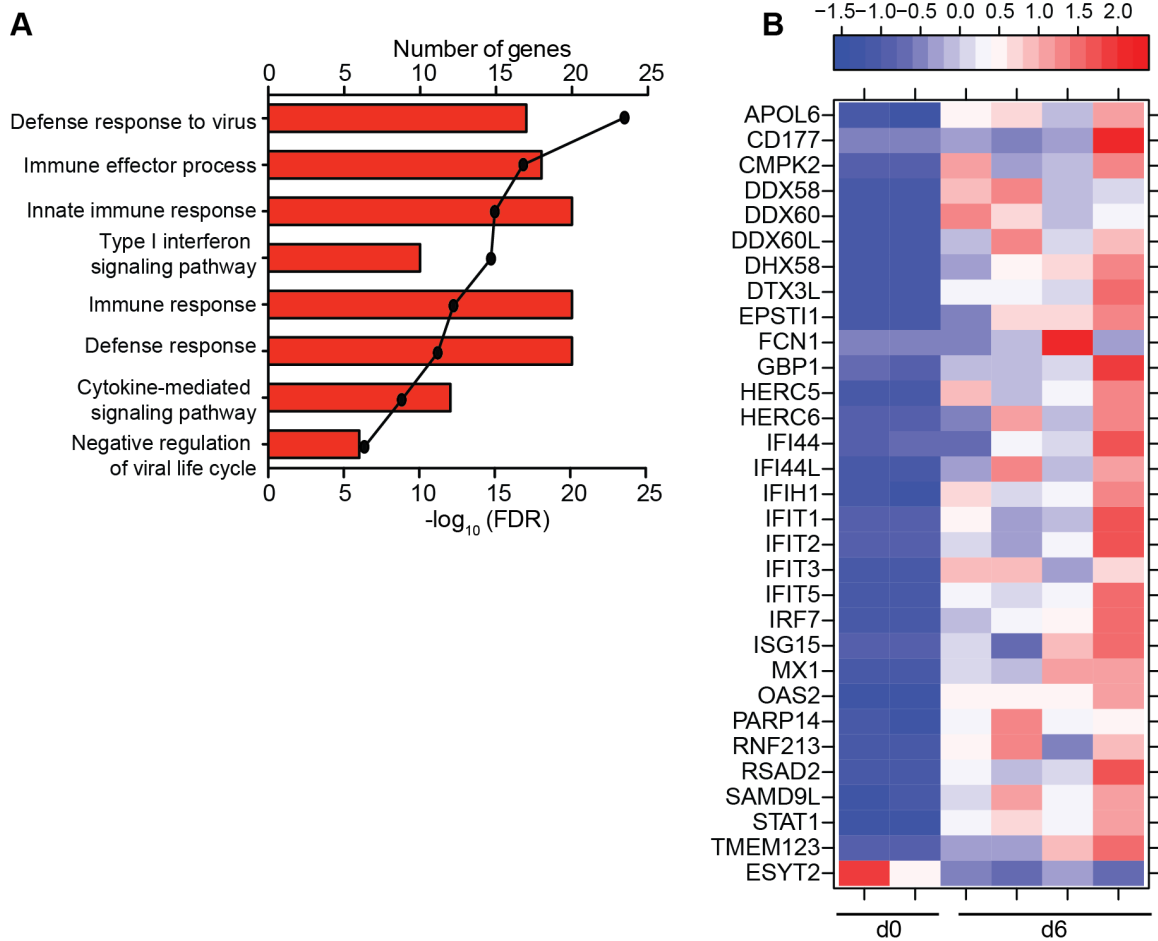


Figure 3.8. ZEBOV-Makona infection induces limited differential gene expression in B-cells. (A) Functional enrichment of upregulated genes detected 6 DPI; horizontal bar graphs represent number of genes that mapped to each GO term listed while line graph represents FDR-corrected p-value. **(B)** Heatmap representing gene expression (shown as absolute normalized RPKM values) of all DEGs 6 DPI; range of colors is based on scaled and centered RPKM values of the entire set of genes (red represents increased expression while blue represents decreased expression); each column represents 1 animal.

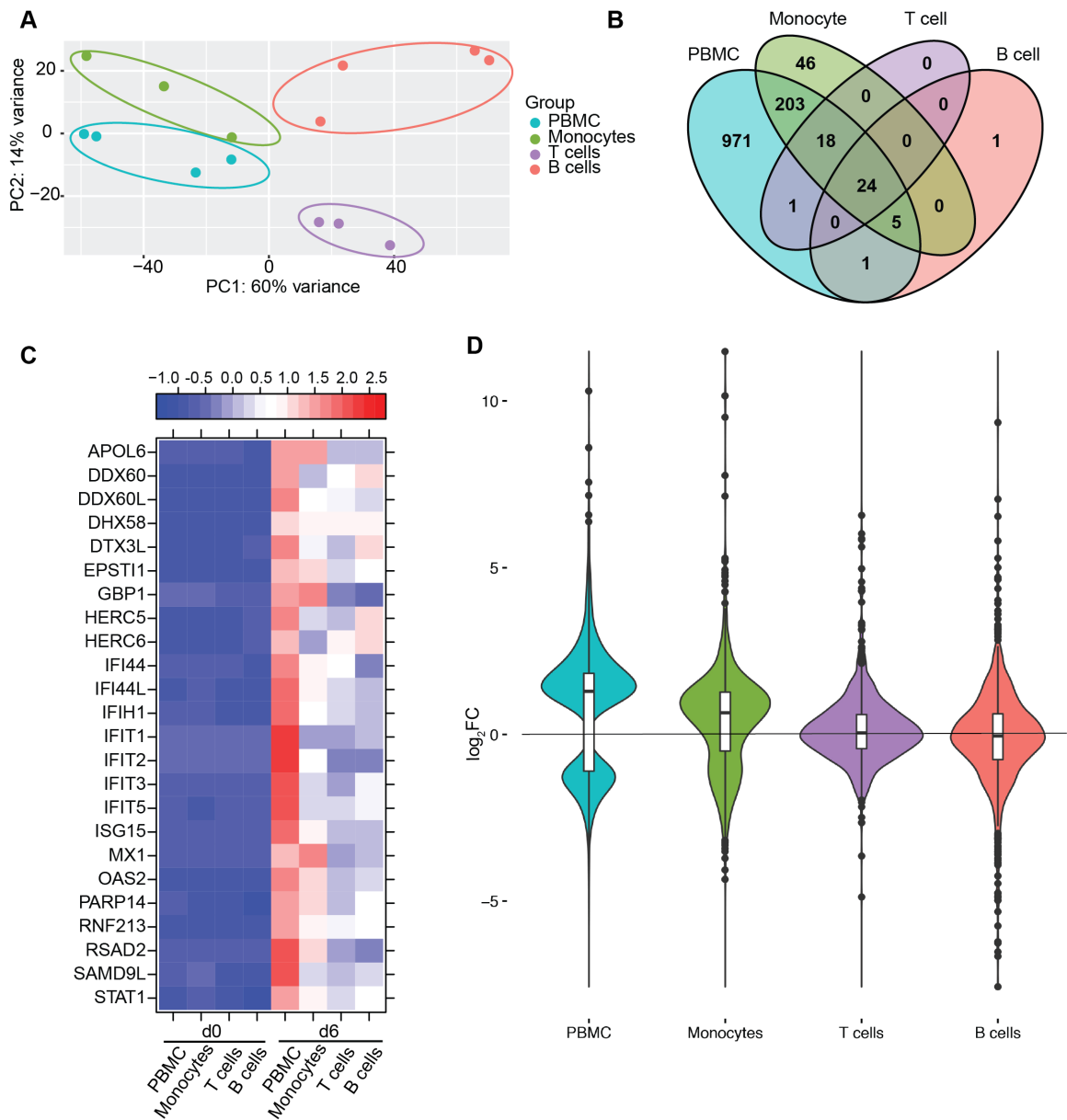


Figure 3.9. Monocytes contribute a significant proportion of transcriptional changes detected in PBMC. (A) Principal component analysis of normalized transcript numbers 6 DPI in PBMC, monocytes, T cells, and B cells. (B) 4 way Venn diagram showing overlap between DEGs detected 6 DPI in PBMC, monocyte, T cells, and B cells. (C) Heatmap representing gene expression (shown as absolute normalized RPKM values) of the 24 DEGs detected in PBMC as well as purified monocytes, T and B cells 6 DPI; range of colors is based on scaled and centered RPKM values of the entire set of genes (red represents increased expression while blue represents decreased expression); each column represents the median RPKM values on each day for each subset. (D) Violin plot of the log₂FC of 971 DEGs that were exclusively detected in PBMC within each cell subset.

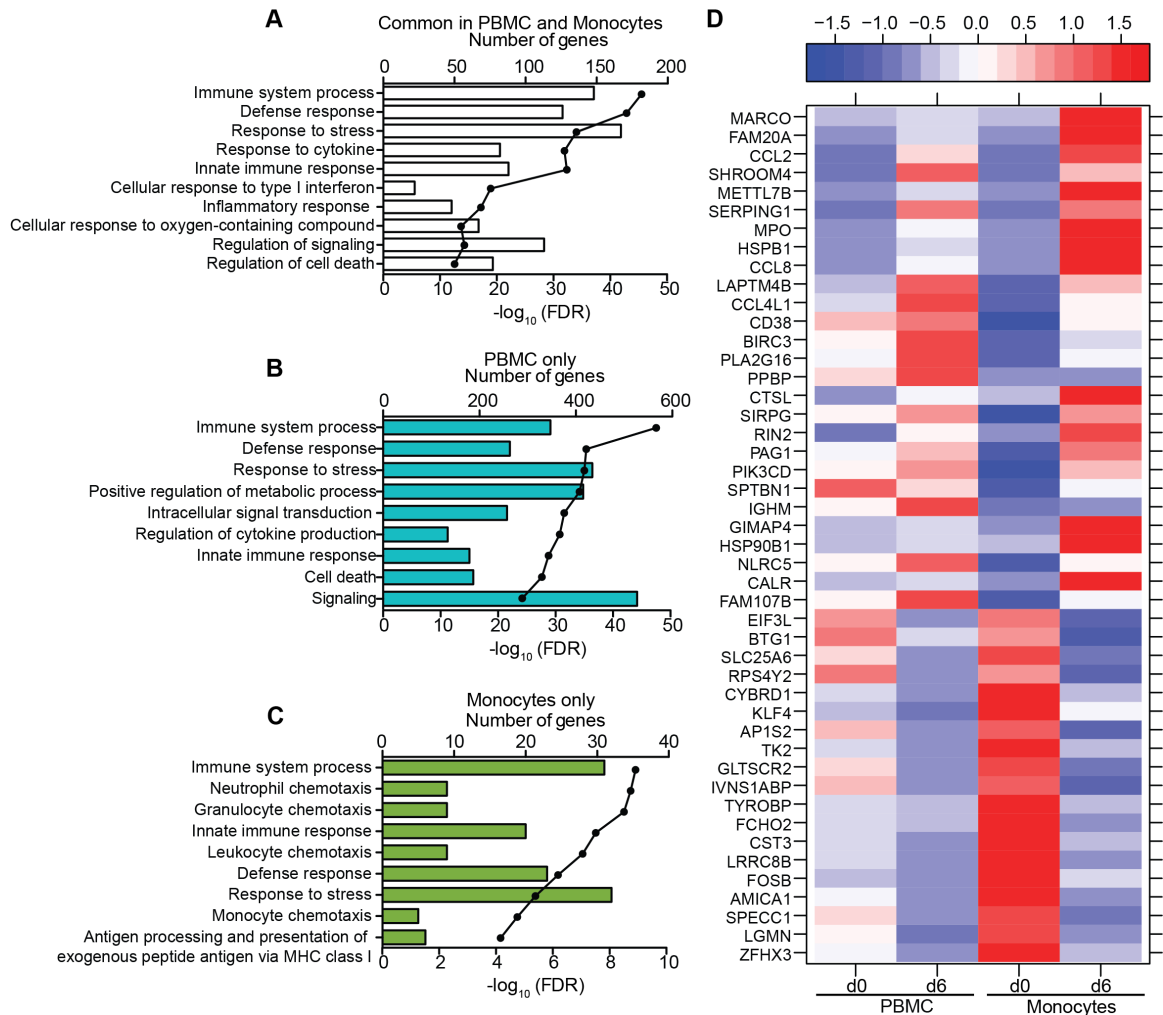


Figure 3.10. Comparison of transcriptional profiles between PBMC and monocytes 6 DPI. (A-C) Functional enrichment of DEGs detected in both monocytes and PBMC (A), PBMC only (B), or monocytes only (C); horizontal bar graphs represent number of genes that mapped to each GO term listed while line graph represents FDR-corrected p-value. (D) Heatmap representing gene expression (shown as absolute normalized RPKM values) of the 46 DEGs that were only detected in monocytes 6 DPI; corresponding RPKM values in PBMC are shown for comparison; range of colors is based on scaled and centered RPKM values of the entire set of genes (red represents increased expression while blue represents decreased expression); each column represents the median RPKM values on each day for each subset.

Discussion

In this manuscript, we report the first *in vivo* longitudinal analysis of viral and host transcriptional changes in purified monocytes, T cells, and B cells isolated from cynomolgus macaques following ZEBOV-Makona infection. The susceptibility of monocytes to ZEBOV infection has been controversial. Some *in vitro* studies showed that filoviruses (MARV, ZEBOV) can replicate in both primary monocytes and monocyte-derived macrophages with similar virus growth kinetics [76, 78, 79], whereas other *in vitro* studies reported delayed ZEBOV entry in undifferentiated monocytes compared to macrophages [229]. Similarly, PMA-naïve THP-1 cells were resistant to virus like particles (VLP) pseudotyped with ZEBOV-GP and become permissive only following differentiation [229]. Our data strongly suggest circulating blood monocytes are permissive to ZEBOV replication *in vivo* given the significant increase in ZEBOV reads 6 DPI. Furthermore, as previously reported in Vero E6 cells, NP was one of the most transcribed genes, whereas L was the least transcribed [47]. These observations are in line with earlier studies reporting viral antigens within DC and monocytes in draining lymph nodes following intramuscular challenge with ZEBOV [58]. In support of the ability of monocytes to permit viral replication, genes involved in receptor-mediated endocytosis 4 DPI (*SIGLEC1* and *HIP1R*) as well as Cathepsin L, which plays a role in ZEBOV-GP mediated entry [257], were upregulated 6 DPI.

DEGs were detected as early as 3 DPI in monocytes, confirming they are amongst the early targets of ZEBOV infection [58]. Although we did not detect increased transcripts of

IFN α/β within monocytes, we saw increased expression of ISGs (e.g. *IFIT1-4*, *OAS1-2*, *OASL*, *RSAD2*, *ISG15*, and *GBP1*). Similarly, ISGs (*IFIT1-2*, *GBP1*, *OASL*) have been detected in monocyte-derived macrophages 6 hours post *in vitro* infection with ZEBOV-Mayinga (ZEBOV strain isolated in 1976) in the absence of increased IFN α/β expression [258]. A possible reason for elevated ISGs in our study is that monocytes may be responding to low levels of IFN α/β secreted from non-infected DCs and monocytes that are activated by viral debris, such as “shed” GP [217]. Moreover, it has been previously shown that ZEBOV virion binding mediated by GP is responsible for early macrophage transcriptional responses before the detection of viral replication [258]. A second possible explanation is that the increased expression of ISGs is independent of the activation of canonical type I IFN signaling. Pulit-Penalosa et al. reported the upregulation of *OAS1a*, *OAS1b*, *IRF1*, and *IRF7* in STAT1^{-/-}, STAT2^{-/-}, and IFN α/β receptor^{-/-} mouse embryonic fibroblasts infected with West Nile Virus [259], indicating that an alternative activation mechanism exists for inducing ISG expression in the absence of type I IFN signaling.

We observed the most transcriptional changes in ZEBOV-Makona infected monocytes 6 DPI. A large number of genes upregulated 6 DPI are important for inflammatory responses such as *CXCL10*, *SERPING1*, *PPBP*, *IL8*, *CSF3R*, *IL1R1*, *MYD88*, *IRAK2*, and *NFKB1A*. The increased expression of chemokines *CCL2*, *CCL4L1*, and *CCL8* may be important for the recruitment of additional monocytes and dendritic cells to sites of infection allowing ZEBOV to disseminate. Furthermore, additional analysis revealed a strong association between DEGs detected in monocytes 6 DPI to circulating levels of inflammatory immune

mediators including IFN α , IL-6, MIP-1 α , and MCP-1 (CCL2). Overall, there was strong agreement between the type of association (positive or negative) with immune mediators and observed changes in gene expression. For instance, expression of most ISGs were positively associated with IFN α . Although some genes were predicted to be negatively regulated by IL1 β and IL18, their expression increased, suggesting that they are positively regulated by other mediators not included in this analysis.

Expression of genes involved in apoptosis (*OLFM4*, *BCL2A1*, *CASP5*, and *BIRC3*) and unfolded protein response (*DDIT3*, *FBX06*, *HSPB1*, and *HSPA5*) were significantly increased. Interestingly, HSPB1 and HSPA5 proteins have been identified as ZEBOV associated host factors, and targeting of HSPA5 *in vivo* using PMOs in mice before challenge increased survival rates [137, 138]. Additionally, we identified an increase in transcripts associated with the production of reactive nitric/oxygen species (*GCHI* and *SOD2*) and vascular function (*ADM*, *MMP9*, *THBS1*, and *SERPINA1*). This is consistent with documented reports of increased nitric oxide in plasma of fatal cases compared to patients who survived [82]. Furthermore, increased expression of *MMP9*, as well as other metalloproteinase genes, in the spleen of mice challenged with mouse adapted (MA)-ZEBOV have been associated with lethality [260]. Interestingly, we did not detect changes in tissue factor (TF) transcripts, which has previously been reported to increase in lymphoid macrophages collected from ZEBOV challenged NHPs [58]. However, TF is produced by tissue macrophages, therefore transcriptional analysis of circulating monocytes may have precluded us from observing changes in TF. In line with a recent study that revealed

increased numbers of T cells expressing inhibitory molecule PD-1 in ZEBOV-Makona infected cases [121], we detected an upregulation of *CD274 (PD-L1)*, which inhibits TCR-mediated activation. Although it did not reach our statistical cutoff, we did detect an increase in inhibitory molecules *PDI*, *CTLA4* and *TIM3* 6 DPI in T cells (**Figure 3.11**). In contrast, genes associated with antigen processing and presentation (*APIS2*, *OBPL1*, *CD74*, *LGGMN*) were downregulated. Collectively, these data suggest that infected monocytes and macrophages are likely to be one of the major drivers of excessive inflammation during ZEBOV infection and provide insight into the failure of initiating an adaptive immune response. We also detected a downregulation of genes associated with translation, including genes encoding for translation initiation factors and ribosomal proteins, a strategy that may be employed by the host to limit ZEBOV replication and spread.

Our observations differ from an *in vitro* study by Wahl-Jensen et al. where they identified 88 DEGs in macrophages within the first six hours after ZEBOV-Mayinga infection [258]. The earlier detection of DEGs in the Wahl-Jensen study correlates with the faster onset of clinical symptoms seen after Mayinga infection compared to Makona [14]. Additionally, the earlier detection of DEGs could be due to the high multiplicity of infection used *in vitro* that may not be reached until later time points during *in vivo*

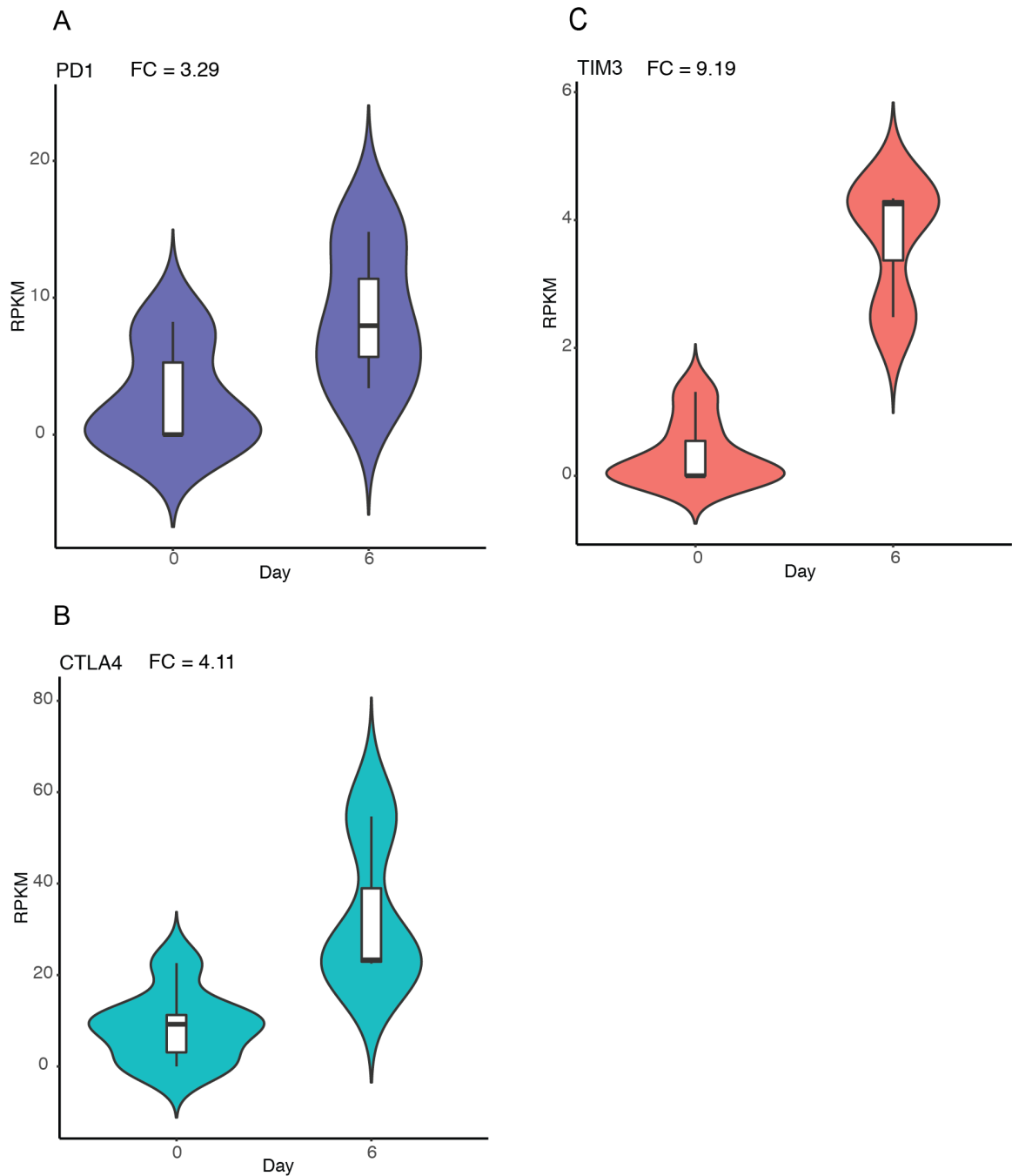


Figure 3.11. Expression of T cell activation inhibitors in purified T cells 6 DPI. (A-C) Violin plot of RPKM values 0 and 6 DPI of *PD1* (A), *CTLA4* (B) and *TIM3* (C). Fold change (FC) at 6 DPI relative to 0 DPI is shown.

infection. Of the 88 DEGs identified in the Wahl-Jensen study, 20 were common with our data set including genes involved in: apoptosis (*TNFAIP3*, *BIRC3*); immune defense, inflammation, and chemotaxis (*TNFAIP6*, *TX3*, *IL8*, *CCL8*, *PPBP*, *TRIM25*, and *IL15RA*); adhesion (*ICAM1*); oxidative stress (*SOD2*, *GCHI*); and ISGs (*IFIT1-2*, *OASL*, *GBP1*). In line with our findings, a recent study by Liu and Speranza et al. showed that patients who succumbed to ZEBOV-Makona infection had a stronger upregulation of acute phase responses and an increased abundance of ISG transcripts compared to survivors [261]. Moreover, longitudinal transcriptomic analysis in peripheral blood from a surviving male health care worker exposed to ZEBOV during the 2013-2016 ZEBOV-Makona epidemic revealed that transcripts that positively correlated with viremia enriched to GO terms associated with activation of antiviral responses (including type I IFN signaling), inflammation, oxidative stress, DNA damage and cell death [262]. Additionally, transcripts with a positive correlation with D-dimer levels and negative correlation with platelet levels functionally enriched to processes associated with macrophage and neutrophil recruitment, macrophage death, antiviral response and phagocytosis [262].

Additional bioinformatics analysis revealed that 62% of DEGs detected within monocytes 6 DPI were shared with the transcriptional changes in monocyte-derived macrophages (MDMs) and macrophages differentiated from human induced pluripotent stem cells (IPSDMs) following 6 hour LPS stimulation (**Figure 3.12A**) [232]. These common genes enriched to GO terms associated with inflammation, response to cytokine, and response to type I interferon (**Figure 3.12B**). This observation suggests that ZEBOV infection may

result in monocyte activation. In contrast, the 40% of DEGs that were unique in our data set enriched to wounding, coagulation, hemostasis and response to oxidative stress, which is in line with the development of EVD (**Figure 3.12C**).

In contrast to monocytes, our data indicate that T and B cells are less permissive to ZEBOV replication, as evidenced by the lower number of viral transcripts in lymphocytes. Additionally, the abundance of viral transcripts was comparable among all ZEBOV ORFs, suggesting abortive transcription. This is consistent with previous *in vivo* and *in vitro* reports that show ZEBOV does not replicate within lymphocytes and that lymphocyte apoptosis is likely an indirect result of ZEBOV induced upregulation of negative regulators and inflammatory mediators [42, 76, 230]. The low number of ZEBOV reads detected in T and B cells 6 DPI may be due to increased amounts of circulating fibrin bound to cells and viral particles resulting in viral genome carry-over during cell separation.

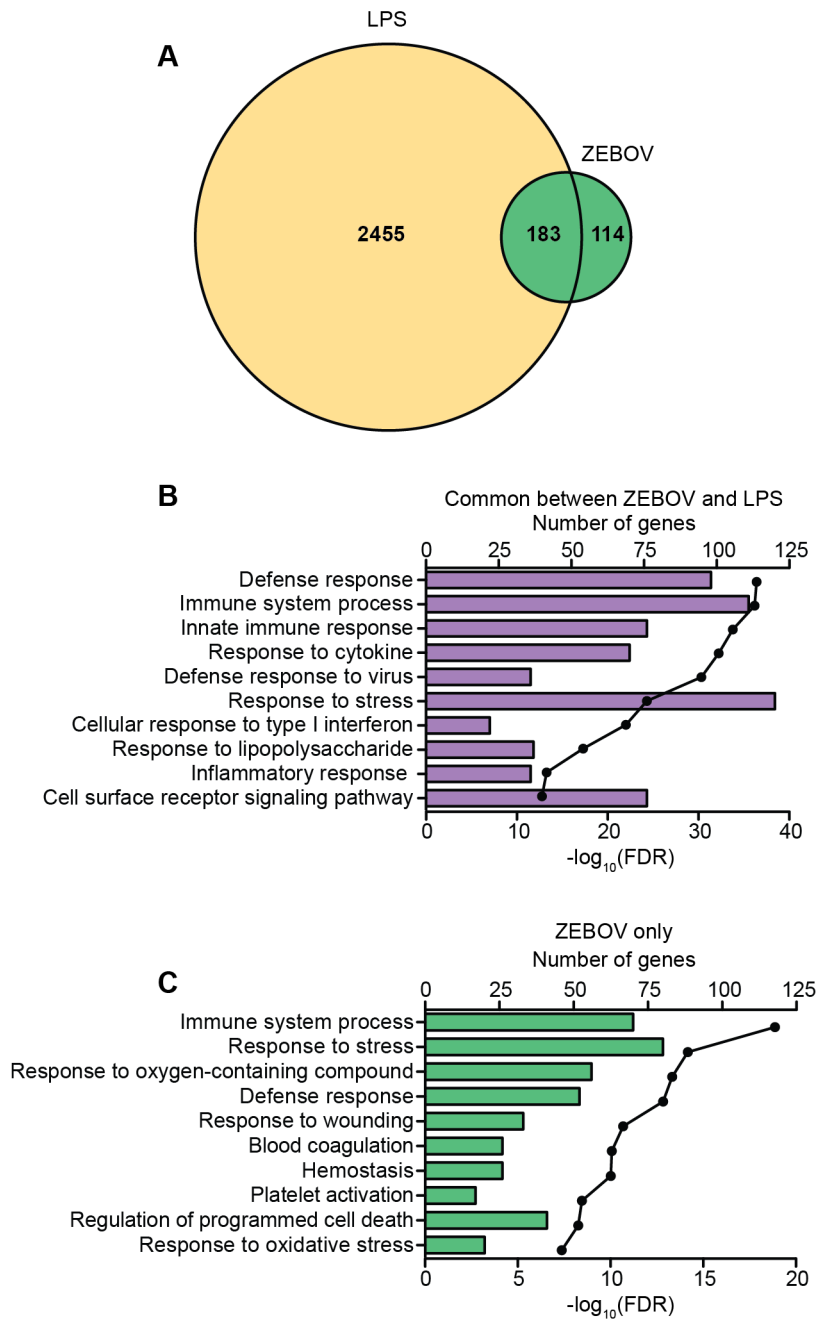


Figure 3.12. Comparison of transcriptional changes in monocytes/macrophages following ZEBOV-Makona infection or LPS stimulation. (A) Venn diagram comparing protein-coding DEGs in monocytes 6 days post ZEBOV-Makona infection and DEGs in macrophages 6 hours post LPS stimulation (29). **(B-C)** Functional enrichment of common DEGs between ZEBOV-Makona infected monocytes and LPS stimulated macrophages **(B)** and DEGs exclusively found in ZEBOV-Makona infected monocytes **(C)**; horizontal bar graphs represent number of genes that mapped to each GO term listed while line graph represents FDR-corrected p-value.

The small number of DEGs detected in T and B cells 6 DPI were overwhelmingly ISGs. This increase in ISG expression within lymphocytes correlates with the large increase in circulating IFN α levels observed 6 DPI. However, fold changes of ISG expression were much lower in lymphocytes compared to monocytes. Previous experiments have demonstrated that IFN α subtypes can activate the JAK/STAT pathway and induce ISGs in T-cells albeit at a lower magnitude compared to DCs [263]. Interestingly, we did not detect changes in the expression of genes that play a role in lymphocyte apoptosis such as *FAS*, *caspase*, and *TRAIL* despite the lymphopenia we observed *in vivo*. In contrast, our previous analysis of transcriptional changes within blood samples isolated from the same animals showed a large decrease in expression of lymphocyte related genes and a robust increase in expression of pro-apoptotic genes [193]. These observations strongly suggest that the absence of such transcripts in this study is due to the fact that T and B cells purified from PBMC, are mostly viable cells not undergoing cell death. Importantly, we were unable to detect any signatures of an adaptive immune response, such as antiviral cytokine IFN γ or cytolytic molecules perforin and granzyme B, needed to clear viral infection and establish memory. A recent study showed production of immunosuppressive mediators IL-10 and PD-L1 is dependent on type I IFN signaling in a mouse model of lymphocytic choriomeningitis virus (LCMV) infection [218, 219]. Therefore, continuous type I IFN response, including sustained expression of ISGs, driven by ZEBOV-Makona infection may inhibit the ability of lymphocytes to develop into an effective defense response. One limitation in our study was the low purity of B cells isolated at early time points post-infection. However, the transcriptional profile within T cells, which had very little

contamination, was similar to B cells, suggesting any contamination had little influence on the gene expression changes we observed. Another limitation is that we were not able to determine transcriptional changes within DCs due to very low cell recovery following sequential isolation using magnetic beads given that this subset make up less than 1% of the PBMC population and was further decreased 6 DPI [193].

In line with the larger transcriptional changes observed, DEGs in monocytes, which make up 10-15% of PBMC, contributed a more significant portion of transcriptional changes (~20% compared to 2-3%) detected in PBMC 6 days post ZEBOV infection compared to T and B cells, which make up to 75% of the PBMC. The 250 common DEGs detected in the purified monocyte fraction and PBMC play a central role in immunity, inflammation, and cell death. However, 971 DEGs that were detected within total PBMC did not meet the criteria for DEGs within purified monocytes, T cells, or B cells. These 971 DEGs enriched to biological processes involved in innate as well as adaptive immunity. Therefore, it is possible that expression changes in these genes are only significant when combining changes in all three cell subsets. Conversely, by enriching for monocytes, changes in expression of genes important for chemotaxis and antigen presentation became more pronounced, likely because the transcription profile was more specific to these cells rather than diluted by the global PBMC transcriptional profile.

In summary, our data revealed that monocytes, but not lymphocytes, are supportive of ZEBOV replication. Our findings also indicate that while ZEBOV replication in monocytes

may suppress IFN α/β mRNA expression [79, 264], it does not suppress ISG induction in infected cells. The gene expression patterns detected identify monocytes as one of the key players in ZEBOV pathogenesis by initiating events that contribute to characteristic symptoms of EVD including inflammation, vascular permeability, coagulation defects and production of reactive oxygen species.

CHAPTER 4: Modulation of host immunity by Ebola VP35

Andrea R. Menicucci¹, Courtney Woolsey^{2,3}, Chad E. Mire^{2,3}, Joan B. Geisbert^{2,3}, Krystle N. Agans^{2,3}, Allen Jankeel⁵, Christopher F. Basler⁴, Thomas W. Geisbert^{2,3*} and Ilhem Messaoudi^{5,*}

¹**University of California-Riverside, Division of Biomedical Sciences, Riverside, CA, USA.**

²**Galveston National Laboratory, Galveston, TX, 77555, USA.**

³**University of Texas Medical Branch, Department of Microbiology and Immunology, Galveston, TX, USA.**

⁴**Georgia State University, Center for Microbial Pathogenesis, GA, USA**

⁵**University of California-Irvine, Department of Molecular Biology and Biochemistry, College of Biological Sciences, Irvine, USA**

***To whom Correspondence should be addressed**

Manuscript under preparation

Abstract

Ebola virus is an RNA virus that causes hemorrhagic fever with up to 90% case fatality. Ebola hemorrhagic fever (EHF) is characterized by an excessive inflammatory response, lymphocyte apoptosis, and hemorrhage and coagulation defects leading to multiorgan failure and shock. The high virulence of ZEBOV in humans and nonhuman primates (NHPs) is largely attributed to the ability of this virus to subvert host innate immune pathways. *In vitro* studies have shown that ZEBOV viral protein 35 (VP35) blocks retinoic acid-inducible gene-I (RIG-I) receptor signaling by binding to dsRNA or binding to PKR activating protein (PACT), which activates RIG-I, thus preventing production of antiviral cytokines (IFN)- α/β in response to viral nucleic acids. However, the importance of this pathway during ZEBOV infection has not been assessed *in vivo*. Therefore, in this study we report the first longitudinal transcriptional changes in peripheral blood collected from cynomolgus macaques following infection with a recombinant ZEBOV containing mutations in VP35 (VP35m) that ablate its type I IFN antagonistic ability. Our data demonstrate, in contrast to wild type ZEBOV, VP35m infection induces large gene expression changes associated with a tightly controlled innate immune response and induction of both cellular and humoral immunity. These animals were effectively protected against subsequent ZEBOV-Makona challenge. These *in vivo* studies highlight the importance of VP35 as a key virulence factor and provide a potential target in the development of antivirals.

Introduction

Ebolaviruses (EBOV) are members of the Filoviridae family and causative agents of hemorrhagic fever. Five species have been identified with the Zaire species (ZEBOV) responsible for the highest mortality rates [36]. Fatal human cases of Ebola virus disease (EVD) are exemplified by high viral titers in blood, excessive inflammation, lack of adaptive immunity, coagulation defects, severe hemorrhaging, and shock [84, 166, 196]. Until 2014, ZEBOV caused sporadic and isolated outbreaks mostly in central Africa. However, the 2014-2016 ZEBOV epidemic that affected over 28,000 individuals and the recent outbreaks in 2017 highlight the importance of understanding factors that influence ZEBOV virulence and pathology [200].

ZEBOV virulence is attributed to its ability to interfere with type I interferon (IFN) responses. Retinoic acid-inducible gene I-like receptors (RLR), which detect viral nucleic acids during infection and replication, are central in promoting downstream phosphorylation of transcription factors IRFs 3 and 7, which relocate to the nucleus and activate transcription of *IFN α* and *IFN β* [66]. Cellular responses to type I IFN induce the expression of numerous interferon stimulated genes (ISGs) that trigger an antiviral state [67]. Several *in vitro* studies have demonstrated that ZEBOV proteins VP35 (an essential cofactor for the viral RNA polymerase complex) and VP24 (a secondary matrix protein) inhibit the production of type I IFN and block the induction of ISGs, respectively [265-267].

Initial studies demonstrated that VP35 complements the growth defect of an influenza virus NS1 deletion mutant that is unable to block type I interferon response [268]. Subsequent *in vitro* studies showed that VP35 binds dsRNA, sequestering it away from retinoic acid-inducible gene-I (RIG-I) recognition, and PKR activating protein (PACT), preventing PACT mediated activation of RIG-I thus suppressing the production of IFN α/β [90, 91] (**Figure 1.3**). Co-immunoprecipitation and reporter gene assays also demonstrated that VP35 prevents the phosphorylation of IRF3 by IKK ϵ and promotes the degradation of IRF3 and IRF7 through the interaction with SUMO E2 enzyme Ubc9 and E3 ligase PIAS [93, 94].

The ability of VP35 to bind to dsRNA resides in its carboxy terminal interferon inhibitory domain (IID). Based on crystal structure analysis, the IID domain has two basic regions: the first basic patch which is important for viral replication but not dsRNA binding and the central basic patch which contain conserved residues required for dsRNA binding and IFN inhibition [269]. Mutations in residues F239, R312, R322 and K319 inhibit VP35 dsRNA binding and suppress IFN β reporter expression but do not affect VP35 function as a viral polymerase co-factor [270, 271]. *In vivo*, a recombinant MA-ZEBOV carrying a VP35 R312A point mutation was greatly attenuated in mice [272]. Furthermore, infection of guinea pigs with recombinant MA-ZEBOV possessing R322 and K319 mutations was avirulent in guinea pigs and protected animals against subsequent wild type (WT) ZEBOV challenge [95]. However, these studies required the use of a mouse adapted ZEBOV, which

contains additional mutations in NP and VP24 [51-53, 95] that render them avirulent in macaques [52]. Therefore, it is critical that these studies be repeated using nonhuman primates, which are susceptible to ZEBOV strains that cause disease in humans [58, 59].

In this study, we report the first longitudinal transcriptional changes in PBMC collected from cynomolgus macaques after infection with a recombinant ZEBOV containing mutations F239A, R322A and K319A in VP35 (VP35m). Our data demonstrate, in contrast to WT ZEBOV, VP35m infection induces significant transcriptional changes associated with regulated innate immunity and induction of both cellular and humoral responses, effectively immunizing animals against subsequent WT challenge. These *in vivo* studies highlight the importance of VP35 as a key virulence factor and provide a potential target in the development of antivirals.

Materials and Methods

Virus and Challenge

Five healthy, filovirus-negative male cynomolgus macaques 3-5 years of age and between 4-8 kg were challenged with 1,000,000 PFU of VP35m, which was generated as previously described [91], intramuscularly with the dose divided equally into the left and right quadriceps. For WT ZEBOV challenge, a laboratory seed stock of the Makona variant was grown from the serum of a 2014 fatal human case in Guékédou, Guinea and passaged twice in authenticated Vero E6 cells (ATCC, CRL-1586) to produce ZEBOV isolate H.sapiens-tc/GIN/2014/ Makona-Gueckedou-C07, accession number KJ660347.2. This clone is one of the earliest isolates from the recent ZEBOV epidemic and was used in recent nonhuman primate studies [14]. Four weeks after VP35m challenge, 4 of the 5 animals were challenged with 1000 PFU of ZEBOV-Makona intramuscularly with the dose divided equally into the left and right quadriceps. Animals were housed in the Biosafety Level 4 (BSL-4) laboratory in the Galveston National Laboratory (GNL) and monitored post challenge for clinical signs of disease. The University of Texas Medical Branch at Galveston Institutional Animal Care and Use Committee (IACUC) and the Institutional Biosafety Committee approved this study and all protocols in accordance with state and federal statutes and regulations relating to experiments involving animals.

Sample Collection and PBMC isolation

Blood was collected by venipuncture into EDTA and serum tubes according to the study design. To separate plasma and serum, tubes were spun at 2500 rpm for 10 minutes at 4°C.

EDTA plasma and serum were stored at -80°C for future analysis and virus quantification. To isolate PBMC, WB was centrifuged over Histopaque (Sigma-Aldrich, St. Louis, MO) using AccuSpin Tubes (Sigma-Aldrich, St. Louis, MO) at 1400 rpm for 45 minutes, room temperature with no brake. The PBMC buffy coat was extracted and washed in RPMI media. Isolated cells were counted on a TC20 Automated Cell Counter (Bio-Rad, Hercules, CA). 1.0×10^6 PBMC were put into Trizol (Invivogen) buffer for RNA isolation. Remaining PBMC cells were frozen and stored at -80°C (stable for 6 months) for future analysis.

Hematology and Clinical Chemistry

WB collected in EDTA was analyzed by a hematological analyzer (Beckman Coulter, Brea, CA) that measures: white blood cell and differentials, red blood cells, platelets, hematocrit values, hemoglobin, mean cell volumes, mean corpuscular volumes, and mean corpuscular hemoglobin concentrations. Serum was collected for clinical chemistry analysis using a Piccolo point-of-care analyzer and Biochemistry Panel Plus analyzer discs (Abaxis, Sunnyvale, CA) to measure concentrations of albumin, amylase, ALT, AST, ALP, GGT, glucose, cholesterol, total protein, total bilirubin (TBIL), blood urea nitrogen (BUN), CRE, and CRP.

Virus detection and quantification

Virus titer was measured by plaque assay on Vero E6 cells. Cells were plated in 6-well plates and grown to confluency. Virus was titrated from 10^{-1} to 10^{-6} in duplicate. Plaques

were counted using neutral red stain; limit of detection was 25 PFU/ml. Viral genome copy number was determined by qRT-PCR using primers/probe targeting the VP30 gene of ZEBOV as recently described [202]. ZEBOV RNA was detected using the CFX96 detection system (BioRad Laboratories) using One-Step Probe qRT-PCR Kits (Qiagen) with the following cycle conditions: 50°C for 10 minutes, 95°C for 10 seconds, and 40 cycles of 95°C for 10 seconds followed by 59°C for 30 seconds. Threshold cycle values representing ZEBOV genome equivalents (GEq) were analyzed with CFX Manager Software, and data are shown as means \pm SD of technical replicates. To create the GEq standard, RNA from ZEBOV stocks was extracted and the number of ZEBOV genomes calculated using Avogadro's number and the molecular weight of the ZEBOV genome.

Library generation and sequencing

RNA was isolated from PBMC using the QIAmp Viral RNA Kit. RNA concentration and integrity was determined using an Agilent 2100 Bioanalyzer. Ribosomal RNA (rRNA) was depleted and libraries were constructed using the TruSeq Stranded Total RNA LT-LS kit. First, rRNA-depleted RNA was fragmented and converted to double stranded cDNA. Adapters were ligated and the ~300 base pair (bp) long fragments were then amplified by PCR and selected by size exclusion. Each library was prepared with a unique indexed primer for multiplexing. In order to ensure proper sizing, quantitation, and quality prior to sequencing, libraries were analyzed on the Agilent 2100 Bioanalyzer. Multiplexed libraries were subjected to single-end 75bp sequencing using the Illumina NextSeq500 platform.

Bioinformatic analysis

Data analysis was performed with the RNA-Seq workflow module of the systemPipeR package available on Bioconductor [204] and as previously described [193]. RNA-Seq reads were demultiplexed, quality filtered and trimmed using Trim Galore with an average phred score cutoff of 30 and minimum length of 75bp. Quality reports were generated with the FastQC function. Because genome annotation for *Macaca fascicularis* is not available, the *Macaca mulatta* genome sequence (Macaca_mulatta.MMUL_1.dna.toplevel.fa) and annotation file from Ensembl (Macaca_mulatta.MMUL_1.78.gtf) was used. In order to determine the level of viral transcription at different time points, either the ZEBOV strain Mayinga genome (H.sapiens-tc/COD/1976/Yambuku-Mayinga) or Makona genome Mayinga genome (H.sapiens-wt/GIN/2014/Makona- Gueckedou-C07) from Virus Pathogen Resource was adjoined to the *Macaca mulatta* reference. RNA-Seq reads were mapped with the alignment suite Bowtie2/Tophat2 against a reference genome containing both *Macaca mulatta* and ZEBOV-Mayinga or Makona genome sequences. Raw expression values in the form of gene-level read counts were generated with the *summarizeOverlaps* function, counting only the reads overlapping exonic regions of genes, and discarding reads mapping to ambiguous regions of exons from overlapping genes. Normalization and statistical analysis of differentially expressed genes (DEGs) was performed using the *edgeR* package. RNA-sequencing data presented in this article were submitted to the National Center for Biotechnology Information Sequence Read Archive (Accession number pending).

Gene clusters following VP35m infection were identified by Short Time-series Expression Miner (STEM) of median normalized reads focusing on transcripts an average RPKM of 5

or greater. The parameter for “model profiles” and “maximum unit change between time points” was set to default 50 and 2, respectively. Only statistically significant clusters with a p-value ≤ 0.05 were included for downstream analysis. Host differentially expressed genes (DEGs) following WT ZEBOV infection were obtained using the RNA-Seq workflow module of systemPipeR and defined as those with a fold change ≥ 2 and a false discovery rate (FDR) corrected p value ≤ 0.05 compared to 0 DPI. Only protein coding genes with human homologs and an average of 5 reads per kilobase of transcript per million mapped reads (RPKM) were included for further analysis. Principal component, heatmaps and venn diagrams were generated using R packages ggplot2 and VennDiagram.

Functional enrichment of these genes was done to identify clusters of genes mapping to specific biological pathways, specifically gene ontology (GO) terms using MetaCore™ (Thomson Reuters, New York, NY).

Statistical Analysis

Statistical analysis of viral load, hematology and clinical chemistry data was conducted using GraphPad Prism software (GraphPad, Software, Inc., La Jolla, CA). Significant values were determined using one-way ANOVA with an alpha value of 0.05 or less.

Results

VP35m infection results in mild clinical disease

Five cynomolgus macaques were challenged with 1×10^6 PFU of recombinant ZEBOV containing mutations in VP35 (VP35m) that abrogate its ability to inhibit IFN α production. Blood samples were collected on 0, 3, 6, 10, 14 and 28 days post infection (DPI) (**Figure 4.1A**). Fever (temperatures 2°F higher than baseline) and anorexia was evident 6 DPI in 2/5 animals. Mild weakness and diarrhea was observed in a third animal. None of these changes reached scorable criteria and no animals succumbed to VP35m challenge. Following VP35m infection, viral titers were measured in plasma by plaque assay and viral RNA was measured in whole blood using RT-qPCR. In one of the animals that had a fever, viral RNA and infectious virus were detected 3 and 6 DPI (**Figure 4.1B-C**). In the animal with mild weakness, viral RNA, but not infectious virus was detected 6 and 10 DPI (**Figure 4.1B**). Levels of circulating C-reactive protein (CRP), indicative of inflammation, increased 3 and 6 DPI in the two animals that developed fever (**Figure 4.1D**). There were no indications of organ damage as levels of liver enzyme aspartate transaminase (AST), blood urea nitrogen (BUN), and pancreas enzyme amylase (AMY) remained unchanged (**Figure 4.1E**). Hematocrit percentage decreased 6, 10 and 28 DPI while platelet numbers increased 10-14 DPI (**Figure 4.1F**). No significant changes were detected in the number of total white blood cells or subsets (**Figure 4.1G**).

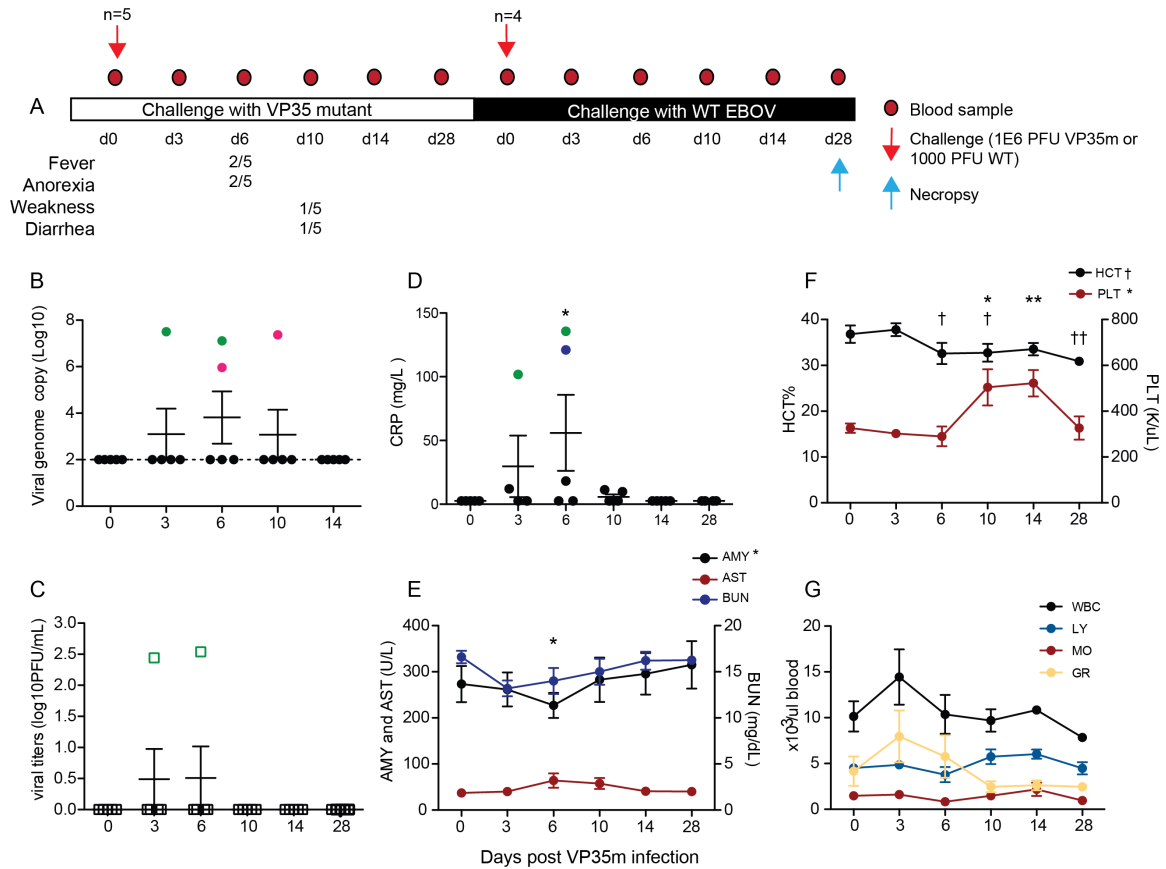


Figure 4.1. VP35m infection results in mild clinical signs. (A) Study time line and clinical observations. (B) Viral loads determined by qRT-PCR using primers/probe targeting VP30; green represents one of the animals that had fever and pink represents the animal that had mild weakness. (C) Infectious virus was quantified by plaque assay on Vero cells; green represents one of the animals that had fever. (D) Plasma levels of C-reactive protein (CRP); green represents the animal that had increased viral titers and fever and blue represents the other animal that developed fever. (E) Amylase (AMY), aspartate transaminase (AST), and blood urea nitrogen (BUN) levels. (F) Percentage of hematocrit and platelet counts. (G) White blood cells (WBC), lymphocyte (LY), monocyte (MO), and granulocyte (GR) counts throughout infection. Symbols (* and †) denote p-value ≤ 0.05 at the indicated time point compared to 0 DPI.

VP35m infection induces robust gene expression changes within PBMC

We next determined longitudinal gene expression changes in PBMC following VP35m infection using RNA-Seq. Principal component analysis of normalized reads showed that transcriptional profiles clustered by time point with the most variability observed at 3 DPI and the largest differences detected between 0 and 10 DPI (**Figure 4.2A**). We used short time-series expression mining (STEM) to delineate distinct temporal expression profiles throughout infection (**Figure 4.2B-E**).

DEGs in each of the clusters that were not statistically significant (FDR corrected p-value ≥ 0.05) during at least 1 time point were excluded from downstream analysis. We identified 4 statistically significant gene clusters: 1) cluster 1 contained 863 DEGs, the expression of which peaked 6 DPI and although it declined 10 DPI, it remained higher than baseline (**Figure 4.2B**); 2) a cluster of 645 DEGs, the expression of which decreased throughout infection (**Figure 4.2C**); 3) cluster 3 contained 424 DEGs, the expression of which peaked 3 and 6 DPI, decreased 10 DPI but remained higher than baseline (**Figure 4.3C**); 4) cluster 4 contained 388 DEGs the expression of which increased slightly 3 and 6 DPI before increasing dramatically 10 DPI (**Figure 4.3D**).

DEGs in Cluster 1, which were highly expressed 6 and 10 DPI, enriched to gene ontology (GO) terms associated with: cellular metabolism, signaling, apoptosis and cell cycle (**Figure 4.3A**). Genes mapping to “Cell cycle” play an important role in promoting cell cycle such as *ANAPC13*, *CCNL1*, *CDC25B* and *DBF4* as well as chromatin condensation

and DNA repair i.e. *SMARCB1*, *NCAPD2*, *XPC* and *LIG1* (**Figure 4.3B**). Additional genes that enriched to this GO term regulate B cell immunity such as: *CD27*, *CD38*, and *IGHV3-23* (**Figure 4.3B**). Of the DEGs in cluster 1 that enriched to GO term “Cellular metabolic process”, 77 (average fold change=22 throughout infection) directly interacted and were regulated by transcription factors *RELA*, *JUND*, and *YY1* (**Figure 4.3C**). Genes in this network play a role in: respiration (*NDUFA13*), innate immunity (*CYBA*, *CSF1R*, *SI00A9* and *NFKBIA*), translation (*EIF3G*, *RPS11*, *CARMI*), signal transduction (*PPP1R1B*), carbohydrate metabolism (*PYGB*, *GPT*), apoptosis (*BAD*), and protein degradation and autophagy (*ATG12* and *UBE2M*) (**Figure 4.3C**).

Similarly, transcripts that decreased throughout infection (cluster 2) mapped to GO terms associated with metabolism and cell cycle in addition to “Organelle organization” and “Gene expression” (**Figure 4.4A**). Downregulated DEGs that mapped to “Cell cycle” play a role in: 1) regulation of mitosis e.g. *CCNA2*, *CCNH*, *RBI*, and *MAD2L1*; 2) DNA repair and replication such as *BRCA2* and *ORC2*; and 3) microtubule formation i.e. *CEP57* and *KIF11* (**Figure 4.4B**). Several genes that enriched to GO term “Cellular metabolic process” interact with one another (**Figure 4.4C**). This network includes several transcription factors (*HIF1A*, *E2F3* and *CEBPZ*), and genes important for mitochondrial respiration (*COX6C* and *CYCS*), MAPK/ERK signaling (*KRAS*, *RAF1* and *PRKD3*), immune regulation (*RIPK2*, *AZI2* and *USP14*) and protein degradation (*PSMD6* and *ATXN3*) (**Figure 4.4C**).

Genes in cluster 3, the expression of which peaked 3 and 6 DPI before returning near baseline, enriched to GO terms related to metabolism, signaling and immunity (**Figure 4.5A**). Genes important for immunity included: ISGs e.g. *IFI35* and *RSAD2*; NFKB signaling e.g. *IKBKE* and *NFKB1*; inflammation e.g. *CD68*, *CCL3* and *TNF*; and antigen presentation such as *TAP1*, proteasome subunits *PSMB3* and *PSMD4*, and genes important for transport to and from the endoplasmic reticulum *SEC24C* and *SEC61A1* (**Figure 4.5B**). Additional genes in this cluster play a role in NK cell cytotoxicity (*NCR3*), T cell differentiation (e.g. *TCF7*) and the differentiation of follicular B helper T cells (i.e. *CXCR5* and *CD40LG*) (**Figure 4.5B**). The most highly expressed DEGs that mapped to “Cellular metabolic process” are involved in glucose metabolism (*ISYNA1*, *PHKG2*, *GYS1* and *GBA2*), fatty acid metabolism (*PPT2* and *ACADVL*), cell cycle (*REC8* and *AKAP8*), MAPK signaling (*MAP3K3* and *MAPK8IP1*) and transcriptional regulation (*MXD3*, *HMGXB3* and *SMARCD3*) (**Figure 4.5C**).

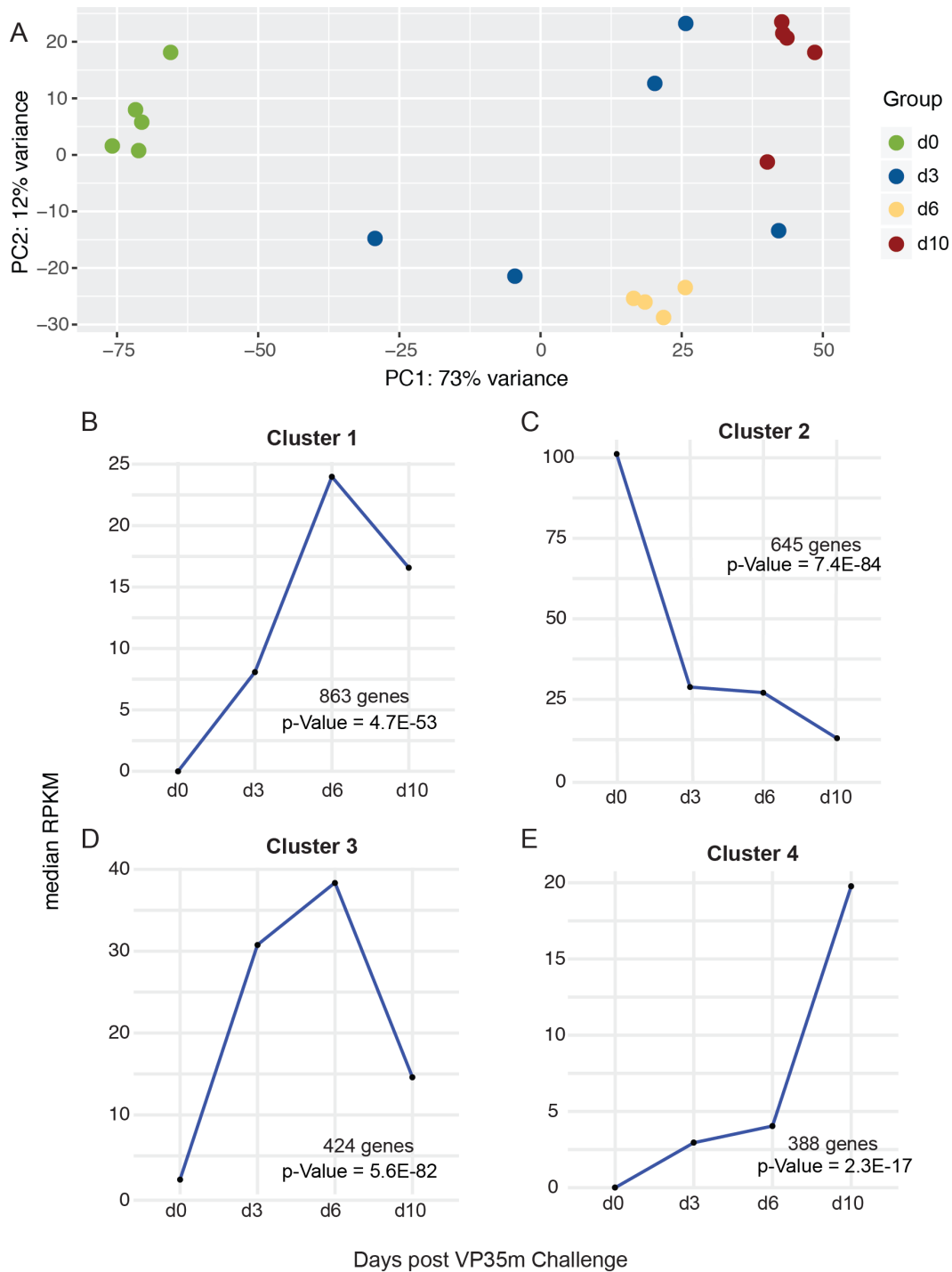


Figure 4.2. VP35m infection induces robust gene expression changes within PBMC. (A) Principal component analysis of normalized reads of each animal detected throughout VP35m infection (B-E) Statistically significant clusters of genes with different transcriptional trends following infection were predicted by STEM clustering of median normalized reads.

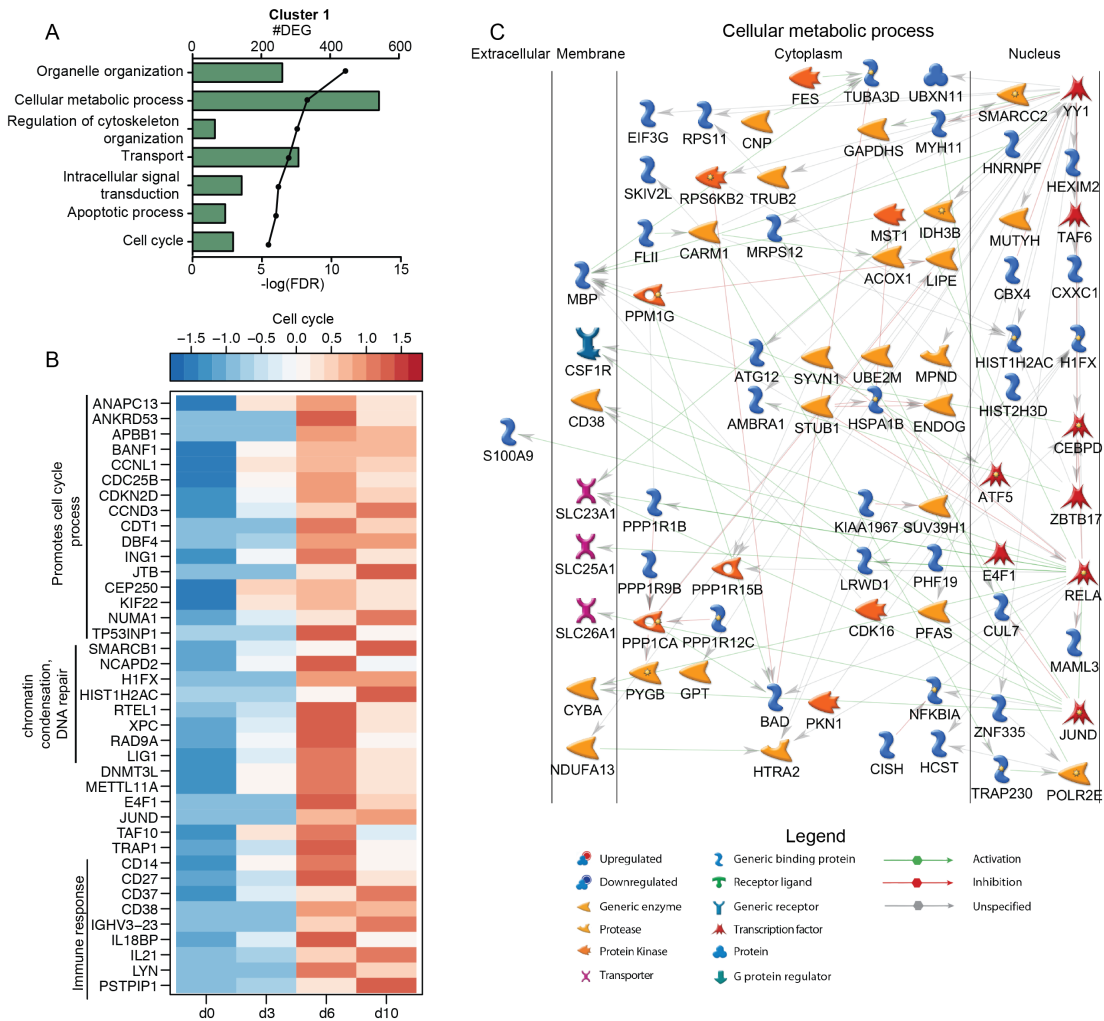


Figure 4.3. Cluster 1 genes are involved in cell cycle and cellular metabolism. (A) Bar graph depicting GO processes to which cluster 1 genes enriched; the line graph represents $-\log_{10}(FDR)$ of the enriched term. (B) Heatmap representing gene expression (shown as absolute normalized RPKM values) of the DEGs in cluster 1 that enriched to “Cell cycle”; range of colors is based on scaled and centered RPKM values of the entire set of genes (red represents increased expression while blue represents decreased expression); each column represents the median RPKM values for each DPI. (C) Network depicting direct interactions of the most upregulated DEGs in cluster 1 that map to GO process “Cellular metabolic process”.

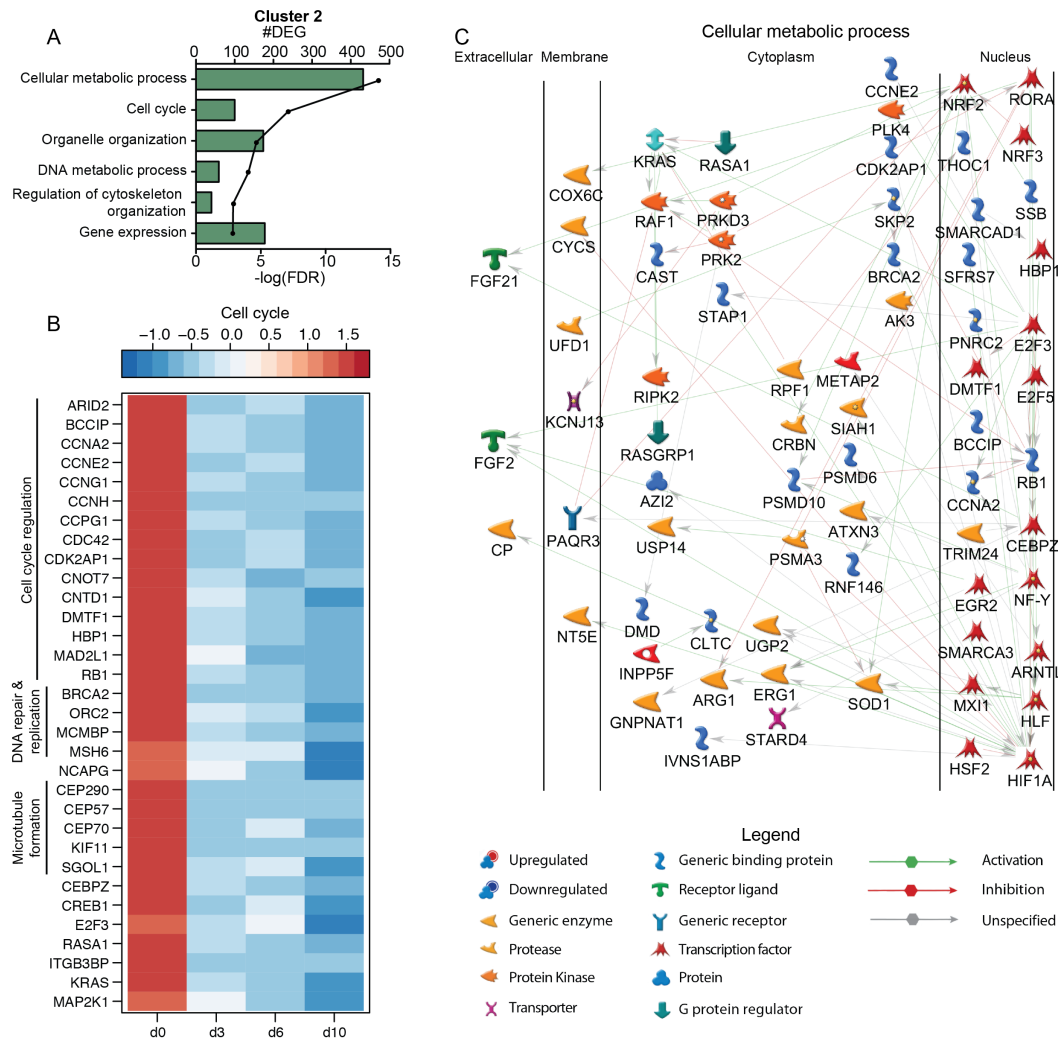


Figure 4.4. Cluster 2 genes are involved in cell cycle and cellular metabolism. (A) Bar graph depicting statistically significant GO processes to which cluster 2 genes enriched; the line graph represents $-\log_{10}(\text{FDR})$ of the enriched term. (B) Heatmap representing gene expression (shown as absolute normalized RPKM values) of the DEGs in cluster 2 that enriched to “Cell cycle”; range of colors is based on scaled and centered RPKM values of the entire set of genes (red represents increased expression while blue represents decreased expression); each column represents the median RPKM values for each DPI. (C) Network depicting direct interactions of the most downregulated DEGs in cluster 2 that map to GO process “Cellular metabolic process”.

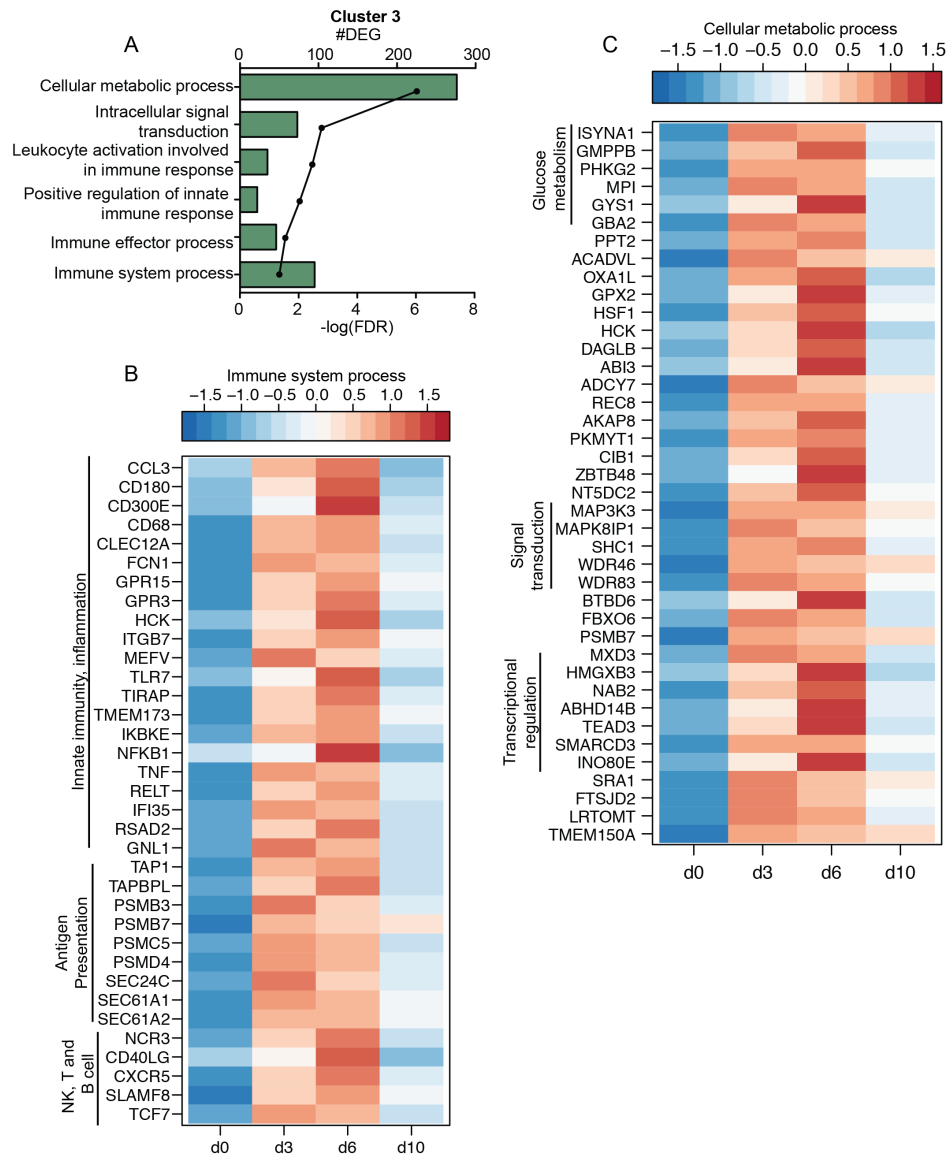
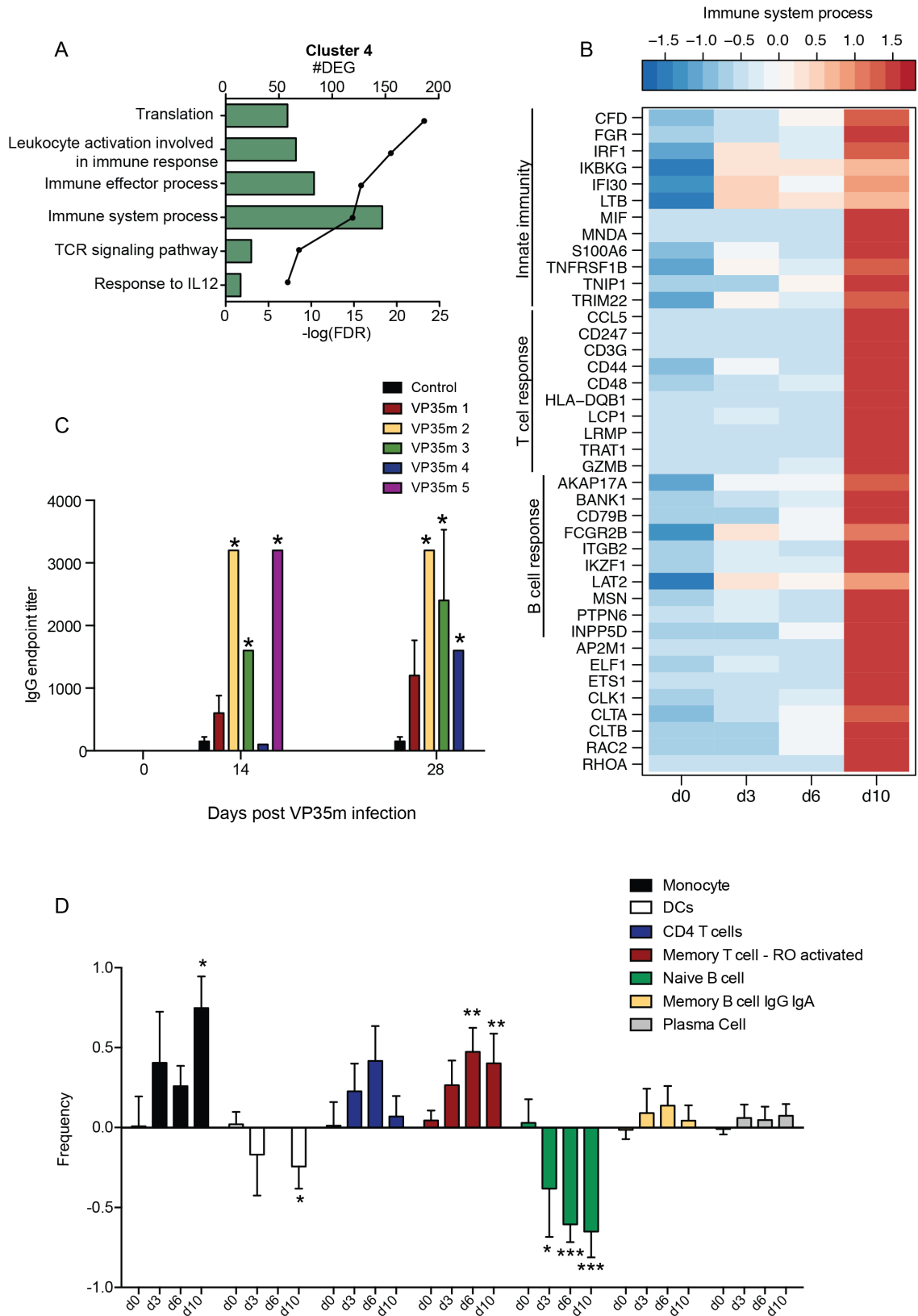


Figure 4.5. VP35m infection induces a regulated innate immune response (A) Bar graph depicting statistically significant GO processes to which cluster 3 genes enriched; the line graph represents $-\log_{10}(\text{FDR})$ of the enriched term. **(B)** Heatmap representing gene expression (shown as absolute normalized RPKM values) of the DEGs in cluster 3 that enriched to “Immune system process”; range of colors is based on scaled and centered RPKM values of the entire set of genes (red represents increased expression while blue represents decreased expression); each column represents the median RPKM values for each DPI. **(C)** Heatmap representing gene expression (shown as absolute normalized RPKM values) of the most upregulated DEGs in cluster 3 that enriched to “Cell metabolic process”; range of colors is based on scaled and centered RPKM values of the entire set of genes (red represents increased expression while blue represents decreased expression); each column represents the median RPKM values for each DPI.

Expression of the 388 DEGs in cluster 4 increased dramatically 10 DPI. These genes mapped primarily to GO terms “Translation” and “Immune system process” (**Figure 4.6A**). Some genes mapping to “Immune system process” played a role in innate immunity like *IRF1*, *IKBKG*, and *MIF* (**Figure 4.6B**). More importantly, a majority of the DEGs that enriched to these GO terms are important for antigen presentation/recognition (*HLA-DQB1* and *CD247*), T cell signaling (*CD3G* and *TRAF1*), T cell activation (*CD44* and *LCPI*), T cell chemotaxis (*CCL5/RANTES*), and effector responses (*GZMB*) (**Figure 4.6B**). Additionally, this cluster included genes that play a role in B cell responses such as *CD79B*, *INPP5D*, *ITGB2*, *BANK1* and *LAT2* (**Figure 4.6B**). In line with transcriptional analysis, ZEBOV-GP specific IgG were detected in 3/5 animals compared to the control animal 14 DPI and in all animals 28 DPI (**Figure 4.6C**).

We used Immquant, which implements the digital cell quantification algorithm to predict changes in immune cell subsets frequencies, based on gene expression. This analysis predicted the transcriptional changes to be associated with a significant increase in monocytes and decrease in dendritic cells 10 DPI, an increase in CD4 T cells 3-6 DPI, and a significant increase in memory T cells 6-10 DPI. This analysis also predicted a decrease in naïve B cells 3-10 DPI with a concomitant increase in memory B cells and plasma cells 3-10 DPI (**Figure 4.6D**).



(Previous Page) Figure 4.6. VP35 infection engenders development of adaptive immunity. (A) Bar graph depicting statistically significant GO processes to which cluster 4 genes enriched; the line graph represents $-\log_{10}(\text{FDR})$ of the enriched term. (B) Heatmap representing gene expression (shown as absolute normalized RPKM values) of the DEGs in cluster 4 that enriched to “Immune system process”; range of colors is based on scaled and centered RPKM values of the entire set of genes (red represents increased expression while blue represents decreased expression); each column represents the median RPKM values for each DPI. (C) IgG antibody titers directed against ZEBOV-GP were measured by ELISA; * denotes $p\text{-value} \leq 0.05$ compared to control animal at each time point. (D) Immquant software, which implements the DCQ deconvolution algorithm, was used to predict changes in immune cell subsets based on DEGs detected throughout VP35m infection.

Animals challenged with VP35m were protected against subsequent WT ZEBOV challenge

To investigate whether host responses induced by VP35m infection were protective, animals were challenged with a lethal dose of WT ZEBOV-Makona (1000 PFU) 4 weeks after VP35m inoculation (**Figure 4.1A**). All animals survived subsequent WT ZEBOV infection, with no detectable viremia or clinical signs (**Figure 4.7**). In contrast, the control animal that did not receive VP35m showed distinct signs of Ebola virus disease (EVD) including anorexia, petechial rash, and weakness that reached a clinical score 6 DPI requiring euthanasia (**Figure 4.7A**). The control animal also exhibited high levels of viremia, decreased platelet levels, increased liver damage as highlighted by increased AST levels, and decreased white blood cells all of which are characteristic hallmarks of EVD (**Figure 4.7B-E**).

Following WT ZEBOV infection, transcriptional changes were detected 10 DPI, with transcriptional profiles 28 DPI clustering near the day of WT ZEBOV infection (**Figure 4.8A-B**). A majority of DEGs 10 DPI were downregulated and enriched to “Cellular metabolic process”, “Cellular response to stress” and “Cell cycle” (**Figure 4.8C**). DEGs 28 DPI were associated with GO terms related to metabolism, transport, regulation of cell death and homeostasis of cell number (**Figure 4.8C**).

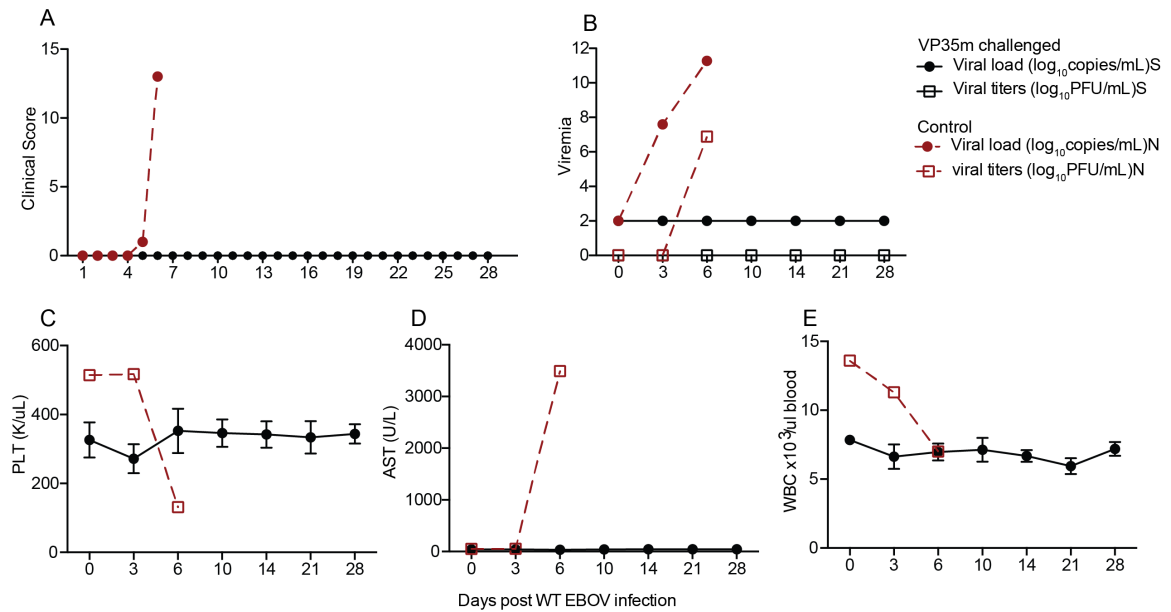


Figure 4.7. Animals challenged with VP35m are protected against subsequent WT ZEBOV challenge. The control animal, which was challenged with WT ZEBOV only is depicted in red while animals that were inoculated with VP35m are depicted in black. **(A)** Clinical score **(B)** Viral genome copies were measured using RT-qPCR and infectious virus was quantified by plaque assay on Vero cells. **(C)** Platelet levels. **(D)** Aspartate transaminase levels. **(E)** White blood cell numbers.

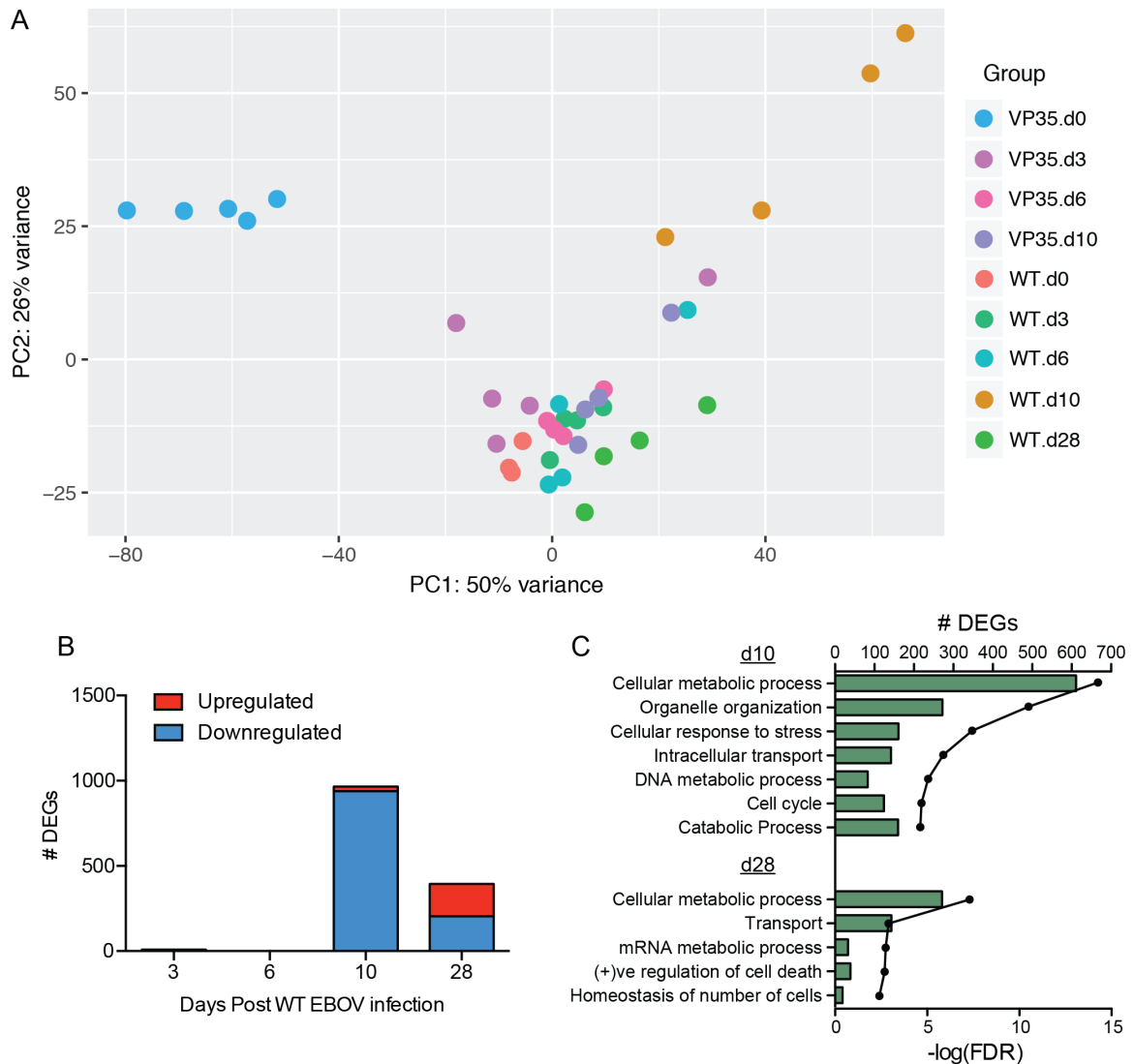


Figure 4.8. Detection of transcriptional changes following WT ZEBOV infection. (A) Principal component analysis of normalized transcript numbers of each animal throughout both VP35m infection and WT ZEBOV infection. **(B)** Bar graph depicts number of protein-coding differentially expressed genes (DEGs; defined as those ≥ 2 fold change compared to 0 DPI and FDR-corrected p-value ≤ 0.05) that have human homologues following infection. **(C)** Bar graph depicting statistically significant GO processes to which DEGs at 10 and 28 DPI enriched; the line graph represents $-\log_{10}(\text{FDR})$ of the enriched term.

Discussion

In this study, we assessed the role of VP35 in modulating ZEBOV pathogenesis for the first time in nonhuman primates. We longitudinally analyzed host transcriptional changes in PBMC isolated from cynomolgus macaques challenged with a recombinant ZEBOV containing 3 point mutations, K319A, R322A and F239A, that abrogate VP35 dsRNA binding activity and impair its suppression of IFN α/β . These VP35 mutations do not interfere with viral replication and were shown to have comparable activity levels as WT VP35 in a minigenome system that assessed the viral RNA polymerase complex function [271]. Additionally, similar growth kinetics and viral loads were observed following infection with WT ZEBOV or a recombinant ZEBOV possessing mutations in K319A and R322A in Vero cells, which are deficient in type I IFN. In contrast, these mutations negatively impacted virus growth in type I IFN competent 293 T cells [95]. In our study, infectious virus and viral RNA were detected in 1 and 2 animals, respectively 3-10 DPI albeit at a significantly lower magnitude compared to WT ZEBOV (4-5 log₁₀ fold lower) [58, 193]. These animals also had mild fever and small increases in levels of inflammatory CRP 3-6 DPI. Importantly, we did not observe significant changes in liver and kidney enzymes or hematocrit percentages. Overall, these data indicate that VP35 is a critical ZEBOV virulence factor. In support of this, previous studies using isothermal titration calorimetry uncovered that VP35 of Reston EBOV, which does not cause disease in humans, has a 2-3 fold lower binding affinity for dsRNA and reduced inhibition of IFN β promoter activation compared to ZEBOV despite high primary sequence homology [273].

Therefore, impaired VP35m growth *in vivo* may be due to its inability to counteract IFN-mediated antiviral responses.

Despite mild clinical signs, we observed large and stable gene expression changes following infection. This is in contrast to transcriptional changes following ZEBOV-Makona infection in which limited transcriptional changes are detected 3-4 DPI followed by widespread changes 5-6 DPI [193, 210]. A majority of genes that were differentially expressed throughout VP35m infection were involved in cell cycle. Specifically, we observed increased expression of genes required for progressing through cell cycle while expression of negative regulators of cell cycle was decreased. Surprisingly, transcript levels of *IFNBI* were only slightly increased 6 DPI in 2/5 animals and only a few ISGs met our statistical and RPKM thresholds. This is in contrast to *in vitro* infection of HEP2G cells with a recombinant ZEBOV carrying K319A and R322A mutations in VP35 that increased expression of several ISGs including *OAS*, *MXI* and *ISG15* [274]. It is possible that type I IFN responses peaked prior to 3 DPI. Another explanation could be that gene signatures of IFN signaling are only significant in specific cell types i.e. DCs, and these changes may have been obscured by the use of total PBMC in our study.

Expression of genes important for innate immunity and inflammation peaked 3-6 DPI before decreasing 10 DPI. This response is distinct from WT ZEBOV in which a larger number of DEGs are involved in inflammation and their magnitude of expression continues to increase throughout infection [193, 210]. We also report significant changes in genes

that play a role in cellular metabolism 3-6 DPI. Up- and downregulated DEGs that enriched to cellular metabolic process are involved in signal transduction, protein degradation and transcriptional regulation. Most noteworthy was an upregulation of genes that are involved in glycogenolysis (*PYGB*), glycolysis (*ISYNA1*) and fatty acid oxidation (*ACADVL*), which may support the energy demands of initiating an immune response.

Previous studies demonstrated that transfection of WT VP35 can block upregulation of DC maturation markers and inhibit stimulation of allogenic T cell responses upon Sendai virus (SeV) infection [89, 275]. In contrast, transfection of VP35 mutants F239A and R322A into primary human monocyte-derived DCs was unable to block upregulation of maturation markers *CD40*, *CD80* and *CD83* resulting in the stimulation of allogenic T cells, based on expression of IFN γ , after SeV infection [275]. In line with these observations, expression of genes that play a role in antigen presentation increased 3-6 DPI.

In contrast to the lymphopenia observed post WT ZEBOV infection [193], VP35m induces expression of genes important for adaptive immunity. Specifically, DEGs that dramatically increased 10 DPI enriched to TCR signaling, B cell activation, and development of plasma B cells. Interestingly, genes associated with development of T follicular helper cells (*CXCR5* and *CD40LG*) significantly increased 3-6 DPI, preceding the peak of B cell activation and differentiation. Although there were no significant changes in the number of white blood cells, there may be differences within immune cell subsets. Indeed, Immquant analysis predicted an increase in the frequency of memory T cells, memory B

cells and plasma cells. Indeed, a humoral response was observed as evidenced by the increase of ZEBOV-GP specific antibodies 14 DPI 3/5 animals, and in all animals by the time of WT-ZEBOV challenge, which likely provided protection.

DEGs were detected 10 and 28 days post WT ZEBOV infection despite the absence of viremia and clinical signs. Since most DEGs 10 DPI, which enriched to metabolism and cell cycle, were downregulated, we propose that transcriptional changes are indicative of the resolution of responses to both VP35m and WT challenge. This is further supported by fewer DEGs 28 DPI, which was transcriptionally more similar to the profiles detected on the day of WT challenge compared to those observed 10 DPI. Moreover, DEGs 28 DPI enriched to GO terms related to homeostasis.

In summary, our data revealed that VP35m infection activate large gene expression changes associated with cellular metabolism, cell cycle and translation. Importantly, our data indicate that VP35m is immunogenic, yielding a strong yet controlled innate immune response and the development of adaptive immunity, which provided protection against ZEBOV challenge. These gene signatures are distinct from those detected in animals infected with WT ZEBOV, which exhibit exacerbated inflammation and absence of adaptive immunity. Together, these data suggest that VP35 plays a key role in mediating Ebola pathogenesis.

CHAPTER 5: rVSV-ZEBOV vaccination induces an antiviral innate response that confers rapid protection

Andrea R. Menicucci¹, Allen Jankeel², Andrea Marzi³, Heinz Feldmann³, Ilhem Messaoudi^{2*}

¹**Division of Biomedical Sciences, School of Medicine, University of California-Riverside, Riverside, CA 92521, USA**

²**Department of Molecular Biology and Biochemistry, University of California-Irvine, Irvine, CA 92697, USA**

³**Laboratory of Virology, Division of Intramural Research, National Institute of Allergy and Infectious Diseases, National Institutes of Health, Hamilton, MT 59840, USA.**

*To whom Correspondence should be addressed

Manuscript in preparation

Abstract

Ebolaviruses (EBOV) are single-stranded RNA viruses that cause Ebola virus disease (EVD) characterized by an excessive inflammatory response, lymphocyte apoptosis, vascular impairment, hemorrhage, and coagulation defects leading to multiorgan failure and shock. Data from Phase III clinical trials show that a recombinant vesicular stomatitis virus expressing the ZEBOV glycoprotein (rVSV-ZEBOV) is safe and 100% efficacious against ZEBOV infection. Additional studies have shown that rVSV-ZEBOV provides complete and partial protection to macaques immunized 7 and 3 days before ZEBOV challenge, respectively. However, the mechanisms by which this live-attenuated vaccine elicits rapid protection are only partially understood. To address this question, we carried out a longitudinal transcriptome analysis of host responses in whole blood samples collected from cynomolgus macaques vaccinated with rVSV-ZEBOV 28, 21, 14, 7 and 3 days before ZEBOV challenge. Our findings showed peak transcriptional changes 7 days following vaccination consistent with the development of innate antiviral immunity as well as B cell activation. ZEBOV challenge 1 week after vaccination results in large gene expression changes consistent with a recall adaptive immune response 14 days post infection. Lastly, the timing of interferon stimulated gene expression correlated with viral burden and disease outcome in animals vaccinated 3 days before challenge.

Introduction

Ebola virus is an enveloped virus containing a negative sense single-stranded genome that causes Ebola virus disease (EVD) characterized by an excessive inflammatory response, lymphocyte death, vascular impairment, and coagulation defects with high case fatality rates. Zaire Ebola virus (ZEBOV) is responsible for the highest case fatality rates (CFRs) and most outbreaks including the 2014-2016 epidemic that resulted in 28,600 potential cases and 11,300 fatalities. This epidemic accelerated the progression of several vaccine platforms through Phase I-III clinical trials. One vaccine platform that has reliably demonstrated 100% efficacy in nonhuman primate (NHP) models and progressed the furthest in clinical trials is the recombinant live-attenuated vesicular stomatitis virus that expresses ZEBOV glycoprotein (GP) in place of the VSV G protein (rVSV-ZEBOV). A single dose of rVSV-ZEBOV provides complete protection against lethal ZEBOV in cynomolgus macaques vaccinated before challenge [151, 153]. Moreover, rVSV-ZEBOV confers 50% protection in rhesus macaques when administered 20-30 minutes after challenge [159, 276]. The results from this NHP study led to the application of rVSV-ZEBOV as a postexposure treatment during the 2014 outbreak when a physician sustained a needle-stick injury while working in an Ebola treatment unit. The patient developed ZEBOV-GP specific antibodies following vaccination and recovered [167]. Multiple Phase I-II clinical trials have demonstrated this vaccine to be safe and immunogenic. Importantly, the Phase III ring vaccination trial in Guinea was the first to show that rVSV-ZEBOV is 100% efficacious.

We previously established antibodies as the primary mode of long-term protection conferred by rVSV-ZEBOV [156]. In a NHP study in which groups of cynomolgus macaques were either depleted of CD4 or CD8 T cells before and during vaccination or depleted of CD4 T cells during challenge, only the animals depleted of CD4 T cells during vaccination, but not before challenge, succumbed to ZEBOV challenge 28 days after immunization. Since this was the only group that lacked GP-specific antibodies at the time of challenge, these data demonstrate that antibodies are required for rVSV-ZEBOV mediated protection. More recently, we reported complete and partial (66%) protection when cynomolgus macaques were immunized 7 and 3 days before challenge, respectively [161]. Given the lack of detectable ZEBOV-GP specific antibodies at the time of challenge, these data suggest that rVSV-ZEBOV can confer rapid protection through mechanisms other than humoral immunity. However, these mechanisms remain incompletely understood. To address this gap in our knowledge, we carried out a longitudinal transcriptome analysis of blood samples collected from cynomolgus macaques that were vaccinated 28, 21, 14, 7 and 3 days before ZEBOV-Makona challenge [161].

Animals vaccinated 2 weeks or more before challenge exhibited small transcriptional changes as we previously reported following challenge with ZEBOV-Kikwit [205]. In contrast, animals vaccinated 1 week prior to challenge had a very robust transcriptional response characterized by high expression of interferon stimulated genes (ISGs), viral RNA sensors, and inhibitors of viral RNA synthesis at the time of challenge. Interestingly, these animals exhibited large transcriptional changes 14 and 28 days post challenge

suggestive of the generation of a recall cellular and humoral immune response. Finally, animals vaccinated 3 days before ZEBOV-Makona challenge also exhibited increased expression of ISGs and RNA sensors at the time of challenge, albeit significantly reduced compared to the animals vaccinated 7 days before challenge. The kinetics and magnitude of these gene expression changes correlated with disease outcome. These data indicate that the robust innate immune response engendered by the rVSV-ZEBOV vaccine can protect against lethal challenge within 3 days and more importantly, can pave the way for the development of a robust adaptive immune response following viral challenge.

Materials and Methods

Library generation and sequencing

RNA was isolated from whole blood using the QIAmp Viral RNA Kit (Qiagen, Valencia, CA). RNA concentration and integrity was determined using an Agilent 2100 Bioanalyzer. Ribosomal RNA (rRNA) was depleted and libraries were constructed using the TruSeq Stranded Total RNA LT-LS kit. First, rRNA-depleted RNA was fragmented and converted to double stranded cDNA. Adapters were ligated and the ~300 base pair (bp) long fragments were then amplified by PCR and selected by size exclusion. Each library was prepared with a unique indexed primer for multiplexing. In order to ensure proper sizing, quantitation, and quality prior to sequencing, libraries were analyzed on the Agilent 2100 Bioanalyzer. Multiplexed libraries were subjected to single-end 75bp sequencing using the Illumina NextSeq500 platform.

Bioinformatic analysis

Data analysis was performed with the RNA-Seq workflow module of the systemPipeR package available on Bioconductor [204]. RNA-Seq reads were demultiplexed, quality filtered and trimmed using Trim Galore with an average phred score cutoff of 30 and minimum length of 75bp. Quality reports were generated with the FastQC function. Because genome annotation for *Macaca fascicularis* is not available, the *Macaca mulatta* genome sequence (Macaca_mulatta.MMUL_1.dna.toplevel.fa) and annotation file from Ensembl (Macaca_mulatta.MMUL_1.78.gtf) was used. In order to determine the level of viral transcription at different time points, the ZEBOV strain Makona genome (H.sapiens-

wt/GIN/2014/Makona- Gueckedou-C07) from Virus Pathogen Resource was adjoined to the *Macaca mulatta* reference. ZEBOV open reading frames (ORFs), intergenic regions (IGRs) and leader and trailing sequences were defined based on the ZEBOV-Makona genome annotation GTF file: NP (470-2689), VP35 (3129-4151), VP40 (4479-5459), GP (6039-8068), VP30 (8509-9375), VP24(10345-11100), L (11581-18219), Leader (1-469), IGR_NP_VP35 (2690-3128), IGR_VP35_VP40 (4152-4478), IGR_VP40_GP (5460-6038), IGR_GP_VP30 (8069-8508), IGR_VP30_VP24 (9376-10344), IGR_VP24_L (11101-11580), Trailing (18220-18959). RNA-Seq reads were mapped with the alignment suite Bowtie2/Tophat2 against a reference genome containing both *Macaca mulatta* and ZEBOV-Makona genome sequences. Raw expression values in the form of gene-level read counts were generated with the *summarizeOverlaps* function, counting only the reads overlapping exonic regions of genes, and discarding reads mapping to ambiguous regions of exons from overlapping genes.

Our previous transcriptional studies demonstrated that the host response to rVSV-ZEBOV is resolved 28 days post vaccination [205]. Thus, day 0 (day of challenge) of the day-28 group (n=2) served as a baseline (BL). Gene expression changes induced by rVSV-ZEBOV were determined by comparing samples collected on the day of challenge from animals vaccinated 21 (n=3), 14 (n=2), 7 (n=2), and 3 days (n=3) before challenge to BL. Following infection, each time point post infection was compared to BL in groups d-7 and d-3 or the respective day 0 for groups d-28, d-21 and d-14.

Normalization and statistical analysis of differentially expressed genes (DEGs) was performed using the *edgeR* package. RNA-sequencing data presented in this article were submitted to the National Center for Biotechnology Information Sequence Read Archive (Accession number pending). Host DEGs were defined as those with a fold change ≥ 2 and a false discovery rate (FDR) corrected p value ≤ 0.05 . Only protein coding genes with human homologs and an average of 5 reads per kilobase of transcript per million mapped reads (RPKM) were included for further analysis. Reads mapping to the ZEBOV-Makona genome were also normalized as RPKM. Statistical analysis of changes in normalized reads mapping to ZEBOV-Makona ORF, IGR, leader, trailing sequences, and entire genome was performed using *edgeR*. MaSigPro was used to obtain lists of significant genes in animals vaccinated 3 days before challenge at early time points of infection. R^2 of the regression model was set to 0.7 and vars set to “all” in the “get.siggenes” function [277]. Heatmaps and venn diagrams were generated using R packages gplot and VennDiagram.

Functional enrichment

Functional enrichment of these genes was done to identify clusters of genes mapping to specific biological pathways, specifically gene ontology (GO) terms using MetaCore™ (Thomson Reuters, New York, NY).

Results

rVSV-ZEBOV vaccination elicits innate immunity and B cell activation

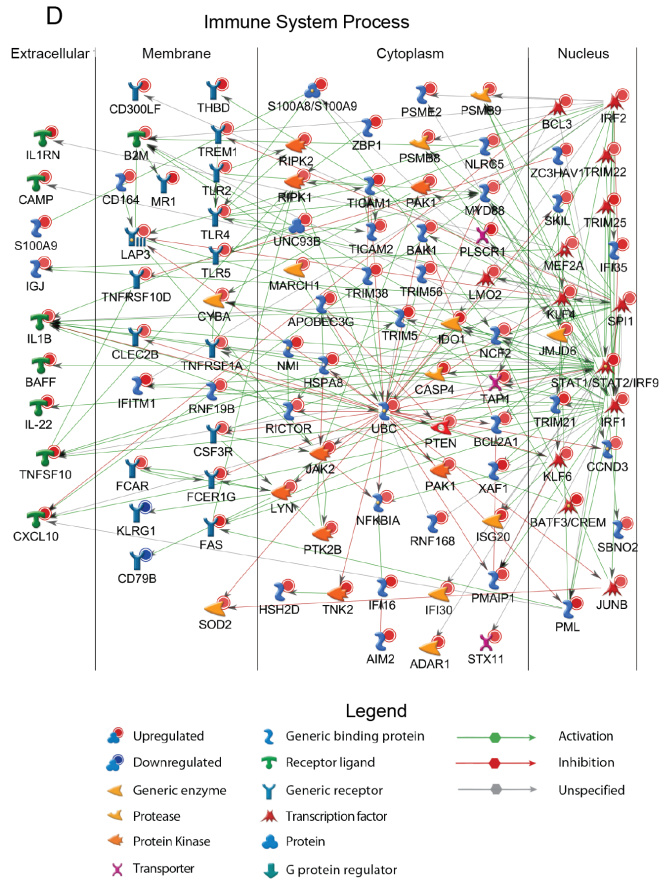
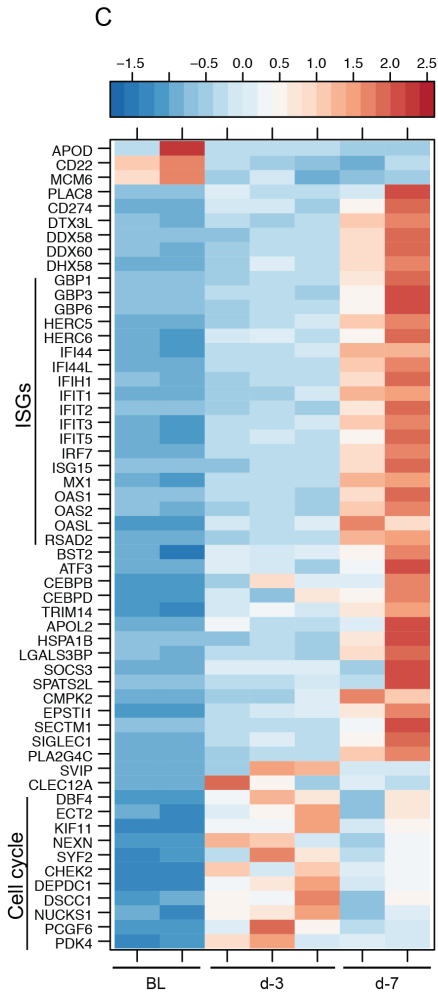
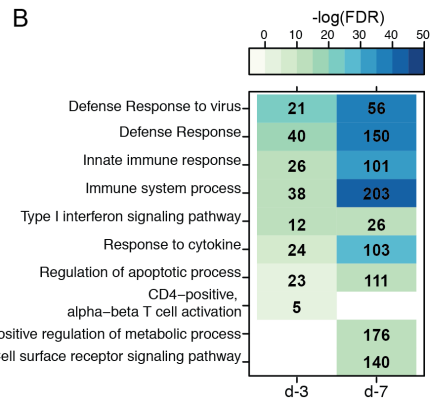
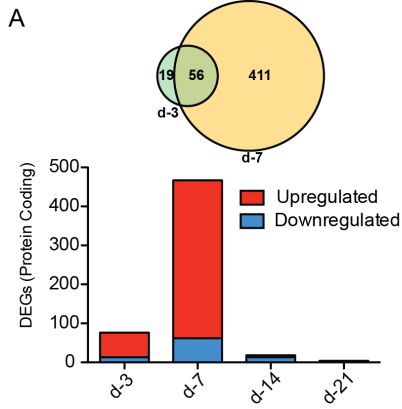
Blood samples were collected from our previous study investigating the time to protective immunity following rVSV-ZEBOV vaccination [161]. Fifteen cynomolgus macaques were divided into groups of 2-3 animals that were immunized with a single intramuscular injection of rVSV-ZEBOV at 28, 21, 14, 7 or 3 days before ZEBOV-Makona challenge. The negative control group was immunized with the VSV-Marburg-GP vaccine (rVSV-MARV), which does not provide cross protection against ZEBOV, 28 days before ZEBOV challenge. Blood was collected on days 0, 3, 6, 14, 21 and 28 post challenge.

Our previous studies using peripheral blood mononuclear cells (PBMC) demonstrated that the host response to rVSV-ZEBOV vaccination peaks 7 days post vaccination and returns to baseline 14 DPI [205]. These transcriptional responses were dominated by changes in the expression genes critical for antiviral immunity and cell proliferation. However, our earlier studies were carried out using PBMC. Therefore, we leveraged access to whole blood samples in the current study in order to gain additional insight into the host response to rVSV-ZEBOV vaccination. Additionally, the current experimental design provided an opportunity to characterize the immune response 3 days post vaccination (DPV) for the first time.

Samples collected on the day of challenge from the day-3, -7, -14, and -21 vaccination groups were compared to those obtained from the day-28 group. On the day of challenge, 75 differentially expressed genes (DEGs) were detected in the animals vaccinated 3 days before challenge and 467 DEGs were detected in the animals vaccinated 7 days before challenge. Very few DEGs were detected in samples collected from animals vaccinated 14 (18 DEGs) and 21 (4 DEGs) days before challenge (**Figure 5.1A**). Functional enrichment revealed that DEGs detected 3 DPV mapped to Gene Ontology (GO) terms associated with defense response and innate immunity (**Figure 5.1B**). Additionally, the expression of most DEGs detected 3 DPV increased 7 DPV (**Figure 5.1A**). These genes consisted primarily of interferon stimulated genes (ISGs), that play an important role in antiviral defense such as *OAS1*, *GBP1*, *MX1* and *IFIT1* as well as viral sensors *DDX58* and *DDX60* (**Figure 5.1C**). Other DEGs that were upregulated 3 DPV played a role in cell cycle such as *DBF4*, *ECT2*, *KIF11* and *CHEK2*, with the highest magnitude of expression occurring 3 DPV (**Figure 5.1C**).

DEGs detected 7 DPV mapped to GO terms associated with immune response, metabolic process, apoptosis, and signaling (**Figure 5.1B**). Of the 203 DEGs exclusively identified 7 DPV that enriched to “Immune system process”, 103 had direct interactions. These genes play a role in antiviral innate immunity including: transcription factors *STAT1*, *STAT2* and *IRF9*; genes that play a role in inflammatory response i.e. *S100A8*, *MYD88*, *NFKBIA*, *IL1B*; and pathogen recognition receptors such as *TLR 2*, *4* and *5* (**Figure 5.1D**). *CXCL10*, which is a chemoattractant for monocytes, NK cells and T cells, was also upregulated. We also

detected increased expression of genes that play role in antigen processing such as proteasome *PSMB9*, *PSME2* and *PSMB8*; and antigen presentation i.e. *TAP1*, *B2M* and *MRI* (**Figure 5.1D**). We also observed signatures of B cell activation as evidenced by increased expression of *SPI1*, *BAFF*, *LYN* and *PRK2B* (**Figure 5.1D**). Other notable upregulated DEGs that are not part of this network include *CD274/PD-L1*; *PRDMI*, also known as *BLIMP1*, which is important for the differentiation of B cells into plasma cells; B-cell related transcripts *MS4A6A* and *MS4A6E*; and *MRI*, which plays a role in antigen presentation. The 18 DEGs detected 14 DPV suggested resolution of immune responses as indicated by the downregulation of *GZMK*, *EMR2*, *CD3G* and *CCR1*.



(Previous Page) Figure 5.1. rVSV-ZEBOV vaccination elicits transcriptional changes suggestive of antiviral innate immunity and B cell activation. (A) Bar graph depicts number of differentially expressed genes following vaccination (DEGs; defined as those ≥ 2 fold change and FDR corrected p value ≤ 0.05) that have human homologues (red indicates upregulated while blue indicates downregulated DEGs). Venn diagram displaying overlap between DEGs detected in day-3 and day-7 vaccinated animals **(B)** Functional enrichment of DEGs 0 DPI in day-3 and day-7 vaccinated animals; color intensity represents the statistical significance shown as negative log of the FDR-corrected p-Value. The number of DEGs enriching to each Gene Ontology (GO) term each day is listed within each box; blank boxes represent no statistical significance. **(C)** Heatmap representing expression (shown as absolute normalized RPKM values) of DEGs detected 3 and 7 DPV; range of colors is based on scaled and centered RPKM values of entire set of genes (red represents increased expression while blue represents decreased expression); each column represents 1 animal. **(D)** Network showing direct interactions between DEGs detected exclusively 7 DPV that enriched to “Immune system Process”.

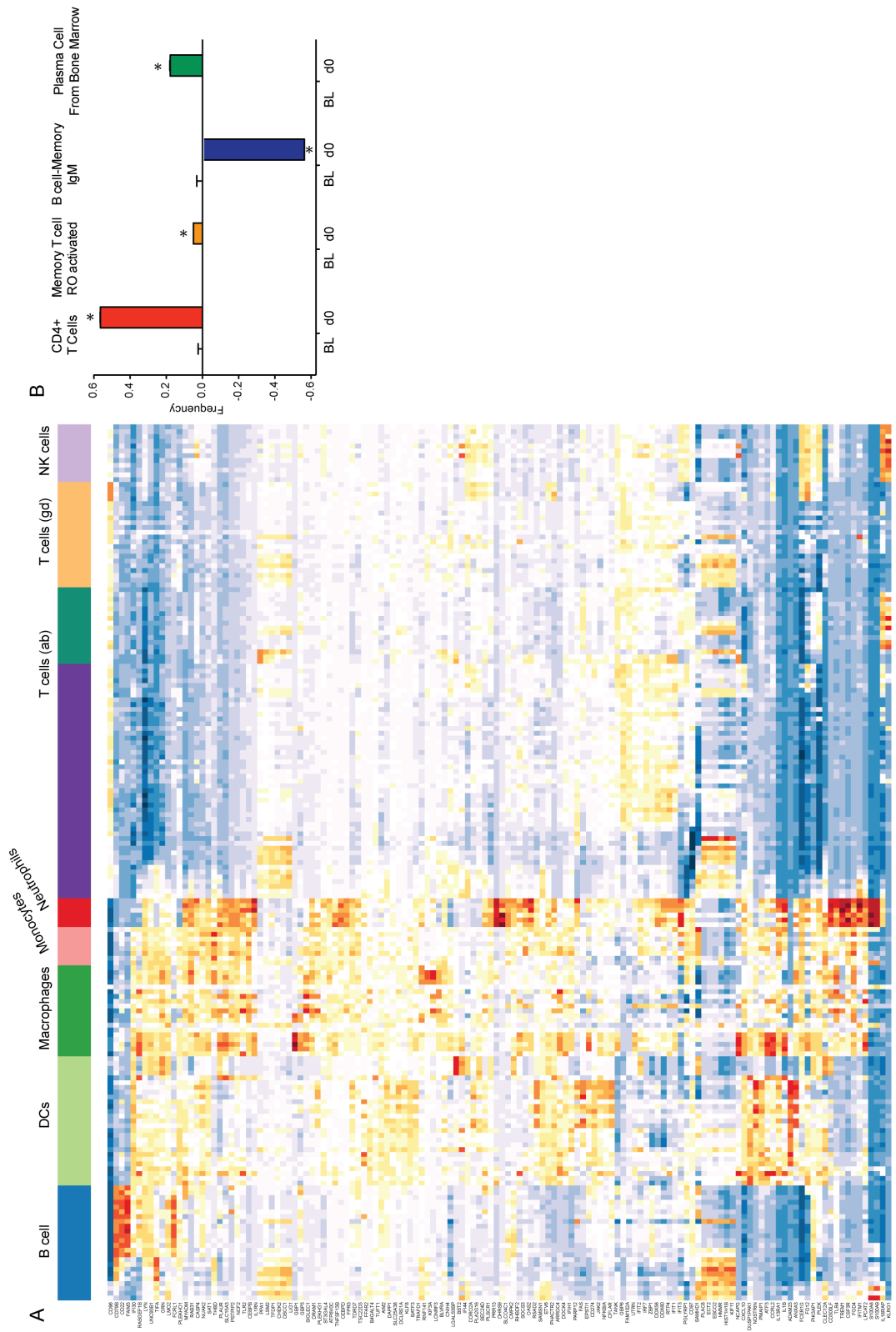
We next used the Immunological Genome Project Consortium (ImmGen) database, which visualizes the distribution of DEGs across immune cell populations in order to infer the source of the gene expression changes detected 7 DPV. This analysis showed that vaccine-induced DEGs are highly expressed by antigen presenting cells (monocytes and dendritic cells) and neutrophils, with some expression in B cells and T cells (**Figure 5.2A**). Additionally, we utilized Immquant, which implements the digital cell quantification algorithm, to predict changes in immune cell subsets based on DEGs detected 7 DPV. This analysis predicted the transcriptional changes to be associated with a significant increase in CD4 T cells, memory T cells, plasma cells and a decrease in IgM memory B cells (**Figure 5.2B**).

Negative control animals exhibit gene expression changes consistent with ZEBOV-Makona infection

Analysis of gene expression following ZEBOV-Makona challenge in negative control animals showed substantial gene expression changes 3 DPI (355 DEGs), with the largest changes observed 5/6 DPI (1,484 DEGs), which correlated with viral transcript counts (**Figure 5.3A**). Expression of the majority of genes upregulated 3 DPI continued to increase 5/6 DPI (**Figure 5.3A**) and enriched to host defense, inflammation, cell death, signaling and metabolic processes as we recently reported [193], (**Figure 5.3B**). Notable upregulated genes that play a role in inflammation include: transcription factors *RELA*, *RELB*, *STAT1*, *CEBPB*, *IRF1*, and *IRF7*; signaling molecules *MYD88*, *TRAF8* and *IRAK2*; chemokines/cytokines *CCL2* and *3*, *CXCL10*, *IL18* and *TNF*; and receptors *FPRI*, *C5AR*,

CCRI TLR2-3, *CD14* and *IFNAR2* (**Figure 5.4A**). Several ISGs were also highly upregulated such as *ISG15*, *IFIT2*, *IFIH1*, *OAS1-2*, and *MX1*. Genes that play a role in cell death including *FAS*, *CASP4*, and *TNFSF10A* were also upregulated (**Figure 5.4A**).

Downregulated DEGs were only detected 5/6 DPI and mapped to gene expression, cell cycle, cellular metabolism, and T cell activation (**Figure 5.3C**). Decreased transcripts that enriched to “Lymphocyte proliferation” included *CD28*, *CD3E*, *CD40LG*, *CD86*, *ZAP70*, *CD27* and *IL7R* (**Figure 5.4B**). The second major group of downregulated genes enriched to cell cycle such as genes that regulate cell cycle progression *CDC25B*, *TOP2A*; and genes important for cell division i.e. *ANAPC10*, *CENPC*, *KIF11*, and *TOP2A* (**Figure 5.4B**). Overall transcriptional changes detected in the negative control animals are characterized by robust inflammation and lymphopenia in line with development of Ebola virus disease. A majority of DEGs detected in the control animals were shared (~60%) with those we recently reported (**Figure 5.3D**) (Chapter 2, [193]).



(Previous Page) Figure 5.2. Immgen and DCQ analysis of transcriptional changes 7 days post rVSV-ZEBOV vaccination. (A-B) Heatmap showing expression profile of DEGs detected 0 DPI in the day-7 group across various immune cell populations as predicted by ImmGen's MyGeneSet application. Red indicates high while blue indicates low likelihood of expression within indicated immune cell population. **(B)** Immquant software, which implements the DCQ deconvolution algorithm, was used to predict changes in immune cell subsets based on DEGs detected 0 DPI in the day-7 group.

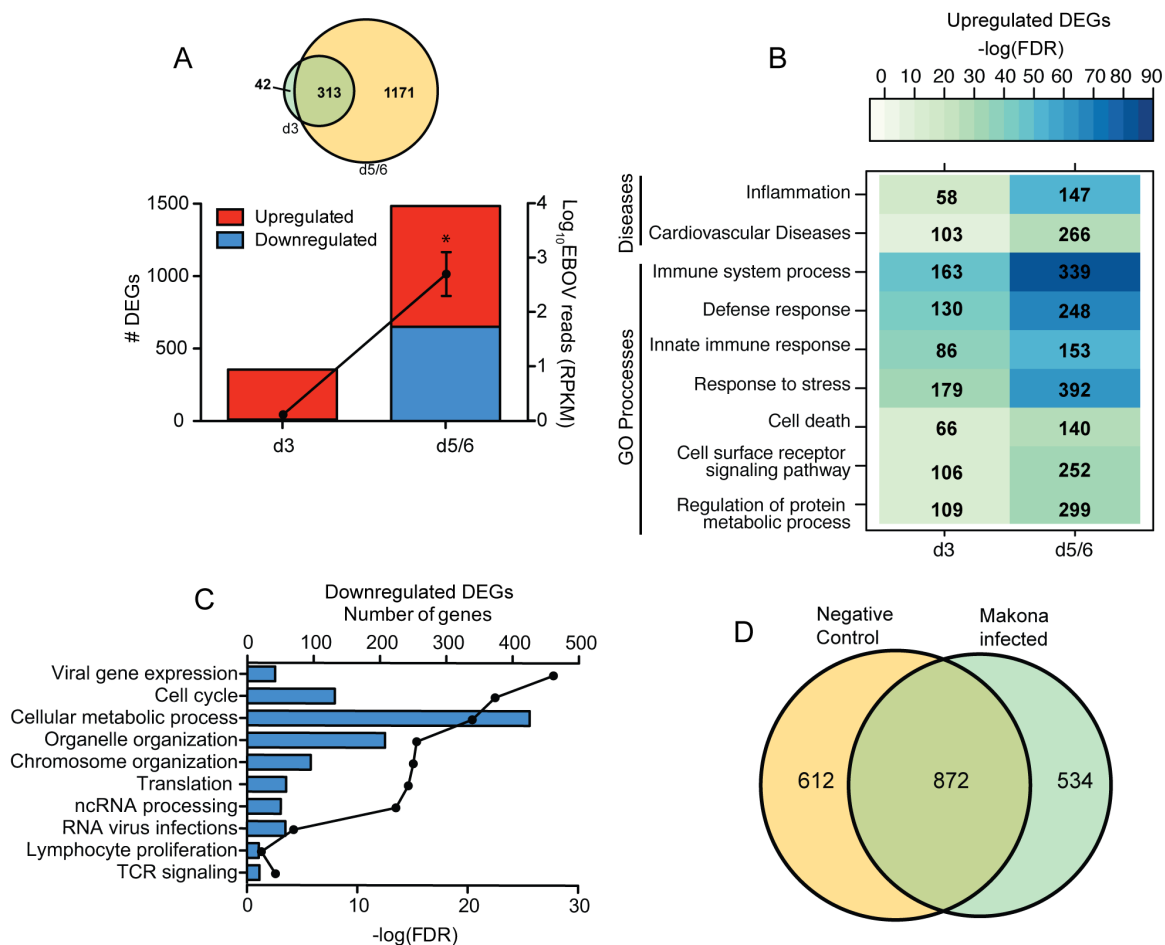


Figure 5.3. Negative control animals exhibit gene expression changes consistent with EVD. (A) Number of differentially expressed genes. Line graph represents number of normalized viral transcripts (RPKM); * p < 0.05 compared to day 0. Venn diagram of DEGs detected 3 and 5/6 DPI in negative control animals. (B) Functional enrichment of upregulated DEGs detected 3 and 5/6 DPI. (C) Functional enrichment of downregulated genes; horizontal bar graphs represent number of genes that mapped to each GO term listed while line graph represents FDR-corrected p-Value. (D) Comparison of DEGs detected between negative control animals 5/6 DPI and cynomolgus macaques challenged with ZEBOV-Makona 6 DPI.

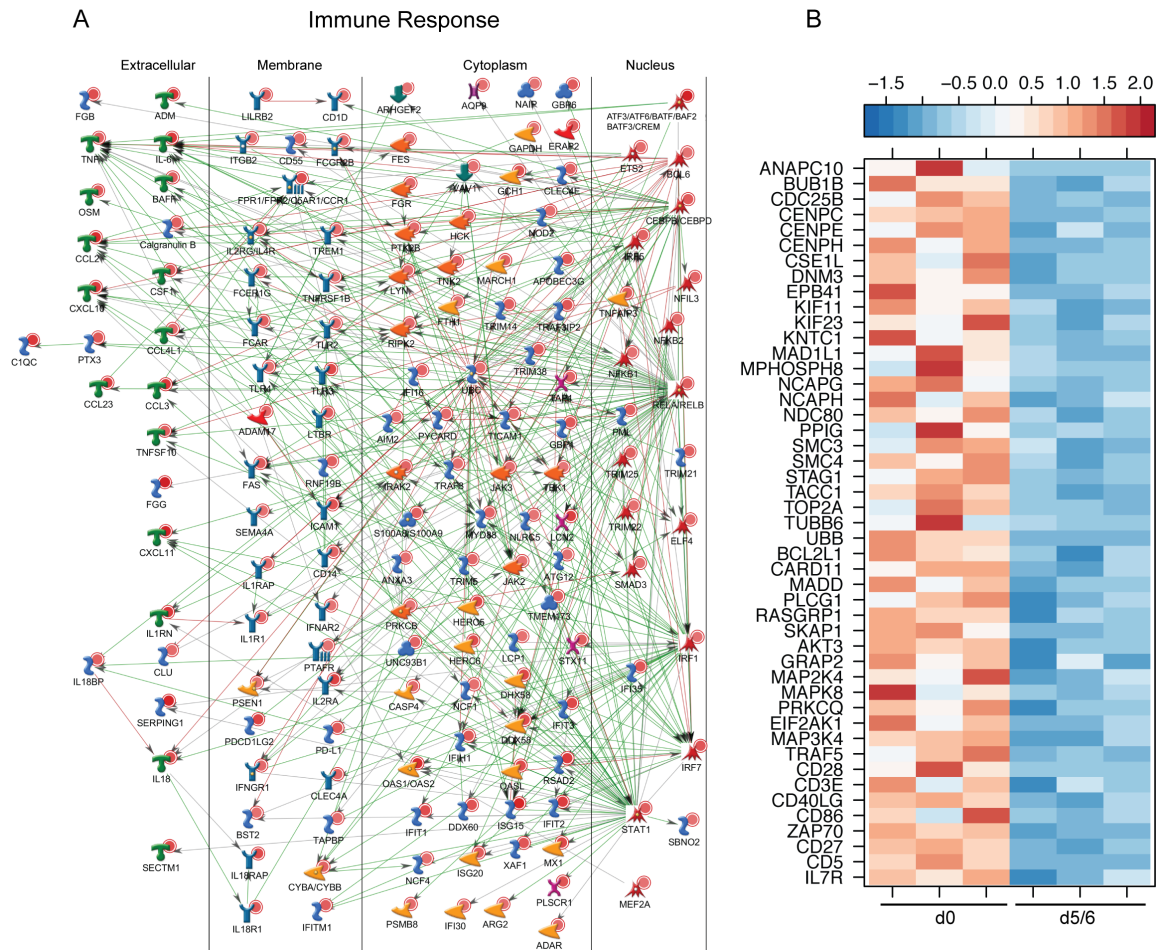
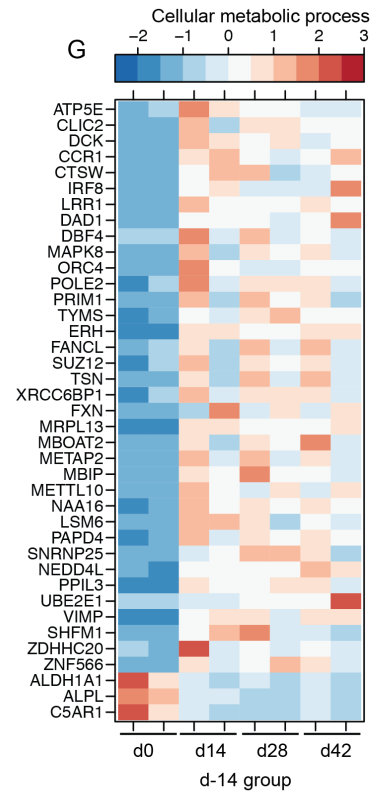
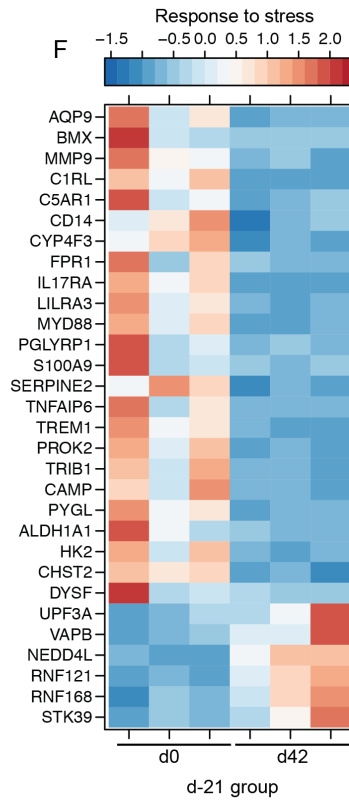
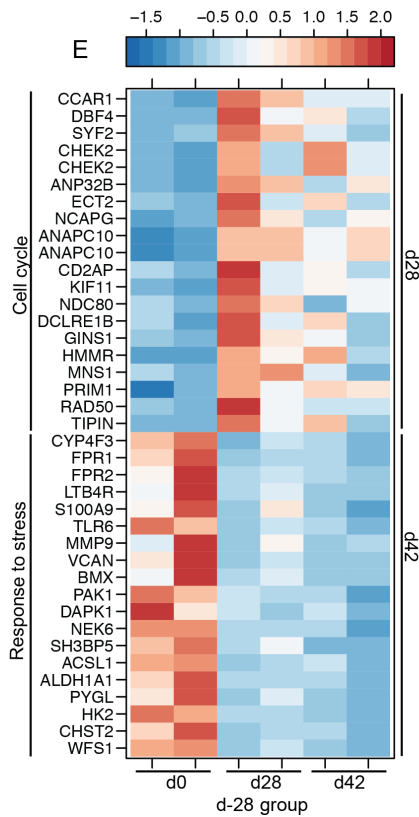
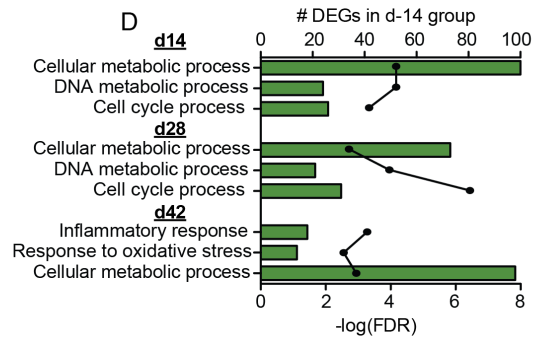
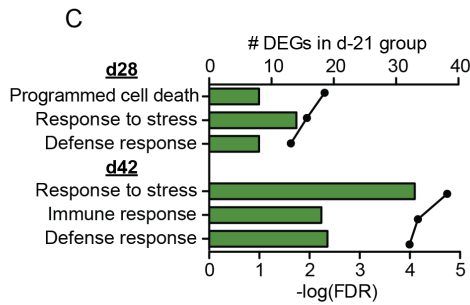
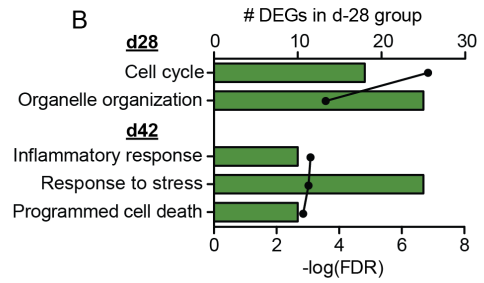
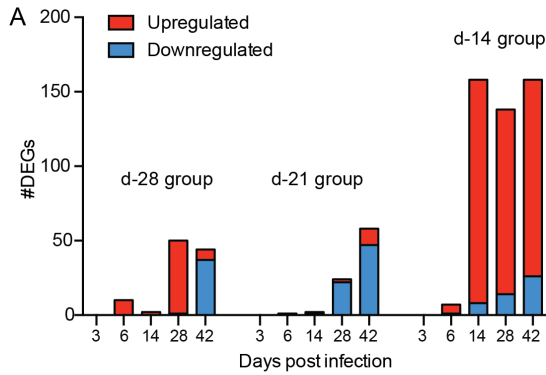


Figure 5.4. Negative control animals display a gene expression changes consistent with dysregulated inflammatory response and lymphopenia. (A) Network image of DEGs upregulated 5/6 DPI in negative control animals that map to “Immune response” with FC ≥ 5.6 and directly interact with each other. (B) Heatmap of genes downregulated 5/6 DPI in negative control animals that map to “Cell cycle” and “TCR signaling”; each column represents 1 animal.

Animals that were vaccinated at least two weeks prior to challenge show limited gene expression changes

Consistent with our earlier study [205], we detected a limited number of DEGs in blood samples collected from the d-28 group following ZEBOV-Makona challenge (**Figure 5.5A**). DEGs detected 28 DPI, which were mostly upregulated, play a role in cell cycle e.g. *CHEK2*, *PRIMI*, *ANAPC10* and *KIF11* (**Figure 5.5B and E**). At 42 DPI, DEGs were mostly downregulated and included genes that play a role in innate immunity and inflammation i.e. *FPR1*, *S100A9* and *TLR6* as well as cell death e.g. *DAPK1* and *SH3BP5* (**Figure 5.5B and E**).

In the day-21 group, DEGs detected 28-42 DPI mostly had decreased expression and play a role in inflammation (e.g. *S100A9*, *C1RL*, *C5AR1*, *CD14*, *FPR1*, *MYD88* and *TREMI*) (**Figure 5.5A, C and F**). A larger number of DEGs were detected in the day-14 group 14, 28 and 42 DPI (**Figure 5.5A**). These DEGs mapped to GO terms associated with metabolic processes and included genes involved in ATP synthesis i.e. *ATP5E*; immunity such as *CCR1*, *CTSW*, *IRF8* and *LRR1*; DNA replication including *ORC4*, *POLE2* and *PRIMI*; and protein degradation e.g. *NEDD4L*, *PPIL3* and *VIMP* (**Figure 5.5D and G**).



(Previous Page) Figure 5.5. Animals that were vaccinated 2 or more weeks prior to challenge show limited gene expression changes. (A) Number of DEGs detected following Makona challenge in animals vaccinated day-28, day-21 and day-14 . **(B-D)** Functional enrichment of DEGs observed in day-28 **(B)**, day-21 **(C)**, and day-14 **(D)** vaccinated animals. **(E)** Heatmap of DEGs in the day-28 group that enriched to “Cell cycle” and/or “Organelle organization” on 28 DPI and “Response to stress” on 42 DPI; each column represents 1 animal. **(F)** Heatmap of DEGs detected 42 DPI in the day-21 group that enriched to “Response to stress”; each column represents 1 animal. **(G)** Heatmap representing DEGs in the day-14 group that overlap at 14, 28 and 42 DPI and enrich to GO terms “Cellular metabolic process”; each column represents 1 animal.

ZEBOV-Makona challenge 1 week after vaccination induces a robust adaptive immune response

Following challenge, a moderate number of DEGs were detected 3 and 6 DPI in the day-7 vaccinated animals. This was followed by a large increase in the number of DEGs 14 and 28 DPI before a return to baseline by 42 DPI (**Figure 5.6A**). DEGs detected 3 and 6 DPI enriched to “Innate immunity”, “Response to stress” and “Type I interferon signaling pathway” (**Figure 5.6B**) and consisted mostly of upregulated ISGs (*ISG15*, *MX1*, *OAS2* and *IFIT1*) (**Figure 5.6C**).

The gene expression changes detected 14 and 28 DPI were largely shared between these two time points (>90%) (**Figure 5.6A**). DEGs upregulated 14 and 28 DPI enriched to GO terms associated with metabolism, cell cycle, and immunity (**Figure 5.7A**). DEGs that mapped to either “Immune system Process”, “T cell differentiation” or “B cell activation” included genes involved in: antigen presentation i.e. *HLA-DQA1*, *CD83* and *CD1C*; lymphocyte proliferation and development i.e. *IL21R*, *TCF7* and *TCF3*; T cell signaling including *CD2*, *CD3G*, *CD4* and *IL2RB*; T cell activation e.g. *CD28* and *ZAP70*; B cell signaling such as *CD19* and *SLAMF1*; and B cell activation e.g. *CD40* and *CD40LG* (**Figure 5.7B**). In silico analysis using the Immquant database indicates that these transcriptional changes are predicted to be associated with a significant increase in CD4 T cells, memory T and B cells 14 DPI (**Figure 5.7C**). DEGs downregulated 14 and 28 DPI also enriched to metabolism, cell cycle, and immunity in addition to signaling and cell death (**Figure 5.7D**). The most downregulated DEGs that enriched to “Myeloid leukocyte

activation” included genes that play a role in chemotaxis and inflammation (*MMP9*, *TNFAIP6* and *S100A9*), neutrophil mediated immunity (*FPRI* and *GCA*), chemotaxis (*CXCR1*, *CXCR2*, and *SIGLEC5*), and pathogen recognition (*TLR 2*, *4* and *6*) (**Figure 5.7E**).

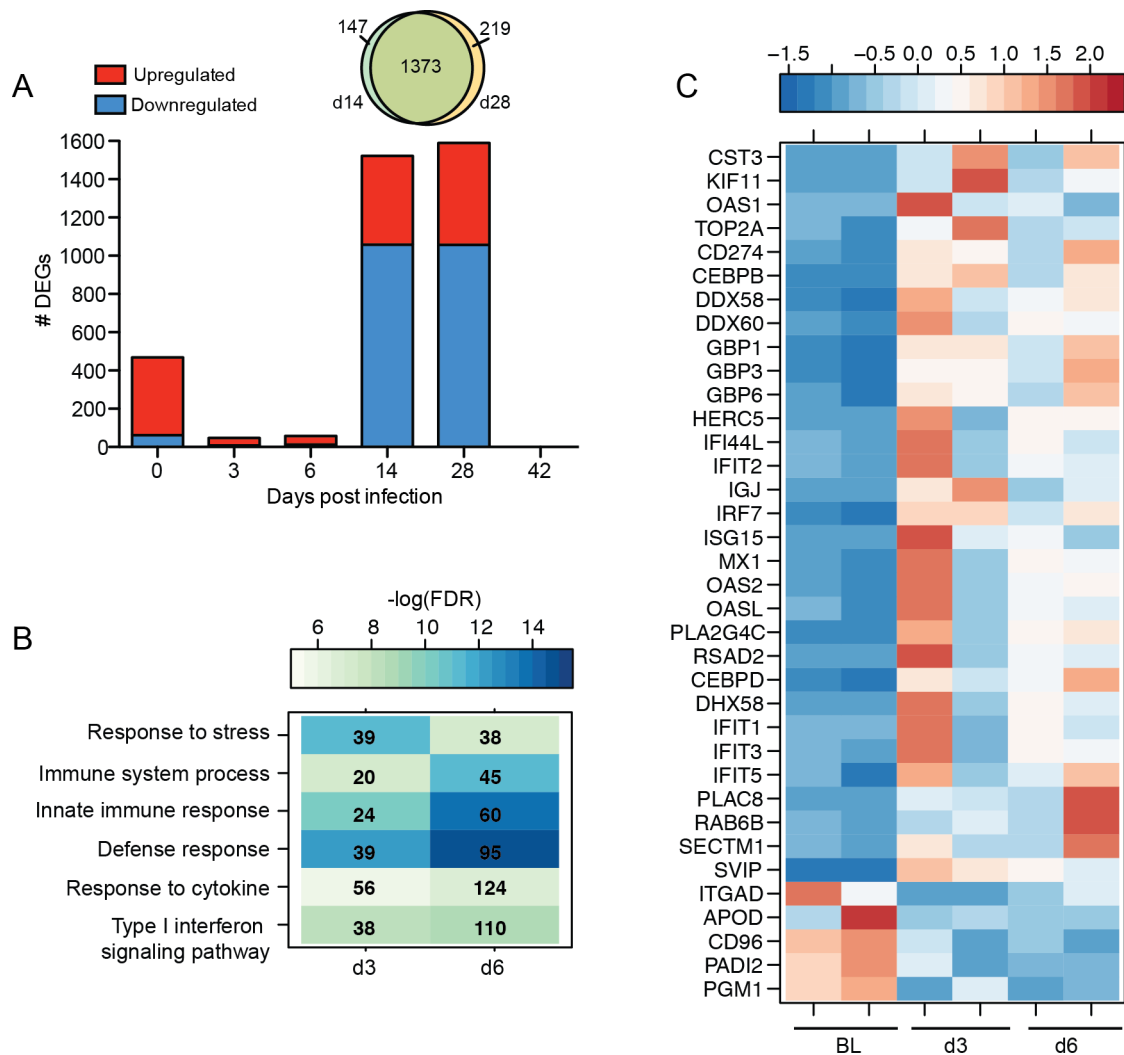
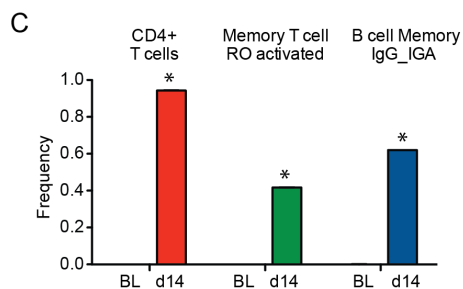
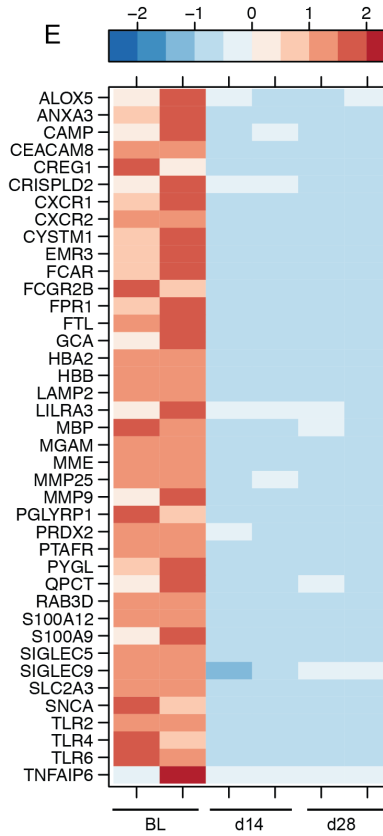
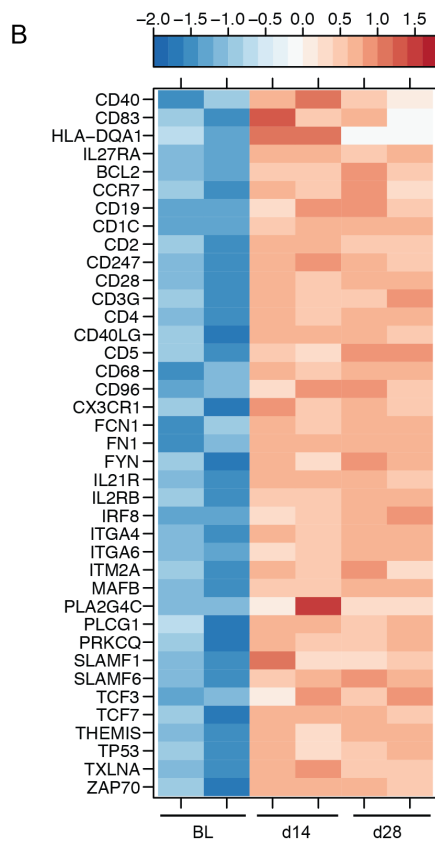
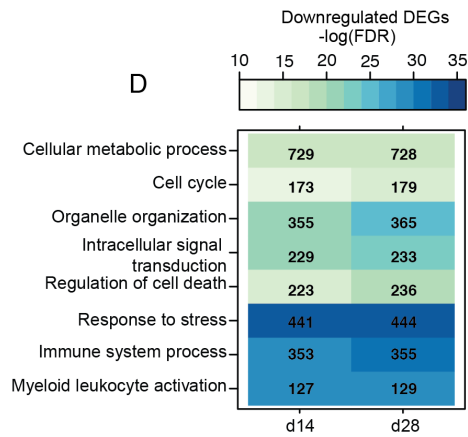
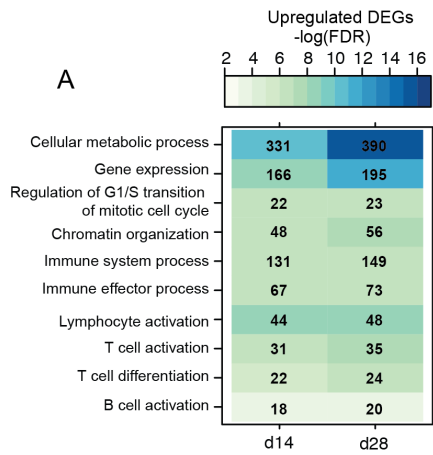


Figure 5.6. ZEBOV-Makona challenge 1 week after vaccination induces a recall response. (A) Number of DEGs detected in day-7 vaccinated animals throughout ZEBOV challenge. Venn diagram of DEGs detected 14 and 28 DPI in the day-28 group. (B) Functional enrichment of DEGs detected 3 and 6 DPI in day-7 vaccinated animals. (C) Heatmap of common DEGs detected 3 and 6 DPI in the day-7 group that enrich to “Immune system process”; each column represents 1 animal; BL represents d-28 animals at 0 DPI.



(Previous Page) Figure 5.7. Animals vaccinated 1 week before challenge exhibit large transcriptional changes associated with adaptive immunity (A) Functional enrichment of upregulated DEGs detected 14 and 28 DPI in the day-7 group. **(B)** Heatmap representing upregulated DEGs detected 14 and 28 DPI in the day-7 group that enriched to “T cell differentiation”, “B cell activation” and “Immune system process”; each column represents 1 animal; BL represents d-28 animals at 0 DPI. **(C)** DCQ analysis predicting changes in immune cell subsets based on DEGs detected 14 DPI in the day-7 group. **(D)** Functional enrichment of downregulated DEGs detected 14 and 28 DPI in the day-7 group. **(E)** Heatmap of downregulated DEGs detected 14 and 28 DPI in the day-7 group that enriched to “Myeloid leukocyte activation” with fold changes greater than 5; each column represents 1 animal; BL represents d-28 animals at 0 DPI.

Animals vaccinated 3 days before challenge display distinct innate immune responses that correlate with disease outcome.

Each of the three animals vaccinated 3 days before challenge displayed distinct disease progression as previously reported [161]. Briefly, one animal (viremic non-survivor; VNS) succumbed 8 DPI after displaying clinical signs consistent with EVD (rash, thrombocytopenia, increased liver enzymes, increased inflammatory mediators) and viremia 6 and 8 DPI. The second animal (viremic survivor; VS) developed mild signs of EVD as well as detectable viral titers 6 DPI but cleared the virus 9 DPI. The third animal exhibited no viremia or EVD symptoms (non-viremic survivor; S). To uncover gene signatures that determine disease outcome, we analyzed transcriptional changes in all three animals separately at early time points post infection. Because edgeR analysis requires more than 1 biological replicate, we used maSigPro, which provides a set of statistically significant DEGs for the entire time-course rather than at each individual time point [277]. Day 0 of the d-28 group served as control and each animal (VNS, VS and S) was treated as a separate experimental condition. This approach identified 546 genes that had temporal expression changes that were significantly different between VNS, VS and S. We next carried out unsupervised gene clustering using a Pearson correlation-based distance measure 0, 3 and 6 DPI to identify groups of co-regulated genes among the three animals (**Figure 5.8**).

On the day of challenge, the viremic animals clustered closer together (**Figure 5.8A**). DEGs that were upregulated only in the non-viremic survivor included: ISGs (e.g. *IFIT1*,

OAS1 and *RSAD2*); antiviral genes (e.g. *TRIM16* and *TRIM38*); and genes important for cell cycle and proliferation (i.e. *RBM38*, *CENPE*, *CDCA5* and *KDR*). Increased transcripts in both surviving animals also included ISGs (*ISG15*, *ISG20*, *IFIT2* and *HERC5*) as well as viral sensors *DHX58* and *TMEM173* (*STING*) [278] (**Figure 5.8A**). Genes that were only upregulated in the non-survivor play a role in inflammation (*TREM2*, *NFKB2*, *CLEC4D* and *PLAC8*) and apoptosis (*PAQR6*, *DDIAS* and *BCL2L14*). Additionally, increased levels of *THBS1*, which plays a role in coagulation, and genes important in oxidative stress such as *NCOA7*, *GLRX*, and *GCHI* a positive regulator of nitric oxide synthesis were detected in both viremic animals.

On DPI 3, expression of ISGs (e.g. *HERC5*, *OAS1*, *ISG15*, *IFIT2* and *GAS6*) remained upregulated only in the animals that developed viremia. Additionally, the VNS animals also showed increased expression of *ISG20*, *GCHI* and *C3AR1* (**Figure 5.8B**). In contrast, the animal that never exhibited clinical signs of EVD exhibited increased expression of genes involved in innate immunity (*CASP4* and *TLR2*), cell adhesion (*SIGLEC11* and *GPR125*), cytoskeleton organization (*RPI* and *RND1*), and cell cycle (*RBM38* and *BIRC5*) (**Figure 5.8B**). Both surviving animals expressed antiviral gene *APOBEC3G* and genes associated with migration such as *MEGF10* and *CRK*, which regulates T cell migration into tissue.

At 6 DPI, the two animals that survived challenge clustered closer. Increased expression of genes important for host defense (*TRIM16*, *TMEM173* and *DEFB108B*) and chemotaxis

(*ENPP2* and *CCL7*) were increased in the animals that survived (**Figure 5.8C**). On the other hand, the animal that succumbed to infection exhibited continued upregulation of ISGs (*ISG20* and *HERC5*) as well as genes that play a role in inflammation (e.g. *CLEC4D* and *C3AR1*). Expression of additional ISGs was increased in both animals that developed viremia (*IFIT1*, *OAS1*, and *ISG15*).

By 14 DPI, no viremia was detected in VS and S, therefore, these two animals were grouped for DEG analysis at subsequent time points (**Figure 5.9**). Most transcriptional changes 14 DPI were upregulated and DEGs with the highest fold change that enriched to “Immune system process” consisted of genes involved in innate immune responses (**Figure 5.9A-C**). In contrast, most DEGs 28 DPI were downregulated and encoded innate immunity related transcripts, suggesting resolution of host response (**Figure 5.9A-B and D**).

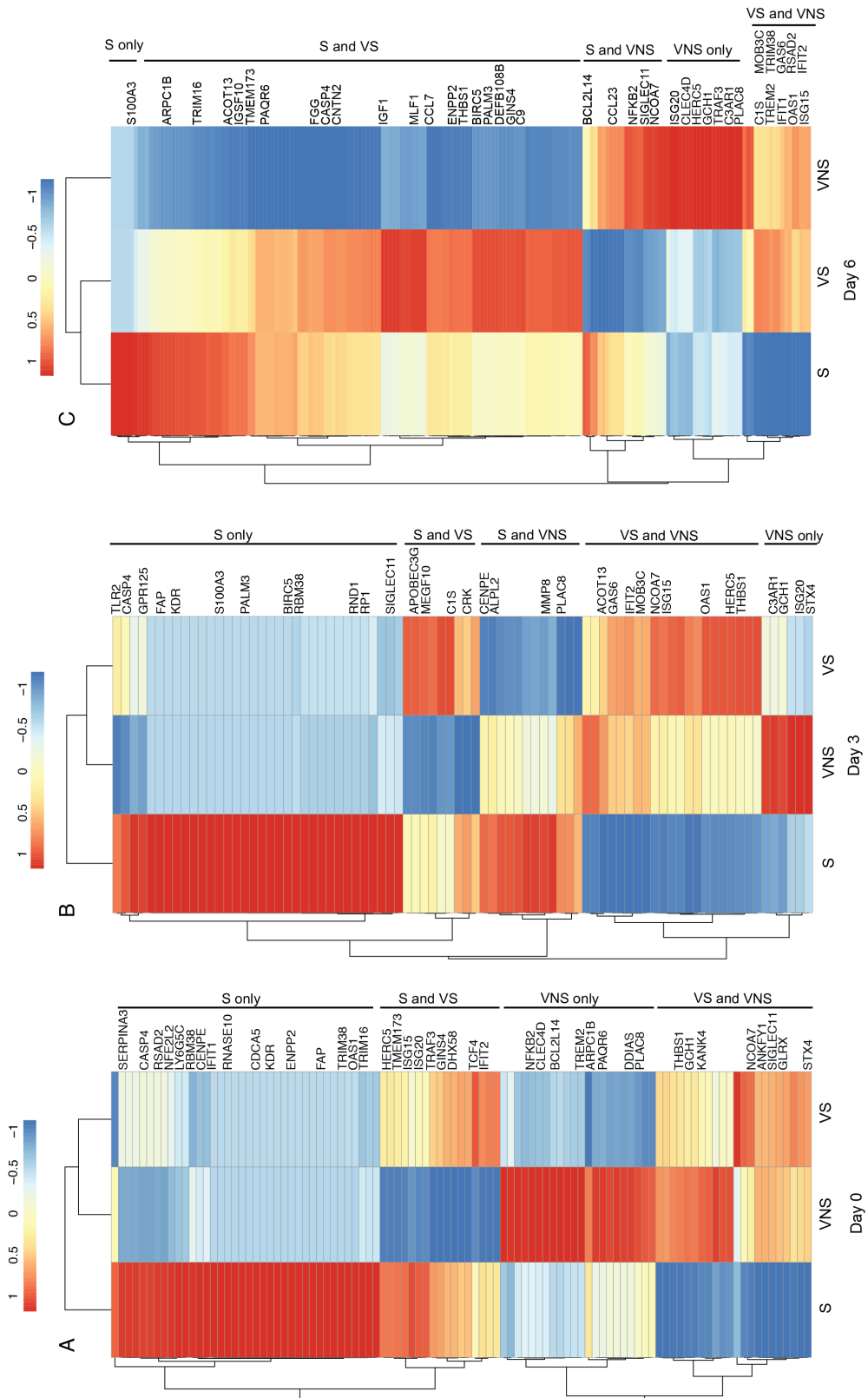


Figure 5.8. Animals vaccinated 3 days before challenge display distinct immune responses that correlate with disease outcome. (A-C) Heatmap representing hierarchical clustering of differentially expressed genes significantly associated with clinical outcome identified by maSigPro on days 0 (A), 3 (B), and 6 (C) post infection. Select genes are shown. Range of colors is based on scaled and centered RPKM values of entire set of genes (red represents increased expression while blue represents decreased expression); each column represents the non-viremic survivor (S), viremic survivor (VS) or viremic non-survivor (VNS).

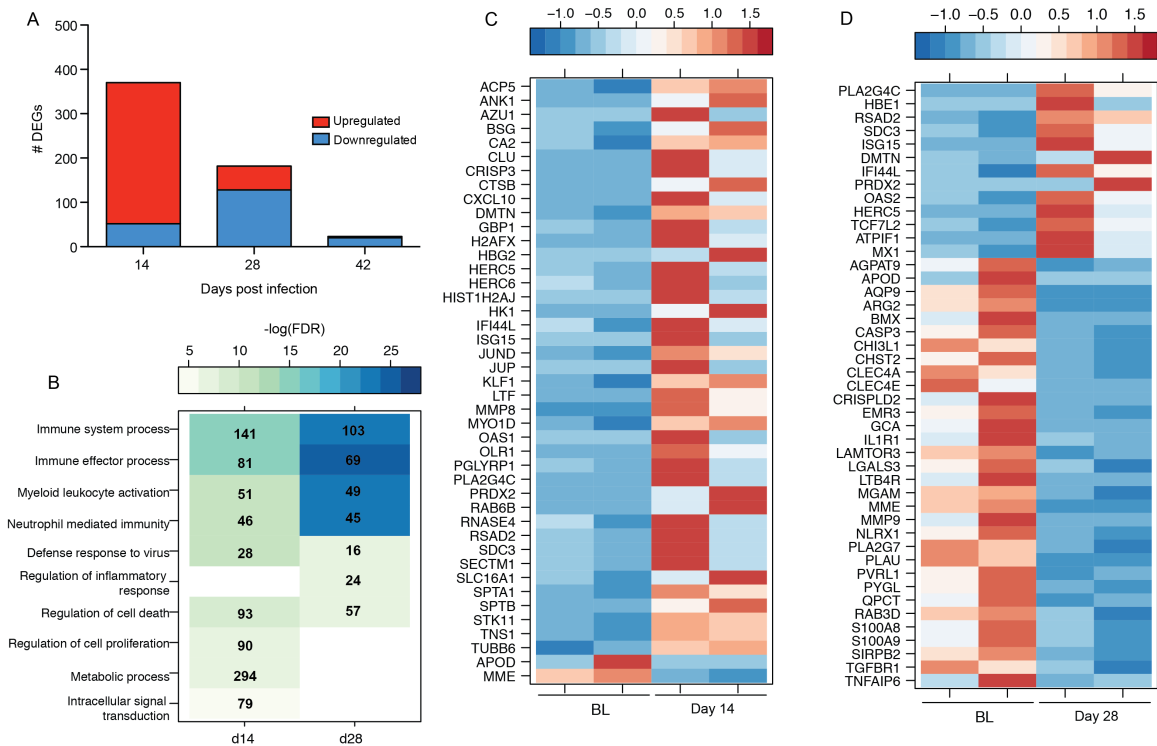


Figure 5.9. Surviving animals in the day-3 group exhibit transcriptional changes consistent with resolution of immune response. (A) Number of DEGs detected in viremic survivor and non-viremic survivor 14, 28 and 42 DPI. **(B)** Functional enrichment of downregulated DEGs detected 14 and 28 DPI in the d-3 surviving animals. **(C)** Heatmap of DEGs detected 14 DPI in the d-3 surviving animals that enriched to “Immune system process” with fold changes greater than 6.8; each column represents 1 animal; BL represents d-28 animals at 0 DPI. **(D)** Heatmap of DEGs detected 28 DPI in the d-3 surviving animals that enriched to “Immune system process” with fold changes greater than 4; each column represents 1 animal; BL represents d-28 animals at 0 DPI.

Discussion

The recombinant live attenuated vaccine rVSV-ZEBOV can confer both rapid and long-term protection against lethal challenge with ZEBOV. While antibodies are the main mode of long-term protection conferred by this vaccine, the mechanisms by which rVSV-ZEBOV elicits rapid protection against ZEBOV are only partially understood. Therefore, in this study, we identified longitudinal changes in peripheral blood transcriptome post ZEBOV-Makona challenge in cynomolgus macaques that were vaccinated 28, 21, 14, 7 and 3 days before challenge.

Although we have recently reported on vaccine-mediated gene expression in PBMC, The current study provided us with an opportunity to define the broader response to the vaccine by analyzing whole blood. Vaccination with rVSV-ZEBOV induced acute gene expression changes 3 and 7 DPV. Consistent with our recent study in PBMC [205], day 7 post rVSV-ZEBOV vaccination is the peak of host transcriptional response. We detected a much larger number of DEGs in WB (467) compared to PBMC (60) 7 DPV, of which only 12 DEGs were shared and consisted of ISGs: *IFIT2*, *IFI44L*, *OAS2*, *OASL*, *IFIT3*, *IFI44* and *GBP6*. This difference is most likely due to responses from neutrophils, which are in WB but not PBMC. Additionally, the current study used a higher vaccine dose compared to our previous study (5×10^7 versus 1×10^7).

The majority of the DEGs detected in WB post rVSV-ZEBOV vaccination are critical for antiviral innate immunity notably ISGs, which had the highest degree of expression 7 DPV.

This is consistent with our previous study in which elevated levels of IFN α were detected 3 and 7 days post vaccination in these animals [161]. At 7 DPV, expression of additional genes important for antiviral innate immunity increased significantly. Notably, expression of genes important for antigen presentation, cell cycle and B cell activation also increased, indicative of the generation of an adaptive immune response. Indeed, we detected increased expression of *LYN*, *BAFF*, and *PRDMI* (aka *BLIMPI*), which are important for B cell activation [279], proliferation [280], and differentiation into plasma cells [281]. Importantly, this B cell signature preceded detection of ZEBOV-GP specific antibodies titers detected at 14 DPV (7 days post ZEBOV infection). We also report increased expression of genes important for cell cycle progression that peaked 3 DPV, consistent with the proliferative burst of lymphocytes that we observed 7 DPV in our previous studies [156]. Also in line with previous reports [156], we did not detect signatures of either CD4 or CD8 T cell responses. Nonetheless, a recent study demonstrated that a single dose of rVSV-ZEBOV (either 2×10^7 or 1×10^8 pfu) induced ZEBOV-GP specific circulating follicular T helper (Tfh) cells, based on the expression of CD40L and CXCR5, which correlated with antibody titers and protection [153]. Furthermore, previous studies have shown type I IFN signaling to be important in generating Tfh cells after viral infection [282-284]. It is possible that the use of whole blood rather than purified CD4 T cells precluded us from detecting transcriptional changes associated with the development of a Tfh cell response.

Following ZEBOV-Makona challenge, we detected robust gene expression changes in negative control animals that correlated with viremia and clinical scores. The transcriptional profile of these animals was characterized by excessive inflammation and lymphopenia consistent with severe EVD and similar to that reported in recent studies [193, 210, 213, 214, 225]. In contrast, animals vaccinated 2 or more weeks before challenge exhibited limited gene expression changes, most likely due to the presence of ZEBOV-GP specific IgG and neutralizing antibody at the time of challenge. As we recently reported [205], animals vaccinated 28 days before challenge displayed limited transcriptional changes post challenge. In our previous study, cynomolgus macaques that were vaccinated with rVSV-ZEBOV and challenged with ZEBOV-Kikwit 28 days later displayed upregulation of genes involved in antiviral defense. However, immune DEGs detected in the animals in this current study were downregulated suggestive of resolution of an immune response. These differences could potentially be attributed to increased vaccine dose and use of Makona strain in the current study. Similarly, we detected the downregulation of genes involved cell death and host defense indicative of immune regulation in day-21 vaccinated animals. Although we observed a larger number of DEGs in day-14 vaccinated animals compared to day-28 and -21 vaccinated animals, these transcriptional changes enriched to metabolic processes, DNA replication and protein degradation, that are not consistent with EVD.

At the time of challenge, day-7 vaccinated animals did not have detectable ZEBOV-GP specific IgG antibody titers but exhibited a large number of transcripts originating from

genes important in antiviral defense. These data strongly suggest that innate defenses engendered by rVSV play a critical role in restricting ZEBOV replication. Additionally, a small number of DEGs involved in inflammation, cell proliferation, antigen presentation and B cell activation were also increased at the time of challenge, indicative of the initial stages of a humoral response. Following challenge, transcriptional changes in these animals strongly suggested the development of a strong recall adaptive immune response 14-28 DPI. Highly expressed genes played a role in antigen presentation, T cell and B cell activation, as well as T and B cell differentiation. Moreover, DCQ analysis predicted an increase in mature B cells with the ability to undergo isotype class switching and CD4 and memory T cells 14-28 DPI. These transcriptional changes strongly suggest that encounter of viral antigen 7 days after vaccination results in the boosting of the initial response. Although GP-specific antibody titers did not increase 14-28 DPI, it is possible that the repertoire and quality of the antibody response changed. Unfortunately, we were also unable to address whether or not these transcriptional changes correlated with the generation of a ZEBOV-specific T cell response. The reason for the delayed appearance of these transcriptional changes (14 days after challenge) is also not understood. These key questions will be the focus of future studies.

Although transcriptional changes that enriched to type I interferon signaling and innate immunity were detected on the day of challenge in the day-3 group, the number of genes and magnitude of fold changes was much smaller compared to that observed in day-7 vaccinated animals. Consequently, immunization 3 days prior to ZEBOV challenge was

not uniformly protective against viremia or fatal disease. Based on our time/group series analysis using maSigPro, gene signatures associated with survival were associated with high expression of ISGs on the day of challenge while viremia and/or fatality was associated with high expression of oxidative stress, inflammatory and apoptotic genes. Specifically, the animal that did not experience any clinical disease expressed the highest number and magnitude of ISGs on the day of challenge. By 3 DPI, expression of ISGs was significantly reduced in this animal, and expression of other inflammatory genes increased, suggesting a tightly regulated innate immune response. This animal also developed ZEBOV-GP specific antibodies 7 DPI. The viremic survivor also expressed ISGs on the day of challenge as well as 3 DPI, which contributed to lower level of viremia compared to the non-survivor. This animal also developed humoral immunity, which was delayed and of lower magnitude compared to the non-viremic survivor.

Unlike the surviving animals, expression of ISGs in the viremic non-survivor was delayed, appearing 3 DPI and peaking 6 DPI. This pattern of expression is reminiscent of that seen in ZEBOV infected unvaccinated cynomolgus macaques and patients who succumbed to EVD [193, 214, 225] and may have instead contributed and exacerbated inflammation characteristic of EVD. Throughout infection, *GCHI*, a positive regulator of nitric oxide production, was only expressed by the viremic non-survivor. This is consistent with our recent report of elevated levels of *GCHI* in monocytes purified from ZEBOV-Makona infected cynomolgus macaques and documented reports of increased nitric oxide in plasma of patients who succumbed to EVD [82, 227].

In summary, we demonstrate that the robust innate antiviral immune response elicited by the rVSV-ZEBOV vaccine facilitates the development of a humoral response. Animals vaccinated 1 week before ZEBOV challenge had high expression antiviral genes at the time of challenge and had vaccine induced antibody titers 7 days post infection. In response to challenge these animals developed a strong recall adaptive immune response 14-28 DPI. In contrast to what we observed in animals vaccinated 7 days before challenge, we did not detect gene expression changes consistent with the generation of a recall response in the animals vaccinated 3 days before challenge. These data are reminiscent of decreased immune responses observed when booster injections are administered too soon following priming vaccination [285]. Future studies should focus on: 1) evaluating the durability of this protective immune response; 2) determining the effector functions elicited by antibodies generated using B cell repertoire sequencing analysis; 3) investigating the role of T cell responses in protection against subsequent infections. Lastly, the timing of ISG expression correlated with regulation of viral replication and disease outcome in animals vaccinated 3 days before challenge. While this analysis provides novel insight into the gene signatures of survival versus fatality, this study should be repeated with a larger cohort and a more in depth longitudinal analysis.

CHAPTER 6: Discussion and Future Directions

ZEBOV causes hemorrhagic fever with high mortality rates and death occurring within a week after symptom onset. The high virulence of ZEBOV is largely attributed to its ability to subvert innate immune responses. *In vitro* studies have shown that ZEBOV infection inhibits antiviral type I interferon responses while promoting uncontrollable inflammation. However, these findings have not been corroborated *in vivo*. Moreover, most gene expression studies conducted in ZEBOV infected nonhuman primates have largely focused on transcriptional changes during final stages of disease. Consequently, ZEBOV-host interactions early during infection *in vivo* are poorly understood. In this dissertation, we address this knowledge gap by investigating longitudinal host responses in peripheral blood collected from cynomolgus macaques inoculated with either wild type ZEBOV, a recombinant ZEBOV that can no longer antagonize type I interferon signaling, or the rVSV-ZEBOV vaccine, using both immunological assays and transcriptomic analysis.

In chapter 2, we report the first comprehensive analysis of the host response to the recently identified ZEBOV variant, Makona, by integrating changes in immune cell frequencies, plasma levels of immune mediators and differentially expressed genes within whole blood and PBMC. Our data revealed that similar to previous variants, ZEBOV-Makona infection results in clinical signs characteristic of EVD including fever, inflammation, lymphopenia, rash, hemorrhaging and organ damage. However, both clinical signs and gene expression

changes appeared later and were less severe than those previously reported for ZEBOV variants Mayinga or Kikwit despite comparable levels of viremia.

In line with data reported in macaques infected with either ZEBOV-Mayinga or ZEBOV-Kikwit, we observed higher pro-inflammatory gene expression 4-6 DPI and increased cytokine and chemokine levels 5-6 days post ZEBOV-Makona infection. Furthermore, we detected for the first time an increase in non-classical monocytes 4 DPI, which are capable of producing large amounts of pro-inflammatory cytokines compared to classical monocytes and may be responsible for the upregulation of inflammatory mediators [220, 221]. Excessive pro-inflammatory cytokine production, is a major contributor in the pathogenesis of viral hemorrhagic fever. Indeed, in chapter 4, animals infected with the recombinant ZEBOV VP35 mutant all survived and displayed a regulated inflammatory response that peaked 3-6 DPI before decreasing near baseline 10 DPI. Similarly, in survivors of ZEBOV infection, the level of circulating cytokines increases briefly and subsides as infection is controlled [80].

Although the responses of monocytes and macrophages infected *in vitro* with ZEBOV suggest these cells as a main source of inflammatory cytokines, these findings had yet to be confirmed *in vivo*. Therefore, in chapter 3 we conducted the first longitudinal transcriptomic analysis in purified immune cell subsets collected from macaques infected with ZEBOV-Makona. Data from this study strongly indicate circulating blood monocytes, but not T or B cells, support productive ZEBOV replication and transcription *in vivo* and

exhibit early expression of genes involved in inflammation followed by increased transcripts associated with coagulation and vascular disease. Importantly, monocytes, which make up 10-15% of PBMC, contributed a more significant portion of transcriptional changes (~20% compared to 2-3%) detected in PBMC 6 days post ZEBOV infection compared to lymphocytes, which make up a majority of the PBMC, thus identifying monocytes as one of the key players in ZEBOV pathogenesis by contributing to the dysregulated inflammatory responses characteristic of EVD.

In vitro studies suggest ZEBOV infection of antigen presenting cells results in the inhibition of expression of co-stimulatory molecules CD80 and CD86, thereby preventing antigen presentation and initiation of adaptive immunity [87, 88, 216]. However, flow cytometry analysis revealed an increased frequency of dendritic cells expressing activation marker CD80. This discrepancy is most likely due to the infection rate being lower *in vivo* resulting in non-infected dendritic cells to become activated by viral debris, such as “shed” GP, which can induce the expression of CD40, CD80, CD83 and CD86 on monocyte-derived DCs [217]. Inhibition of DC activation is believed to be attributed to VP35, which was shown to block upregulation of dendritic cell activation markers CD40, CD80 and CD83 and prevent stimulation of allogeneic T cells [275]. In support of this hypothesis, we report downregulation of genes associated with antigen processing and presentation in infected monocytes. This is in contrast to data from animals infected with the VP35 mutant where we detect the increased expression of genes important for antigen processing and development of adaptive immunity. Future studies should focus on delineating host

immune responses within infected antigen presenting cells (monocytes and DCs) using techniques that address population heterogeneity, such as single cell RNA-Seq.

Inhibition of type I IFN production and suppression of cellular responses to type I IFN by ZEBOV VP35 and VP24 have been documented *in vitro* [87, 88, 216]. However, our data show that ZEBOV-Makona infection *in vivo* induces expression of interferon stimulated genes (ISGs), which continue to increase throughout infection and correlate with peak levels of circulating IFN α 6 DPI. This contrasts the transient peak of type I IFN responses observed in non-lethal viral infections [286-288]. This observation was reported after the onset of symptoms in ZEBOV infected macaques [210, 214]. We also report similar kinetics of ISG expression in purified monocytes 3-6 days post ZEBOV infection.

Despite the high levels of circulating IFN α and expression of ISGs, ZEBOV viral titers continue to rise resulting in uniform fatality. Positive correlations of type I IFN signaling and severity of disease have recently been reported. For instance, Liu and Speranza et al. showed that patients who succumbed to ZEBOV-Makona infection had a stronger upregulation of acute phase responses and an increased abundance of ISG transcripts compared to survivors [261]. In another example, longitudinal transcriptomic analysis in peripheral blood from a surviving male health care worker exposed to ZEBOV during the 2013-2016 ZEBOV-Makona epidemic revealed that type I IFN related transcripts positively correlated with viremia [262].

Our data indicate that the kinetics of type I IFN signaling is important in controlling ZEBOV replication. In chapter 4, we assessed the role of ZEBOV VP35 in mediating pathogenesis for the first time by infecting animals with a recombinant ZEBOV carrying mutations in VP35, which ablate its ability to suppress type I IFN production. Replication of the VP35 mutant was impaired most likely due to its inability to counteract IFN-mediated antiviral responses in infected cells resulting in survival and protection of animals against subsequent infection. We did not detect type I IFN related gene expression in these animals, which may have peaked prior to sample collection, be diluted by the transcriptional contribution of other cells in PBMC, or is only expressed locally (e.g. lymph node tissues).

Additionally, in chapter 5, animals that were challenged with ZEBOV 7 days after vaccination with rVSV-ZEBOV did not have a detectable adaptive immune response but did exhibit a strong upregulation of ISGs, strongly suggesting that antiviral defenses induced by the vaccine play a critical role in restricting viral replication. Furthermore, previous studies show type I IFN signaling to be important in generating Tfh cells after viral infection [282-284]. Thus, the detection of ISGs may influence promotion of humoral immunity as evidenced by elevated expression of DEGs involved in inflammation, cell proliferation, antigen presentation and B cell activation at the time of challenge. To further highlight the importance type I IFN signaling, previous studies using isothermal titration calorimetry uncovered that VP35 of Reston EBOV, which does not cause disease in

humans, has a 2-3 fold lower binding affinity for dsRNA and inhibits IFN β promoter activation at lower levels compared to ZEBOV [273].

In chapter 5, immunization with rVSV-ZEBOV 3 days prior to ZEBOV challenge was not uniformly protective resulting in distinct disease outcomes. This gave us the unique opportunity to investigate differences in early host responses that distinguish survival from fatality. Although this study is limited by the lack of biological replicates, we were able to determine that signatures of survival were associated with an early and high expression of ISGs on the day of challenge. In contrast, expression of ISGs in the non-surviving animal was delayed, appearing 3 DPI and peaking 6 DPI, similar to what is observed in unvaccinated macaques and patients who succumbed to EVD.

Thus the timing and magnitude of type I IFN critically modulate antiviral immunity and disease outcome following ZEBOV infection. Early type I IFN responses may be critical in controlling ZEBOV replication while allowing time for the development of adaptive immune responses. Early treatment of macaques with either IFN- α 2b or IFN β only delayed viremia and death [289, 290]. However, this may be explained by the amount of time required for cells to respond to type I IFNs and produce ISGs, which are the effector molecules of antiviral defense. The delayed ISGs observed in fatal cases may be due to the ablation of early type I IFN production in key cells like plasmacytoid DCs, which are potent IFN α/β producers. Unfortunately one of our limitations was that we were not able to determine transcriptional changes within DCs due to very low cell recovery. Future studies

should employ the use of single cell approaches to define the impact of ZEBOV infection on the production of type I IFN, based on the expression of DC markers (i.e. CD123, CD11c) and detection of viral transcripts.

On the other hand, excessive type I IFN responses after onset of viremia can instead be detrimental, exacerbating inflammatory responses and potentially suppressing T cell activation. In a chronic LCMV infection, production of PD-L1, which inhibits TCR-mediated activation, was dependent on type I IFN signaling [218, 219]. Accordingly, we observed increased transcription of PD-L1 in whole blood and purified monocytes. This preceded the lymphopenia and reduced expression of genes expressed by lymphocytes. Moreover, purified T cells did not have any signatures of T cell activation following infection. This is in line with recent clinical studies that report increased numbers of T cells expressing inhibitory molecules CTLA-4 and PD-1 in ZEBOV Makona fatalities [121]. Therefore, sustained expression of ISGs, driven by ZEBOV-Makona infection may inhibit the ability of lymphocytes to develop an effective defense response.

The data presented in this dissertation provide novel insights into ZEBOV pathogenesis *in vivo* and indicate that ZEBOV interactions with the innate immune system play an important role in determining disease outcome. Future studies should investigate tissue-based responses to ZEBOV as early viral replication can occur in both lymph node and spleen. Finally, the use of single cell technology will enable the comparison of

transcriptional changes in infected monocytes and dendritic cells versus uninfected bystander cells in order to better elucidate the consequences of infection.

References

1. Feldmann, H., W. Slenczka, and H.D. Klenk, *Emerging and reemerging of filoviruses*. Arch Virol Suppl, 1996. **11**: p. 77-100.
2. Slenczka, W. and H.D. Klenk, *Forty years of marburg virus*. J Infect Dis, 2007. **196 Suppl 2**: p. S131-5.
3. Siegert, R., et al., [*On the etiology of an unknown human infection originating from monkeys*]. Dtsch Med Wochenschr, 1967. **92**(51): p. 2341-3.
4. Towner, J.S., et al., *Marburgvirus genomics and association with a large hemorrhagic fever outbreak in Angola*. J Virol, 2006. **80**(13): p. 6497-516.
5. Bausch, D.G., et al., *Marburg hemorrhagic fever associated with multiple genetic lineages of virus*. N Engl J Med, 2006. **355**(9): p. 909-19.
6. Johnson, K.M., et al., *Isolation and partial characterisation of a new virus causing acute haemorrhagic fever in Zaire*. Lancet, 1977. **1**(8011): p. 569-71.
7. Jahrling, P.B., et al., *Preliminary report: isolation of Ebola virus from monkeys imported to USA*. Lancet, 1990. **335**(8688): p. 502-5.
8. Formenty, P., et al., *Human infection due to Ebola virus, subtype Cote d'Ivoire: clinical and biologic presentation*. J Infect Dis, 1999. **179 Suppl 1**: p. S48-53.
9. Amman, B.R., et al., *Oral shedding of Marburg virus in experimentally infected Egyptian fruit bats (*Rousettus aegyptiacus*)*. J Wildl Dis, 2015. **51**(1): p. 113-24.
10. Paweska, J.T., et al., *Virological and serological findings in *Rousettus aegyptiacus* experimentally inoculated with vero cells-adapted hogan strain of Marburg virus*. PLoS One, 2012. **7**(9): p. e45479.
11. Negrodo, A., et al., *Discovery of an ebolavirus-like filovirus in europe*. PLoS Pathog, 2011. **7**(10): p. e1002304.
12. CDC. *Outbreaks Chronology: Ebola Virus Disease*. 2015 January 2, 2015]; Available from: <http://www.cdc.gov/vhf/ebola/outbreaks/history/chronology.html>.
13. (CDC), C.f.D.C.a.P. *Ebola Outbreaks 2000-2017*. 2017 May 4, 2017]; Available from: <https://www.cdc.gov/vhf/ebola/outbreaks/history/summaries.html>.
14. Marzi, A., et al., *Delayed Disease Progression in Cynomolgus Macaques Infected with Ebola Virus Makona Strain*. Emerg Infect Dis, 2015. **21**(10): p. 1777-83.

15. Dowell, S.F., et al., *Transmission of Ebola hemorrhagic fever: a study of risk factors in family members, Kikwit, Democratic Republic of the Congo, 1995. Commission de Lutte contre les Epidemies a Kikwit*. J Infect Dis, 1999. **179 Suppl 1**: p. S87-91.
16. Qin, E., et al., *Clinical Features of Patients With Ebola Virus Disease in Sierra Leone*. Clin Infect Dis, 2015. **61**(4): p. 491-5.
17. Hunt, L., et al., *Clinical presentation, biochemical, and haematological parameters and their association with outcome in patients with Ebola virus disease: an observational cohort study*. Lancet Infect Dis, 2015. **15**(11): p. 1292-9.
18. Feldmann, H. and T.W. Geisbert, *Ebola haemorrhagic fever*. Lancet, 2011. **377**(9768): p. 849-62.
19. Bwaka, M.A., et al., *Ebola hemorrhagic fever in Kikwit, Democratic Republic of the Congo: clinical observations in 103 patients*. J Infect Dis, 1999. **179 Suppl 1**: p. S1-7.
20. Howley, D.M.K.a.P.M., *Fields Virology*. 2013, Philadelphia, PA: Lippincott Williams & Wilkins.
21. Kiley, M.P., et al., *Filoviridae: a taxonomic home for Marburg and Ebola viruses?* Intervirology, 1982. **18**(1-2): p. 24-32.
22. Crary, S.M., et al., *Analysis of the role of predicted RNA secondary structures in Ebola virus replication*. Virology, 2003. **306**(2): p. 210-8.
23. Muhlberger, E., et al., *Three of the four nucleocapsid proteins of Marburg virus, NP, VP35, and L, are sufficient to mediate replication and transcription of Marburg virus-specific monocistronic minigenomes*. J Virol, 1998. **72**(11): p. 8756-64.
24. Muhlberger, E., et al., *Comparison of the transcription and replication strategies of marburg virus and Ebola virus by using artificial replication systems*. J Virol, 1999. **73**(3): p. 2333-42.
25. Kawaoka, Y., *How Ebola virus infects cells*. N Engl J Med, 2005. **352**(25): p. 2645-6.
26. Sanchez, A., et al., *Sequence analysis of the Ebola virus genome: organization, genetic elements, and comparison with the genome of Marburg virus*. Virus Res, 1993. **29**(3): p. 215-40.

27. Will, C., et al., *Marburg virus gene 4 encodes the virion membrane protein, a type I transmembrane glycoprotein*. J Virol, 1993. **67**(3): p. 1203-10.
28. Volchkov, V.E., et al., *Release of viral glycoproteins during Ebola virus infection*. Virology, 1998. **245**(1): p. 110-9.
29. Sanchez, A., et al., *The virion glycoproteins of Ebola viruses are encoded in two reading frames and are expressed through transcriptional editing*. Proc Natl Acad Sci U S A, 1996. **93**(8): p. 3602-7.
30. Volchkov, V.E., et al., *GP mRNA of Ebola virus is edited by the Ebola virus polymerase and by T7 and vaccinia virus polymerases*. Virology, 1995. **214**(2): p. 421-30.
31. Feldmann, H., et al., *Marburg virus, a filovirus: messenger RNAs, gene order, and regulatory elements of the replication cycle*. Virus Res, 1992. **24**(1): p. 1-19.
32. Noda, T., et al., *Ebola virus VP40 drives the formation of virus-like filamentous particles along with GP*. J Virol, 2002. **76**(10): p. 4855-65.
33. Dolnik, O., L. Kolesnikova, and S. Becker, *Filoviruses: Interactions with the host cell*. Cell Mol Life Sci, 2008. **65**(5): p. 756-76.
34. Misasi, J. and N.J. Sullivan, *Camouflage and misdirection: the full-on assault of ebola virus disease*. Cell, 2014. **159**(3): p. 477-86.
35. Chan, S.Y., et al., *Folate receptor-alpha is a cofactor for cellular entry by Marburg and Ebola viruses*. Cell, 2001. **106**(1): p. 117-26.
36. Feldmann, H., A. Sanchez, and T.W. Geisbert, *Fields Virology*. 6th ed. Filoviridae: Marburg and Ebola Viruses. Vol. 1. 2013: Wolters Kluwer.
37. Nanbo, A., et al., *Ebolavirus is internalized into host cells via macropinocytosis in a viral glycoprotein-dependent manner*. PLoS Pathog, 2010. **6**(9): p. e1001121.
38. Aleksandrowicz, P., et al., *Ebola virus enters host cells by macropinocytosis and clathrin-mediated endocytosis*. J Infect Dis, 2011. **204 Suppl 3**: p. S957-67.
39. Ito, H., et al., *Ebola virus glycoprotein: proteolytic processing, acylation, cell tropism, and detection of neutralizing antibodies*. J Virol, 2001. **75**(3): p. 1576-80.
40. Watanabe, S., et al., *Functional importance of the coiled-coil of the Ebola virus glycoprotein*. J Virol, 2000. **74**(21): p. 10194-201.

41. Weissenhorn, W., et al., *The central structural feature of the membrane fusion protein subunit from the Ebola virus glycoprotein is a long triple-stranded coiled coil*. Proc Natl Acad Sci U S A, 1998. **95**(11): p. 6032-6.
42. Wool-Lewis, R.J. and P. Bates, *Characterization of Ebola virus entry by using pseudotyped viruses: identification of receptor-deficient cell lines*. J Virol, 1998. **72**(4): p. 3155-60.
43. Cote, M., et al., *Small molecule inhibitors reveal Niemann-Pick C1 is essential for Ebola virus infection*. Nature, 2011. **477**(7364): p. 344-8.
44. Carette, J.E., et al., *Ebola virus entry requires the cholesterol transporter Niemann-Pick C1*. Nature, 2011. **477**(7364): p. 340-3.
45. Chandran, K., et al., *Endosomal proteolysis of the Ebola virus glycoprotein is necessary for infection*. Science, 2005. **308**(5728): p. 1643-5.
46. Wang, H., et al., *Ebola Viral Glycoprotein Bound to Its Endosomal Receptor Niemann-Pick C1*. Cell, 2016. **164**(1-2): p. 258-68.
47. Sanchez, A. and M.P. Kiley, *Identification and analysis of Ebola virus messenger RNA*. Virology, 1987. **157**(2): p. 414-20.
48. Ball, L.A. and G.W. Wertz, *VSV RNA synthesis: how can you be positive?* Cell, 1981. **26**(2 Pt 2): p. 143-4.
49. Weik, M., et al., *Ebola virus VP30-mediated transcription is regulated by RNA secondary structure formation*. J Virol, 2002. **76**(17): p. 8532-9.
50. Klenk, H.-D. and H. Feldman, *Ebola and Marburg Viruses*. Molecular and Cellular Biology, 2004.
51. Bray, M., et al., *A mouse model for evaluation of prophylaxis and therapy of Ebola hemorrhagic fever*. J Infect Dis, 1998. **178**(3): p. 651-61.
52. Bray, M., et al., *Haematological, biochemical and coagulation changes in mice, guinea-pigs and monkeys infected with a mouse-adapted variant of Ebola Zaire virus*. J Comp Pathol, 2001. **125**(4): p. 243-53.
53. Ebihara, H., et al., *Molecular determinants of Ebola virus virulence in mice*. PLoS Pathog, 2006. **2**(7): p. e73.
54. Collaborative Cross, C., *The genome architecture of the Collaborative Cross mouse genetic reference population*. Genetics, 2012. **190**(2): p. 389-401.

55. Rasmussen, A.L., et al., *Host genetic diversity enables Ebola hemorrhagic fever pathogenesis and resistance*. *Science*, 2014. **346**(6212): p. 987-91.
56. Bird, B.H., et al., *Humanized Mouse Model of Ebola Virus Disease Mimics the Immune Responses in Human Disease*. *J Infect Dis*, 2016. **213**(5): p. 703-11.
57. Bente, D., et al., *Disease modeling for Ebola and Marburg viruses*. *Dis Model Mech*, 2009. **2**(1-2): p. 12-7.
58. Geisbert, T.W., et al., *Pathogenesis of Ebola hemorrhagic fever in cynomolgus macaques: evidence that dendritic cells are early and sustained targets of infection*. *Am J Pathol*, 2003. **163**(6): p. 2347-70.
59. Geisbert, T.W., et al., *Pathogenesis of Ebola hemorrhagic fever in primate models: evidence that hemorrhage is not a direct effect of virus-induced cytolysis of endothelial cells*. *Am J Pathol*, 2003. **163**(6): p. 2371-82.
60. Nathan, C., *Neutrophils and immunity: challenges and opportunities*. *Nat Rev Immunol*, 2006. **6**(3): p. 173-82.
61. Randolph, G.J., C. Jakubzick, and C. Qu, *Antigen presentation by monocytes and monocyte-derived cells*. *Curr Opin Immunol*, 2008. **20**(1): p. 52-60.
62. Banchereau, J. and R.M. Steinman, *Dendritic cells and the control of immunity*. *Nature*, 1998. **392**(6673): p. 245-52.
63. O'Keeffe, M., W.H. Mok, and K.J. Radford, *Human dendritic cell subsets and function in health and disease*. *Cell Mol Life Sci*, 2015. **72**(22): p. 4309-25.
64. Pyzik, M. and S.M. Vidal, *Natural killer cells: NK cells stroll down the memory lane*. *Immunol Cell Biol*, 2009. **87**(4): p. 261-3.
65. Thompson, M.R., et al., *Pattern recognition receptors and the innate immune response to viral infection*. *Viruses*, 2011. **3**(6): p. 920-40.
66. Schneider, W.M., M.D. Chevillotte, and C.M. Rice, *Interferon-stimulated genes: a complex web of host defenses*. *Annu Rev Immunol*, 2014. **32**: p. 513-45.
67. Schoggins, J.W., *Interferon-stimulated genes: roles in viral pathogenesis*. *Curr Opin Virol*, 2014. **6**: p. 40-6.
68. Chaplin, D.D., *Overview of the immune response*. *J Allergy Clin Immunol*, 2010. **125**(2 Suppl 2): p. S3-23.
69. Milstein, O., et al., *CTLs respond with activation and granule secretion when serving as targets for T-cell recognition*. *Blood*, 2011. **117**(3): p. 1042-52.

70. Mosmann, T.R. and S. Sad, *The expanding universe of T-cell subsets: Th1, Th2 and more*. Immunol Today, 1996. **17**(3): p. 138-46.
71. De Carli, M., et al., *Human Th1 and Th2 cells: functional properties, regulation of development and role in autoimmunity*. Autoimmunity, 1994. **18**(4): p. 301-8.
72. Hale, J.S. and R. Ahmed, *Memory T follicular helper CD4 T cells*. Front Immunol, 2015. **6**: p. 16.
73. Dorner, T. and A. Radbruch, *Antibodies and B cell memory in viral immunity*. Immunity, 2007. **27**(3): p. 384-92.
74. Caraux, A., et al., *Circulating human B and plasma cells. Age-associated changes in counts and detailed characterization of circulating normal CD138- and CD138+ plasma cells*. Haematologica, 2010. **95**(6): p. 1016-20.
75. Jegaskanda, S., et al., *Antibody-dependent cellular cytotoxicity is associated with control of pandemic H1N1 influenza virus infection of macaques*. J Virol, 2013. **87**(10): p. 5512-22.
76. Geisbert, T.W., et al., *Apoptosis induced in vitro and in vivo during infection by Ebola and Marburg viruses*. Lab Invest, 2000. **80**(2): p. 171-86.
77. Hensley, L.E., et al., *Proinflammatory response during Ebola virus infection of primate models: possible involvement of the tumor necrosis factor receptor superfamily*. Immunol Lett, 2002. **80**(3): p. 169-79.
78. Stroher, U., et al., *Infection and activation of monocytes by Marburg and Ebola viruses*. J Virol, 2001. **75**(22): p. 11025-33.
79. Gupta, M., et al., *Monocyte-derived human macrophages and peripheral blood mononuclear cells infected with ebola virus secrete MIP-1alpha and TNF-alpha and inhibit poly-IC-induced IFN-alpha in vitro*. Virology, 2001. **284**(1): p. 20-5.
80. Baize, S., et al., *Inflammatory responses in Ebola virus-infected patients*. Clin Exp Immunol, 2002. **128**(1): p. 163-8.
81. Ebihara, H., et al., *Host response dynamics following lethal infection of rhesus macaques with Zaire ebolavirus*. J Infect Dis, 2011. **204 Suppl 3**: p. S991-9.
82. Sanchez, A., et al., *Analysis of human peripheral blood samples from fatal and nonfatal cases of Ebola (Sudan) hemorrhagic fever: cellular responses, virus load, and nitric oxide levels*. J Virol, 2004. **78**(19): p. 10370-7.

83. Villinger, F., et al., *Markedly elevated levels of interferon (IFN)-gamma, IFN-alpha, interleukin (IL)-2, IL-10, and tumor necrosis factor-alpha associated with fatal Ebola virus infection.* J Infect Dis, 1999. **179 Suppl 1**: p. S188-91.
84. Wauquier, N., et al., *Human fatal zaire ebola virus infection is associated with an aberrant innate immunity and with massive lymphocyte apoptosis.* PLoS Negl Trop Dis, 2010. **4**(10).
85. Baize, S., et al., *Apoptosis in fatal Ebola infection. Does the virus toll the bell for immune system?* Apoptosis, 2000. **5**(1): p. 5-7.
86. Geisbert, T.W., et al., *Mechanisms underlying coagulation abnormalities in ebola hemorrhagic fever: overexpression of tissue factor in primate monocytes/macrophages is a key event.* J Infect Dis, 2003. **188**(11): p. 1618-29.
87. Mahanty, S., et al., *Cutting edge: impairment of dendritic cells and adaptive immunity by Ebola and Lassa viruses.* J Immunol, 2003. **170**(6): p. 2797-801.
88. Bosio, C.M., et al., *Ebola and Marburg viruses replicate in monocyte-derived dendritic cells without inducing the production of cytokines and full maturation.* J Infect Dis, 2003. **188**(11): p. 1630-8.
89. Lubaki, N.M., et al., *The lack of maturation of Ebola virus-infected dendritic cells results from the cooperative effect of at least two viral domains.* J Virol, 2013. **87**(13): p. 7471-85.
90. Cardenas, W.B., et al., *Ebola virus VP35 protein binds double-stranded RNA and inhibits alpha/beta interferon production induced by RIG-I signaling.* J Virol, 2006. **80**(11): p. 5168-78.
91. Luthra, P., et al., *Mutual antagonism between the Ebola virus VP35 protein and the RIG-I activator PACT determines infection outcome.* Cell Host Microbe, 2013. **14**(1): p. 74-84.
92. Basler, C.F., et al., *The Ebola virus VP35 protein inhibits activation of interferon regulatory factor 3.* J Virol, 2003. **77**(14): p. 7945-56.
93. Prins, K.C., W.B. Cardenas, and C.F. Basler, *Ebola virus protein VP35 impairs the function of interferon regulatory factor-activating kinases IKKepsilon and TBK-1.* J Virol, 2009. **83**(7): p. 3069-77.
94. Chang, T.H., et al., *Ebola Zaire virus blocks type I interferon production by exploiting the host SUMO modification machinery.* PLoS Pathog, 2009. **5**(6): p. e1000493.

95. Prins, K.C., et al., *Mutations abrogating VP35 interaction with double-stranded RNA render Ebola virus avirulent in guinea pigs*. J Virol, 2010. **84**(6): p. 3004-15.
96. Mateo, M., et al., *Ebolavirus VP24 binding to karyopherins is required for inhibition of interferon signaling*. J Virol, 2010. **84**(2): p. 1169-75.
97. Reid, S.P., et al., *Ebola virus VP24 binds karyopherin alpha1 and blocks STAT1 nuclear accumulation*. J Virol, 2006. **80**(11): p. 5156-67.
98. Reid, S.P., et al., *Ebola virus VP24 proteins inhibit the interaction of NPI-1 subfamily karyopherin alpha proteins with activated STAT1*. J Virol, 2007. **81**(24): p. 13469-77.
99. Xu, W., et al., *Ebola virus VP24 targets a unique NLS binding site on karyopherin alpha 5 to selectively compete with nuclear import of phosphorylated STAT1*. Cell Host Microbe, 2014. **16**(2): p. 187-200.
100. Mohamadzadeh, M., et al., *Activation of triggering receptor expressed on myeloid cells-1 on human neutrophils by marburg and ebola viruses*. J Virol, 2006. **80**(14): p. 7235-44.
101. Reed, D.S., et al., *Depletion of peripheral blood T lymphocytes and NK cells during the course of ebola hemorrhagic Fever in cynomolgus macaques*. Viral Immunol, 2004. **17**(3): p. 390-400.
102. Jaax, N.K., et al., *Lethal experimental infection of rhesus monkeys with Ebola-Zaire (Mayinga) virus by the oral and conjunctival route of exposure*. Arch Pathol Lab Med, 1996. **120**(2): p. 140-55.
103. Bradfute, S.B., et al., *Lymphocyte death in a mouse model of Ebola virus infection*. J Infect Dis, 2007. **196 Suppl 2**: p. S296-304.
104. Gupta, M., C. Spiropoulou, and P.E. Rollin, *Ebola virus infection of human PBMCs causes massive death of macrophages, CD4 and CD8 T cell sub-populations in vitro*. Virology, 2007. **364**(1): p. 45-54.
105. Baize, S., et al., *Defective humoral responses and extensive intravascular apoptosis are associated with fatal outcome in Ebola virus-infected patients*. Nat Med, 1999. **5**(4): p. 423-6.
106. Bradfute, S.B., et al., *Mechanisms and consequences of ebolavirus-induced lymphocyte apoptosis*. J Immunol, 2010. **184**(1): p. 327-35.
107. Rath, P.C. and B.B. Aggarwal, *TNF-induced signaling in apoptosis*. J Clin Immunol, 1999. **19**(6): p. 350-64.

108. Simon, H.U., A. Haj-Yehia, and F. Levi-Schaffer, *Role of reactive oxygen species (ROS) in apoptosis induction*. Apoptosis, 2000. **5**(5): p. 415-8.
109. Snyder, C.M., et al., *Nitric oxide induces cell death by regulating anti-apoptotic BCL-2 family members*. PLoS One, 2009. **4**(9): p. e7059.
110. Bah, E.I., et al., *Clinical presentation of patients with Ebola virus disease in Conakry, Guinea*. N Engl J Med, 2015. **372**(1): p. 40-7.
111. Leroy, E.M., et al., *Early immune responses accompanying human asymptomatic Ebola infections*. Clin Exp Immunol, 2001. **124**(3): p. 453-60.
112. Bradfute, S.B., K.L. Warfield, and S. Bavari, *Functional CD8+ T cell responses in lethal Ebola virus infection*. J Immunol, 2008. **180**(6): p. 4058-66.
113. Jeffers, S.A., D.A. Sanders, and A. Sanchez, *Covalent modifications of the ebola virus glycoprotein*. J Virol, 2002. **76**(24): p. 12463-72.
114. Yang, Z.Y., et al., *Identification of the Ebola virus glycoprotein as the main viral determinant of vascular cell cytotoxicity and injury*. Nat Med, 2000. **6**(8): p. 886-9.
115. Francica, J.R., et al., *Steric shielding of surface epitopes and impaired immune recognition induced by the ebola virus glycoprotein*. PLoS Pathog, 2010. **6**(9): p. e1001098.
116. Lee, J.E., et al., *Structure of the Ebola virus glycoprotein bound to an antibody from a human survivor*. Nature, 2008. **454**(7201): p. 177-82.
117. Reynard, O., et al., *Ebolavirus glycoprotein GP masks both its own epitopes and the presence of cellular surface proteins*. J Virol, 2009. **83**(18): p. 9596-601.
118. Mehedi, M., et al., *A new Ebola virus nonstructural glycoprotein expressed through RNA editing*. J Virol, 2011. **85**(11): p. 5406-14.
119. Mohan, G.S., et al., *Antigenic subversion: a novel mechanism of host immune evasion by Ebola virus*. PLoS Pathog, 2012. **8**(12): p. e1003065.
120. McElroy, A.K., et al., *Human Ebola virus infection results in substantial immune activation*. Proc Natl Acad Sci U S A, 2015. **112**(15): p. 4719-24.
121. Ruibal, P., et al., *Unique human immune signature of Ebola virus disease in Guinea*. Nature, 2016. **533**(7601): p. 100-4.
122. Kang, E.S., et al., *Hypotension during hemodialysis: role for nitric oxide*. Am J Med Sci, 1997. **313**(3): p. 138-46.

123. Neumann, F.J., et al., *Effect of human recombinant interleukin-6 and interleukin-8 on monocyte procoagulant activity*. *Arterioscler Thromb Vasc Biol*, 1997. **17**(12): p. 3399-405.
124. Mattia, J.G., et al., *Early clinical sequelae of Ebola virus disease in Sierra Leone: a cross-sectional study*. *Lancet Infect Dis*, 2015.
125. Qureshi, A.I., et al., *Study of Ebola Virus Disease Survivors in Guinea*. *Clin Infect Dis*, 2015. **61**(7): p. 1035-42.
126. Clark, D.V., et al., *Long-term sequelae after Ebola virus disease in Bundibugyo, Uganda: a retrospective cohort study*. *Lancet Infect Dis*, 2015. **15**(8): p. 905-12.
127. Deen, G.F., et al., *Ebola RNA Persistence in Semen of Ebola Virus Disease Survivors - Preliminary Report*. *N Engl J Med*, 2015.
128. Mate, S.E., et al., *Molecular Evidence of Sexual Transmission of Ebola Virus*. *N Engl J Med*, 2015. **373**(25): p. 2448-54.
129. Varkey, J.B., et al., *Persistence of Ebola Virus in Ocular Fluid during Convalescence*. *N Engl J Med*, 2015. **372**(25): p. 2423-7.
130. Fink, S. *Ebola Survivor From Scotland Is Critically Ill*. 2015 [cited 2016 February 8]; Available from: <http://www.nytimes.com/2015/10/15/world/europe/scottish-nurse-who-had-ebola-is-back-in-hospital-and-critically-ill.html>.
131. Baggi, F.M., et al., *Management of pregnant women infected with Ebola virus in a treatment centre in Guinea, June 2014*. *Euro Surveill*, 2014. **19**(49).
132. Kaplan, H.J. and J.Y. Niederkorn, *Regional immunity and immune privilege*. *Chem Immunol Allergy*, 2007. **92**: p. 11-26.
133. de La Vega, M.A., et al., *Ebola viral load at diagnosis associates with patient outcome and outbreak evolution*. *J Clin Invest*, 2015. **125**(12): p. 4421-8.
134. Zhang, X., et al., *Prognostic Analysis of Patients with Ebola Virus Disease*. *PLoS Negl Trop Dis*, 2015. **9**(9): p. e0004113.
135. Schieffelin, J.S., et al., *Clinical illness and outcomes in patients with Ebola in Sierra Leone*. *N Engl J Med*, 2014. **371**(22): p. 2092-100.
136. Rollin, P.E., D.G. Bausch, and A. Sanchez, *Blood chemistry measurements and D-Dimer levels associated with fatal and nonfatal outcomes in humans infected with Sudan Ebola virus*. *J Infect Dis*, 2007. **196 Suppl 2**: p. S364-71.

137. Reid, S.P., et al., *HSPA5 is an essential host factor for Ebola virus infection*. Antiviral Res, 2014. **109**: p. 171-4.
138. Spurgers, K.B., et al., *Identification of essential filovirion-associated host factors by serial proteomic analysis and RNAi screen*. Mol Cell Proteomics, 2010. **9**(12): p. 2690-703.
139. Sanchez, A., K.E. Wagoner, and P.E. Rollin, *Sequence-based human leukocyte antigen-B typing of patients infected with Ebola virus in Uganda in 2000: identification of alleles associated with fatal and nonfatal disease outcomes*. J Infect Dis, 2007. **196 Suppl 2**: p. S329-36.
140. Wauquier, N., et al., *Association of KIR2DS1 and KIR2DS3 with fatal outcome in Ebola virus infection*. Immunogenetics, 2010. **62**(11-12): p. 767-71.
141. Friedrich, B.M., et al., *Potential vaccines and post-exposure treatments for filovirus infections*. Viruses, 2012. **4**(9): p. 1619-50.
142. Sullivan, N.J., et al., *Immune protection of nonhuman primates against Ebola virus with single low-dose adenovirus vectors encoding modified GPs*. PLoS Med, 2006. **3**(6): p. e177.
143. Sullivan, N.J., et al., *CD8+ cellular immunity mediates rAd5 vaccine protection against Ebola virus infection of nonhuman primates*. Nat Med, 2011. **17**(9): p. 1128-31.
144. Ledgerwood, J.E., et al., *A replication defective recombinant Ad5 vaccine expressing Ebola virus GP is safe and immunogenic in healthy adults*. Vaccine, 2010. **29**(2): p. 304-13.
145. Zhu, F.C., et al., *Safety and immunogenicity of a novel recombinant adenovirus type-5 vector-based Ebola vaccine in healthy adults in China: preliminary report of a randomised, double-blind, placebo-controlled, phase 1 trial*. Lancet, 2015. **385**(9984): p. 2272-9.
146. Geisbert, T.W., et al., *Recombinant adenovirus serotype 26 (Ad26) and Ad35 vaccine vectors bypass immunity to Ad5 and protect nonhuman primates against ebolavirus challenge*. J Virol, 2011. **85**(9): p. 4222-33.
147. Stanley, D.A., et al., *Chimpanzee adenovirus vaccine generates acute and durable protective immunity against ebolavirus challenge*. Nat Med, 2014. **20**(10): p. 1126-9.
148. Ledgerwood, J.E., et al., *Chimpanzee Adenovirus Vector Ebola Vaccine - Preliminary Report*. N Engl J Med, 2014.

149. Rampling, T., et al., *A Monovalent Chimpanzee Adenovirus Ebola Vaccine - Preliminary Report*. N Engl J Med, 2015.
150. Kennedy, S.B., et al., *Phase 2 Placebo-Controlled Trial of Two Vaccines to Prevent Ebola in Liberia*. N Engl J Med, 2017. **377**(15): p. 1438-1447.
151. Jones, S.M., et al., *Live attenuated recombinant vaccine protects nonhuman primates against Ebola and Marburg viruses*. Nat Med, 2005. **11**(7): p. 786-90.
152. Jones, S.M., et al., *Assessment of a vesicular stomatitis virus-based vaccine by use of the mouse model of Ebola virus hemorrhagic fever*. J Infect Dis, 2007. **196** Suppl 2: p. S404-12.
153. Qiu, X., et al., *Mucosal immunization of cynomolgus macaques with the VSVDeltaG/ZEBOVGP vaccine stimulates strong ebola GP-specific immune responses*. PLoS One, 2009. **4**(5): p. e5547.
154. Wong, G., et al., *Immunization with vesicular stomatitis virus vaccine expressing the Ebola glycoprotein provides sustained long-term protection in rodents*. Vaccine, 2014. **32**(43): p. 5722-9.
155. Mire, C.E., et al., *Durability of a vesicular stomatitis virus-based marburg virus vaccine in nonhuman primates*. PLoS One, 2014. **9**(4): p. e94355.
156. Marzi, A., et al., *Antibodies are necessary for rVSV/ZEBOV-GP-mediated protection against lethal Ebola virus challenge in nonhuman primates*. Proc Natl Acad Sci U S A, 2013. **110**(5): p. 1893-8.
157. Geisbert, T.W., et al., *Vesicular stomatitis virus-based ebola vaccine is well-tolerated and protects immunocompromised nonhuman primates*. PLoS Pathog, 2008. **4**(11): p. e1000225.
158. Geisbert, T.W., et al., *Single-injection vaccine protects nonhuman primates against infection with marburg virus and three species of ebola virus*. J Virol, 2009. **83**(14): p. 7296-304.
159. Feldmann, H., et al., *Effective post-exposure treatment of Ebola infection*. PLoS Pathog, 2007. **3**(1): p. e2.
160. Geisbert, T.W., et al., *Recombinant vesicular stomatitis virus vector mediates postexposure protection against Sudan Ebola hemorrhagic fever in nonhuman primates*. J Virol, 2008. **82**(11): p. 5664-8.

161. Marzi, A., et al., *EBOLA VACCINE. VSV-EBOV rapidly protects macaques against infection with the 2014/15 Ebola virus outbreak strain*. *Science*, 2015. **349**(6249): p. 739-42.
162. Agnandji, S.T., et al., *Phase 1 Trials of rVSV Ebola Vaccine in Africa and Europe - Preliminary Report*. *N Engl J Med*, 2015.
163. Regules, J.A., et al., *A Recombinant Vesicular Stomatitis Virus Ebola Vaccine - Preliminary Report*. *N Engl J Med*, 2015.
164. Henao-Restrepo, A.M., et al., *Efficacy and effectiveness of an rVSV-vectored vaccine expressing Ebola surface glycoprotein: interim results from the Guinea ring vaccination cluster-randomised trial*. *Lancet*, 2015. **386**(9996): p. 857-66.
165. Huttner, A., et al., *Determinants of antibody persistence across doses and continents after single-dose rVSV-ZEBOV vaccination for Ebola virus disease: an observational cohort study*. *Lancet Infect Dis*, 2018.
166. Gunther, S., et al., *Management of accidental exposure to Ebola virus in the biosafety level 4 laboratory, Hamburg, Germany*. *J Infect Dis*, 2011. **204** **Suppl 3**: p. S785-90.
167. Lai, L., et al., *Emergency Postexposure Vaccination With Vesicular Stomatitis Virus-Vectored Ebola Vaccine After Needlestick*. *JAMA*, 2015.
168. Oestereich, L., et al., *Successful treatment of advanced Ebola virus infection with T-705 (favipiravir) in a small animal model*. *Antiviral Res*, 2014. **105**: p. 17-21.
169. Smither, S.J., et al., *Post-exposure efficacy of oral T-705 (Favipiravir) against inhalational Ebola virus infection in a mouse model*. *Antiviral Res*, 2014. **104**: p. 153-5.
170. Trompiz, G., H. Lawson, and S. Powell. *First French Ebola patient leaves hospital*. 2014; Available from: <http://www.reuters.com/article/2014/10/04/us-health-ebola-france-idUSKCN0HT0D720141004>.
171. Sissoko, D., et al., *Experimental Treatment with Favipiravir for Ebola Virus Disease (the JIKI Trial): A Historically Controlled, Single-Arm Proof-of-Concept Trial in Guinea*. *PLoS Med*, 2016. **13**(3): p. e1001967.
172. Warren, T.K., et al., *Protection against filovirus diseases by a novel broad-spectrum nucleoside analogue BCX4430*. *Nature*, 2014. **508**(7496): p. 402-5.
173. Litterman, N., C. Lipinski, and S. Ekins, *Small molecules with antiviral activity against the Ebola virus*. *F1000Res*, 2015. **4**: p. 38.

174. Gulland, A., *Ebola drug trial is terminated after fall in number of new cases*. BMJ, 2015. **350**: p. h664.
175. Warren, T.K., et al., *Therapeutic efficacy of the small molecule GS-5734 against Ebola virus in rhesus monkeys*. Nature, 2016. **531**(7594): p. 381-5.
176. Warren, T.K., et al., *Advanced antisense therapies for postexposure protection against lethal filovirus infections*. Nat Med, 2010. **16**(9): p. 991-4.
177. Heald, A.E., et al., *Safety and pharmacokinetic profiles of phosphorodiamidate morpholino oligomers with activity against ebola virus and marburg virus: results of two single-ascending-dose studies*. Antimicrob Agents Chemother, 2014. **58**(11): p. 6639-47.
178. Geisbert, T.W., et al., *Postexposure protection of guinea pigs against a lethal ebola virus challenge is conferred by RNA interference*. J Infect Dis, 2006. **193**(12): p. 1650-7.
179. Geisbert, T.W., et al., *Postexposure protection of non-human primates against a lethal Ebola virus challenge with RNA interference: a proof-of-concept study*. Lancet, 2010. **375**(9729): p. 1896-905.
180. Young, S. *FDA allows expanded use of experimental Ebola drug*. 2014 December 12, 2014]; Available from: <http://www.cnn.com/2014/09/22/health/ebola-drug-tekmira/>.
181. Oswald, W.B., et al., *Neutralizing antibody fails to impact the course of Ebola virus infection in monkeys*. PLoS Pathog, 2007. **3**(1): p. e9.
182. Marzi, A., et al., *Protective efficacy of neutralizing monoclonal antibodies in a nonhuman primate model of Ebola hemorrhagic fever*. PLoS One, 2012. **7**(4): p. e36192.
183. Dye, J.M., et al., *Postexposure antibody prophylaxis protects nonhuman primates from filovirus disease*. Proc Natl Acad Sci U S A, 2012. **109**(13): p. 5034-9.
184. Qiu, X., et al., *Successful treatment of ebola virus-infected cynomolgus macaques with monoclonal antibodies*. Sci Transl Med, 2012. **4**(138): p. 138ra81.
185. Olinger, G.G., Jr., et al., *Delayed treatment of Ebola virus infection with plant-derived monoclonal antibodies provides protection in rhesus macaques*. Proc Natl Acad Sci U S A, 2012. **109**(44): p. 18030-5.
186. Qiu, X., et al., *Reversion of advanced Ebola virus disease in nonhuman primates with ZMapp*. Nature, 2014. **514**(7520): p. 47-53.

187. McCarthy, M., *US signs contract with ZMapp maker to accelerate development of the Ebola drug*. BMJ, 2014. **349**: p. g5488.
188. Group, P.I.W., et al., *A Randomized, Controlled Trial of ZMapp for Ebola Virus Infection*. N Engl J Med, 2016. **375**(15): p. 1448-1456.
189. WHO, W.H.O. *Ebola vaccines, therapies, and diagnostics*. 2015 [cited 2015; Available from: http://www.who.int/medicines/emp_ebola_q_as/en/].
190. Jacobs, M., et al., *Post-exposure prophylaxis against Ebola virus disease with experimental antiviral agents: a case-series of health-care workers*. Lancet Infect Dis, 2015. **15**(11): p. 1300-4.
191. Corti, D., et al., *Protective monotherapy against lethal Ebola virus infection by a potently neutralizing antibody*. Science, 2016. **351**(6279): p. 1339-42.
192. Misasi, J., et al., *Structural and molecular basis for Ebola virus neutralization by protective human antibodies*. Science, 2016. **351**(6279): p. 1343-6.
193. Versteeg, K., et al., *Infection with the Makona variant results in a delayed and distinct host immune response compared to previous Ebola virus variants*. Sci Rep, 2017. **7**(1): p. 9730.
194. MacNeil, A., et al., *Proportion of deaths and clinical features in Bundibugyo Ebola virus infection, Uganda*. Emerg Infect Dis, 2010. **16**(12): p. 1969-72.
195. Gupta, M., et al., *Serology and cytokine profiles in patients infected with the newly discovered Bundibugyo ebolavirus*. Virology, 2012. **423**(2): p. 119-24.
196. Larsen, T., et al., *Pathologic findings associated with delayed death in nonhuman primates experimentally infected with Zaire Ebola virus*. J Infect Dis, 2007. **196** Suppl 2: p. S323-8.
197. Cross, R.W., et al., *The Domestic Ferret (Mustela putorius furo) as a Lethal Infection Model for 3 Species of Ebolavirus*. J Infect Dis, 2016. **214**(4): p. 565-9.
198. Geisbert, T.W., J.E. Strong, and H. Feldmann, *Considerations in the Use of Nonhuman Primate Models of Ebola Virus and Marburg Virus Infection*. Journal of Infectious Diseases, 2015. **212**: p. S91-S97.
199. Davis, K.J., et al., *Pathology of experimental Ebola virus infection in African green monkeys. Involvement of fibroblastic reticular cells*. Arch Pathol Lab Med, 1997. **121**(8): p. 805-19.

200. CDC. *2014 Ebola Outbreak in West Africa - Case Counts*. 2016 [cited 2016 November 16, 2016]; Available from: <http://www.cdc.gov/vhf/ebola/outbreaks/2014-west-africa/case-counts.html>.
201. Baize, S., et al., *Emergence of Zaire Ebola virus disease in Guinea*. N Engl J Med, 2014. **371**(15): p. 1418-25.
202. Thi, E.P., et al., *Lipid nanoparticle siRNA treatment of Ebola-virus-Makona-infected nonhuman primates*. Nature, 2015. **521**(7552): p. 362-5.
203. Autissier, P., et al., *Immunophenotyping of lymphocyte, monocyte and dendritic cell subsets in normal rhesus macaques by 12-color flow cytometry: clarification on DC heterogeneity*. J Immunol Methods, 2010. **360**(1-2): p. 119-28.
204. TW, H.B. and T. Girke, *systemPipeR: NGS workflow and report generation environment*. BMC Bioinformatics, 2016. **17**: p. 388.
205. Menicucci, A.R., et al., *Transcriptomic analysis reveals a previously unknown role for CD8(+) T-cells in rVSV-EBOV mediated protection*. Sci Rep, 2017. **7**(1): p. 919.
206. Holm, S., *A simple sequentially rejective multiple test procedure*. Scandinavian Journal of Statistics, 1979. **6**(2): p. 65-70.
207. Salhia, B., et al., *Integrated genomic and epigenomic analysis of breast cancer brain metastasis*. PLoS One, 2014. **9**(1): p. e85448.
208. Heng, T.S., M.W. Painter, and C. Immunological Genome Project, *The Immunological Genome Project: networks of gene expression in immune cells*. Nat Immunol, 2008. **9**(10): p. 1091-4.
209. Barrenas, F., et al., *Next-generation sequencing reveals a controlled immune response to Zaire Ebola virus challenge in cynomolgus macaques immunized with vesicular stomatitis virus expressing Zaire Ebola virus glycoprotein (VSVDeltaG/EBOVgp)*. Clin Vaccine Immunol, 2015. **22**(3): p. 354-6.
210. Rubins, K.H., et al., *The temporal program of peripheral blood gene expression in the response of nonhuman primates to Ebola hemorrhagic fever*. Genome Biol, 2007. **8**(8): p. R174.
211. Dietzel, E., et al., *Functional Characterization of Adaptive Mutations during the West African Ebola Virus Outbreak*. J Virol, 2017. **91**(2).
212. Diehl, W.E., et al., *Ebola Virus Glycoprotein with Increased Infectivity Dominated the 2013-2016 Epidemic*. Cell, 2016. **167**(4): p. 1088-1098 e6.

213. Garamszegi, S., et al., *Transcriptional correlates of disease outcome in anticoagulant-treated non-human primates infected with ebolavirus*. PLoS Negl Trop Dis, 2014. **8**(7): p. e3061.
214. Caballero, I.S., et al., *In vivo Ebola virus infection leads to a strong innate response in circulating immune cells*. BMC Genomics, 2016. **17**: p. 707.
215. Yen, J.Y., et al., *Therapeutics of Ebola hemorrhagic fever: whole-genome transcriptional analysis of successful disease mitigation*. J Infect Dis, 2011. **204 Suppl 3**: p. S1043-52.
216. Ilinykh, P.A., et al., *Different Temporal Effects of Ebola Virus VP35 and VP24 Proteins on Global Gene Expression in Human Dendritic Cells*. J Virol, 2015. **89**(15): p. 7567-83.
217. Escudero-Perez, B., et al., *Shed GP of Ebola virus triggers immune activation and increased vascular permeability*. PLoS Pathog, 2014. **10**(11): p. e1004509.
218. Wilson, E.B., et al., *Blockade of chronic type I interferon signaling to control persistent LCMV infection*. Science, 2013. **340**(6129): p. 202-7.
219. Teijaro, J.R., et al., *Persistent LCMV infection is controlled by blockade of type I interferon signaling*. Science, 2013. **340**(6129): p. 207-11.
220. Yang, J., et al., *Monocyte and macrophage differentiation: circulation inflammatory monocyte as biomarker for inflammatory diseases*. Biomark Res, 2014. **2**(1): p. 1.
221. Mukherjee, R., et al., *Non-Classical monocytes display inflammatory features: Validation in Sepsis and Systemic Lupus Erythematosus*. Sci Rep, 2015. **5**: p. 13886.
222. Ludtke, A., et al., *Ebola Virus Disease Is Characterized by Poor Activation and Reduced Levels of Circulating CD16+ Monocytes*. J Infect Dis, 2016.
223. Fisher-Hoch, S.P., et al., *Physiological and immunologic disturbances associated with shock in a primate model of Lassa fever*. J Infect Dis, 1987. **155**(3): p. 465-74.
224. Glatman Zaretsky, A., J.B. Engiles, and C.A. Hunter, *Infection-induced changes in hematopoiesis*. J Immunol, 2014. **192**(1): p. 27-33.
225. Liu, X., et al., *Transcriptomic signatures differentiate survival from fatal outcomes in humans infected with Ebola virus*. Genome Biology, 2017. **18**(1): p. 4.

226. Gauss, K.A., et al., *Role of NF-kappaB in transcriptional regulation of the phagocyte NADPH oxidase by tumor necrosis factor-alpha*. *J Leukoc Biol*, 2007. **82**(3): p. 729-41.
227. Menicucci, A.R., et al., *Transcriptome Analysis of Circulating Immune Cell Subsets Highlight the Role of Monocytes in Zaire Ebola Virus Makona Pathogenesis*. *Front Immunol*, 2017. **8**: p. 1372.
228. Geisbert, T.W., et al., *Treatment of Ebola virus infection with a recombinant inhibitor of factor VIIa/tissue factor: a study in rhesus monkeys*. *Lancet*, 2003. **362**(9400): p. 1953-8.
229. Martinez, O., et al., *Ebola virus exploits a monocyte differentiation program to promote its entry*. *J Virol*, 2013. **87**(7): p. 3801-14.
230. Connolly, B.M., et al., *Pathogenesis of experimental Ebola virus infection in guinea pigs*. *J Infect Dis*, 1999. **179 Suppl 1**: p. S203-17.
231. Yaddanapudi, K., et al., *Implication of a retrovirus-like glycoprotein peptide in the immunopathogenesis of Ebola and Marburg viruses*. *FASEB J*, 2006. **20**(14): p. 2519-30.
232. Alasoo, K., et al., *Transcriptional profiling of macrophages derived from monocytes and iPS cells identifies a conserved response to LPS and novel alternative transcription*. *Sci Rep*, 2015. **5**: p. 12524.
233. Dong, C., R.J. Davis, and R.A. Flavell, *MAP kinases in the immune response*. *Annu Rev Immunol*, 2002. **20**: p. 55-72.
234. Hofer, T.P., et al., *slan-defined subsets of CD16-positive monocytes: impact of granulomatous inflammation and M-CSF receptor mutation*. *Blood*, 2015. **126**(24): p. 2601-10.
235. Grunin, M., et al., *Transcriptome Analysis on Monocytes from Patients with Neovascular Age-Related Macular Degeneration*. *Sci Rep*, 2016. **6**: p. 29046.
236. Lacey, D.C., et al., *Defining GM-CSF- and macrophage-CSF-dependent macrophage responses by in vitro models*. *J Immunol*, 2012. **188**(11): p. 5752-65.
237. Reiman, J.M., et al., *Tumor immunoediting and immunosculpting pathways to cancer progression*. *Semin Cancer Biol*, 2007. **17**(4): p. 275-87.
238. Frankenberger, M., et al., *Transcript profiling of CD16-positive monocytes reveals a unique molecular fingerprint*. *Eur J Immunol*, 2012. **42**(4): p. 957-74.

239. O'Reilly, M.K. and J.C. Paulson, *Siglecs as targets for therapy in immune-cell-mediated disease*. Trends in Pharmacological Sciences, 2009. **30**(5): p. 240-248.
240. Daly, C. and B.J. Rollins, *Monocyte chemoattractant protein-1 (CCL2) in inflammatory disease and adaptive immunity: Therapeutic opportunities and controversies*. Microcirculation, 2003. **10**(3-4): p. 247-257.
241. Modi, W.S., *CCL3L1 and CCL4L1 chemokine genes are located in a segmental duplication at chromosome 17q12*. Genomics, 2004. **83**(4): p. 735-738.
242. Muralidharan, S. and P. Mandrekar, *Cellular stress response and innate immune signaling: integrating pathways in host defense and inflammation*. J Leukoc Biol, 2013. **94**(6): p. 1167-84.
243. Manns, J.M., I. Isordia-Salas, and R.A. DeLa Cadena, *Thrombospondin-1 (TSP) binds to the heavy chain of elastase (HNE) activated coagulation factor V (FVa(HNE)) and enhances thrombin generation on the surface of a monocytic cell line*. Blood, 2000. **96**(11): p. 16a-16a.
244. Vogler, M., *BCL2A1: the underdog in the BCL2 family*. Cell Death and Differentiation, 2012. **19**(1): p. 67-74.
245. Weisiger, R.A. and I. Fridovich, *Mitochondrial Superoxide Dismutase - Site of Synthesis and Intramitochondrial Localization*. Journal of Biological Chemistry, 1973. **248**(13): p. 4793-4796.
246. McNeill, E., et al., *Regulation of iNOS function and cellular redox state by macrophage Gch1 reveals specific requirements for tetrahydrobiopterin in NRF2 activation*. Free Radic Biol Med, 2015. **79**: p. 206-16.
247. Johnson, C., et al., *Matrix metalloproteinase-9 is required for adequate angiogenic revascularization of ischemic tissues - Potential role in capillary branching*. Circulation Research, 2004. **94**(2): p. 262-268.
248. Butte, M.J., et al., *Programmed death-1 ligand 1 interacts specifically with the B7-1 costimulatory molecule to inhibit T cell responses*. Immunity, 2007. **27**(1): p. 111-122.
249. Hammond, M.E.W., et al., *Il-8 Induces Neutrophil Chemotaxis Predominantly Via Type-I Il-8 Receptors*. Journal of Immunology, 1995. **155**(3): p. 1428-1433.
250. Van Damme, J., et al., *Structural and functional identification of two human, tumor-derived monocyte chemotactic proteins (MCP-2 and MCP-3) belonging to the chemokine family*. J Exp Med, 1992. **176**(1): p. 59-65.

251. Tsai, S.F., et al., *Isochailulactone-induced DDIT3 causes ER stress-PERK independent apoptosis in glioblastoma multiforme cells*. *Oncotarget*, 2016.
252. Feder, M.E. and G.E. Hofmann, *Heat-shock proteins, molecular chaperones, and the stress response: evolutionary and ecological physiology*. *Annu Rev Physiol*, 1999. **61**: p. 243-82.
253. Irmeler, M., et al., *Inhibition of death receptor signals by cellular FLIP*. *Nature*, 1997. **388**(6638): p. 190-5.
254. Ma, O., et al., *MMP13, Birc2 (cIAP1), and Birc3 (cIAP2), amplified on chromosome 9, collaborate with p53 deficiency in mouse osteosarcoma progression*. *Cancer Res*, 2009. **69**(6): p. 2559-67.
255. Rahman, N., G. Stewart, and G. Jones, *A role for the atopy-associated gene PPH11 in T-cell activation and viability*. *Immunol Cell Biol*, 2010. **88**(8): p. 817-24.
256. Hashiguchi, M., et al., *Triggering receptor expressed on myeloid cell-like transcript 2 (TLT-2) is a counter-receptor for B7-H3 and enhances T cell responses*. *Proc Natl Acad Sci U S A*, 2008. **105**(30): p. 10495-500.
257. Schornberg, K., et al., *Role of endosomal cathepsins in entry mediated by the Ebola virus glycoprotein*. *J Virol*, 2006. **80**(8): p. 4174-8.
258. Wahl-Jensen, V., et al., *Ebola virion attachment and entry into human macrophages profoundly effects early cellular gene expression*. *PLoS Negl Trop Dis*, 2011. **5**(10): p. e1359.
259. Pulit-Penalosa, J.A., S.V. Scherbik, and M.A. Brinton, *Type 1 IFN-independent activation of a subset of interferon stimulated genes in West Nile virus Eg101-infected mouse cells*. *Virology*, 2012. **425**(2): p. 82-94.
260. Cilloniz, C., et al., *Functional genomics reveals the induction of inflammatory response and metalloproteinase gene expression during lethal Ebola virus infection*. *J Virol*, 2011. **85**(17): p. 9060-8.
261. Liu, X., et al., *Transcriptomic signatures differentiate survival from fatal outcomes in humans infected with Ebola virus*. *Genome Biol*, 2017. **18**(1): p. 4.
262. Kash, J.C., et al., *Longitudinal peripheral blood transcriptional analysis of a patient with severe Ebola virus disease*. *Sci Transl Med*, 2017. **9**(385).

263. Hilkens, C.M., J.F. Schlaak, and I.M. Kerr, *Differential responses to IFN-alpha subtypes in human T cells and dendritic cells*. J Immunol, 2003. **171**(10): p. 5255-63.
264. Leung, L.W., et al., *Ebolavirus VP35 suppresses IFN production from conventional but not plasmacytoid dendritic cells*. Immunol Cell Biol, 2011. **89**(7): p. 792-802.
265. Valmas, C., et al., *Marburg virus evades interferon responses by a mechanism distinct from ebola virus*. PLoS Pathog, 2010. **6**(1): p. e1000721.
266. Harcourt, B.H., A. Sanchez, and M.K. Offermann, *Ebola virus inhibits induction of genes by double-stranded RNA in endothelial cells*. Virology, 1998. **252**(1): p. 179-88.
267. Kash, J.C., et al., *Global suppression of the host antiviral response by Ebola- and Marburgviruses: increased antagonism of the type I interferon response is associated with enhanced virulence*. J Virol, 2006. **80**(6): p. 3009-20.
268. Basler, C.F., et al., *The Ebola virus VP35 protein functions as a type I IFN antagonist*. Proc Natl Acad Sci U S A, 2000. **97**(22): p. 12289-94.
269. Leung, D.W., et al., *Structure of the Ebola VP35 interferon inhibitory domain*. Proc Natl Acad Sci U S A, 2009. **106**(2): p. 411-6.
270. Prins, K.C., et al., *Basic residues within the ebolavirus VP35 protein are required for its viral polymerase cofactor function*. J Virol, 2010. **84**(20): p. 10581-91.
271. Leung, D.W., et al., *Structural basis for dsRNA recognition and interferon antagonism by Ebola VP35*. Nat Struct Mol Biol, 2010. **17**(2): p. 165-72.
272. Hartman, A.L., et al., *Inhibition of IRF-3 activation by VP35 is critical for the high level of virulence of ebola virus*. J Virol, 2008. **82**(6): p. 2699-704.
273. Leung, D.W., et al., *Structural and functional characterization of Reston Ebola virus VP35 interferon inhibitory domain*. J Mol Biol, 2010. **399**(3): p. 347-57.
274. Hartman, A.L., et al., *Whole-genome expression profiling reveals that inhibition of host innate immune response pathways by Ebola virus can be reversed by a single amino acid change in the VP35 protein*. J Virol, 2008. **82**(11): p. 5348-58.
275. Yen, B., et al., *Molecular basis for ebolavirus VP35 suppression of human dendritic cell maturation*. J Virol, 2014. **88**(21): p. 12500-10.

276. Marzi, A., Hanley P.W., Haddock E., Martellaro C., Kobinger G., Feldmann H. , *Efficacy of Vesicular stomatitis virus-Ebola virus postexposure treatment in rhesus macaques infected with Ebola virus Makona*. Journal of Infectious Diseases, 2016.
277. Nueda, M.J., S. Tarazona, and A. Conesa, *Next maSigPro: updating maSigPro bioconductor package for RNA-seq time series*. Bioinformatics, 2014. **30**(18): p. 2598-602.
278. Nakhaei, P., J. Hiscott, and R. Lin, *STING-ing the antiviral pathway*. J Mol Cell Biol, 2010. **2**(3): p. 110-2.
279. Gauld, S.B. and J.C. Cambier, *Src-family kinases in B-cell development and signaling*. Oncogene, 2004. **23**(48): p. 8001-6.
280. Mackay, F. and J.L. Browning, *BAFF: a fundamental survival factor for B cells*. Nat Rev Immunol, 2002. **2**(7): p. 465-75.
281. Cattoretti, G., et al., *PRDM1/Blimp-1 is expressed in human B-lymphocytes committed to the plasma cell lineage*. J Pathol, 2005. **206**(1): p. 76-86.
282. Le Bon, A., et al., *Type I interferons potently enhance humoral immunity and can promote isotype switching by stimulating dendritic cells in vivo*. Immunity, 2001. **14**(4): p. 461-70.
283. Deenick, E.K. and C.S. Ma, *The regulation and role of T follicular helper cells in immunity*. Immunology, 2011. **134**(4): p. 361-7.
284. Sprokholt, J.K., et al., *RIG-I-like receptor activation by dengue virus drives follicular T helper cell formation and antibody production*. PLoS Pathog, 2017. **13**(11): p. e1006738.
285. Siegrist, C.-A., *Vaccine immunology*. Vaccines, ed. S.A. Plotkin and W.A. Orenstein. 2008, Philadelphia, PA: Elsevier Inc.
286. Baize, S., et al., *Early and strong immune responses are associated with control of viral replication and recovery in lassa virus-infected cynomolgus monkeys*. J Virol, 2009. **83**(11): p. 5890-903.
287. Malleret, B., et al., *Primary infection with simian immunodeficiency virus: plasmacytoid dendritic cell homing to lymph nodes, type I interferon, and immune suppression*. Blood, 2008. **112**(12): p. 4598-608.

288. Jacquelin, B., et al., *Nonpathogenic SIV infection of African green monkeys induces a strong but rapidly controlled type I IFN response*. J Clin Invest, 2009. **119**(12): p. 3544-55.
289. Jahrling, P.B., et al., *Evaluation of immune globulin and recombinant interferon-alpha2b for treatment of experimental Ebola virus infections*. J Infect Dis, 1999. **179 Suppl 1**: p. S224-34.
290. Smith, L.M., et al., *Interferon-beta therapy prolongs survival in rhesus macaque models of Ebola and Marburg hemorrhagic fever*. J Infect Dis, 2013. **208**(2): p. 310-8.